Lawrence Berkeley National Laboratory
LBL Publications

Title

DECOVALEX-2023 Task F2 Salt Final Report

Permalink

https://escholarship.org/uc/item/2874s3kv

Authors

Faybishenko, Boris
LaForce, Tara

Publication Date

2024-04-12

Copyright Information

Peer reviewed

DECOVALEX-2023
Task F2 Salt Final Report

Tara LaForce[1]

With contributions from:

Jeroen Bartol[4], Dirk-Alexander Becker[2], Steven Benbow[3], Alexander Bond[3], Carl Rudolf Dietl[5], Tanja Frank[2], Rick Jayne[1], Ingo Kock[5], Fabiano Magri[5], Josh Nicholas[3], Marek Pekala[5], Philip H. Stauffer[6], Emily Stein[1], Jodie Stone[3], Jens Wolf[2]

[1]Sandia National Laboratories, [2]GRS, [3]Quintessa, [4]COVRA, [5]BASE, [6]Los Alamos National Laboratory

Dec 2023

DECOVALEX 2023

Disclaimer

This document was prepared as an account of the international research project DECOVALEX-2023 comprising participants from industry, government and academia, with funding organizations--Andra, BASE, BGE, BGR, CAS, CNSC, COVRA, U.S. DOE, Enresa, ENSI, JAEA, KAERI, NWMO, NWS, SÚRAO, SSM and Taipower. The statements made in the report are, however, solely those of the authors and do not necessarily reflect those of the Funding Organizations. While this document is believed to contain correct information, neither the United States Government nor any agency thereof, nor the Regents of the University of California, nor any of their employees, makes any warranty, express or implied, or assumes any legal responsibility for the accuracy, completeness, or usefulness of any information, apparatus, product, or process disclosed, or represents that its use would not infringe privately owned rights. Reference herein to any specific commercial product, process, or service by its trade name, trademark, manufacturer, or otherwise does not necessarily constitute or imply its endorsement, recommendation, or favoring by the United States Government or any agency thereof or the Regents of the University of California. The views and opinions of the authors expressed herein do not necessarily state or reflect those of the United States Government, any agency thereof, or the Regents of the University of California.

This technical document does not consider contractual limitations or obligations under the Standard Contract for Disposal of Spent Nuclear Fuel and/or High-Level Radioactive Waste (Standard Contract) (10 CFR Part 961).

To the extent discussions or recommendations in this document conflict with the provisions of the Standard Contract, the Standard Contract governs the obligations of the parties, and this presentation in no manner supersedes, overrides, or amends the Standard Contract.

No inferences should be drawn from this document regarding future actions by DOE, which are limited by the terms of the Standard Contract and Congressional appropriations for the Department to fulfill its obligations under the Nuclear Waste Policy Act, including licensing and constructing a spent nuclear fuel repository.

DECOVALEX-2023

Task F2 Final Report

Main Authors :

Tara LaForce
Sandia National Laboratories

Contributing Authors (alphabetical by organisation) :

Carlo Dietl, Ingo Kock, Fabiano Magri, Marek Pekala
BASE

Jeroen Bartol
COVRA

Dirk-Alexander Becker, Tanja Frank, Jens Wolf
GRS

Philip Stauffer
LANL

Steven Benbow, Alex Bond, Josh Nicholas, Jodie Stone
Quintessa

Richard Jayne, Emily Stein
SNL

Preface

The DECOVALEX Project is an ongoing international research collaboration established in 1992 to advance the understanding and modeling of coupled Thermal (T), Hydrological (H), Mechanical (M), and Chemical (C) processes in geological systems. DECOVALEX was initially motivated by recognising that predicting these coupled effects is essential to the performance and safety assessment of geologic disposal systems for radioactive waste and spent nuclear fuel. Later, it was realized that these processes also play a critical role in other subsurface engineering activities, such as subsurface CO_2 storage, enhanced geothermal systems, and unconventional oil and gas production through hydraulic fracturing. Research teams from many countries (e.g., Canada, China, Czech Republic, Finland, France, Germany, Japan, Netherlands, Republic of Korea, Spain, Sweden, Switzerland, Taiwan, United Kingdom, and the United States) various institutions have participated in the DECOVALEX Project over the years, providing a wide range of perspectives and solutions to these complex problems. These institutions represent radioactive waste management organizations, national research institutes, regulatory agencies, universities, and industry and consulting groups.

At the core of the collaborative work within DECOVALEX is the collaborative analysis and comparative modeling of state-of-the-art field and laboratory experiments. DECOVALEX engages model comparison in a broad and comprehensive sense, including the modelers' interpretation of experimental data, selection of boundary conditions, rock and fluid properties, etc., and their choice of coupling schemes and simulators. This recent phase of DECOVALEX has expanded the work scope to include the modelers being challenged to gain an understanding of the representation coupled processes in generic 'whole system' or 'performance assessment' models. In-depth and detailed discussions among the teams yield insight into the coupled THMC processes and stimulate the development of modeling capabilities and measurement methods. This would have been impossible if only one or two groups had studied the data.

Since the project initiation, DECOVALEX has been organized in several four-year phases, each featuring several modeling tasks of importance to radioactive waste disposal and other geoscience applications. Seven project phases were successfully concluded between 1992 and 2019, the results of which have been summarized in several overview publications (e.g., Tsang et al., 2009; Birkholzer et al., 2018; Birkholzer et al., 2019, Birkholzer et al., 2024). The most recent phase, DECOVALEX-2023, started in 2020 and ended in 2023. Seven tasks were conducted in DECOVALEX-2023, as follows:

- **Task A: HGFrac** – Thermal- and gas- induced fracturing of the Callovo-Oxfordian Clay, France
- **Task B: MAGIC** – Migration of gas in compacted clay
- **Task C: FE Experiment** – Thermal-hydro-mechanical (THM) modelling of the FE experiment at Mont Terri, Switzerland
- **Task D: Horonobe EBS Experiment** - THM modelling of the Horonobe EBS experiment at the Horonobe URL, Japan
- **Task E: BATS** – THM modeling for the Brine Availability Test in Salt (BATS) at the WIPP, New Mexico, USA

- **Task F: Performance Assessment** – Comparative generic performance assessment models in crystalline and salt formations
- **Task G: SAFENET** – Laboratory-scale TH and THM analyses of single fractures

The DECOVALEX Project would not have been possible without the support and engagement of the participating organizations who jointly support the coordination of the project within a given project phase, propose and coordinate modeling tasks, including the necessary experimental data, and deploy their research team (or teams) working on a selection of the tasks conducted in the project. The partner organizations in DECOVALEX-2023 were:

- Andra, National Radioactive Waste Management Agency, *France*
- BASE, Federal Office for the Safety of Nuclear Waste Management*, Germany*
- BGE, Federal Company for Radioactive Waste Disposal, *Germany*
- BGR, Federal Institute for Geosciences and Natural Resources, *Germany*
- CAS, Chinese Academy of Sciences, *China*
- CNSC, Canadian Nuclear Safety Commission, *Canada*
- COVRA, Central Organisation for Radioactive Waste, *Netherlands*
- DOE, Department of Energy, *USA*
- Enresa, National Radioactive Waste Management Agency, *Spain*
- ENSI, Swiss Federal Nuclear Safety Inspectorate, *Switzerland*
- JAEA, Japan Atomic Energy Agency, *Japan*
- KAERI, Korea Atomic Energy Research Institute, Republic of Korea
- NWMO, Nuclear Waste Management Organization, *Canada*
- NWS, Nuclear Waste Services, *United Kingdom*
- SSM, Swedish Radiation Safety Authority, *Sweden*
- SÚRAO, Radioactive Waste Repository Authority, *Czech Republic*
- Taipower, Taiwan Power Company, *Taiwan*

We are extremely grateful to these organizations for their financial and technical support of DECOVALEX-2019.

Jens Birkholzer (Chairman of the DECOVALEX project) and Alex Bond (Technical Coordinator of the DECOVALEX Project).

Berkeley, California, USA, October 2024

References:
Birkholzer, J.T., Bond, A.E., Hudson, J.A., Jing, L., Tsang, C.-F., Shao, H., Kolditz, O. (2018): DECOVALEX-2015 - An International Collaboration for Advancing the Understanding and Modeling of Coupled Thermo-Hydro-Mechanical-Chemical (THMC) Processes in Geological Systems, Environmental Earth Sciences, 77(14). https://doi.org/10.1016/j.ijrmms.2022.105097

Birkholzer, J.T., Tsang, C.-F., Bond, A.E., Hudson, J.A., Jing, L., and Stephansson, O. (2019): 25 Years of DECOVALEX - Scientific Advances and Lessons Learned from an International Research Collaboration in Coupled Subsurface Processes, Invited Review, International Journal and Rock Mechanics and Mining Sciences, 122. https://doi.org/10.1016/j.ijrmms.2019.03.015

Birkholzer, J.T., Bond, A.E. and Tsang, C.-F. (2024). The DECOVALEX international collaboration on modeling of coupled subsurface processes and its contribution to confidence building in

radioactive waste disposal. Hydrogeology Journal, https://doi.org/10.1007/s10040-024-02799-7

Tsang, C.-F., Stephansson, O., Jing, L., and Kautsky, F. (2009): DECOVALEX Project: from 1992 to 2007. Environmental Geology, 57(6). https://doi.org/10.1007/s00254-008-1625-1

Summary

The subject of Task F of DECOVALEX-2023 concerns performance assessment modelling of radioactive waste disposal in deep mined repositories. The primary objectives of Task F are to build confidence in the models, methods, and software used for performance assessment (PA) of deep geologic nuclear waste repositories, and/or to bring to the fore additional research and development needed to improve PA methodologies. In Task F2-(salt), these objectives have been accomplished through staged development and comparison of the models and methods used by participating teams in their PA frameworks. Coupled-process submodels and deterministic simulations of the entire PA model for a reference scenario for waste disposal in domal salt have been conducted. The task specification has been updated continuously since the initiation of the project to reflect the staged development of the conceptual repository model and performance metrics.

Thermal, hydrological, mechanical, and chemical properties of individual components of the engineered and natural system were chosen for relevance by participating teams. The salt reference case system was characterized using data and measurements collected at relevant underground research laboratories (URLs), field sites, and simulation results from teams with specialized modelling capability. Participating teams made a wide range of model assumptions from compartmentalized networks to full 3D models of the salt formation. No single contributed model includes full-fidelity representation of all the features, events, and processes (FEPs) detailed in the task specification, but almost all features and processes are represented in at least one model.

Despite differences in the modelling strategies developed by participating teams, all models indicate that salt compaction and radionuclide diffusion are key processes in the repository, and for the FEPs and model scenario considered, little of the disposed radionuclides will migrate beyond the repository seal over the 100,000 year simulations. In general, the model output quantities have the largest differences over the short term and near the waste. The models tend to be more similar further from waste and at later time. Disparities between the models are believed to be due to differing simplifications from the task specification, some of which are chosen simplifications to reduce complexity, and some are restrictions imposed by the modelling tools.

A second round of this task has been accepted for DECOVALEX-2027 in conjunction with Task F1 on crystalline PA modelling. The future round includes waste package heating, improved modelling of salt creep closure, additional comparisons of coupled-process

sub-models, and the impact of repository engineering design on radionuclide migration in the repository. Participants will also propose and finalize a set of uncertain inputs for the reference case simulations, propagate these uncertainties in a set of realizations, and conduct sensitivity analyses on the simulation results.

Contents

1 Introduction

Task F of DECOVALEX-2023 involves comparison of the models and methods used in post-closure performance assessment of deep geologic repositories in either salt or crystalline basement rock. Task F2 is a sub-task of Task F that is focused on radioactive waste disposal in salt repositories. The participating teams in Task F2 are shown in Table 1-1. The primary objectives of Task F are to build confidence in the models, methods, and software used for performance assessment (PA) of deep geologic repositories, and/or to bring to the fore additional research and development needed to improve PA methodologies. The objectives have been accomplished through a staged comparison of the models and methods used by participating teams including coupled-process submodels (e.g., salt creep closure, spent fuel dissolution, radionuclide transport) and deterministic simulation(s) of the entire PA model for the defined reference scenario. The detailed task specification has been updated continuously since the initiation of the project as complexity has been added to the PA conceptual model. The final version, Revision 10, contains the final specification for creation of deterministic crystalline and salt reference cases and is given by LaForce et. al (2023).

PA is a decision management tool that provides information from quantitative evaluations of the behaviour of a complex system to decision makers. PA involves evaluating the level of confidence (taking into account identified uncertainties) in the estimated performance of the system and seeks to provide reasonable assurance that the repository system will meet applicable safety standards throughout the lifetime of a repository program. PA is used in an iterative fashion to support site selection, site characterization, and repository design, and to inform data collection and model development.

At any iteration, the first steps of the PA process are to establish the assessment context, part of which is to develop performance measures and conceptual models of the repository system from knowledge of the natural and engineered system components (Figure 1-1). One or more computational models appropriate for forward simulation of the problem and calculation of performance measures is developed. Then performance measures are calculated, uncertainty and sensitivity analysis are performed, and results are synthesized.

Forward modelling requires information characterizing the repository system and its subsystems. For Task F it is assumed that sufficient geological and engineering data are

available to develop a suitable PA model and that key FEPs and associated uncertainties have been identified for uncertainty quantification and sensitivity assessment, so this is not a data interpretation exercise. Task F focuses on performance measures indicative of the ability of the repository system to isolate radionuclides from the biosphere through containment and retardation. Performance measures include those related to the overall performance of the repository system and those related to the performance of individual components of the engineered or natural system, such as pressurization and saturation of the excavated drifts and radionuclide transport from one component of the system to another.

Conceptual models describe the key FEPs affecting repository performance measures and their interactions. Each participating team works from a common data set provided in the task specification (LaForce et al., 2023) to develop their own conceptual and computational models for evolution of the repository system. Teams chose to include or neglect some processes or feedback between processes in their conceptual models, to use a more or less mechanistic model, and to couple processes more or less tightly. Values of performance measures resulting from deterministic simulations of the reference case scenario will be compared in subsequent sections.

A schematic for the development of PA models is shown in Figure 1-1. Task F2 focused on the second and third blocks of iteratively developing conceptual and computational models of increasing levels of complexity. The initial model focused on flow modelling, then transport, and finally salt creep closure was added. Participating teams agreed on the characteristics of the natural and engineered systems, performance measures, and conceptual models describing processes affecting fluid flow, radionuclide mobilization, and transport in the repository system. Each team developed their own forward model(s) and calculated performance measures of the conceptual model in an iterative fashion. Performance measures were added to the task in parallel with additional FEPs.

Table 1-1. Participating teams in Task F2.

Abbreviation of team	Team
BASE	The Federal Office for the Safety of Nuclear Waste Management (Bundesamt für die Sicherheit der nuklearen Entsorgung)
COVRA	Central Organisation for Radioactive Waste (Centrale Organisatie Voor Radio-actief Afval)
DOE	US Department of Energy/Sandia National Laboratories
GRS	Gesellschaft für Anlagen- und Reaktorsicherheit (GRS) gGmbH
Quintessa	Quintessa Ltd
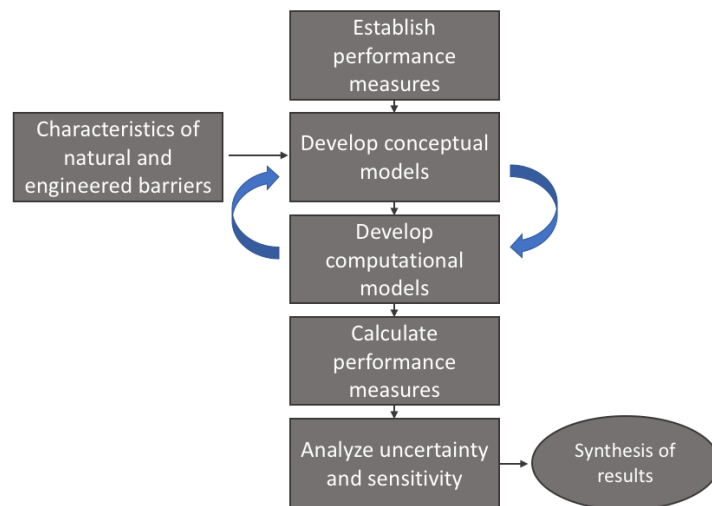
Figure 1-1. The performance assessment process (modified from OCRWM, 1990).

1.1 Research teams and sponsors

1.1.1 BASE

The Federal Office for the Safety of Nuclear Waste Management (BASE) is the German government's central authority for safely dealing with the legacy of nuclear energy. BASE performs regulatory, licensing and supervisory tasks related to disposal, storage, handling and transport of high-level radioactive waste (HLW) (https://www.base.bund.de/EN/bfe/about-base/about-base_node.html).

BASE was established in 2014 and has continued to develop since 2016. BASE provides specialist expertise to supervise nuclear safety and advises the Federal Ministry for the Environment, Nature Conservation and Nuclear Safety (BMUV) on disposal of nuclear waste. Among its various tasks, BASE regulates the site selection procedure for a final repository for HLW and coordinates public participation in the process.

To carry out its tasks in line with the scientific and technological state-of-the-art, BASE engages in academic research. The office initiates and supports research projects in the field of nuclear disposal safety and conducts its own research. This involves a variety of aspects from the natural sciences, technology as well as social sciences.

BASE is participating in Task F2 because site selection for a future HLW repository in Germany is currently underway. Besides crystalline rock and claystone, salt rock is one of three host rocks under consideration. Safety assessment (SA) is an important element of the decision-making process as stipulated by the Site Selection Act (https://www.bmuv.de/en/law/repository-site-selection-act-standag). In this context, BASE is developing a comprehensive set of numerical SA tools with a focus on reliability and transparency.

BASE is one of the funding organizations for the current phase of DECOVALEX-2023 and actively contributes to Task F of the project with the aim to:

- Exchange state-of-the-art modelling approaches and methodologies
- Further develop competence in process modelling (within Task F2: with a focus on safety-relevant processes in HLW repository hosted in a salt rock)
- Test functionalities, identify strengths and development needs of safety and performance assessment codes
- Develop a workflow for large-scale deployment of the PFLOTRAN code as a potential SA tool

1.1.2 COVRA

The Central Organization for Radioactive Waste (COVRA) is the only company in the Netherlands that is qualified to collect, process, and store all the Dutch radioactive waste. COVRA is also responsible for disposal of the radioactive waste. The current policy in the Netherlands is that radioactive waste is collected, treated, and stored for at least 100 years above ground, until approximately 2130. After this period of storage, this waste is envisioned to be disposed (Ministry of Infrastructure and the Environment, 2016).

While a definitive decision on the disposal method has not been taken yet, the Netherlands started research on geological disposal in the early 80's. Research initially focused on the Zechstein rock salt but more recently the focus has shifted to poorly indurated clay: both are considered potential host rocks for disposal in the Netherlands.

At the start of 2024, a non-site-specific, conditional, safety case is expected to be published in the Netherlands. An important part of the safety case is the safety assessment to demonstrate the safety of the repository through time and to optimize the design, identify knowledge gaps, and steer research and development. While there are differences between the Netherlands safety concept and the DECOVALEX case, this generic safety assessment can be used as a starting point for the Dutch safety assessment.

1.1.3 DOE

Sandia National Laboratories (SNL) is one of 17 US national research laboratories funded by the US Department of Energy (DOE) to develop strategic scientific and technological capabilities. Sandia is leading Task F of DECOVALEX-2023 on behalf of the Spent Fuel and Waste Science and Technology (SFWST) Campaign of the US Department of Energy Office of Nuclear Energy (DOE-NE) office of Spent Fuel and Waste Disposition (SFWD). The goal of SFWST is to develop US technological readiness and expertise on generic performance assessment modelling in three host rocks: salt, crystalline, and argillite. International leadership and learning from international best-practice have been identified an important part of developing expertise. This goal is furthered by DOE participation in DECOVALEX-2023.

The primary objectives of Task F are to build confidence in the models, methods, and software used for performance assessment (PA) of deep geologic repositories, and/or to bring to the fore additional research and development needed to improve PA

methodologies. As part of the DOE contribution to the Task F2-salt project, this team is building a simulation model and utilizing the task to develop an early career scientist at SNL (Rick Jayne) to provide training to the next generation of scientists. Both of these DECOVALEX-2023 goals align closely with the goals of SFWST.

1.1.4 GRS

Gesellschaft für Anlagen- und Reaktorsicherheit (GRS) gGmbH is a non-profit technical-scientific research and expert organization. Since 1977, GRS has been Germany's central expert organization for nuclear safety issues. GRS research focuses on reactor safety, decommissioning and dismantling, interim storage, disposal, physical protection, and radiation protection as well as environment and energy in general. GRS carried out long-term safety analyses for generic and real radioactive waste repositories in various national and international projects. Research activities are carried out to continuously expand knowledge regarding several questions related to safe disposal of radioactive waste.

GRS gGmbH is participating in Task F to examine the need for further development of their performance assessment code, enhance the features of the applied code and learn about different approaches and methods in performance assessment.

1.1.5 Quintessa

Quintessa's vision is to provide leading-edge scientific, mathematical, and strategic consultancy, scientific software development and research to public and private science-based organisations to facilitate a low carbon energy future. Quintessa was founded in 1999 with the aim of providing an enjoyable and fulfilling working environment in which talented scientists and mathematicians can use their problem-solving skills to help clients address key issues. Quintessa operates at the interface between academia and industry, facilitating the application of leading-edge knowledge in a timely and cost-effective manner. Quintessa has been heavily involved in radioactive waste management since its inception and has been active in DECOVALEX since 2007.

Quintessa's contribution to Task F is self-funded with a team comprising of Alex Bond, Steven Benbow, Josh Nicholas, and Jodie Stone. Quintessa has a general interest in building models that are comprehensive enough to include all relevant processes at an appropriate level, but simple enough that they can be readily understood and run repeatedly. The ability to strike this balance between complexity and simplicity is critical

to producing models that can be used to generate insights into the potential performance of complex coupled systems while being sufficiently transparent that the results can be presented with confidence. This task provides an excellent opportunity to understand how to construct numerically robust models that are transparent, representative, and practicable for detailed sensitivity/conceptual uncertainty analysis.

1.2 Task objectives and structure

Task F is atypical for a DECOVALEX task, as it does not include a comparison to experimental data and does not seek to develop or parameterise models that explain a specific dataset. Task F is focused on methodological development for PA, and assumes key FEPs have already been identified and suitable parameters described. The repository concept and parameters are defined collaboratively so that each team builds their individual model with the same dataset. Finally, through comparison of forward models of increasing complexity, Task F seeks to understand the uncertainty introduced by modelling choices (model fidelity, alternative models, methods of coupling).

The three distinct sub-tasks in the Task F specification for Task F2-Salt are:

Deterministic Reference Case Creation (Step S0): Creation of a series of reference case models of increasing complexity that address coupling between processes. The scenario developed for comparison is a 'what if' scenario and assumes failure of the seals in the shaft connecting the repository to the surface as well as early waste package failure, as discussed in Section 2. The initial conditions and level of fidelity of flow, transport, and salt compaction processes are developed in this step, along with performance measures for model comparison. The reference case is briefly outlined in Section 2.

Benchmarks and Process Models (Step S1): Comparison of codes and process model implementations on relatively simple problems that address a subset of the features and/or processes included in the full reference case simulation. These comparisons develop a common understanding among participants and identify differences in model behaviour that may propagate through the more complex analyses. There is one one-dimensional (1D) and one two-dimensional (2D) chemical solute transport problem available for comparison, as discussed in Section 3.

Deterministic Reference Case Model Comparison (Step S2): Comparison of the simulation models and results for each team's implementation of the reference case simulation. Repository performance predicted by each team's model is compared in this step to identify differences in model behaviour that appear to arise from methods of

coupling, omission of FEPs, or models of differing fidelity. A comparison of modelling approaches is given in Section 4 and the comparison of modelling results is given in Section 5.

Two additional model comparisons are presented in Section 5.6 that are not in the task specification. These comparisons are a case with low initial saturation and slower salt compaction mechanism, and cases with earlier and later shaft seal failure. These variants were proposed during compilation of the team results to assess the impact of these two modelling assumptions. Because the variant cases were added very late to the task, not all teams were able to participate in the comparisons.

2 Reference case development

The salt reference scenario has been developed collaboratively between the teams since the initiation of Task F2-Salt and development continued and complexity was added until the end of the second year of DECOVALEX-2023. The base case focuses on a disturbed scenario for a salt repository. Multiple performance assessments (e.g., RESUS, KOMTESS, ISIBEL and VSG – Bollingfehr et al., 2008; Beuth et al., 2012; Bollingfehr et al., 2017; Bollingfehr et al., 2018; Bertrams et al., 2020) have calculated no significant radiological consequences via liquid-phase transport within 1,000,000 years for undisturbed disposal in salt formations because of salt's very low permeability and moisture content. The task specification conceptual model is a simplified scenario that has pessimistic assumptions about the engineered barriers: First, the shaft seals fail 1,000 years after repository closure, allowing an influx of brine from overlying aquifers down the shafts and into the repository. Second, the vitrified glass begins dissolving at the start of the simulation and the SNF waste packages simultaneously fail at 500 years.

Staged development of models building up to a full PA model is part of the work of Task F2 and the final task specification is itself a project result. This stepwise process is followed to ensure the consistency between each team's modelling efforts as complexities are added. The staged development was:

1. Model flow in the repository for variably saturated initial conditions.
2. Add tracers, then radionuclide waste form release, mobilization and transport.
3. Include drift convergence by salt creep and backfill consolidation.
4. Consider alternative scenarios.

The original plan for Task F2 was to add heat flow and model uncertainty, but this was not achieved in the present DECOVALEX stage. The final description of the base case model is discussed in detail in the task specification (LaForce et al., 2023), and briefly summarized here.

2.1 Geological setting and repository structure

The geological model is a generic geological cross section of a salt dome developed for the RESUS project (Bertrams et al. 2020) that has been simplified to 6 homogeneous geologic units as shown in Figure 2-1. It is assumed that the salt dome geometry extends 9 km perpendicular to the plane of the cross section. The repository is mined at a depth of 850 m below the ground surface, as shown in Figure 2-1.

Figure 2-2 shows that the repository is also symmetrical, allowing teams to model the half-symmetry domain, if desired. Within the repository there are three sets of 25 emplacement drifts. For the spent nuclear fuel (SNF) waste, the waste packages are placed end-to-end in 50 emplacement drifts 90 m long with 10 waste packages per drift for a total of 500 POLLUX-10 waste packages. The vitrified waste emplacement area consists of 25 emplacement drifts and each 45-m-long drift contains 10 vertical boreholes with two waste packages per borehole, giving a total of 500 waste packages containing vitrified waste.

The waste areas are isolated from the infrastructure area and shafts connecting the repository to the surface by two seals that consist of 300 m of run-of-mine salt between two concrete abutments, as shown in Figure 2-2. The infrastructure area is filled with gravel to accommodate fluid influx from the surface or gas generated by the waste (though this FEP is not currently considered). All other waste and non-waste areas are filled with run-of-mine salt backfill. The shaft is a layered sequence of gravel, sealing elements, and concrete, but may be modelled as homogenous in the task specification.
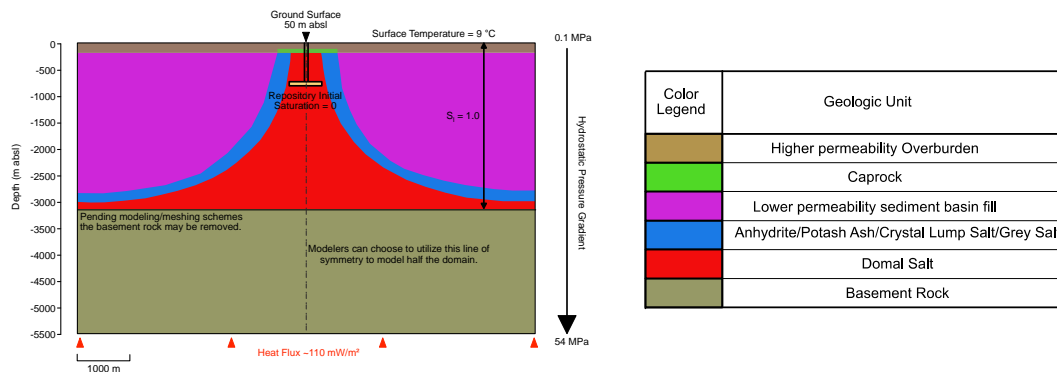
Figure 2-1. Geological cross-section with model units for the generic salt reference case. The model units are simplified from Bertrams et al. (2020). The repository location and initial model conditions are shown.
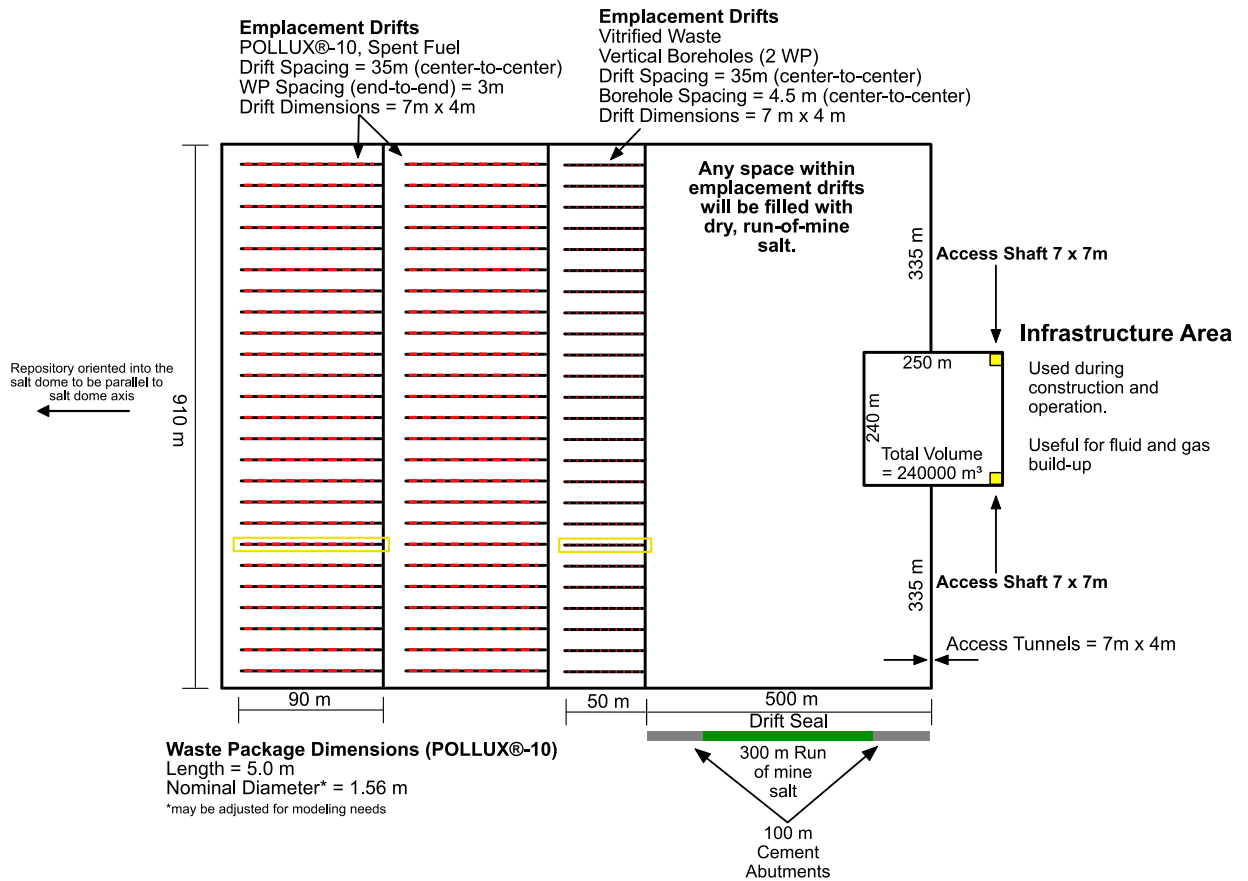
Figure 2-2. Schematic of the waste repository in a generic salt dome. The drifts outlined in yellow will be for used for comparisons between each teams' results.

2.2 Flow and transport modelling

Simulations are run for 100,000 years. The initial condition of the repository is 20% saturated with brine and fluid flow is modelled as variably saturated single-phase flow (frequently called Richards' model flow). This is likely to be an unrealistically high initial saturation, however it was necessary because several teams could not start a Richards' flow simulation at or near liquid residual saturation without unrealistic liquid pressure in the numerical model, as the two are not independent variables. The impact of this assumption will be investigated as a variant in Section 5.6.

Transport modelling includes a simplified ^{238}U decay chain (^{238}U$\rightarrow$ ^{234}U$\rightarrow^{230}$Th$\rightarrow^{226}$Ra) and two long-lived radionuclide fission products: ^{129}I, which is only in the SNF canisters and ^{99}Tc, which is only in the vitrified waste. The initial inventories of the SNF canisters and vitrified waste both contain the ^{238}U decay chain radionuclides. Transport of three ideal (non-reacting, non-adsorbing, and non-decaying) tracers are also modelled. Tracer 1 is only in the SNF and is representative of the instant release fraction of ^{129}I from the

SNF canisters when they breach at 500 years. Tracer 2 is in the SNF canisters and represents the fraction of ^{129}I slowly released from the SNF as it degrades. Tracer 3 is only in the vitrified waste and represents the ^{99}Tc that is slowly released as the glass dissolves, starting at the beginning of the simulation. The tracer simulation results are the focus of this report because they satisfy the need to compare the models as simply as possible and comparison of radioactive contaminants resulted in similar observations. Moreover, the tracers represent a simple scenario for transport through the repository towards the biosphere. The tracers also provide information about the origin of contaminants in the repository, as Tracers 1 and 2 are only in the SNF and Tracer 3 is only in the vitrified waste.

2.3 Salt closure model

The teams chose to model the drift convergence based on Gorleben data (Bertrams et al., 2020) as implemented in the GRS LOPOS software. Salt creep begins at the start of the simulation. The drift convergence rate and resulting porosity as a function of time are calculated in LOPOS using the initial condition and parameters in the task specification. Creep of the salt only takes a few decades to close to below 2%, which is highly optimistic. Closure is rapid because wet salt creep is faster than dry salt creep, and the initial water saturation is 20%. This data was provided by GRS to the other teams as Excel tables in the task specification. Teams could use the tabular data or calculate the porosity from the equations provided in the task specification.

It is assumed that the run-of-mine salt backfill returns to intact salt permeability once the drifts have fully closed. A Kozeny-Carmen type equation for permeability as a function of porosity is provided in the task specification.

2.4 Development of the reference case as a task result

Unlike most DECOVALEX tasks, the initial task specification for Task F (Stein, 2020) did not contain the salt PA model and it was developed throughout the first two years of the project. Ten revisions of the specification were created as FEPs were added and removed to create a tractable PA case that is relevant and accessible to all five participating teams. The PA model itself represents a valuable output for the radioactive waste community as it is a publicly available domal salt PA conceptual model that contains realistic data for many of the key FEPs and is amenable to a wide variety of modelling approaches.

Two examples of collaborative revisions of the task specification are the initial liquid saturation and flow model specification. Early versions of the task called for either Richards' (water phase plus infinitely mobile gas) or two-phase flow and residual initial liquid saturation in the repository. However, it quickly became apparent that the initial condition of residual liquid saturation was numerically too challenging for several teams' models. Moreover, it is impossible to enforce both the atmospheric pressure and low liquid saturation initial conditions using Richards' model without liquid pressure becoming large and negative, which can cause numerical instability due to approximations in the solver. Relative permeability curves can also create numerical instability as they go to zero as mobile liquid fraction goes to zero. The decision was made to enforce a realistic liquid-pressure constraint and accept resultant higher initial water saturation (20% in the repository, 35% in the shaft) and revisit the original initial condition as a variant case later in the project.

At the same time, some teams were using full two-phase flow models and others were using Richards' model flow. It became apparent that the early flow comparisons were 'apples to oranges' because of the differing assumptions behind the two flow models. As it was not possible for all teams to implement two-phase flow into their models, consensus was reached that the task specification should only explicitly include Richards' model for single-phase variably-saturated flow, which all except one team was able to implement into their software. Differences introduced by two-phase flow physics could then be investigated as part of the variant exercises (see Appendix E).

The iterative task development process also serves to demonstrate the level of necessary complexity to capture important FEPs in the model. One example of a feature that was added to the task specification, and then later removed, is a detailed representation of the shaft. The original task specification had homogeneous properties in the shaft. However, a detailed shaft model was available and introduced as an option, alongside a new homogenised shaft with average heterogeneous shaft properties. GRS investigated the two variants (see Appendix D) early in the task, and DOE did a series of one-dimensional simulations comparing the two variants as discussed in the interim report (LaForce et al., 2022). Both show that the flow into the repository is sufficiently similar that the additional complexity is not necessary. Based partly on these results, the homogeneous shaft model was chosen for the base case, with the heterogeneous shaft as an optional variant. All the teams used the homogenised shaft model for their reference cases but GRS and Quintessa also investigated the heterogeneous shaft case as variants.

3 Benchmark modelling

Two transport benchmark models are conducted to compare the simulation software that teams were using. A very brief survey is presented here. Further discussion is in the interim report (LaForce et al., 2022).

3.1 One-dimensional transport benchmark

The one-dimensional (1D) transport benchmark is from Kolditz et al. (2015) Section 2.5.2. The domain is a 10 m × 1 m × 1 m beam extending in the positive x direction. A steady-state flow field is applied. At the inflow face, a pulse of three tracers (conservative, decaying and adsorbing) are introduced to the system. Concentrations are compared to the analytical solution after the end of the tracer pulse.

Figure 3-1 shows a comparison of the analytical solution and simulated solution by the DOE, GRS, COVRA, and Quintessa teams for the ideal tracer. Overall, the 1D simulations capture the analytical solution extremely well. The COVRA and Quintessa simulation with numerical dispersion correction are indistinguishable from the analytical solution while the DOE simulation and Quintessa simulation without dispersion correction slightly under-estimate the tracer peak. There is some difference in the solution upstream of the tracer peak for the GRS solution because it was necessary to approximate the boundary condition in the GRS software, LOPOS. All teams capture the tail of the analytical solution accurately.
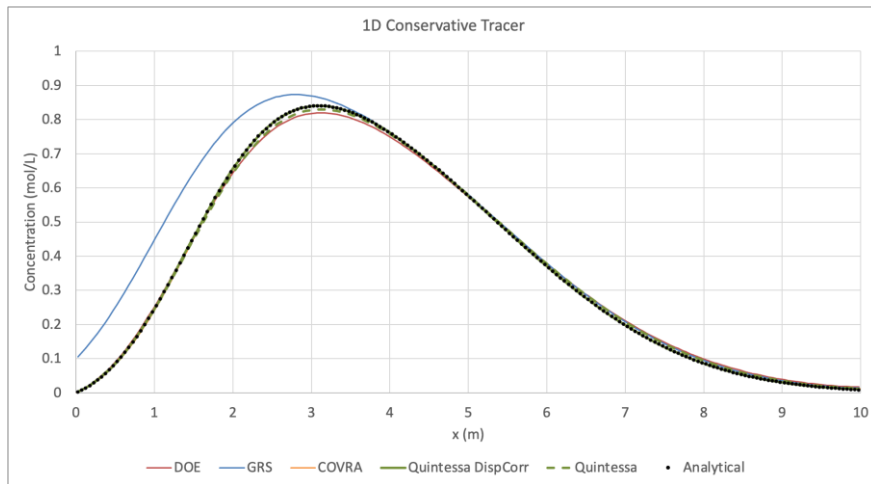
Figure 3-1. Comparison of analytical and simulated conservative tracer solutions by all the teams for 1D tracer benchmark. 'Quintessa DispCorr' is solution with numerical dispersion correction and 'Quintessa' is solution without dispersion correction.

3.2 Two-dimensional transport benchmark

The analytical model for the 2D transport benchmark is given in Example 3-9 in Section 3.3.2.2 of Batu (2006). The model has steady-state groundwater flow in the x-direction and tracers introduced by a line source perpendicular to the direction of flow. This model is intended to be representative of radionuclides leaking from a failed shaft into the overburden. Solutions are calculated for a conservative tracer and adsorbing tracer for a constant rate source, and a conservative tracer from a decaying rate source. Comparisons were conducted at lines across the domain at snapshots in time and as a function of time at discrete points in the domain. One example comparison is shown below, and others are in the interim report (LaForce et al., 2022).

Figure 3-2 shows the ideal tracer from a constant source on an x parallel section at z = 1005 m and time 10 years. Quintessa and DOE were able to model the ideal tracer simulation accurately with small differences due to the impact of numerical diffusion in the simulated solution. The GRS profile is for a 1D approximation to the 2D simulation, as their GeoTREND software is one-dimensional. This results in an overestimate of the tracer profiles, as shown in Figure 3-2. Quintessa ran the same 1D approximation for the conservative tracer using both QPAC and COMSOL and got similar results, confirming it is the 1D approximation, not the software which is causing the difference in the tracer profiles.

Figure 3-2. Simulation and analytical model for ideal tracer comparison of 2D tracer benchmark on the slice through the simu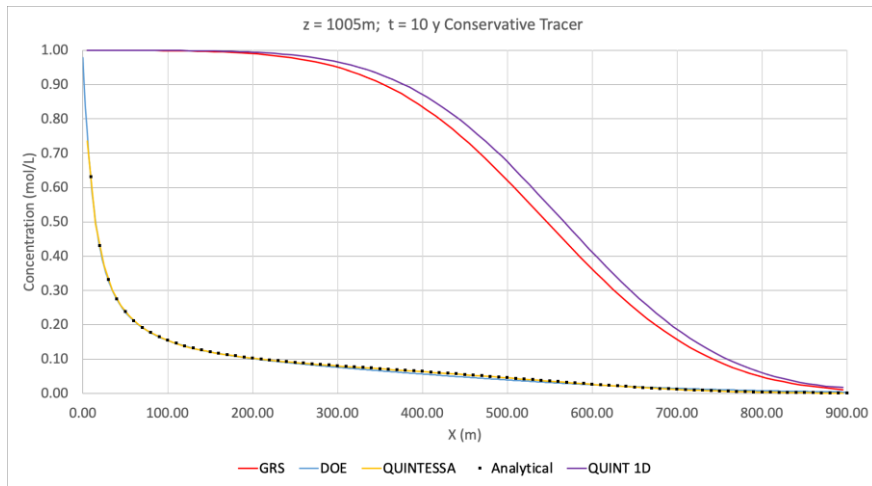lation domain at z = 1005 m and time 10 years. QUINTESSA is a 2D simulation of the problem, while QUINT 1D is for comparison with GRS LOPOS 1D results.

4   Modelling approaches

The software used by each team participating in the task is shown in Table 4-1. A brief summary of each teams' computational approach is also shown.

Table 4-1. Software utilized by each team and their modelling approaches.

Team	Modeling Tools	Modeling Approach
BASE	PFLOTRAN	3D model with detailed representation of the repository Geosphere is omitted
COVRA	COMSOL	Detailed representation of repository 3 stage 1D and 2D models Neglect impermeable host rock
DOE	PFLOTRAN	Include all geological volumes/materials Simplified representation of repository, shaft
GRS	RepoTREND (LOPOS)	"Looped structures in repositories" Segmented model of 1D components
Quintessa	COMSOL and GoldSim (benchmarks only) and QPAC	Sequence of tank, 1D and 2D models linked together to create a 3D structure.

4.1 BASE

The BASE model and modelling results are discussed in detail in Appendix A. Simulations were performed using the PFLOTRAN code version 4.0 on the model shown in Figure 4-1. The flow model simulates single phase, variably water saturated isothermal conditions using the Richards' model. Model parameterization (e.g. characteristic curves) is carried out as per the Task Specification. Solute transport is assumed to occur in the liquid phase under isothermal conditions due to advection and diffusion. Solute transport is coupled to chemical reactions using a global implicit approach.

Source terms are implemented individually for SNF and vitrified waste drifts as per the Task Specification. Radionuclide decay occurs across all phases, i.e. in the solid waste as well as in the dissolved and precipitated forms. To represent the source term,

radionuclide partitioning and decay in PFLOTRAN, the "Waste Form" and "UFD Decay" process models are used.

As discussed in more detail in Appendix A, salt creep (convergence) is represented simplistically by reducing material porosity in a pre-defined manner based on results obtained externally from the code   as provided by the team from GRS. The PFLOTRAN porosity reduction model does not aim to reproduce the results of LOPOS in any specific detail – rather, it reflects general trends and value ranges with a particular focus on matching the endpoint porosity in the task specification. Porosity changes feed directly into advective flow and transport (via intrinsic permeability) and diffusive transport (via the effective diffusion coefficient). Importantly, this approach ensures mass conservation during porosity reduction. Therefore, for example, water pressurization due to salt convergence is represented.

Simplifications from the task specification are:

- Advantage is taken of a vertical plane of symmetry in the disposal system (Figure 4-1), which allows the geometry to be reduced to a half.
- For computational efficiency, the geometry ignores the presence of the host rock (seen Figure 4-1). This is done in order to decrease the computational burden on model solution and is based on the expectation that the impact of the host rock on the system's hydraulic evolution is small or negligible.
- Approximated porosity evolution as discussed in more detail in Appendix A.
- Individual deposition holes within the deposition drifts are not represented and the initial radionuclide inventories are averaged across the entire volume of the deposition drifts.
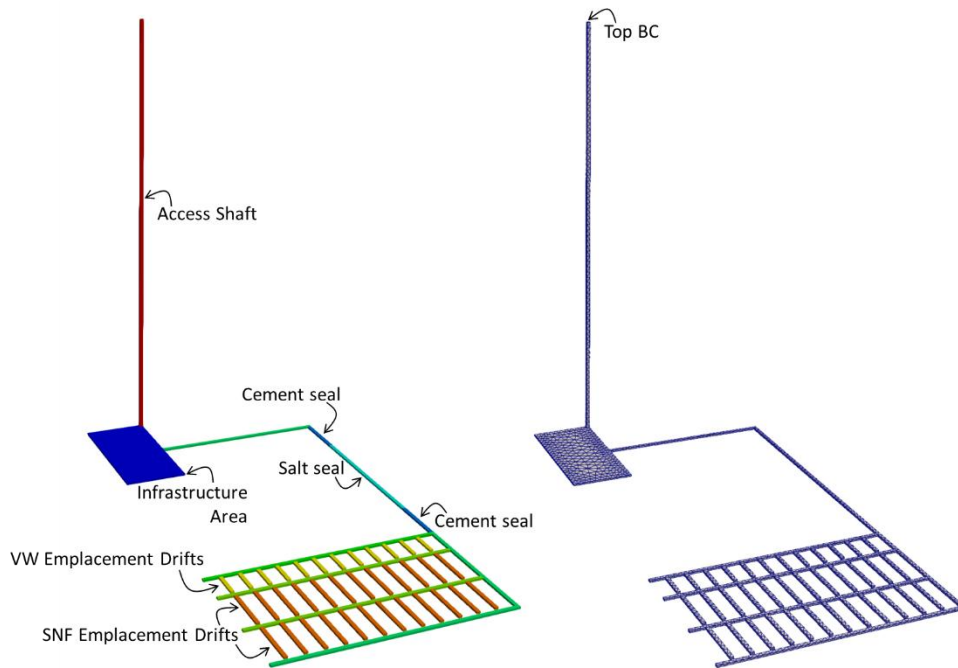
Figure 4-1. The BASE computational model geometry (left) and the corresponding finite volume grid (right) indicating the position of the top boundary condition (Top BC). VW – vitrified waste, SNF – spent nuclear fuel.

4.2 COVRA

The COVRA model and modelling results are discussed in detail in Appendix B. The simulator used by COVRA is COMSOL Multiphysics ®. The simulation model is divided into two sub-models that run separately, one for the shaft and one for the repository as shown in Figure 4-2. The shaft model is a vertical 1D model with homogeneous properties, a saturated top boundary condition and closed bottom boundary condition. Water flows down the shaft under the force of gravity until the shaft is almost fully liquid saturated, but not entirely (~99% saturation). Keeping the model just below fully saturated conditions will significantly reduce the computational time needed. The pressure head at the bottom of the shaft is subsequently used as input boundary conditions for the 2D repository model, which is run as a separate model.

Porosity evolution depends on the head pressure. Head pressure would become zero when fully saturated, but for computational efficiency the model is kept to slightly undersaturated, which is anticipated to have little influence on the simulation results. The dependence of the porosity change on the head pressure results in slower evolution of the porosity than in the task specification, as discussed in more detail in Appendix B.

Simplifications from the task specification are:

- Half symmetry domain to improve computational efficiency.
- Geosphere surrounding the repository is not represented in the model.
- Simplified porosity reduction curve.
- 1D shaft model runs separately from the 2D repository model. Gravity is neglected in the repository model.
- Individual waste packages are not explicitly represented.
- Effective diffusivity is calculated by multiplying the initial porosity (not changing), the porosity (changing in time) and the molecular diffusion coefficient in free water.
- Effective permeability equals the saturation.
- Repository does not reach full saturation, but only 99%.
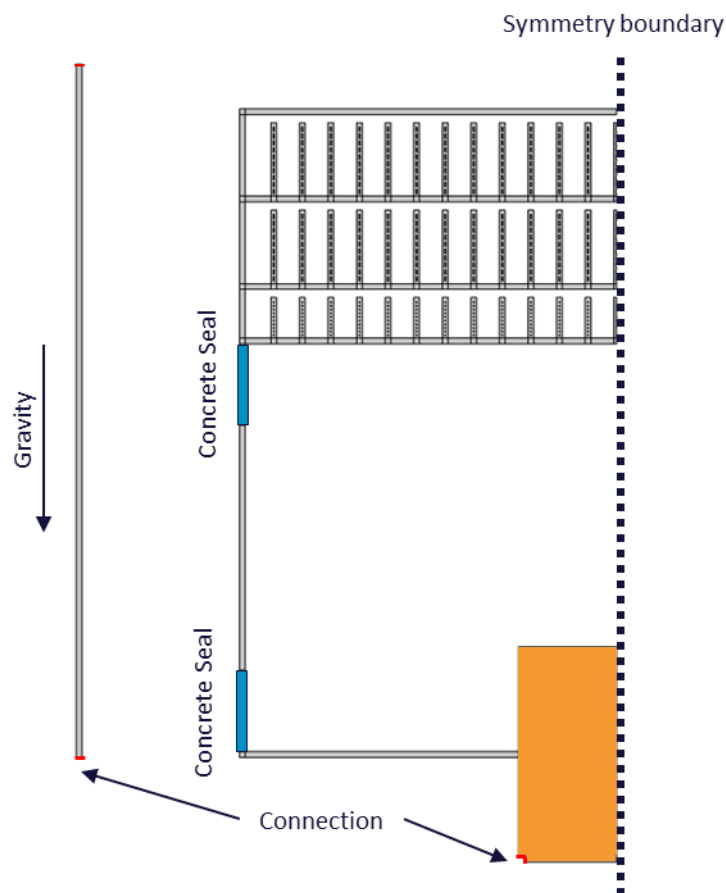- Dissolution of vitrified HLW is directly into the disposal gallery; the salt seal is bypassed.

Figure 4-2. Conceptual model developed by COVRA. The shaft model is shown on the left, and the repository model is on the right.

4.3 DOE

The DOE model and modelling results are discussed in detail in Appendix C. The simulator used for this study is PFLOTRAN (Hammond et al., 2014). Richards' mode is chosen to simulate mass transport within the repository which applies to single phase, variably saturated, isothermal systems. The final model (Figure 4-3) utilizes ½ symmetry to reduce computational demand associated with the given repository scenario. The model domain explicitly meshes the SNF and vitrified waste drifts, drift seal, infrastructure area, the homogenous shaft, salt surrounding the repository, and an overburden layer where an aquifer is located.

Simplifications are made to implement the geomechanical effects of drift convergence. Porosity does not change with time to have conservation of mass with the current Richards' mode and material property change implementations in PFLOTRAN. Instead, a stepped permeability change with time is used so that when the shaft fails the drift convergence is considered complete, and all crushed salt within the repository assumes the permeability of intact salt. Diffusivity is coupled to the original crushed salt porosity, which impacts effective diffusivity in the model.

Simplifications from the task specification are:

- Half-symmetry domain to reduce computational demand associated with the given repository scenario.
- The domal salt and overburden are accounted for explicitly in the model but all other geological units are omitted.
- Drifts are meshed, but individual waste packages are not. Each disposal drift is treated as source containing all the radionuclides from each waste package.
- Neglecting change in porosity during salt compaction and changing permeability in a stepwise fashion, as discussed above and in more detail in Appendix C.
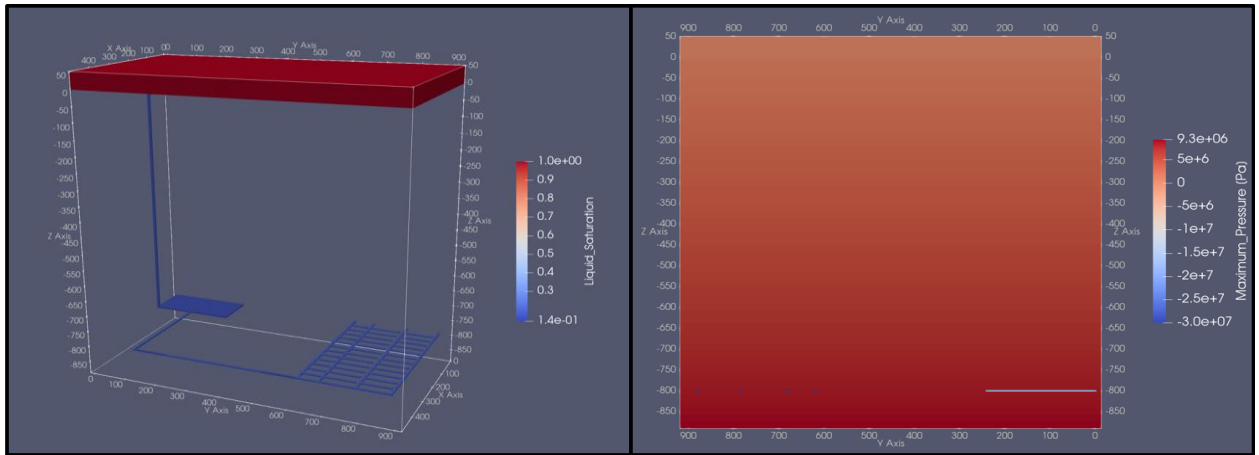
Figure 4-3. The DOE simulation model domain. Left: The repository, shaft, and overlying aquifer showing initial fluid saturation. Right: A Y-Z plane view of the model domain illustrates fluid pressure is hydrostatic within the intact salt and negative within the repository to create atmospheric gas phase pressure.

4.4 GRS

The GRS model and modelling results are discussed in detail in Appendix D. The features of their model are briefly summarized here. GRS used a sequentially coupled model framework called RepoTREND. RepoTREND is a modularly structured code, that contains modules for simulating processes in the near-field, the far-field and the biosphere (Reiche et al., 2016). The integrated near-field code LOPOS is a compartment model (Hirsekorn et al., 1999).

In LOPOS, a compartment structure can be defined to represent a network of chambers, drifts, shafts, and boreholes. The layout of the repository as represented in the LOPOS near-field model is shown in Figure 4-4. The salt reference case was set up according to the requirements of the task specification (LaForce, et al., 2023). Both creep closure model options in the task specification were taken from the LOPOS equations and calculations (Hirsekorn et al., 1999; Noseck et al., 2005).

Simplifications from the task specification are:

- The natural barrier system is not modelled, because there is no significant radionuclide release from the shaft.
- Only half of the specified repository geometry is defined as LOPOS compartments, due to the line of symmetry through the repository and salt dome for computational efficiency.

- Each of the three sets of 25 emplacement drifts is realized as one compartment and the waste packages are not explicitly modelled as defined.

- LOPOS uses single-phase Darcy flow and radionuclide transport (Hirsekorn et al., 1999), instead of utilizing a single-phase variably saturated (Richards Equation type) model; therefore relative permeability and capillary pressure functions cannot be taken into account.

- Tortuosity and compressibility of the engineered barrier system are not considered.

- Since the LOPOS approach is one-dimensional transverse dispersion is neglected (Hirsekorn et al., 1999).

- Since LOPOS simulates single-phase radionuclide transport, the transport equation is only solved for compartments that have reached full liquid saturation.

- In 100,000 years, all compartments except Seal-1 reach full saturation. Since diffusion can also occur in partly saturated compartments, liquid saturation of the Seal-1 compartment is manually set to 1 after 50 years for the simulation of radionuclide transport. This time was chosen because at this time radionuclides reach the neighbouring salt compartment.
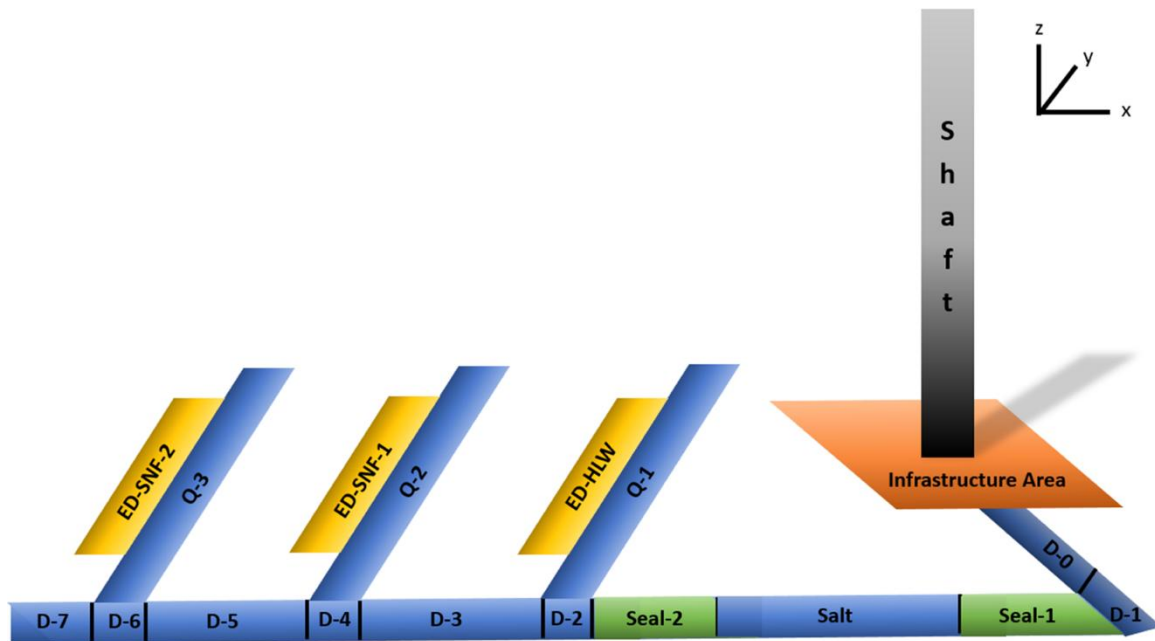
Figure 4-4. Reference case LOPOS layout for the GRS performance assessment case model. Note that ED stands for "Engineered Drift" and refers to the disposal drifts and associated engineering.

4.5 Quintessa

The Quintessa model and modelling results are discussed in detail in Appendix E. For the reference case calculations, the primary simulation tool was the Quintessa multi-physics code QPAC. For the purposes of the base case calculations, the Richards' equation flow and tracer transport modules were used, though multiphase flow variants are available for variant calculations. As discussed in detail in Appendix E, bespoke physical relationships were implemented to represent release of contaminants from the waste. The creep closure equations of the access drifts as given in the task specification were adopted directly including coupling to local water pressure.

QPAC is primarily a finite volume code, with the additional flexibility of being able to specify variables on the interfaces between finite volumes ('compartments'), as well as on the volume centroid. All calculations are monolithic (all equations solved simultaneously) using a fully implicit time stepping approach, which allows full coupling of all simulated processes including creep closure.

A relatively coarse finite volume mesh was used to represent the system. Only the engineered components of the system (access shaft, tunnels, and drifts) were

represented explicitly. Simple calculations showed that for the purposes of fate and transport (primarily diffusion) through the salt dome, the only pathway that could credibly cause any impact to surface would be via the engineered components. The schematic of the model implementation and the gridded model are shown in Figure 4-5 and Figure 4-6.

With the exception of the infrastructure area and waste panels, each 'subgrid' in the model is represented by a 1D section. In particular, tunnels are represented as 1D sections with no vertical discretisation.

Simplifications from the task specification are:

- Due to the symmetry of the system, only half the repository was modelled.
- The host rock was neglected from the calculations, being represented only via a boundary condition that can be optionally included to impose a brine source from the geosphere, but was only included as a variant case considered in Appendix E as geosphere inflow was not included in the final task specification.
- Transverse dispersion is not considered in the 1D segments of the model as it was judged that it would only serve to artificially disperse into the host-rock (if it was included) and would have no impact if the host-rock isn't present.
- One simplification of the model was in the waste areas. Rather than model the tunnels explicitly, they were homogenised into larger panels which can contain a non-integer number of disposal tunnels.
- Waste disposal packages were also not modelled explicitly because the release mechanisms specified do not require an individual treatment due to a lack of spatial variability and no local processes.
- The aquifer was not included in this version of the model because no significant radionuclide concentrations were observed leaving the shaft top.
- To improve computation time, the van-Genuchten retention curves were linearised between 90% water saturation and 100% water saturation. Testing showed that this simplification reduced run-time but made no significant difference to the results.
- Creep convergence starts after 0.2 y. The capability to allow for delayed convergence was a defensive measure to initially stabilise the model. The (very small) impact on the porosity evolution of having convergence starting immediately is discussed in Appendix E.
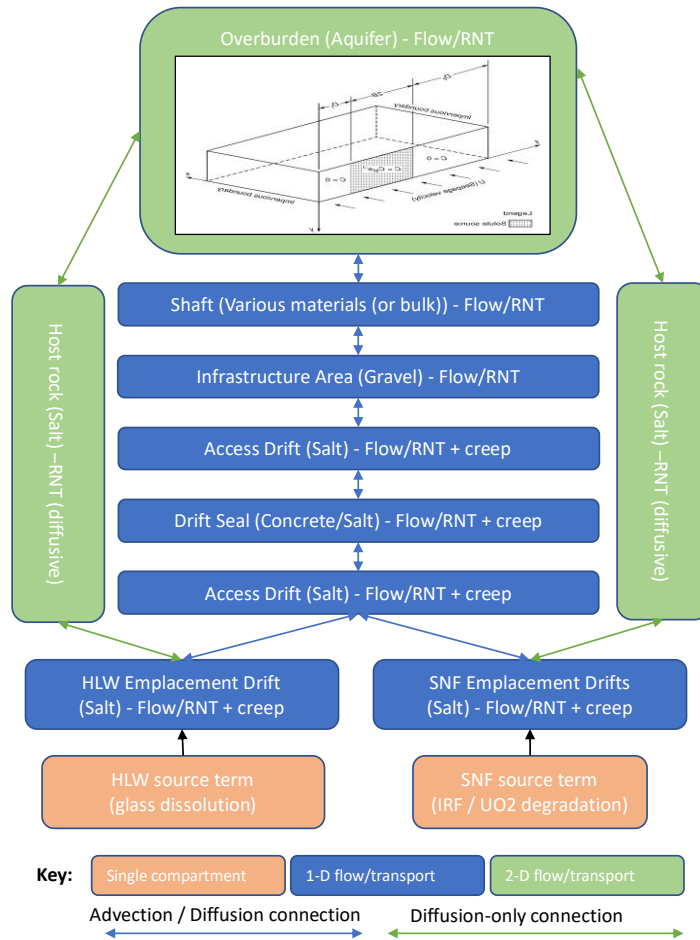
Figure 4-5. Conceptualisation of the reference salt repository model (note that RNT stands for radionuclide transport)
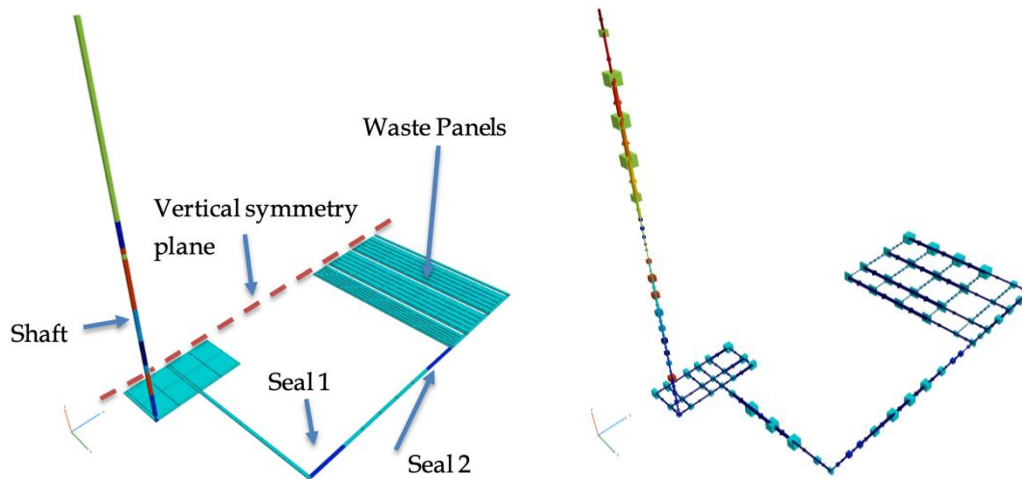
Figure 4-6. The Quintessa model grid in QPAC (coloured by intrinsic permeability on a log scale) showing the volumetric representation (left) and the 1D legs making up the model (right). The heterogenous shaft infill is shown here.

4.6 Comparison of modelling approaches

As can be seen in the preceding sections and summarized in Table 4-1, Table 4-2, and Table 4-3 teams have different conceptual models, software capabilities, and make different simplifying assumptions from the model in the task specification. This results in different features and events in the models and higher or lower fidelity representations of some aspects of the models. Two simplifying assumptions that were made by all teams was to omit discretization of the individual waste packages and utilize the half-symmetry of the domain to reduce computational overhead.

Each teams' model invokes simplifications in some places to capture more complexity in others. In particular, the complex, fully-coupled, salt closure model in LOPOS was challenging to reproduce in some of the other software. Teams' porosity modelling assumptions are summarized in Table 4-4. Differences in the rate of salt compaction, and how compaction is coupled to other processes is believed to be influential in flow modelling of the reference case, as discussed in Section 5.

Diffusion is believed to be an important mechanism for transport of radionuclides in all the models. The diffusivity assumptions of each team are shown in Table 4-5. All teams used the effective diffusion coefficients in the task specification and linked them to porosity, but the difference in porosity evolution between the models (Table 4-4) means that the models potentially have different effective diffusion coefficients during the simulation. In particular, the BASE, GRS, and Quintessa models have the effective diffusivity as a function only of the current porosity, while COVRA assumes that the

effective diffusivity depends on the initial porosity times the changing porosity. Numerical dispersion is also a concern in all the models. In the finite volume models of BASE, DOE, and Quintessa, advective numerical dispersion is about ½ the local grid spacing, but is different for each model as they have different levels of grid resolution. Calculating the numerical dispersion in the COVRA and GRS models is not as clear cut. Diffusive transport in the simulations will be determined by a combination of the numerical dispersion and diffusion resulting from the effective diffusion in the model. Depending on the numerical scheme and model resolution, numerical dispersion may be larger than physical diffusion and dominate diffusive transport. Thus, differences in effective diffusivity and numerical dispersion are both potential sources of discrepancies between the teams' models.

Table 4-2. Features in teams' model.

Feature	BASE	COVRA	DOE	GRS	Quintessa
Software	PFLOTRAN	COMSOL	PFLOTRAN	LOPOS	QPAC
Dimensionality	3D	1D/2D	3D	1D	3D
Includes host rock?	No	No	Yes	No	No
Full repository?	No, symmetric	No, symmetric	No, symmetric	No, symmetric	No, symmetric
Numerical Method	Finite Volume	Finite Element	Finite Volume	Finite Difference	Finite Volume
Includes overburden?	No	No	Yes	No	No
Continuous or compartments model?	Continuous	Continuous	Continuous	Compartment	Continuous

Table 4-3. Processes in teams' model.

Process	BASE	COVRA	DOE	GRS	Quintessa
Repository resaturation	Richards' equation	Richards' equation followed by diffusive transport	Richards' equation	Darcy equation	Richards' equation (multi-phase flow as variant)
Solubility limits?	Yes	No	No	Yes	Yes
Inflow from the geosphere	No	No	Intact salt included	No	Geosphere inflow can be modelled (only used as variant)
Maximum Fluid Pressure	Hydrostatic	Hydrostatic	Hydrostatic	Lithostatic	Hydrostatic (but configurable)

Table 4-4. Porosity evolution in teams' models.

Question	BASE	COVRA	DOE	GRS	Quintessa
Using the provided compaction?	No, prescribed porosity reduction	No, exponential decay of porosity	No, simple stepped approach to reduce permeability	Yes	Yes
If so, what variables is it coupled to?	Pressure and saturation	Pressure only	N/A	Pressure and saturation	Pressure and saturation
One way or two-way coupling?	One-way (porosity impacts saturation and pressure)	Two-way	N/A	Two-way	Two-way
Is convergence parameterization different between repository areas?	Yes, Two models: one for the seal, another for all other areas	No, but convergence rate varies locally	N/A	Yes	Yes
How did permeability vary with porosity?	Yes, according to task specification	Yes, according to task specification	No, permeability was stepped down	Yes, according the task specification	Yes, according to task specification

Table 4-5. Diffusion modelling in teams' models.

Question	BASE	COVRA	DOE	GRS	Quintessa
Does the model use the effective diffusion coefficients in task specification?	Yes	Yes	Yes	Yes	Yes
Are the diffusion coefficients coupled to porosity?	Yes	Yes	Yes, but porosity is fixed in the simulation	Yes	Yes
Does the model have numerical dispersion associated with advection?	Yes	Yes	Yes	Yes, from coupling between regions, but not within regions	Yes

5 Results

In the task specification (LaForce et al., 2023) a total of 206 comparison quantities are proposed. The teams compared 3-4 quantities at each monthly meeting for six months to narrow down the initial list to quantities that were informative and eliminate quantities that provided redundant information. The 21 quantities of interest (QOI) shown in Table 5-1 and discussed in this section are the result of that iterative process. Comparison of local porosity is not in the task specification but was determined to be essential for understanding and comparing simulation results and added as a QOI for the final report.

Comparison QOI between models are focused on two parts of the repository; quantities in the disposal drifts and quantities related to the safety functions of the repository. The first group of comparisons serve to demonstrate similarities and differences in how the models simulate initial radionuclide release into the repository, while the second explores how the models simulate radionuclide transport towards the biosphere. The first location where the model outputs are compared is the example SNF drift and the second is the example vitrified waste drift. Both are highlighted yellow in Figure 2-2. These are the radionuclide release locations and as the SNF and vitrified waste have fundamentally different release mechanisms it is necessary to consider both. The third point of comparison is the salt in the repository seals, shown in green on the bottom right of Figure 2-2. The final point of comparison is one of the lower shafts, where the location of the shafts are shown in yellow on the right of Figure 2-2.

QOI in the disposal drifts and seal salt are further broken down into three subsets; local evolution of porosity, quantities related to flow, and quantities related to radionuclide transport. This additional breakdown is necessary because differences in porosity evolution drives differences in the flow quantities, which in turn may drive radionuclide transport. The porosity and fluid flow QOI that were determined to be the most useful are average porosity, average liquid saturation, and liquid flow rate(s), as shown in Table 5-1.

The original 180 transport comparison quantities in the task specification included the radionuclides in the ^{238}U decay chain ($^{238}U \rightarrow ^{234}U \rightarrow ^{230}Th \rightarrow ^{226}Ra$), two long-lived radionuclide fission products: ^{129}I, present only in the SNF drift, and ^{99}Tc, present only in the vitrified waste drift, and three tracers. Tracer 1 is an ideal (non-decaying and non-adsorbing) tracer that is present only in the SNF drift and represents the 10% of ^{129}I inventory instantly released from the SNF canisters when they breach at 500 years. Tracer 2 is an ideal tracer that is present only in the SNF drift and represents the 90% of

^{129}I inventory gradually released from the SNF canisters over one million years after they breach. Tracer 3 is an ideal tracer that is present only in the vitrified waste drift and represents the ^{99}Tc inventory gradually released from the vitrified waste over one million years.

The radionuclides and tracers were found to provide largely the same information on transport in the repository. Tracers 1 and 3 were chosen as the transport QOI because they provide a simple model for radionuclide transport to the shaft, and as they neither adsorb nor decay they will tend to overestimate transport. Furthermore, as Tracer 1 is initially present only in the SNF drift and Tracer 3 is initially present only in the vitrified waste drift, they provide information on the origin of radionuclides in the seal that cannot be obtained from radionuclides in the ^{238}U decay chain that originate in both waste types in teams' current models. Table 5-1 shows that the transport QOI selected are the mass and transport of Tracer 1 and Tracer 3 into or out of the repository regions.

The final QOI is fluid flow through the lower shaft. This QOI is used to demonstrate the direction of the driving forces between the surface and the repository. No transport quantities are investigated here, as no team's model shows the presence of significant radionuclides or tracers in the shaft at any time in the simulation.

Table 5-1: QOI location and model output used for comparison of team simulation results.

Location (number of QOI)	QOI
SNF drift (5)	- Porosity - Liquid saturation, liquid flow out of drift - Tracer 1 mass, Tracer 1 transport out of drift
Vitrified waste drift (5)	- Porosity - Liquid saturation, liquid flow out of drift - Tracer 3 mass, Tracer 3 transport out of drift
Salt in repository seal (10)	- Porosity - Liquid saturation, liquid flow between cement abutment and repository seal salt on the repository side, liquid flow between repository seal salt and cement abutment on the infrastructure area/shaft side - Tracer 1 mass, Tracer 1 transport between cement abutment and repository seal salt on the repository side, Tracer 1 transport between repository seal salt and cement abutment on the infrastructure area/shaft side - Tracer 3 mass, Tracer 3 transport between cement abutment and repository seal salt on the repository side, Tracer 3 transport between repository seal salt and cement abutment on the infrastructure area/shaft side
Lower shaft (1)	Liquid flow between access tunnel and lower shaft

5.1 SNF drift

The example SNF drift is highlighted yellow in Figure 2-2. Five QOI are compared in this drift, as shown in Table 5-1. This location is chosen to demonstrate how radionuclides are released in the SNF disposal drift and are transported into the rest of the repository. The waste package spacing, dimensions, and design of the POLLUX-10 canisters are provided in section 4.3.2 of the task specification. No team decided to mesh the

individual waste packages, so all the teams' simulation models are simplified from the original task specification.

BASE, COVRA, and DOE mesh the combined drift/waste package region into multiple grid cells and use average properties for the buffer and SNF canisters in the region. Quintessa homogenises the SNF drift into several, larger compartments in their model. GRS investigated two scenarios, one with individual compartments for each SNF drift and the second lumping the SNF drifts into two compartments of the 25 drifts farthest from the seal (on the left of Figure 2-2) and the 25 drifts in the centre of the repository (centre of Figure 2-2). They discovered there is no difference in the model results. In the final GRS model the SNF drifts are lumped into two compartments for computational efficiency. It is unlikely that these simplifications will cause differences between the models as all teams make similar assumptions, the task specification has all the POLLUX-10 canisters fail simultaneously at 500 years, any containment provided by the SNF waste package is neglected, while the SNF waste form gradually dissolves throughout the simulation. This assumption may cause increased migration of radionuclides inside the drift as compared with a fully resolved model, but this question cannot be addressed with any of the current team models.

5.1.1 Porosity evolution

As shown in Table 4-3, teams make a wide variety of assumptions about the compaction of salt in their models. They cover the full range of possibilities: fully-coupled compaction according to the task specification for GRS and Quintessa, simplified compaction for BASE and COVRA, and changing permeability only for DOE.

As can be seen in Figure 5-1, the porosity evolution curves in the SNF drift reflect these differing compaction assumptions. GRS and Quintessa have very similar curves. This is because the GRS compaction model is used to create the compaction equations in the task specification (see Section 4.4 and Appendix D) and the Quintessa model fully couples these equations into their simulation model (see Section 4.5 and Appendix E). These two models also have the highest rate of compaction.

As discussed in Section 4.1 and Appendix A, BASE uses the mineral reaction functionality in PFLOTRAN to create a porosity reduction curve that approximates the tabular data in the task specification subject to the requirement that liquid mass must be preserved (see Table 4-4). These simplifications and forward coupling approach result in a salt compaction curve that is similar in shape, if slightly slower than the task specification on the scale of the 100,000 year simulation.

COVRA also uses a coupling technique in their salt compaction model, as discussed in Section 4.2 and Appendix B. This results in a compaction curve that was similar in shape, but slower than the task specification compaction curve. The COVRA model has the curve with the slowest compaction rate, as can be seen in Figure 5-1.

Finally, DOE does not explicitly include porosity reduction in their model, as discussed in Section 4.3 and Appendix C so it never changes from the original 10% porosity throughout the simulation. They choose instead to only model the permeability reduction in the parts of the model that experience compaction.

Porosity is reduced to around 2% by 20 years for the BASE, GRS, and Quintessa models and by 50 years for COVRA. This is due to the 20% initial water saturation and resulting rapid salt compaction in the task specification. Clearly the differing assumptions about changing porosity in the SNF drift will impact the liquid saturation and flow in the drift. However, differences between the four models with porosity reduction may not have a significant impact on the radionuclide transport because the drifts are all nearly fully compacted long before the SNF waste packages breach at 500 years.
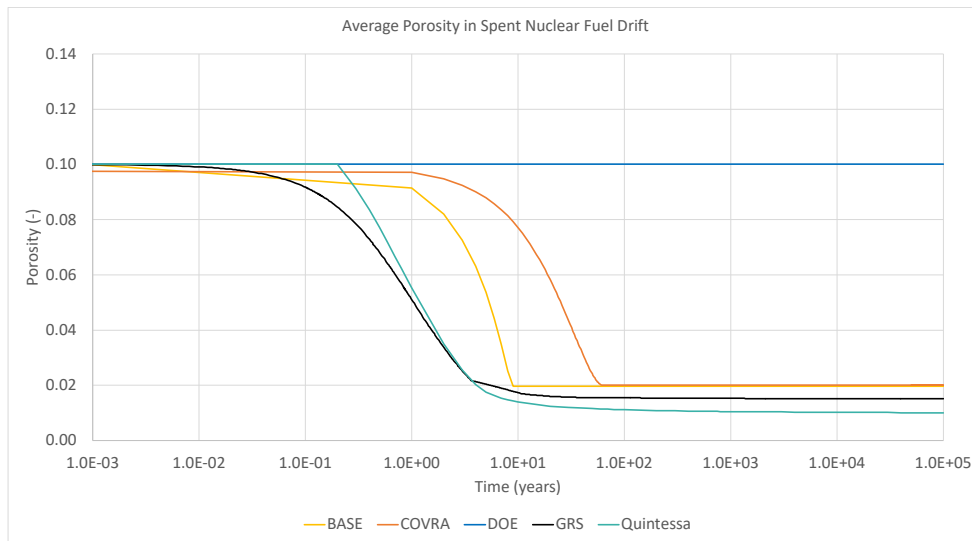

Figure 5-1 Porosity evolution for the example SNF drift.

5.1.2 Fluid flow

Figure 5-2 shows the liquid saturation (top) and liquid flow out of the SNF drift (bottom) for each of the team's simulation models. As anticipated, in the BASE, COVRA, GRS, and Quintessa models, as the porosity decreases the liquid saturation increases in a very clear inverse relationship (see Figure 5-1). This is because early in the simulation there

is little external force in these models to drive changes in liquid saturation, and saturation increases almost entirely due to the decreasing pore space.

Starting around 500 years there is a gradual decrease in liquid saturation in the BASE model. This is because at the interface of the concrete plugs and the seal salt, the model doesn't fully resaturate with liquid. At later times, the concrete plugs of the seal start draw water from nearby tunnels (not shown) to re-equilibrate the repository. Different grid refinements were considered, but the same result was obtained, so this does not appear to be a grid-related numerical artefact. The desaturation of the drift accelerates around 1,000 years when the shaft seal fails, creating flow in the parts of the repository adjacent to the shaft and seal. If shaft failure occurs at a different time the models may fully saturate. This equilibration process continues until around 10,000 years, when the new equilibrium saturation of about 94% is reached in the SNF drift.

As the liquid saturation increases, pressure (not shown) begins to build in the SNF drift, creating flow of liquid out of the drift in the BASE, COVRA, GRS, and Quintessa models, as seen at the bottom of Figure 5-2. There is a clear correlation between the peak flow rate of liquid and reaching full resaturation of the SNF drift in the BASE, GRS, and Quintessa models. The COVRA model has peak liquid flowrate during the resaturation process. Liquid flowrate peaks first the GRS model at 2.4 m^3/yr at 3.7 year and the Quintessa model flow peaks at 1.72 m^3/yr after 6.0 years, which are strikingly similar results. The next highest peak is the BASE model and has peak flowrate of 0.09 m^3/yr at 12 years, over an order of magnitude lower. The COVRA model has peak liquid flowrate at nearly the same time, after 13 years, but the peak rate is two orders of magnitude lower, at 5×10^{-4} m^3/yr. As the flow out of the repository is driven by creep closure, it makes intuitive sense that the models with the most rapid reduction in porosity have the highest and earliest peak in liquid flowrate. On the scale of the 100,000 year simulations, the timing of the peak flow out of the SNF drift is remarkably similar between these four models.

The DOE model resaturation process is driven by fundamentally different physical mechanisms than the other four models. Recall that this model has no creep closure, but it is the only model that includes influx of liquid from the geosphere, as geosphere influx was not included the task specification, but is a consequence of DOE meshing the surrounding geosphere in their model. Prior to shaft failure at 1,000 years, the driving forces for resaturation in this model are influx from the geosphere and influx from the rest of the repository at a rate on the order of -10^{-5} m^3/yr (not visible on Figure 5-2 as it is a log-log plot). The DOE model is the only model that has appreciable liquid flow into the drift from the rest of the repository. Resaturation by these two mechanisms is a slow process, as can be seen on the top of Figure 5-2. The DOE model shows a very short-

lived spike in liquid flow out of the SNF drift when saturation is reached after 14,000 years.
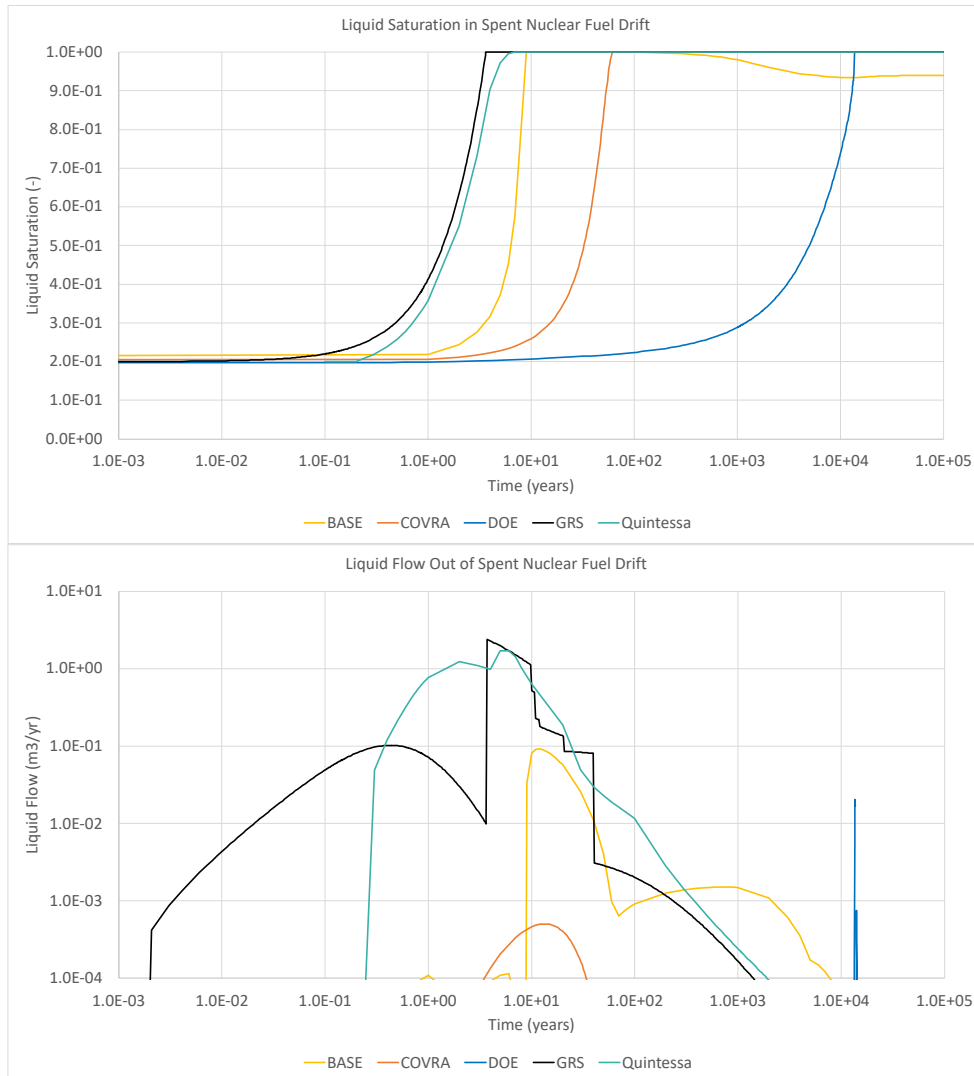

Figure 5-2. Flow quantities for the example SNF drift. Top: Liquid saturation. Bottom: Liquid flow. Positive flow is defined as flow out of the drift towards the shaft.

5.1.1 Tracer 1 mass and transport

Figure 5-3 shows the mass of Tracer 1 in the SNF drift (top) and the transport of tracer out of the drift (bottom). The BASE, COVRA, DOE, and Quintessa models show zero moles of tracer from the start of the simulation to 500 years, when the waste packages all breach simultaneously. The GRS software LOPOS does not calculate mass in the waste compartment, so is not shown.

The trend of the mass of Tracer 1 in all the models is remarkably consistent, especially considering the differences in liquid flowrate shown in Figure 5-2. This is in large part because the peak flowrate of water in all the models with compaction occurs before 13 years, long before the waste packages breach at 500 years. The liquid flowrate is on the order of 1 x 10^{-3} m^3/yr or lower at 500 years in every model, including the DOE model, which has liquid flow into the drift at 500 years.

The bottom of Figure 5-3 shows the Tracer 1 transport out of the SNF drift for the five teams. In all the models there is a spike in transport of Tracer 1 out of the SNF drift as the result of the waste packages breaching at 500 years followed by a rapid decline as the mass of Tracer 1 in the SNF drift decreases. In the BASE, GRS, and Quintessa models, this decline follows the decline in the liquid flowrate 500 years in each of these models, as can be seen in Figure 5-2. Comparison of Tracer 1 transport in the BASE, GRS, and Quintessa models in Figure 5-3 with the liquid flowrate for these models in Figure 5-2 indicates that there is a clear trend between high fluid flowrates and high transport rate of Tracer 1 after 500 years: the BASE model has both the highest Tracer 1 transport and the highest liquid flowrate, Quintessa is second, and GRS is third. Analysis by the individual teams in Appendix A and D indicates that the BASE and GRS models have some advection but have diffusion dominated transport of Tracer 1. The Quintessa model also has diffusion as the primary transport mechanism, as discussed in Appendix E.

At 500 years the liquid flowrate in the COVRA model is very low (below the minimum rate shown in Figure 5-2) and the Tracer 1 transport in Figure 5-3 is similarly low. This model also appears to have transport of Tracer 1 mass via diffusion. In the DOE model the liquid is flowing into the SNF drift at 500 years, so Tracer 1 can only be transported out of the drift by diffusion. In the DOE model the transport of Tracer 1 by diffusion is much larger than the COVRA and GRS models and comparable to the Quintessa model. This is likely because the DOE model effective diffusivity depends on the crushed salt porosity, which is higher than the intact salt porosity. The spike in Tracer 1 transport around 14,000 years aligns with the spike in liquid flow in Figure 5-2.
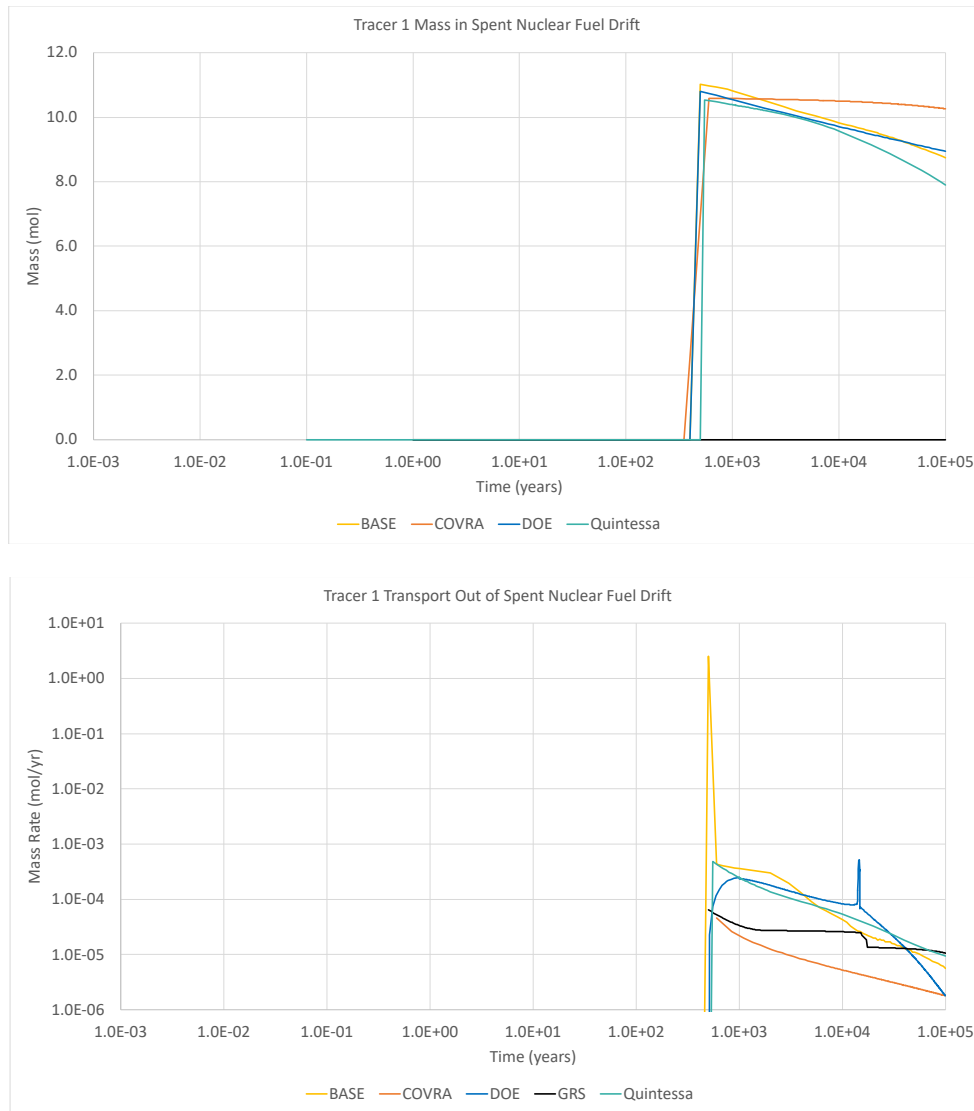
Figure 5-3 Tracer 1 transport quantities in the SNF drift. Top: Tracer 1 mass in the drift. GRS is not shown as the LOPOs software does not output this quantity. Bottom: Tracer 1 transport out of the drift. Positive is defined as transport out of the repository and towards the shaft.

5.2 Vitrified waste drift

The example vitrified waste drift is highlighted yellow in Figure 2-2. Five QOI are compared in this drift, as shown in Table 5-1. This location is chosen to demonstrate how radionuclides are released in the vitrified waste disposal drift and are transported into the rest of the repository. The waste form and container specifications, overpack dimensions, and description of the emplacement scheme with two waste packages in vertical boreholes in the floor of the drift are provided in section 4.3.3 of the task specification. As with the SNF drifts, no team decided to mesh the individual waste

packages, which are specified to be placed in boreholes with two packages per borehole and salt seals surrounding them. Thus, all the teams' simulation models are simplified from the original task specification. Like the SNF drifts, BASE, COVRA, and DOE meshed the combined drift/canister region into multiple grid cells, Quintessa lumped the vitrified waste drifts into a smaller number of compartments and GRS lumped the vitrified waste drifts into one compartment. Again, it is unlikely that these simplifications cause differences between the models as all teams made similar assumptions, the task specification omits performance provided by the vitrified waste canister, and the glass waste has rate-limited dissolution starting at the beginning of the simulation. This assumption may cause increased migration of radionuclides inside the drift as compared with a fully resolved model, but this question cannot be addressed by any of the teams' models.

5.2.1 Porosity

As can be seen in Figure 5-4 the porosity evolution curves in the vitrified waste drift follow the same trend as the porosity in the SNF drift shown in Figure 5-1. One difference in the porosity evolution between the models is that the GRS model begins at a higher initial porosity of 14%, while the other models begin at a porosity of 10%. This is the result of differing simplifications from the task specification: GRS chose to use the vitrified waste emplacement borehole porosity for the entire vitrified waste drift, while the other teams chose to use the crushed salt value. The higher GRS initial porosity results in the Quintessa model having the fastest porosity decrease of all the models with compaction. Also, in this drift the GRS porosity declines to about 2% within 100 years, whereas in the SNF drift the final porosity was 1.5%. The other porosity evolution curves are extremely similar to the curves for the SNF drift in Figure 5-1.
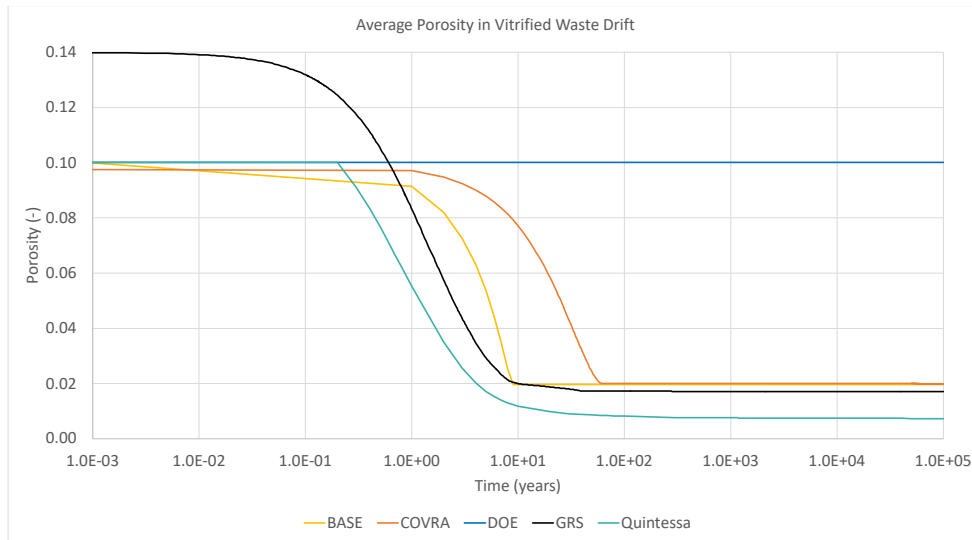
Figure 5-4. Average porosity for the vitrified waste drift.

5.2.2 Fluid flow

Figure 5-5 shows the liquid saturation (top) and liquid flow out of the vitrified waste drift (bottom) for each of the team's simulation models. As in the SNF drift, in the BASE, COVRA, GRS, and Quintessa models the liquid saturation increases in a very clear inverse relationship with the porosity (see Figure 5-4). The liquid saturation in the vitrified waste drift increases at almost the same rate in the GRS and Quintessa models, while in the SNF drift the GRS model resaturated first. This difference from the SNF drift is likely because the Quintessa model has the fastest drift closure in the vitrified waste drift, which shifts the Quintessa resaturation curve to the left relative to the others.

The BASE model liquid saturation begins to decrease in the vitrified waste drift around 100 years in Figure 5-5. The mechanism is the same as the SNF drift, with the concrete plugs drawing in water, particularly after shaft seal failure. The desaturation is larger in the vitrified waste drift than SNF drift shown in Figure 5-2 because the vitrified waste drift is closer to the seal. The liquid saturation reaches a minimum of 88% at 2,000 years, before rebounding to about 94%, the same saturation as the SNF drift, around 10,000 years when the final equilibrium saturation of the repository is reached.

As the liquid saturation increases due to compaction, it begins to flow out of the drift in the BASE, COVRA, GRS, and Quintessa models, as seen at the bottom of Figure 5-5. There is again a clear correlation between the peak flow rate of liquid and full resaturation of the vitrified waste drift in the BASE, GRS, and Quintessa models, and peak liquid flowrate during resaturation in the COVRA model. Liquid flowrate peaks first the GRS model at 6.04 m^3/yr at 4.8 years and the Quintessa model flow peaks at 1.71 m^3/yr after 5.0 years,

which are again strikingly similar results. The BASE model has peak liquid flowrate of 0.26 m^3/yr at 17 years, while the COVRA model again peaks at a very similar time with a rate of 3.98 x 10^{-3} m^3/yr at 14 years. On the scale of the 100,000 simulations, the timing of the peak flow out of the vitrified waste drift is again remarkably similar between the four models with compactions.

The DOE model resaturation process is driven by influx of liquid from the geosphere the rest of the repository, a much slower process. Unlike the SNF drift, starting around 500 years there is liquid flow out of the vitrified waste drift. The difference is likely because the vitrified waste drift is shorter and adjacent to a large volume of intact salt near where the drift connects to the access tunnel connecting it to the rest of the repository. The flow out of the drift increases until shaft seal failure at 1,000 years when it drops off, then begins to increase again until 10,000 years, when the maximum liquid flowrate of 0.017 m^3/yr is reached before dropping sharply off again.
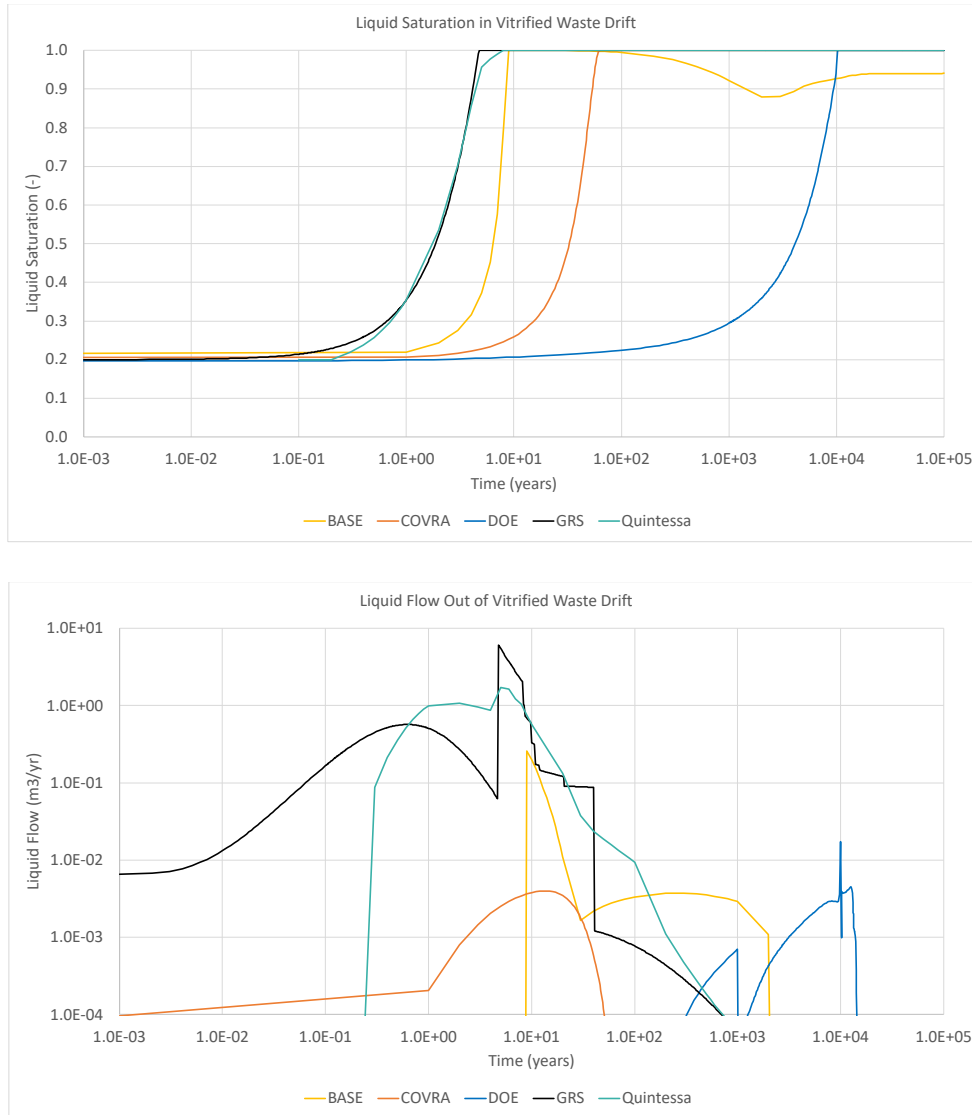
Figure 5-5. Flow quantities for the vitrified waste (HLW) drift. Top: Liquid saturation. Bottom: Liquid flowrate. Positive flow is defined as flow out of the drift towards the shaft.

5.2.3 Tracer 3 mass and transport

The mechanism for release of Tracer 3 in the vitrified waste containers is gradual dissolution of glass. The vitrified glass waste begins to dissolve at a slow, constant dissolution rate from the start of the simulation. The result is that there is very little Tracer 3 in the drift until 1,000 years and the mass increases uniformly with time in all the simulations, as can be seen in Figure 5-6. This is a much later release than the sudden breach of the SNF waste packages at 500 years that releases Tracer 1 in Figure 5-3.

The top of Figure 5-6. shows the gradual release of Tracer 3 in all the models except GRS, as LOPOS does not output this quantity. It takes 10,000 years to accumulate more than 2 mol of Tracer 3 in the vitrified waste drift in every model. By this time all the models predict fluid flowrates of less than 0.01 m^3/year out of the drift (see Figure 5-5). The Tracer 3 transport rates are similarly low and relatively constant in time, as shown on the bottom of Figure 5-6.. Thus, the transport of Tracer 3 out of the vitrified waste drift appears to be diffusion-dominated in every model because of the later release. This is a fundamental divergence from the SNF drift, where the models with compaction had an advection-driven component of Tracer 1 transport, peaked right after waste package breach at 500 years and had largely died out by 10,000 years.
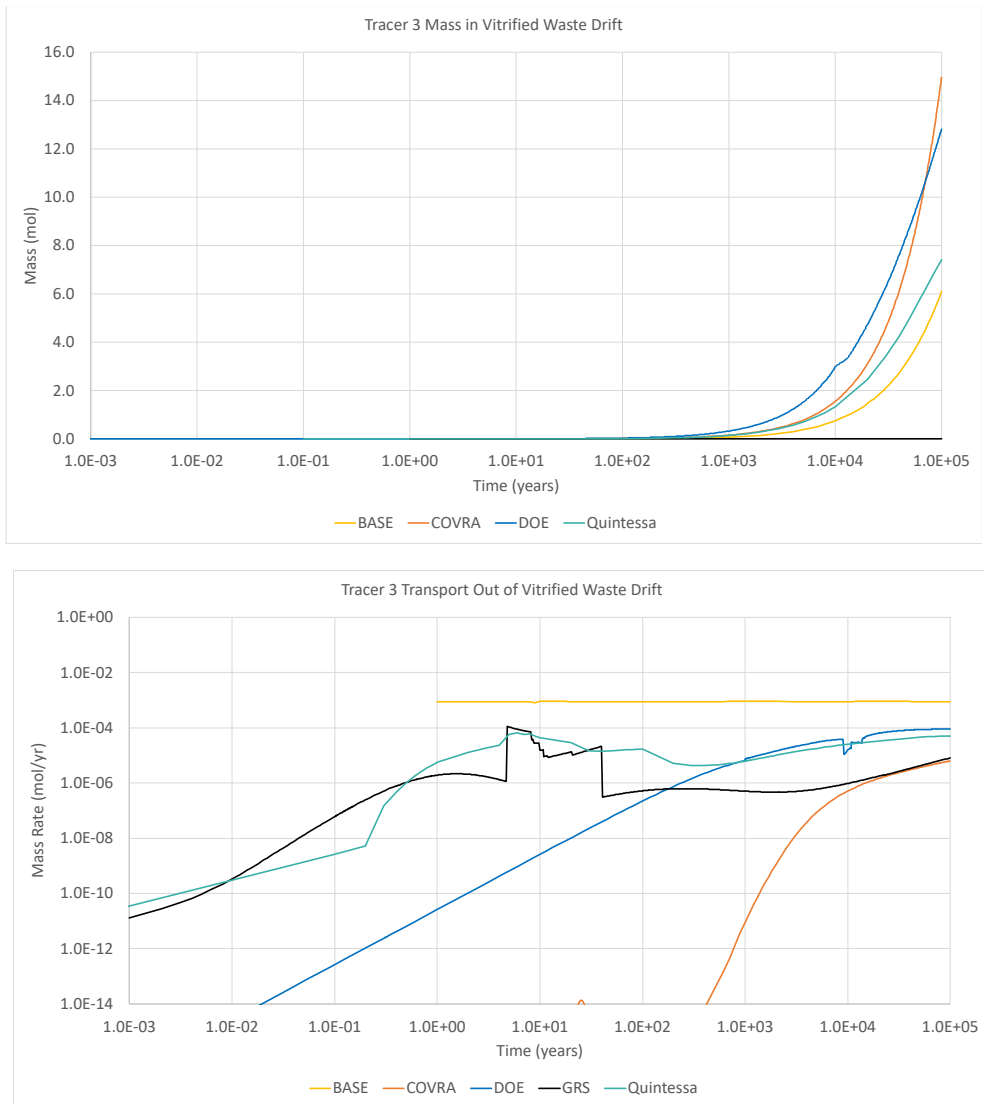
Figure 5-6. Tracer 3 transport quantities in the vitrified waste (HLW) drift. Top: Tracer 3 mass in the drift. GRS is not shown as the LOPOs software does not output this quantity. Bottom: Tracer 3 transport out of the drift. Positive is defined as transport out of the repository and towards the shaft.

5.3 Repository seal salt

The third location where QOI are compared is the run of mine salt in the repository seal, shown in green in Figure 2-2. This location is chosen to demonstrate performance of the repository engineered barrier system. The seal salt is chosen as the third performance metric because it is the part of the engineered barrier system furthest from the waste drifts that contains radionuclides. In most models no radionuclides pass through the salt seal into the parts of the repository nearer the biosphere in the 100,000 year simulation (not shown).

Ten QOI are compared in this drift, as shown in Table 5-1. The QOI are consistent with those chosen for the waste drifts, but there are twice as many because the seal salt contains both Tracer 1 and Tracer 3 and there is flow and transport at both ends of the seal. The only simplification of the seal salt that was made by the teams was the modified compaction models.

5.3.1 Porosity

Figure 5-7 shows that the porosity evolution as modelled by the BASE, GRS, and Quintessa models is extremely similar. Once again, the Quintessa and GRS modes are the same because the Quintessa model is developed using the equations from GRS software LOPOS presented in the task specification. Recall from Table 4-4 and Appendix A that the BASE model uses a porosity reduction curve that approximates the tabular data in the task specification subject to the requirement of preservation of liquid mass. The BASE compaction curve more closely matches the GRS curve here than in the waste drifts.

As the BASE curve was fitted to the tabular data created by GRS, these two models have nearly the same porosity of 0.002 at 100,000 years. COVRA and Quintessa have higher porosities at the end of the simulations of 0.006 and 0.007, respectively. Like the waste drifts, the COVRA model has slower compaction of the porosity because this is necessary to ensure their model could run while satisfying the coupled porosity evolution and pressure constraint in their model.
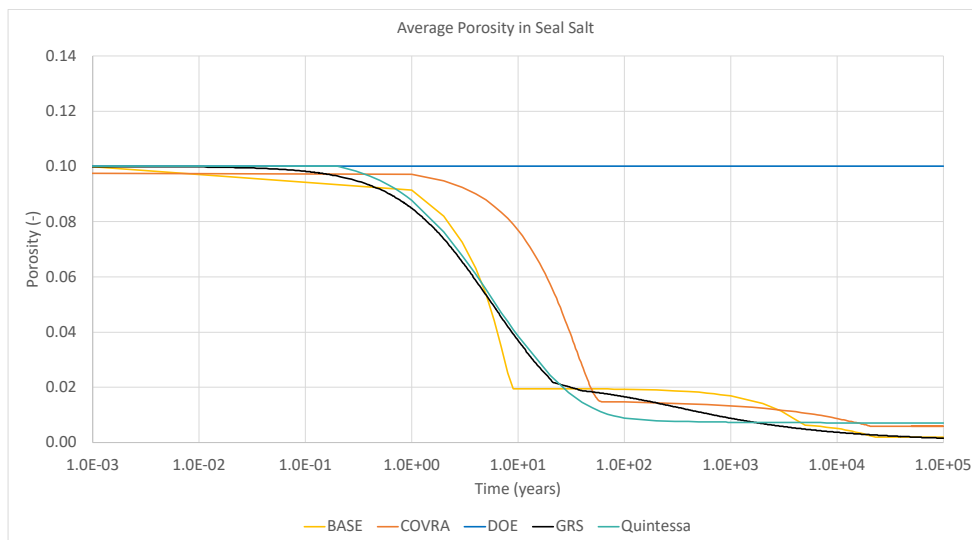

Figure 5-7. Average porosity in the salt in the repository seal.

5.3.2 Fluid flow

The top of Figure 5-8 shows liquid saturation in the seal salt. As in the waste drifts, in the BASE, COVRA, GRS, and Quintessa models the liquid saturation increases in a very clear inverse relationship with the porosity (see Figure 5-7). The liquid saturation begins to increase at almost the same time in the BASE, GRS, and Quintessa models, while the COVRA model begins to resaturate later and the DOE model resaturates much later due to influx from the geosphere and surrounding repository. In the seal, the BASE and COVRA models both experience desaturation due to fluid loss to the concrete seals, though this occurs on different timescales for the two models. The COVRA model may begin to desaturate earlier than some of the other models because it has a higher endpoint porosity and different relative permeability function than the task specification. Quintessa sees a similar impact at other locations in the model, and desaturation would be visible in the seal salt if the simulation were run for more than 100,000 years (not shown).

The middle and bottom of Figure 5-8 show liquid flow from the cement abutments on the repository side into the seal salt, and flow from the seal salt into the cement abutment on the side of the seal salt closest to the infrastructure and shafts to the surface, respectively. The BASE, COVRA, and Quintessa models all show a very similar trend in liquid flow. As the salt begins to compact, the liquid saturation increases and is pushed out of the seal salt in both directions. This squeezing effect results in flow in the direction of the waste area (negative) from the left side of the salt (middle of Figure 5-8) and flow in the direction of the shaft (positive) from the right side of the salt (bottom of Figure 5-8). In the BASE and COVRA models the peak flowrate occurs when the salt is nearly fully saturated, around 7 years and 30 years, respectively. This makes intuitive sense, as prior to full saturation the higher-mobility gas phase is also flowing out of the salt, and the rate of compaction sharply declines once the seal salt is fully liquid saturated, decreasing the driving force (see Figure 5-7). In the Quintessa model the peak flowrates occur earlier during compaction at 7 years, likely due to the fully coupled compaction model, and there is a secondary peak at 40 years when the salt becomes fully saturated.

The GRS model shows a similar trend, but there is little flow until the seal is fully saturated, followed by a sharp spike and, at around 40 years, a reversal of the flow direction. The difference between the GRS model and the other models with compaction is believed to be because in LOPOS squeezing the fluid out of the seal starts after the seal is fully saturated. The BASE, Quintessa, and DOE models also show this reversal of flow direction after full saturation, but at a much smaller scale (not visible on

the scale of Figure 5-8). The DOE model does not have compaction, so the flow of liquid out of the salt seal is much lower and delayed relative to the other models. However, it follows a similar trend to the GRS model.

By 15,000 years all the models have flow into the salt seal from the repository below 4 x 10^{-4} m^3/yr. The BASE and DOE model have flow in the negative direction towards the waste after 22,000 and 5,500 years, respectively (not visible on the scale of the graph). For the BASE model the flow into the inner repository persists for the rest of the simulation. In the DOE model there is an additional flow reversal at 15,000 years. The COVRA, DOE, and Quintessa models have flow out of the salt seal towards the shaft on the order of 1 x 10^{-3} m^3/yr or lower after 15,000 years. Thus after 15,000 years there is little or no advective force driving repository liquid towards the shaft in any model.
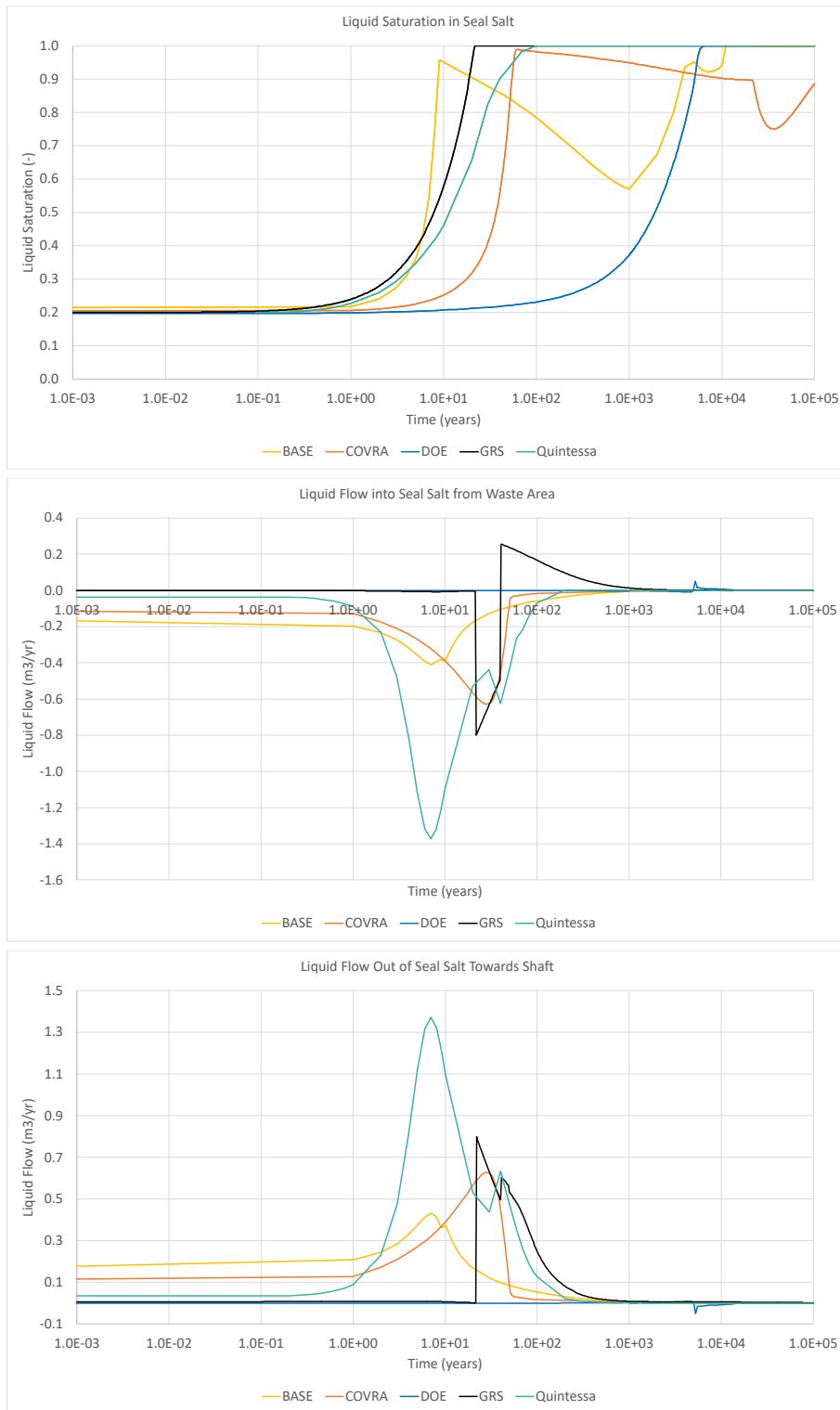
Figure 5-8 Flow quantities for the run of mine salt in the repository seal. Top: Liquid saturation. Centre: Liquid flowrate between the salt and concrete abutment connecting to the waste area. Bottom: Liquid flowrate between the salt and concrete abutment connecting to the infrastructure area and shaft. Positive flow is defined as flow in the direction of the shaft.

5.3.3 Tracers 1 and 3 mass and transport

Figure 5-9. shows the transport quantities for Tracer 1 in the seal salt. The top subfigure shows the mass of Tracer 1 in the seal salt. There is a great deal of variability in the timing of the appearance of Tracer 1 in the seal salt, from 1,400 for the Quintessa model to almost 90,000 years for the COVRA model. This does not appear to correlate with the differences in flow rates in the preceding section, as most models have very slow or negative fluid flow into the seal salt at the time of Tracer 1 appearance. All models predict monotonically increasing Tracer 1 concentration with time. The GRS, DOE, and COVRA models show a similar slope in the increasing trend on the log-log plot. The variation in breakthrough time between the GRS, COVRA, and DOE models leads to differences in the maximum Tracer 1 mass in the seal salt at the end of the simulation at 100,000 years for these models. The BASE model has a more gradual increase in the Tracer 1 mass, so that even though breakthrough is at nearly the same time as the GRS model, the final Tracer 1 mass is much lower at the end of the simulation. The Quintessa model shows the most gradual increase in the Tracer 1 mass in the seal salt so that even though Tracer 1 appears over 5,000 years earlier in this model than any of the others it has nearly the same mass as the DOE and BASE models at the end of the simulation.

The centre and bottom of Figure 5-9. show the transport of Tracer 1 into the seal salt from the waste area (centre) and out of the seal salt towards the infrastructure area and shaft (bottom). As can be seen, there is increasing rate of transport of tracer into the seal salt with time that parallels the increase in Tracer 1 mass for each model on the log-log plots, but at later time. For the COVRA model, transport into the seal salt is always below the 1×10^{-14} mol/yr in the 100,000 year simulation, though Tracer 1 mass does accumulate to above 1×10^{-14} mol before 100,000 years due to transport at rates below the minimum shown in the centre of Figure 5-9.

The bottom of Figure 5-9. verifies that there is very little transport of Tracer 1 out of the seal salt towards the shaft. In the BASE, COVRA, and DOE models there is no transport of Tracer 1 above the minimum concentration shown of 1×10^{-14} mol/yr. The Quintessa model shows a small amount of transport between 1×10^{-14} to 1×10^{-13} mol/yr the last 10,000 years of the simulation, while the GRS model has the highest transport through the salt seal, with a maximum of 3.8×10^{-7} mol/yr at the end of the simulation. These low transport rates of Tracer 1 indicate that, in every model, the salt in the repository seal provides containment and is keeping the radionuclides from migrating through the seal towards the infrastructure area and the shaft. However, rates of transport of Tracer 1 past the seal salt increase up to 100,000 years in the GRS, Quintessa, and DOE (not visible on the scale of the plot) models.

Comparison of the liquid flowrates in Figure 5-8 and the Tracer 1 transport in Figure 5-9. shows that there is very little liquid flow into or out of the seal salt in any model after 1,000 years. This indicates that Tracer 1 transport through the seal salt is diffusion-dominated in every model. As discussed in Section 4.6, in all the models there are different levels of numerical dispersion in addition to physical diffusion resulting from the effective diffusion in the simulation models. Numerical dispersion and diffusivity/porosity coupling could drive some of the differences in Tracer 1 transport between the models.
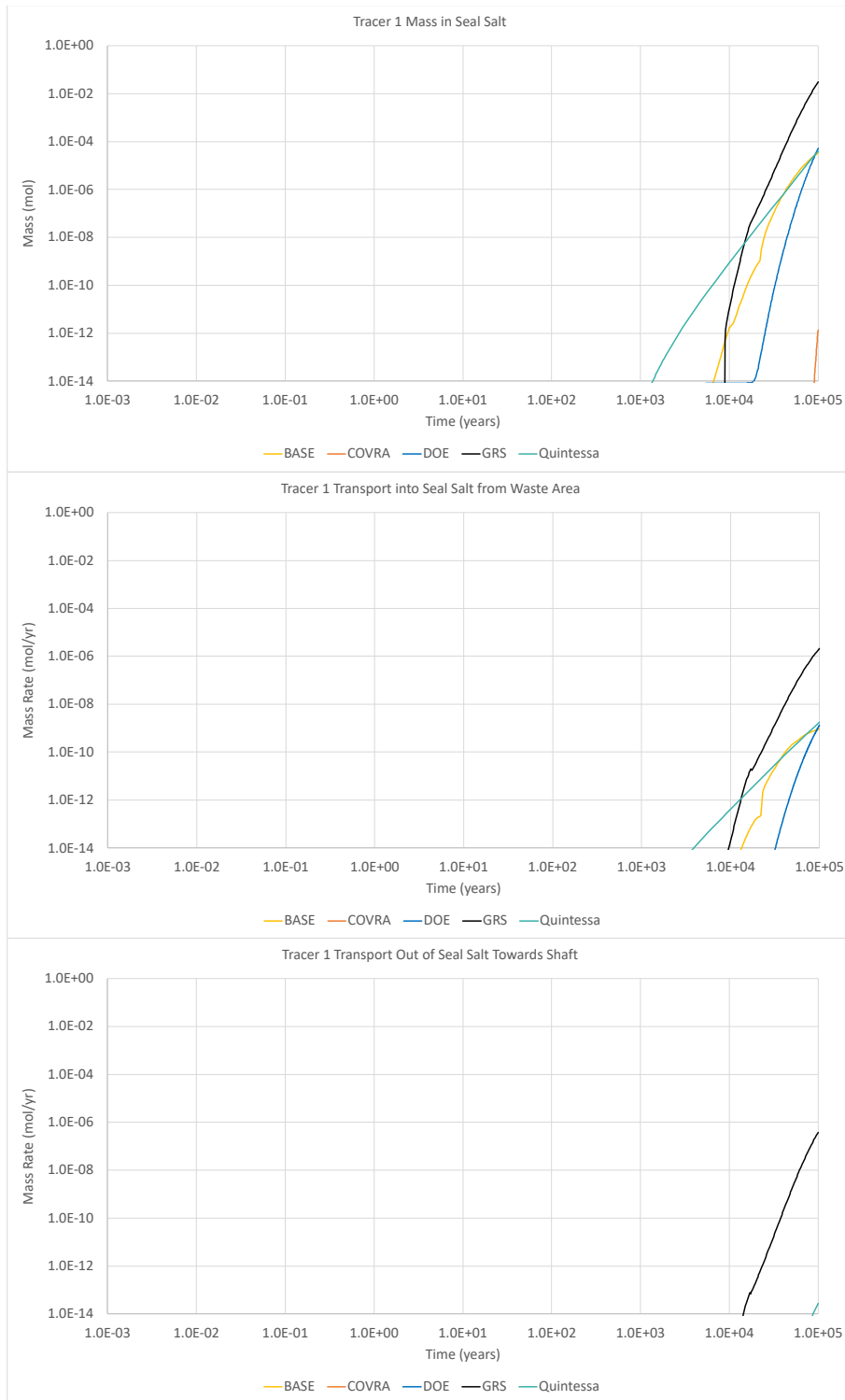
Figure 5-9. Tracer 1 transport quantities the salt in the repository seal. Top: Tracer 1 mass. Centre: Tracer 1 transport between the salt and drifts connecting to the waste area. Bottom: Tracer 1 transport between the salt and drifts connecting to the shaft. Positive is defined as flow out of the repository and towards the shaft.

Figure 5-10 shows the transport quantities for Tracer 3 in the seal salt. Comparison of Figure 5-10 and Figure 5-9. reveals that in all the models Tracer 3 appears earlier than Tracer 1. This makes intuitive sense as the vitrified waste drift containing Tracer 3 is closer to the seal than the SNF drift containing Tracer 1 (see Figure 2-2). Recall also that the tracers are released into the model by different mechanisms; Tracer 1 is released suddenly at 500 years and there is an advective component to Tracer 1 transport at early time in some models (see Figure 5-1 and Figure 5-4), while Tracer 3 is released throughout the simulation from the start and is diffused at low concentrations out of the vitrified waste drift in every model (see Figure 5-5 and Figure 5-6.).

In the Quintessa model, Tracer 3 appears at 40 years and coincides with the secondary peak in negative liquid flowrate (out of the seal salt into the waste area) shown in the centre of Figure 5-8. In the BASE model Tracer 3 appears at 900 years, when the liquid flowrate is small and negative at -7×10^{-3} m^3/yr, but not negligible. This indicates that the transport regime into the seal salt for Tracer 3 must be diffusive in these two models, as the fluid flow is in the opposite direction of Tracer 3 transport.

In the DOE and COVRA models there is very little fluid flow that could contribute to advective transport of Tracer 3 into the seal salt. In The GRS model Tracer 3 appears at 41 years and exactly coincides with the reversal of the liquid flow direction from negative to positive (see Figure 5-8). Thus, transport of Tracer 3 may be partly driven by advection in the GRS model, though it too is believed to be largely diffusive.

In the COVRA and DOE models, Tracer 3 mass and transport into the seal salt from the waste area curves that are similar in shape, but earlier in time than the Tracer 1 curves. Neither model shows transport of Tracer 3 out of the seal salt towards the shaft in the bottom of Figure 5-10.

For the BASE, GRS, and Quintessa models, comparison of Figure 5-9. and Figure 5-10 shows that the Tracer 1 and Tracer 3 mass curves are very different in shape and Tracer 3 appears at least an order of magnitude earlier in time than Tracer 1 within each model. In these models, the mass of Tracer 3 quickly increases right after breakthrough and then more gradually at later time. In the GRS and Quintessa models the transport of Tracer 3 into the seal salt declines after breakthrough and then increases again after 50,000 years. The BASE model shows a more complex, but apparently similar trend. This is unlike Tracer 1, where the rate of transport into the seal salt was uniformly increasing in a nearly linear trend on the log-log plot (see the middle of Figure 5-9.). The difference between the shape of the mass and transport into the seal salt in these three models may be caused by the different mechanisms of tracer release or may be a late-time trend that is only observable in Tracer 3 because it arrives at the seal earlier than Tracer 1.

The bottom of Figure 5-10 shows that, as with Tracer 1, only the GRS and Quintessa model predict transport of Tracer 3 from the seal salt towards the shaft. Because Tracer 3 appears much earlier than Tracer 1 in these models, transport of Tracer 3 towards the shaft also begins earlier and reaches a higher level. However, the maximum transport of Tracer 3 is still very low, with a maximum rate of 2.3 x 10^{-8} mol/yr at the end of the GRS simulation. These results indicate that Tracer 3 is entirely or mostly trapped in the seal salt for the duration of the 100,000 year simulation. However, transport of Tracer 3 out of the seal is still increasing in every simulation at 100,000 years.

Figure 5-10 Tracer 3 transport quantities the salt in the repository seal. Top: Tracer 3 mass. Centre: Tracer 3 transport between the salt and drifts connecting to the waste area. Bottom: Tracer 3 transport between the salt and drifts connecting to the shaft. Positive is defined as transport out of the repository and towards the shaft.

5.4 Fluid flow in the repository shaft

The final QOI to be compared across all the teams is liquid flow in the lower shafts (see

Table 5-1 Table 5-1), defined as bottom 25 m of the shaft above the infrastructure area. The reason only a liquid QOI is compared here is that no model shows significant presence of either tracer at this location or at any location nearer to the biosphere.

Figure 5-11 shows the liquid flow across the lower shaft for all the teams' models. As can be seen, the dominant direction of flow in every model is flow of liquid from the surface downwards into the repository. In all the models, prior to the failure of the shaft seal at 1,000 years, flow through the lower shaft is small and negative (not visible on the scale of the plot), with the greatest magnitude flow in the GRS model at around -0.1 m^3/yr and the smallest in the DOE model at -8 x 10^{-7} m^3/yr.

In every model there is a large, sudden, pulse of liquid down the shaft into the repository associated with shaft seal failure due to the instant failure of the shaft, as represented by a step change in permeability (see Figure 5-11). All models also have a sharp decrease in flow once the gravel-filled infrastructure area is saturated. The GRS model shows the lowest and longest pulse of water from the surface, beginning immediately upon shaft seal failure and maintaining a relatively constant rate of about -2 m^3/yr until 15,500 years. The DOE model shows the largest and briefest influx of water from the surface beginning 100 years after the shaft fails. The DOE flowrate peaks at -8 m^3/yr then declines sharply, before dying off around 4,000 years. The flowrate in the DOE model is likely higher than the others because the lack of compaction in this model means that flow within the repository is less restricted at the time of shaft seal failure, when most of the other models are nearly fully compacted. The BASE and Quintessa models start downward flow at similar times, 3,000 and 2,000 years, respectively, and end at 10,000 years, however the Quintessa model has a higher flowrate.

Recall from Section 4.2 and Appendix B that the COVRA model consists of two sub-models that are calculated separately, one for the shaft, and one for the repository. The COVRA shaft model allows for flow down the shaft starting immediately at 1,000 years, with the greatest flowrate of the water pulse at -8.75 m^3/yr after 2530 years. The flowrate declines to -2.0 m^3/yr by 2620 years, when the shaft is nearly fully saturated. The head pressure corresponding to the final shaft flowrate is used as a boundary condition for the repository model from 2620 years until the end of the simulation. The negative of the inflow into the repository is shown for times greater than 2620 years as a dashed line on Figure 5-11 for comparison purposes with the other models. As can be seen, the flow into the repository varies with time, but declines to a very low rate by 3,000 years, (similar to the BASE and Quintessa models) and remains low until the end of the simulation.

The BASE, DOE, GRS, and Quintessa models show comparable volumes of water influx from the surface to the repository on the order of 1 x 10^4 m^3 of water during the water pulse. Interestingly the model with the lowest total water volume entering the repository is the DOE model, which is the only model without compaction and the resulting reduction of porosity. This may be because it is also the only model with geosphere influx as a second mechanism for filling the repository with liquid, despite the very low (1 x 10^{-22} m^2) permeability of the surrounding salt.

The BASE, DOE, and Quintessa models also predict that at later time, after 6,000 to 15,000 years there is a reversal of the flow direction and there is a small amount of flow upwards towards the surface. In the BASE and Quintessa models, the upwards flow is believed to be caused by slow compaction of the repository and the difference between the hydrostatic and lithostatic pressure in the models, and compaction drives the repository pressure towards lithostatic. The flow is on the order of 4 x 10^{-5} m^3/yr and appears to be declining towards the end of the simulation. In the DOE model the upwards flow plateaus around 1 x 10^{-2} m^3/yr from 19,000 years to the end of the simulation.
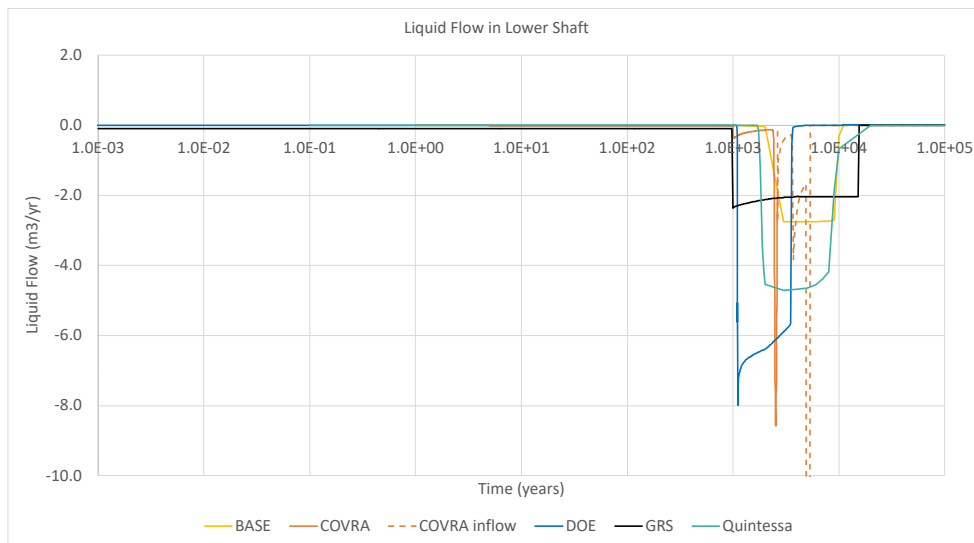
Figure 5-11 Liquid flow in the lower shaft. Positive flow is defined as flow from the repository upward toward the surface.

5.5 Observations

Figure 5-1 through Figure 5-11 show a comparison of the 21 QOI outlined in Table 5-1. In some of the QOI, there is a great deal of difference between the models, but in other areas the differences are modest.

5.5.1 Importance of salt compaction

The largest differences between the models are in quantities related to liquid saturation and flow and are most pronounced at early time, before 1,000 years, as shown in Figure 5-2, Figure 5-5, and Figure 5-8. These differences are believed to be driven largely by the difference in the rate of reduction of porosity in the BASE, COVRA, GRS, and Quintessa models, which in turn depends on the coupling and assumptions in the compaction models (see Table 4-4). The DOE model is believed have the slowest resaturation and generally lower liquid flow rates because there is no reduction in porosity in their compaction model, however this is somewhat counteracted by the fact that this is the only model allowing influx from the geosphere, as this was omitted from the reference case but is a consequence of including the intact salt in the model. These differences in liquid flow QOI reflect the **importance of implementing a high-fidelity salt compaction mechanism** in this salt conceptual model to study performance of the repository, especially at early times post-closure.

5.5.2 Importance of diffusive transport

The large differences in the short-term flow field have relatively little impact on the transport of Tracer 1 and Tracer 3 out of the SNF and vitrified waste drifts, respectively. This is believed to be because in the BASE, COVRA, and Quintessa models with compaction there is no Tracer 1 in the SNF drift, and very little Tracer 3 in the vitrified waste drift until after salt compaction is nearly complete. (Recall that the GRS software does not provide data about tracer concentration in the waste drifts.) The liquid flowrates out of the waste drifts are very small when the SNF canisters fail at 500 years, as shown in Figure 5-3, and when Tracer 3 mass begins to increase exponentially after 1,000 years, as shown in Figure 5-6. Similarly, in all the models the tracers appear in the salt seal either while liquid flow driven by salt compaction is in the negative direction, or after it has decreased to a low value, as shown in Figure 5-9. and Figure 5-10. In the DOE model, the liquid flow in the waste drifts and seal salt is uniformly small.

Consequently, transport of the tracers out of the waste drifts and though the seal salt is believed to be largely diffusive in all models. Though the differences in diffusive transport are generally smaller than the fluid flow differences, this indicates that **diffusion, or effective diffusivity, is a key physical mechanism** that impacts long-term transport of radionuclides in the repository. Diffusion is closely linked to the salt creep closure mechanism via porosity reduction and the coupling between porosity and effective diffusivity. Moreover, diffusion in the numerical models may be impacted by numerical dispersion.

5.5.3 System performance implications

Finally, the three QOI related to potential for the release of radionuclides to the biosphere are transport of Tracer 1 and Tracer 3 from the seal salt towards the shaft, and liquid flow in the shaft. (Recall that Tracer 1 and Tracer 3 were chosen as a high radionuclide mobility scenario as they do not adsorb, decay, and have no solubility limit, unlike the radionuclides in the task specification.) These three QOI show a remarkable degree of agreement across all the models, despite the widely varying levels of geometric complexity, differing salt compaction models, and numerical dispersion adding to the physical diffusion mechanism in all models.

Figure 5-9. and Figure 5-10 show that little or no tracer is transported past the seal salt in any model during the 100,000 year simulations, though rates are increasing at the end of the simulation. Figure 5-11 shows that in all models the dominant direction of water flow in the shaft is from the surface downwards into the repository, and that large flowrates through the shaft are limited to a pulse of water downward into the repository beginning at the time of shaft seal failure.

This is due to the hydraulic decoupling of the 'inner' and 'outer' repository that was observed in every model with salt compaction. The inner repository is defined as all volumes in the repository from the waste drifts to the repository seal. Flow and transport in the inner repository are driven by salt convergence. The outer repository is defined as all repository volumes from the seal to the surface. The seal in the example PA model functions as a highly effective hydraulic barrier, so the inner repository is impacted very little by the shaft seal failure. The outer repository is significantly impacted by shaft seal failure, which floods most of the outer repository. The water migrates into the gravel-filled infrastructure area, which has a large pore space to accommodate the influx of water because the gravel has no compaction in the task specification.

Due to the combination of the large volume of pore space in the outer repository to accommodate water migrating down from the surface, and the highly effective repository seal, no model predicts significant migration of radionuclide tracers in the outer model. For the parameters used and the FEPs and model scenarios considered in the task specification, the simplified disposal system in the conceptual model provides containment during the simulated period of 100,000 years.

This result is similar to the expected and alternative scenario of the generic case of Bertrams et al. (2020). In those scenarios, the release of radionuclides within the assessment period is negligibly small. The diffusive transport velocities are very low, and the transport distances are long. A significant discharge of radionuclides from the repository into the overburden only occurs at times greater than one million years.

5.6 Variants

Based on the results of the base case, two variant cases are considered by several of the teams. The first variant considers changes in initial saturation and a slower compaction rate. The second considers the impact of earlier or later failure of the shaft seal.

5.6.1 Initial saturation and compaction rate

This variant is prompted by the importance of the compaction rate as a driver for fluid flow, as discussed above in Section 5.5.1. The initial liquid saturation of the repository was 20% in the task specification (LaForce et al., 2023). However, 20% initial saturation is almost certainly unrealistically high and, because wet salt compacts more quickly than dry salt, results in rapid compaction of the salt in the base case models, as shown in Sections 5.1-5.5.

In this variant the initial saturation is set to the residual saturation of the crushed salt backfill, which is 3%. The salt convergence parameters are also changed to a slower compaction to reflect the reduced water content. New compaction curves were created in LOPOS by GRS and circulated to the teams. The equations in the task specification can also be used to model creep with the new initial condition and compaction parameters. Two teams chose to participate in this variant, GRS and Quintessa. Recall that GRS and Quintessa both have fully-coupled compaction (Table 4-4) based on the LOPOS equations in the task specification, and as a result, resulted in similar porosity decline curves in Figure 5-1 and Figure 5-7, while differing assumptions about the average

porosity in the vitrified waste drift resulted in different initial porosity in the initial porosity for the curves in Figure 5-4.

Flow and porosity in the disposal drifts

Figure 5-12 shows the porosity, liquid saturation, and fluid flow out of the SNF drift for the GRS and Quintessa base case and low initial saturation/slow compaction variant. These quantities are not shown for the vitrified waste drift as the trends are similar. The top and centre subfigures show that the shape of the porosity decline and liquid saturation curves are very similar to the base case (in log-time). In the low saturation/slow compaction variant the onset of creep closure is delayed until nearly 100 years (instead of less than 1 year), and porosity doesn't drop to less than 2% until after 10,000 years (instead of before 50 years).

The centre subfigure of Figure 5-12 shows that, like the base-case (see Figure 5-1 and Figure 5-2), there is a clear inverse relationship between porosity and liquid saturation. Again, this is because there is little external force driving flow in the SNF drift and so saturation increases primarily due to the decreasing pore space until full saturation is reached. The bottom subfigure of Figure 5-12 shows that the GRS and Quintessa low saturation/slow compaction models both show a peak in fluid flow out of the model corresponding to the time of full saturation. However, because drift closure is so much slower, the peak flow rates are about four orders of magnitude lower than the base case.

The centre subfigure of Figure 5-12 also shows the re-saturation curve from the DOE base case model that has resaturation driven only by influx from the geosphere and the rest of the repository. The DOE model reaches full saturation at nearly the same time as the GRS model, indicating that in the low initial saturation/slow compaction variant, influx of water from the geosphere may be a more important physical mechanism for driving fluid flow in the repository. Geosphere influx is excluded from the GRS and Quintessa base case models, but is considered as a variant by Quintessa in Appendix E and shown to have negligible impact on the base case.
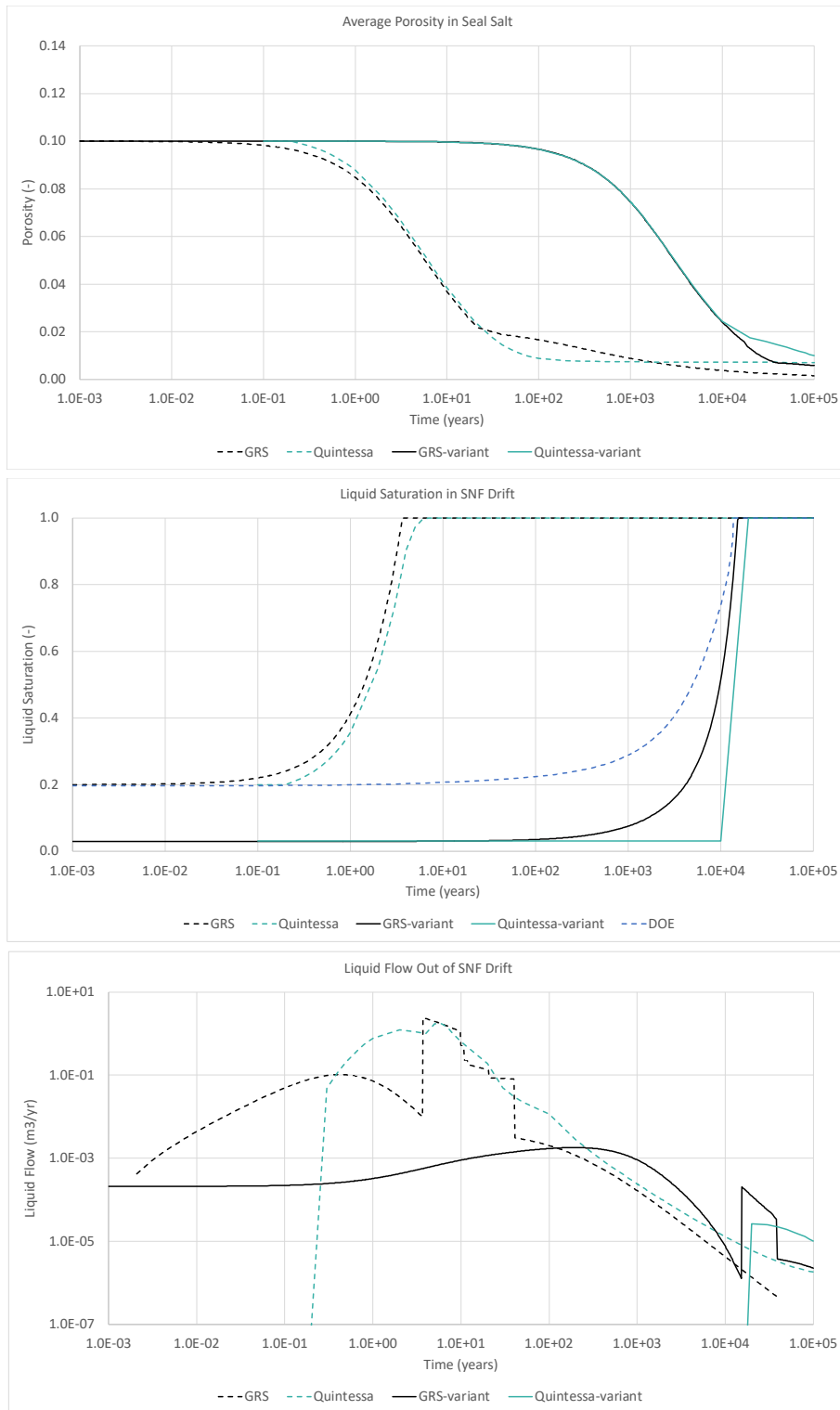
Figure 5-12. Porosity and flow quantities for the SNF drift for the base (dashed lines) and low initial saturation/slow compaction (solid lines) case. Top: Average porosity. Middle: Average liquid saturation. Bottom: Fluid flow where positive is flow out of the drift. The base case (dashed lines) and low initial saturation variant (solid lines).

Tracer transport out of the disposal drifts

Transport of Tracer 1 and Tracer 3 out of their respective disposal drifts are shown in Figure 5-13 for the base case and low initial saturation/slow compaction variant GRS and Quintessa models. Tracer mass in the disposal drifts is not shown.

The top of Figure 5-13 shows that for the SNF drift, in both models the low initial saturation/slow compaction variant has a maximum transport of Tracer 1 after waste package failure at 500 years, though in the GRS model the maximum Tracer 1 transport is significantly higher than the base case, and in the Quintessa model the maximum is significantly lower. Tracer 1 transport in both teams' models then decline to about two orders of magnitude below the base case after 10,000 years and increases again at the peak in liquid flow corresponding to full liquid saturation of the SNF drift. Thus, for Tracer 1 transport the low initial saturation/slow compaction variant is clearly impacted by the liquid flow field, indicating that Tracer 1 transport out of the SNF drift has a significant advective component, as opposed to diffusion-dominated transport of Tracer 1 in the SNF drift observed in the base case in Section 5.1.1.

Figure 5-13 shows that, in the vitrified waste drift, transport of Tracer 3 shows a conceptually consistent trend between the base case and low initial saturation/slow compaction variant models, though transport in the variant case is slower for the first 1,000 years in both teams' models. Transport is relatively low and gradually increasing (on the log-log plot) at short time, increases slightly during compaction and then returns to the gradually increasing trend. This indicates that the transport of Tracer 3 is diffusion-dominated for both the GRS and Quintessa low initial saturation/slow compaction models, as was the case for the base case models.
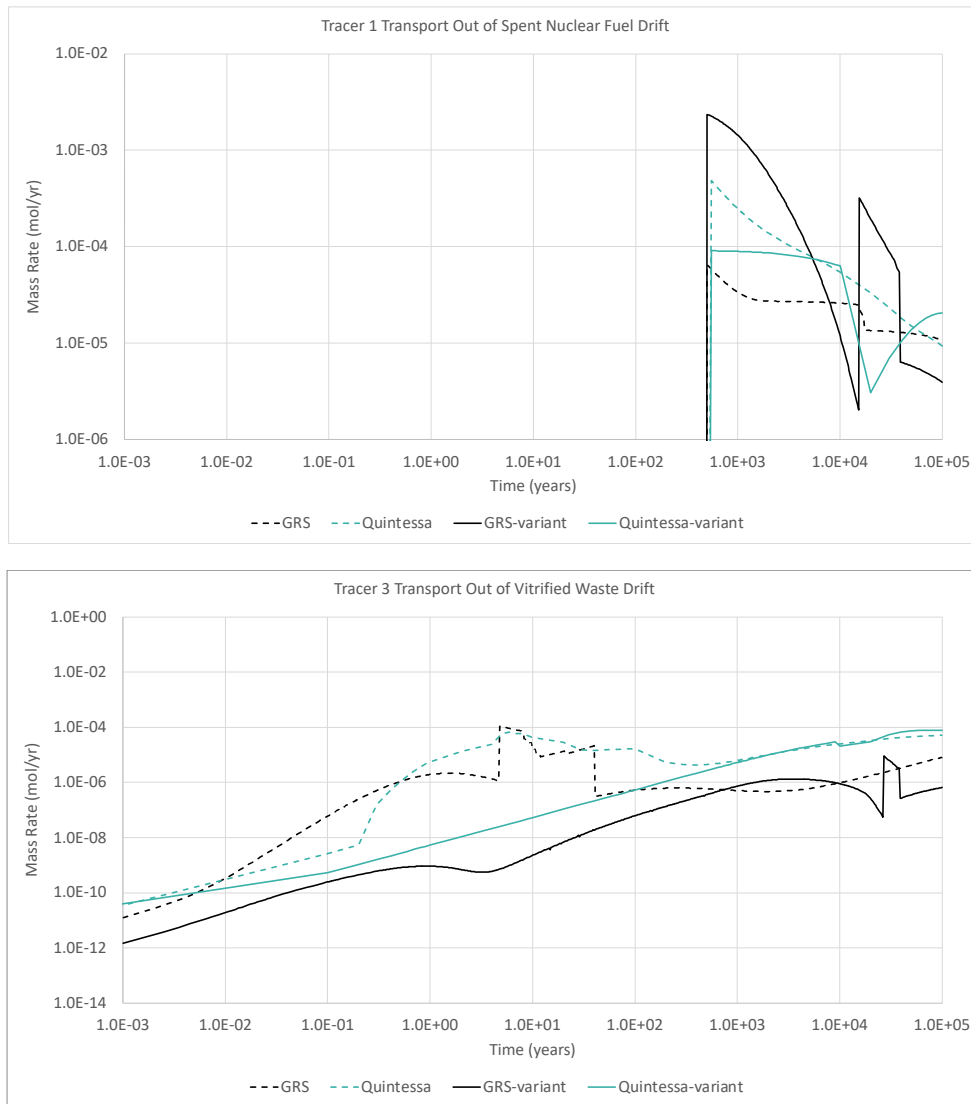
Figure 5-13. Transport of Tracers out of the disposal drifts for the base (dashed lines) and low initial saturation/slow compaction (solid lines) case. Top: Tracer 1 transport out of the SNF drift. Bottom: Tracer 3 transport out of the Vitrified waste drift. Positive transport is defined as flow out of the repository and towards the shaft.

Flow and transport in the seal salt

The liquid flow through the seal salt from the concrete abutments are shown in Figure 5-14. The trend for flow through the seal salt in the GRS and Quintessa models is fundamentally different for the low initial saturation/slow compaction case than the base case. It appears that, rather than fluid being squeezed out of both ends of the seal salt as it compacts saturates, fluid is being pushed through the seal at a slow rate from the infrastructure area towards the waste (negative flow in both subfigures of Figure 5-14). The rate for the Quintessa model is significantly larger than the GRS model, but

both show the same trend. This is likely because the shaft fails at 1,000 years, which saturates the infrastructure area and access tunnels connecting it to the seal prior to significant closure of the seal salt in this variant. The access tunnels are also backfilled with crushed salt, and, having higher water saturation due to the shaft failure, may close earlier than the seal salt and inner repository.

Figure 5-15 shows the transport of Tracer 1 in the seal salt. The GRS low initial saturation/slow compaction model shows arrival of Tracer 1 via diffusive transport earlier than in the base case, while the Quintessa model shows arrival of Tracer 1 later than the base case. Tracer 1 breakthrough in the GRS model is followed by a sharp decline of Tracer 1 transport from the repository side as the seal closes to 2% porosity around 10,000 years. After the seal is compacted, Tracer 1 resumes transport into the seal salt via diffusion in the GRS model, and appears in the Quintessa model. Tracer 1 is transported out of the seal salt only after the flow into the repository generated by compaction has largely died out. For the GRS model, Tracer 1 diffusion out of the seal salt is broadly similar to the base case, but for the Quintessa model, Tracer 1 transport out of the seal towards the shaft is higher than the base case.

Tracer 3 transport through the seal salt for the low initial saturation/slow compaction variant is very similar to the transport of Tracer 1 and is not shown. This represents a very different outcome than the base case, where Tracer 3 arrived one to two orders of magnitude in time earlier than Tracer 1 and showed a more complex trend in the rate of transport into the seal salt from the waste area (see Figure 5-10).
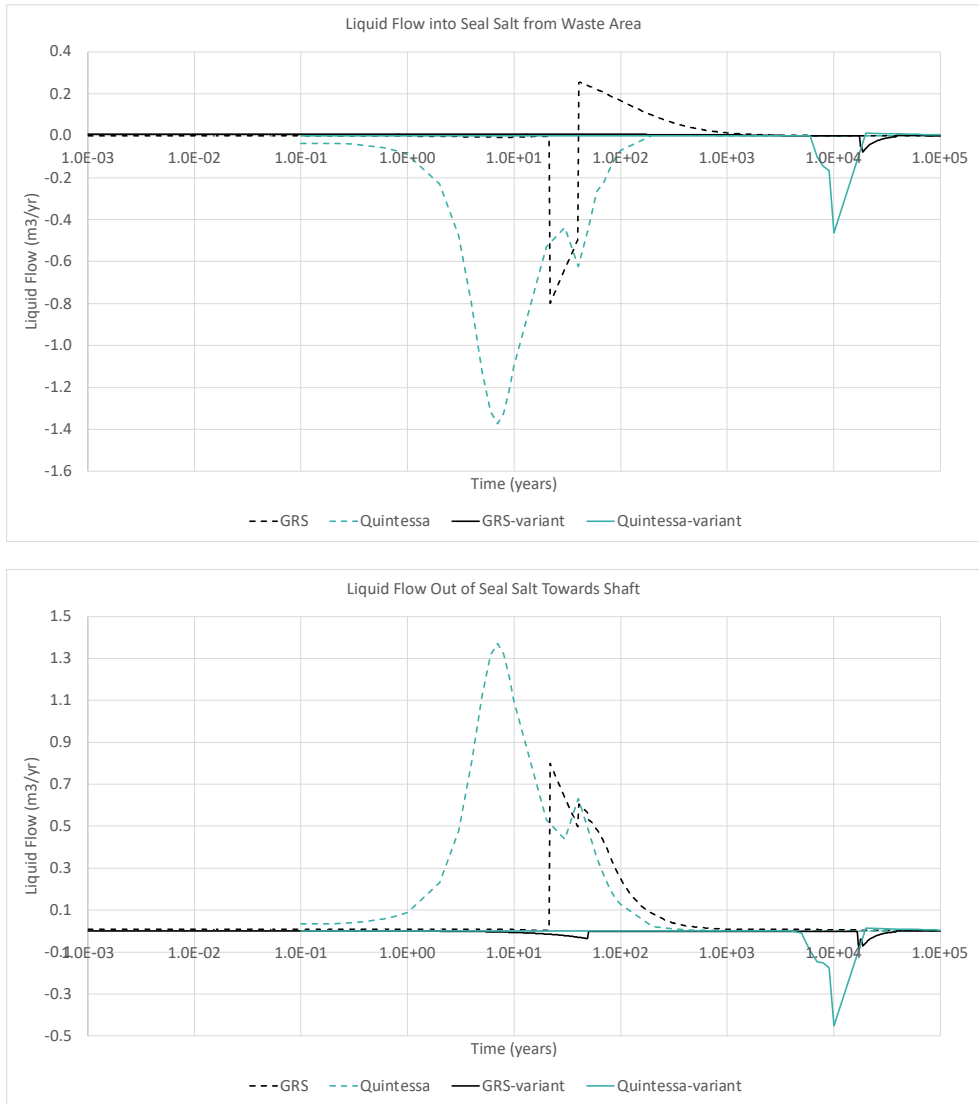
Figure 5-14. Flow quantities for the run of mine salt in the repository seal for the base (dashed lines) and low initial saturation/slow compaction (solid lines) case. Top: Liquid flowrate between the salt and concrete abutment connecting to the waste area. Bottom: Liquid flowrate between the salt and concrete abutment connecting to the infrastructure area and shaft. Positive flow is defined as flow in the direction of the shaft.
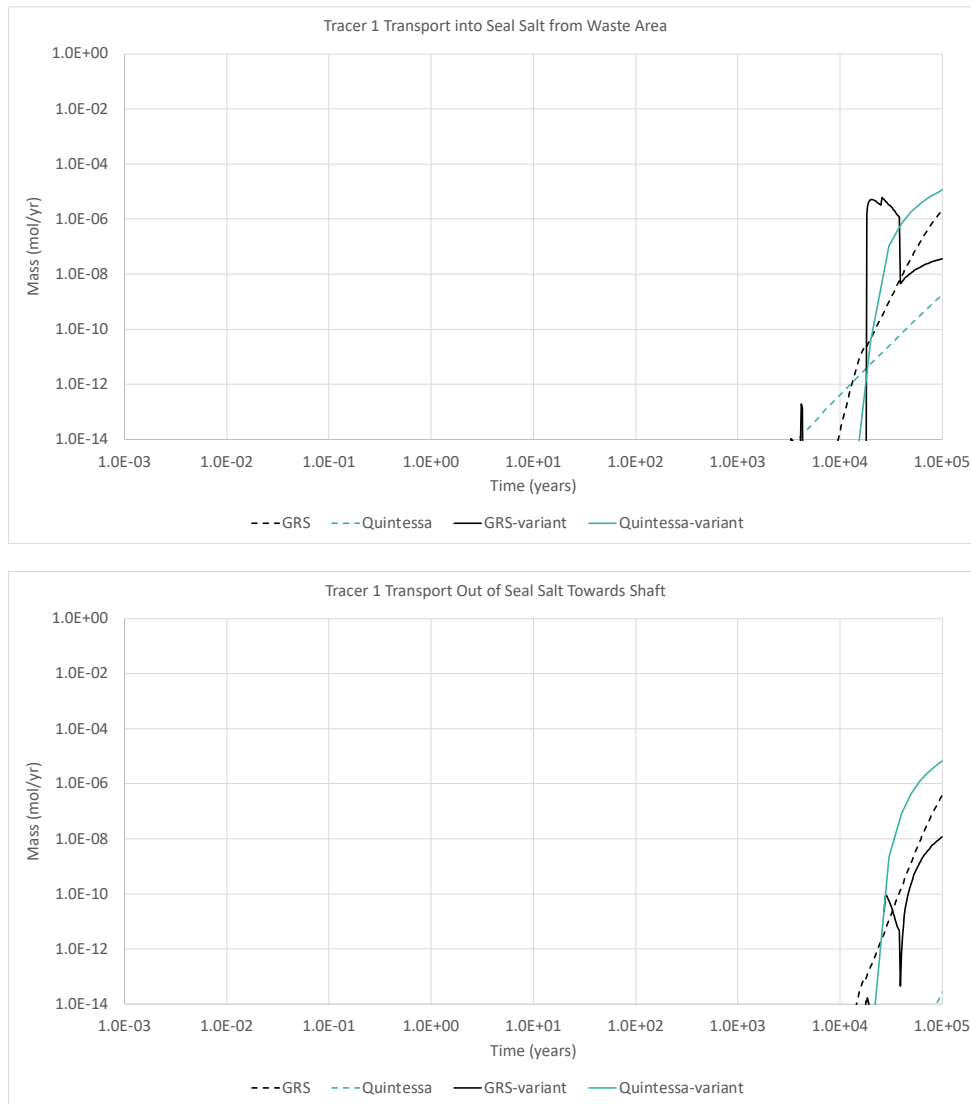
Figure 5-15. Tracer 1 transport for the run of mine salt in the repository seal for the base (dashed lines) and low initial saturation/slow compaction (solid lines) case. Top: Tracer 1 transport between the salt and concrete abutment connecting to the waste area. Bottom: Tracer 1 transport between the salt and concrete abutment connecting to the infrastructure area and shaft.

Flow in the shaft

The flow into the shaft for the low initial water saturation variant is shown in Figure 5-16. Both the GRS and Quintessa models have a delay in the pulse of water flowing down the shaft into the infrastructure area in the low saturation/slow compaction variant as compared with the base case, but the maximum flowrates are very similar to the base case. For the GRS model the total volume of water that flows down the lower shaft is lower, but for the Quintessa the volume is higher, though the difference in the water volumes are not large. The delay in flow down the shaft is because the shaft has

a lower initial saturation (3% vs 35%) so there is less water available in the shaft at the time of shaft seal failure and so less flow.

It is counterintuitive that the total mass of water in the pulse is lower in the low initial saturation/slow compaction model than the base case for the GRS model (see Figure 5-16). The later compaction and lower initial water saturation mean that more porosity is available in the repository at 1,000 years because the crushed salt is only beginning to have significant compaction (see Figure 5-12). However, in both variants the porosity and permeability of all the crushed salt-filled regions (see Figure 2-2) declines much more slowly when the regions become liquid saturated. Further compaction requires squeezing liquid out of the crushed salt. Thus, porosity and permeability in some parts of the repository are lower at later time in the low initial saturation/slow compaction variant because there is less liquid available to hinder reduction of pore volume in crushed-salt segments of the repository. The inner repository is less able to accommodate additional water, because those compartments are fully saturated and squeezing fluid out, and the only flow pathway for the liquid is the low-permeability seal. This acts against the influx of water from the shaft, and may be the cause of the smaller total volume of water flowing down the shaft in the GRS model.
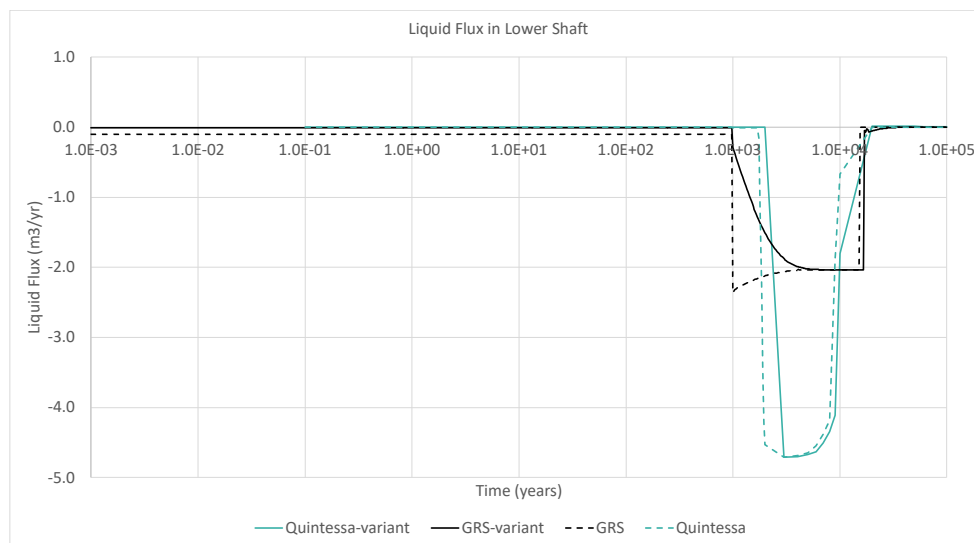
Figure 5-16. Liquid flow in the lower shaft for the base (dashed lines) and low initial water saturation/slow compaction (solid lines) variant. Positive flow is defined as flow from the repository upward toward the surface.

Discussion

The results of the low initial saturation/slower compaction variant suggest that future salt performance assessment models incorporating uncertainty and sensitivity analysis should include investigation of sensitivity to initial liquid saturation and the creep closure model parameters. The GRS and Quintessa models both show that the more realistic initial liquid saturation and the slower and later creep closure of the salt backfill fundamentally changed the fluid flow and tracer transport in the seal salt.

The delayed creep closure has a clear impact on QOI related to the safety function of the seal salt. The later compaction results in very similar transport of the two tracers through the repository in the variant case. Both tracers clearly had diffusion-dominated transport in the seal because of the low flowrates, and Tracer 3 transport into the seal salt is orders of magnitude later in time than the base case. The impact of later compaction on transport of the tracers from the seal salt towards the infrastructure area and shaft is unclear, as the Quintessa model predicts increased transport of the tracers than the base case, and the GRS model predicts similar transport at late time.

5.6.2 Time of shaft seal failure

The failure of the shaft seal at 1,000 years appears to have relatively little impact on fluid flow or radionuclide transport in the base case scenario presented in the task specification. This is believed to be because salt compaction is largely complete in the models with compaction prior to shaft failure and the repository was either saturated or nearly at an equilibrium saturation by 1,000 years when the shaft seal failed. Moreover, the tracers have not yet reached the seal salt. To test this hypothesis two variants were proposed. The first has early failure of the shaft seal at 100 years, while compaction is underway and the second is later failure at 10,000 years, when there are tracers in the seal salt.

Earlier shaft seal failure at 100 years

Three teams participated in the early shaft seal failure variant: DOE, GRS, and Quintessa. Fluid flow down the shaft for the base and 100 year shaft failure case is shown in Figure 5-17. In the GRS model liquid begins to flow down the shaft at 100 years, while in the DOE model it is delayed until 200 years, due to the time it takes to saturate the upper shaft. The Quintessa model doesn't show significant flow of liquid down the shaft until nearly 1,000 years, which consistent the 900-year delay for flow down the lower shaft after shaft seal failure at 1,000 years in the base case. In the DOE model, for the early

shaft failure case, significantly less fluid mass flows down the shaft than the base case, while in the GRS model there is significantly more liquid mass flow down the shaft, and in the Quintessa model it appears to be similar to the base case.

Due to the decoupling of the inner and outer repository, the early shaft seal failure results in essentially no changes in flow or transport in the waste disposal drifts and these QOI are not shown. Fluid flow from the repository into the salt seal is also nearly identical to the base case and not shown. Flow out of the seal salt towards the shaft is slightly higher in the GRS model with early shaft failure, as shown in Figure 5-18 but is nearly identical in the other two models.

Tracer 1 and Tracer 3 transport in the seal salt are also very similar for the early shaft seal failure scenario and the base case. The only visible difference is that the GRS transport of Tracer 1 into and out of the seal is slightly lower with the early shaft seal failure, so these are not shown.
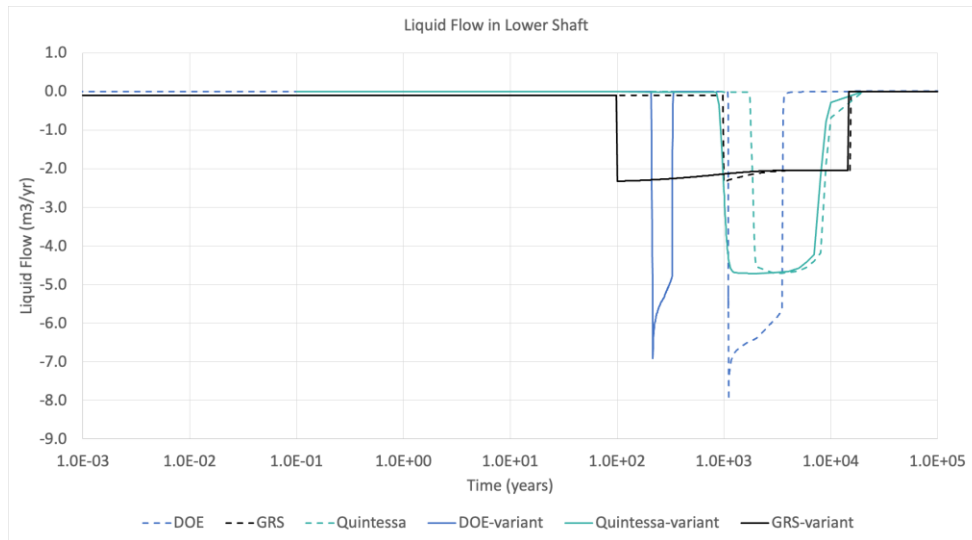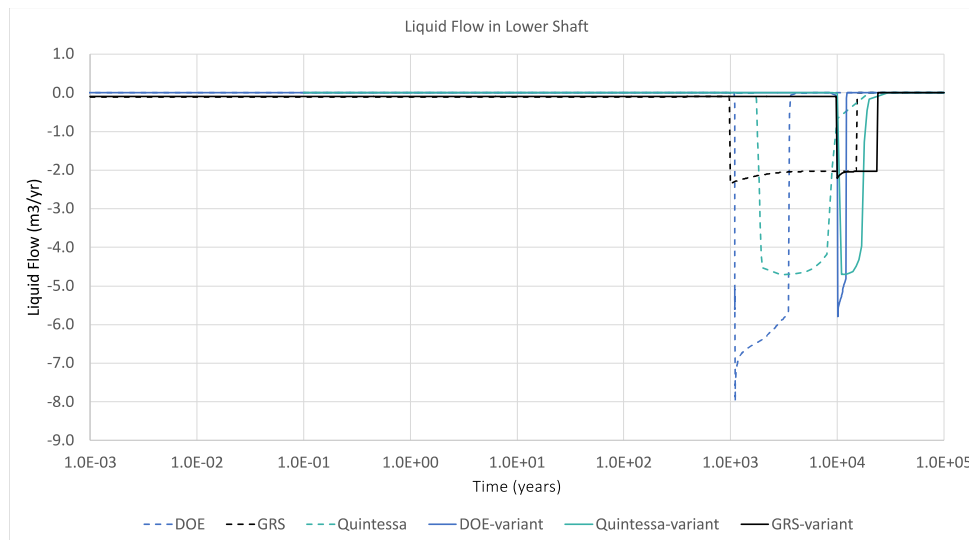

Figure 5-17 Liquid flow in the lower shaft for the base and shaft failure at 100 years case. Positive flow is defined as flow from the repository upward toward the surface.
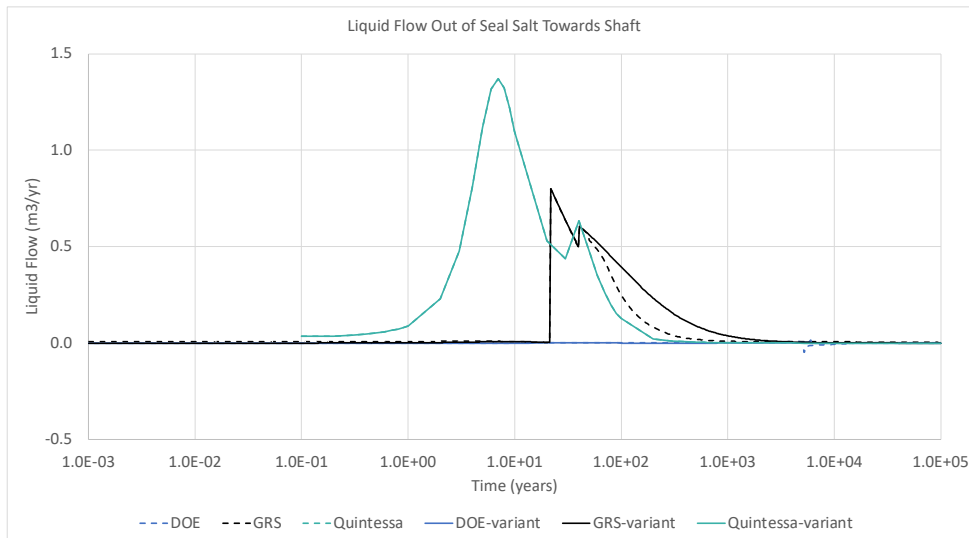
Figure 5-18. Liquid flowrate between the salt and concrete abutment connecting to the infrastructure area and shaft for the base (dashed lines) and shaft failure at 100 years case (solid lines). Positive flow is defined as flow in the direction of the shaft.

Later shaft seal failure at 10,000 years

The same three teams participated in the late shaft seal failure variant: DOE, GRS, and Quintessa. Fluid flow down the shaft for the base and 10,000 year shaft failure case is shown in Figure 5-19. In the GRS and DOE models liquid begins to flow down the shaft around 10,000 years, The Quintessa model again has a 900 year delay due to the shaft resaturation time before there is flow down the shaft at 11,000 years. In the DOE model, for the later shaft failure case, less fluid mass flows down the shaft than the base case, while in the GRS and Quintessa models the fluid volume flowing down the shaft is very similar to the base case.

As with the early shaft failure case, due to the decoupling of the inner and outer repository region there is little change in the drifts or flow through the seal salt, so these QOI are not shown.

Tracer 1 transport into the salt from the repository (not shown) shows only modest changes, with the GRS model showing slightly higher Tracer 1 transport through the seal salt at most times. Tracer 3 transport through the seal salt is also not shown because it is the same as the base case for the GRS and Quintessa, but Tracer 3 diffusion in the DOE model is below the rates shown on the plot. This is believed to be because the vitrified waste drifts are not yet liquid saturated at 10,000 years in the DOE model and Tracer 3 is not yet diffusing out of the vitrified waste drifts. The influx of water from the shaft flows through the repository and pushes Tracer 3 back into the far ends of the vitrified waste drifts with the water. This does not occur in the earlier shaft seal failure scenarios because the concentration of Tracer 3 is still low at earlier time.

Figure 5-19 Liquid flow in the lower shaft for the base and shaft failure at 10,000 years case. Positive flow is defined as flow from the repository upward toward the surface.

Discussion

The early and late shaft seal failure scenarios change the timing of the influx of water from the surface, and also impact the volume of water that floods the repository. The early shaft failure cases have an inconsistent trend between the models, with DOE having less flow down the shaft and GRS significantly more. The later shaft seal failure scenario results in similar (GRS and Quintessa) or less (DOE) water flowing down the shaft.

Though the timing of shaft seal failure results in some changes in flow in the shaft, early failure has little impact on fluid flow and tracer transport in the inner repository region. Transport of Tracer 1 with early or late shaft failure was similar for all the models. Later shaft seal failure reduced the transport of Tracer 3 in the DOE model, but not the GRS and Quintessa models with compaction.

The differences in the three model results are not fully consistent with each other, so it is difficult to draw conclusions about the differing impact of early vs late shaft seal failure on repository performance. However, with the repository seal operating as designed, shaft seal failure at 100, 1,000 or 10,000 years does not appear to have a significant impact on flow and transport in the inner repository where the waste is located due to the decoupling of the inner and outer repository. Furthermore, in all three scenarios the repository provides containment during the simulated period of 100,000 years.

6   Conclusions and future work

6.1 Conclusions

Task F2-salt of DECOVALEX-2023 is a comparison of the models and methods for a simplified post-closure performance assessment model of a deep geologic repository in domal salt host rock over 100,000 years. Five teams participated in the task: BASE, COVRA, DOE, GRS, and Quintessa. The detailed task specification was updated continuously with contributions from all teams as complexity has been added to the conceptual model.

Task F2-salt focuses on forward PA modelling of a simplified repository system and its subsystems. This final report focuses on a comparison of 21 QOI, which are performance measures of the flow and radionuclide transport in the repository, and the ability of the repository system to isolate radionuclides through containment and retardation. Teams chose to include or neglect some processes or feedback between processes, to use a more or less mechanistic model, and to couple processes more or less tightly. All teams make simplifying assumptions in their models relative to the task specification. The simplifications made by all teams are simulating on a half-symmetry domain and not meshing individual waste packages. The other most common simplifications are omitting the geosphere, reducing dimensionality of the model, and simplifying the salt creep-closure model.

Despite differences in the modelling strategies developed by participating teams (see Table 4-1 to Table 4-5), all models indicate that salt compaction and radionuclide diffusion are key physical processes in the simplified repository system. All models also showed the engineered barriers are effective for containing the radionuclides in the repository. The repository models are largely decoupled at the seal salt into an inner model, containing the disposal drifts, access tunnels, and concrete abutment on the repository side of the salt seal, and an outer model, containing the infrastructure, shafts, and concrete abutment on the infrastructure side of the salt seal (see Figure 2-2).

For the four team models that include a reduction in porosity as a result of creep closure (BASE, COVRA, GRS, and Quintessa), the differences in the rate of salt compaction have a large impact on fluid flow in the repository during the first few hundred years. All four models indicate that most of the flow in the inner repository is driven by salt compaction, that liquid is pushed out of the waste disposal drifts by compaction, and that liquid is then squeezed out of the seal salt in both directions into the adjacent

concrete abutments. However, the timing of the liquid flow and flow rate are determined in large part by the timing and rate of the porosity reduction. The DOE team has resaturation of the inner model by influx of fluid from the geosphere, which is a much slower process. The liquid flow in the outer model is driven by the influx of surface water caused by the shaft seal failure in every team model.

The QOI related to radionuclide transport that are compared in this report were Tracer 1 (present only in the SNF) and Tracer 3 (present only in the vitrified waste). These are a high mobility scenario because they are ideal tracers. They also provide information about the source of contaminants reaching the seal that can't be extracted from the radionuclides in the ^{238}U decay chain, which is present in both types of waste. Transport of both tracers is largely diffusive in every team model, with indications of some contribution of advective transport of Tracer 1 out of the SNF drift in the BASE, GRS, and Quintessa models. The rate of tracer diffusion throughout the repository is determined by a combination of the effective diffusion coefficients and how they interacted with the reduction in porosity and numerical dispersion, which is different for every model and difficult to accurately quantify at this point. Tracer transport takes place on very different timescales in the models, though the trends are qualitatively similar. Tracer 1 and Tracer 3 have very different tracer transport behaviour both at the drifts and at the seal salt, likely due to the different release mechanisms from the waste forms.

Two variant cases are also considered by some of the teams to test the impact of the high initial saturation and rapid creep-closure of the salt, and the timing of the shaft seal failure. The low initial saturation/slow compaction case results are very different from the base case with flow through the seal salt reduced by orders of magnitude, and the models giving differing predictions on the impact on tracer transport. This comparison highlights the importance of considering uncertainty in both initial conditions and parameters in the creep closure model in future stochastic simulation cases. The early and late shaft failure cases demonstrate that, though the timing of the shaft seal failure had a large impact on flow in the outer repository, the inner repository is relatively unaffected because of the effective hydraulic and transport barrier provided by the repository seal. This highlights the importance of the seal salt as the primary barrier between the waste drifts and the surface, and indicates the importance of further investigating assumptions around the effectiveness of the seal as a barrier.

6.2 Current and future work

In addition to the overview, two collaborative posters were presented by the DECOVALEX Task F2 teams for the DECOVALEX symposium Nov 14-16, 2023 in Troyes, France with the goal of turning them into journal publications in the coming months. The first paper, led by GRS, is a more detailed comparison of the levels of abstraction participating team models, the value of abstraction for simplifying models and speeding calculations, and the inherent trade-offs of utilizing lower fidelity models. This paper has been submitted for peer-review. The second paper, led by COVRA, investigates the impact of engineering decisions on repository performance. In particular, they plan to investigate the impact of changes in the design of the concrete seals, salt seal, and infrastructure area.

A second round of this task has been funded for DECOVALEX-2027 in conjunction with Task F1 on crystalline PA modelling. The future round includes physics that are believed to be important to repository performance that were left out of the current conceptual model. The next stage will include waste package heating, improved modelling of salt creep closure, and additional comparisons of coupled-process sub-models. Sensitivity analysis and uncertainty quantification will also be an integral part of the DECOVALEX-2027 task. Participants will create a set of uncertain inputs for the reference case simulations, propagate these uncertainties in a set of realizations, and conduct sensitivity analyses on the simulation results. As indicated by the low initial saturation/slow compaction variant and the importance of the seal salt in isolating the inner repository, these inputs should include initial saturation, creep convergence parameters, parameters impacting seal performance (or failure), as well as other uncertain parameters.

7 Planned and completed publications

Table 7-1 gives the planned and completed publications under this task, correct at the time of writing.

Table 7-1: Planned and completed journal and conference papers for Task F2.

Author(s)	Title	Journal/ Conference	Status
Lead: Tara LaForce (DOE) To include: all teams	Comparing Modeling Approaches for a Generic Nuclear Waste Repository in Salt	DECOVALEX-2023 Special Issue	Writing draft
Lead: Tanja Frank (GRS) DOE, GRS, Quintessa	Value of abstraction – learning about the modelling and consequences of choices	DECOVALEX-2023 Special Issue	Submitted
Lead: Jeroen Bartol (COVRA) Tentatively to include all teams	Study details of different processes/engineering decisions. –practical learning about engineering and what would we build	DECOVALEX-2023 Special Issue	Collating simulation results
Lead: Carlo Dietl (BASE) Teams TBD	Trust in Models	Safety of Nuclear Waste Disposal	Concept stage

8   Acknowledgements

9 References

Batu, V. 2006. *Applied Flow and Solute Transport Modelling in Aquifers*. CRC Taylor and Francis.

Bertrams, N., Bollingerfehr, W., Eickemeier, R., Fahland, S. Flügge, J., Frenzel, B., Hammer, J., Kindlein, J. Liu, W., Maßmann, J., Mayer, K.-M., Mönig, J., Mrugalla, S., Müller-Hoeppe, N., Reinhold, K., Rübel, A., Schubarth-Engel- schall, N., Simo, E., Thiedau, J., Thiemeyer, T., Weber, J.R., Wolf, J. 2020. *Grundlagen zur Bewertung eines Endlagersystems in flach lagernden Salzformationen (S1) - Ergebnisse aus dem Vorhaben RESUS*. BGE TEC 2020.

Beuth, T., Bracke, G., Buhmann, D., Dresbach, C., Keller, S., Krone, J., Lommerzheim, A., Mönig, A., Mrugalla, S., Rübel, A., and Wolf, J. 2012. *Szenarienentwicklunng: Methodic und Anwendung. Bericht zum Arbeitspaket 8. Vorläufige Sicherheitsanalyse für den Standort Gorleben*, Gesellschaft für Anlagen und Reaktorsicherheit (GRS) mbH, GRS-284, Köln, ISBN 978-3939355-60-1.

Bollingerfehr, W., Bertrams, N., Buhmann, D., Eickemeier, R., Fahland, S., Filbert, W., Hammer, J., Kindlein, J., Knauth, M., and Wenting, L. 2018. *Concept developments for a generic repository for heat-generating waste in bedded salt formations in Germany*. Synthesis Report (No. BGE TEC 2018-13). BGE TECHNOLOGY GmbH.

Bollingerfehr, W., Buhmann, D. and Doerr, S. 2017. *Evaluation of methods and tools to develop safety concepts and to demonstrate safety for an HLW repository in salt*. Final Report (No. TEC-03-2017-AB). BGE TECHNOLOGY GmbH.

Bollingerfehr, W., Filbert, W., Pöhler, M., Tholen, M., and Wehrmann, J. 2008. *Konzeptionelle Endlagerplanung und Zusammen- stellung des endzulagernden Inventars (Design planning of a final repository and summary of the inventory to be stored) – Project ISIBEL*, Peine, April 2008.

Hammond, G.E., Lichtner, P.C., & Mills, R.T. 2014. *Evaluating the performance of parallel subsurface simulators: An illustrative example with PFLOTRAN*. Water Resources Research 50:208–228.

Hirsekorn, Rolf-Peter, Brigitte Boese, Dieter Buhmann. (1999). *LOPOS: Programm zur Berechnung der Schadstofffreisetzung aus netzwerkartigen Grubengebäuden*. GRS Germany, GRS - 157

Kolditz, O., H. Shao, W. Wang, and S. Bauer 2015. *Thermo-Hydro-Mechanical-Chemical Processes in Fractured Porous Media: Modelling and Benchmarking Closed-Form*

Solutions (O. Kolditz, H. Shao, W. Wang, & S. Bauer Eds.). Switzerland: Springer International Publishing.

LaForce, T., Bartol, J., Becker, D., Benbow, S., Bond, A., Dietl, C., Frank,T., Magri, F., Jayne, R., Leone, R., Stauffer, P., Stein, E., and Wolf, J., 2022. *DECOVALEX-2023 Task F2-Salt Interim Report*, Sandia National Laboratories, Albuquerque, NM.

LaForce, T., Jayne, R.S., Leone, R., Mariner, P., Stein, E., Nguyen, S., and Frank, T. 2023. D*ECOVALEX-2023 Task F Specification Revision 10.* SAND2023-04005R. Sandia National Laboratories, Albuquerque, NM.

Ministry of infrastructure and the Environment, 2016. The national programme for the management of radioactive waste and spent fuel, p. 61.

Noseck, Ulrich, Wernt Brewitz, Dirk-Alexander Becker, Dieter Buhmann, Christine Fahrenholz, Eckhard Fein, Peter Hirsekorn, Sven Keesmann, Klaus-Peter Kröhn, Ingo Müller-Lyda, André Rübel, Anke Schneider, Richard Storck. (2005). *Wissenschaftliche Grundlagen zum Nachweis der Langzeitsicherheit von Endlagern.* GRS, Germany, GRS-204.

OCRWM. 1990. *Performance Assessment Strategy Plan for the Geologic Repository Program*. DOE-RW-0266P. U.S. Department of Energy, Office of Civilian Radioactive Waste Management, Washington, DC.

Reiche, T. 2016. RepoTREND – *Das Programmpaket zur integrierten Langzeitsicherheitsanalyse von Endlagersystemen.* GRS-413, Gesellschaft für Anlagen- und Reaktorsicherheit (GRS) gGmbH, ISBN 978-3-944161-95-2, BMWi-FKZ 02E10367, Braunschweig.

Stein, E. R., 2020. D*ECOVALEX-2023 Task F Specification.* SAND2020-4598 O. Sandia National Laboratories, Albuquerque, NM.

Appendix A: BASE

A.1 Introduction

A.1.1 Brief introduction to team

The Federal Office for the Safety of Nuclear Waste Management (BASE) is the German government's central authority for safely dealing with the legacy of nuclear energy. BASE performs regulatory, licensing and supervisory tasks related with disposal, storage, handling and transport of high-level radioactive waste (HLW) (https://www.base.bund.de/EN/bfe/about-base/about-base_node.html).

BASE provides specialist expertise to supervise nuclear safety and advises the Federal Ministry for the Environment, Nature Conservation and Nuclear Safety (BMUV) on disposal of nuclear waste. Among its various tasks, BASE regulates the site selection procedure for a final repository for HLW and coordinates public participation in the process.

To carry out its tasks in line with the scientific and technological state-of-the-art, BASE engages in academic research. The office initiates and supports research projects in the field of nuclear disposal safety and conducts its own research. This involves a variety of aspects from the natural sciences, technology as well as social sciences.

BASE was set up in 2014 and has continued to develop since 2016.

A.1.2 Why team is participating

Site selection for a future HLW repository in Germany is currently underway. Besides crystalline rock and claystone, salt rock is one of three host rocks under consideration. Safety assessment (SA) is an important element of the decision-making process as stipulated by the Site Selection Act (https://www.bmuv.de/en/law/repository-site-selection-act-standag).

In this context, BASE is developing a comprehensive set of numerical SA tools with a focus on reliability and transparency.

BASE is one of the funding organizations for the current phase of DECOVALEX-2023 (running from 2020 to 2023) and actively contributes to Task F of the project (https://www.base.bund.de/DE/themen/fa/soa/projekte-aktuell/projekte-

– "Beteiligung an der internationalen Forschungskooperation DECOVALEX") with the aim to:

- Exchange state-of-the-art modelling approaches and methodologies

- Further develop competence in process modelling (within Task F2: with a focus on safety-relevant processes in HLW repository hosted in a salt rock)

- Test functionalities, identify strengths and development needs of safety and performance assessment codes

- Develop a work-flow for large-scale deployment of the PFLOTRAN code as a potential SA tool

A.2 Reference case construction

A.2.1 Software (versions), method of calculations

Simulations were performed using the PFLOTRAN code version 4.0 (downloaded on 04.11.2022) using PETSC version 3.16.2.

PFLOTRAN is an open source, state-of-the-art massively parallel subsurface flow and reactive transport code. PFLOTRAN uses the finite volume method to solve a system of generally nonlinear partial differential equations describing multiphase, multicomponent and multiscale reactive flow and transport in porous materials (www.pflotran.org). Detailed information regarding the technical capabilities of the code can be found in Hammond et al. (2012, 2014 and 2019).

A.2.2 Flow and transport model construction

How the space is represented and gridded

Full model geometry is shown in (Figure A.1). For computational efficiency, the geometry ignores the presence of the host rock and of individual deposition holes within the deposition drifts. Furthermore, advantage is taken of a vertical plane of symmetry in the disposal system (Figure A.1), which allows the geometry to be reduced to a half.

The half-size computational geometry (indicating main engineered system elements) and the finite volume grid (consisting of 4910 tetrahedral cells) is shown in Figure A.2 (left and right, respectively).
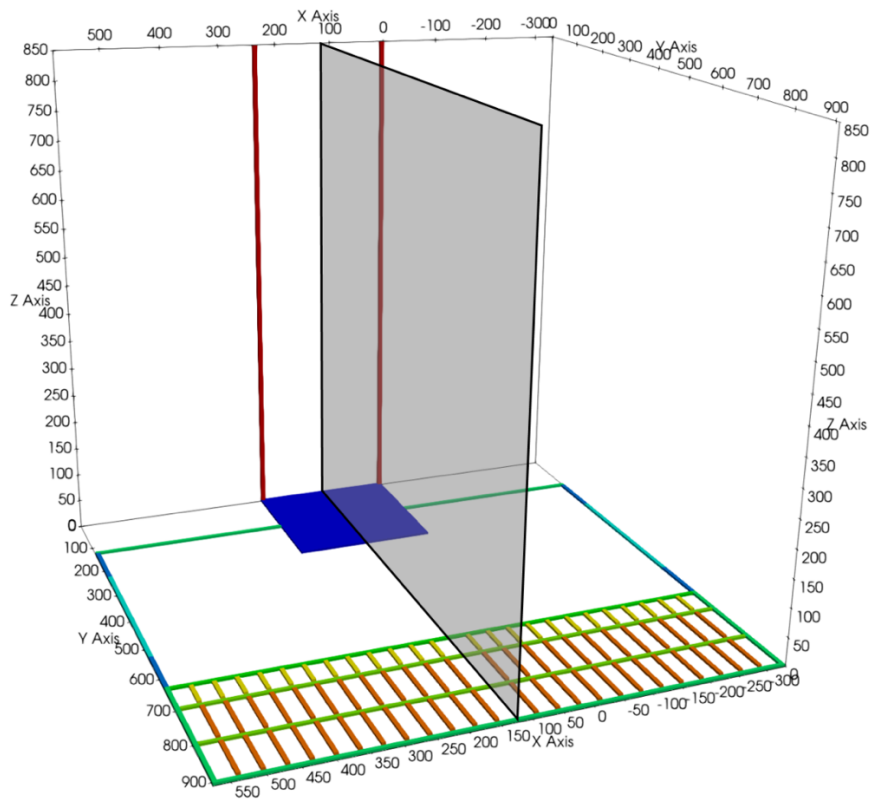
Figure A.1: Full model geometry indicating a vertical symmetry plane (grey) used for the reduction to a half-size computational geometry.
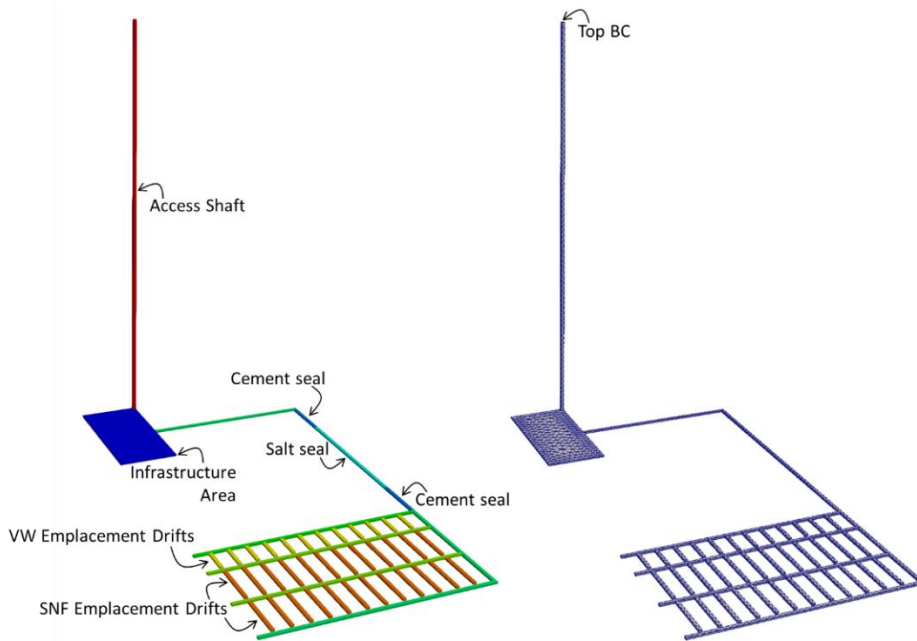
Figure A.2: Half-size computational model geometry (left) and the corresponding finite volume grid (right) indicating the position of the top boundary condition (Top BC). VW – vitrified waste, SNF – spent nuclear fuel.

Flow and transport models

The flow model simulates single phase, variably water saturated isothermal conditions using the Richard's model (www.pflotran.org/documentation/theory_guide/mode_richards.html). Model parameterization (e.g. characteristic curves) is carried out as per Task Specification.

Solute transport is assumed to occur in the liquid phase under isothermal conditions due to advection and diffusion (https://www.pflotran.org/documentation/theory_guide/mode_reactive_transport.html). Solute transport is coupled to chemical reactions using a global implicit approach. No aqueous activity and speciation models are applied.

Liquid flow and solute transport are solved sequentially. The coupling scheme allows chemical reactions to alter material properties such as porosity, permeability, and tortuosity thereby altering the flow field. This functionality is used to simplistically simulate salt convergence as discussed in more detail in Section A.2.3.

Initial and boundary conditions (if different from base case)

As indicated earlier in this section, presence of the salt host rock is ignored. This is done in order to decrease the computational burden on model solution and is based on the expectation (later corroborated by preliminary calculations by other teams) that, owing to very low permeability, the impact of the host rock on the system's hydraulic evolution is small or negligible. Therefore, fluid flow and solute transport occur exclusively within the interconnected elements of the disposal system (drifts, tunnels, seals, infrastructure area and access shaft).

Initial relative liquid saturation is set at 35 % in the access shaft and 20 % elsewhere in the repository system. Initial solute tracer/radionuclide concentrations are set at 10^{-20} mol/L_{water} – an arbitrarily small number representing "zero concentration".

For solving the flow and transport models, all boundaries are assumed to be closed (no flux), except for the top of the access shaft (located at the terrain surface level, indicated in Figure A.2, right). For solving flow, this boundary is defined to be at full liquid saturation throughout the simulation. For solving transport, the boundary is held at the initial "zero concentration" (represented by an arbitrary concentration of 10^{-20} mol/L_{water}) at all times.

Implementation of tracer/radionuclide source terms, solubility limits, partitioning

Source terms (including canister breach times, tracer/radionuclide initial inventories, release mechanisms and release rates) are implemented individually for SF (spent fuel) and VW (vitrified waste) as per Task Specification. Where applicable, radionuclide decay and decay chains are implemented in agreement with Task Specification.

Radionuclide decay occurs across all phases, i.e. in the solid waste as well as in the dissolved and precipitated forms (where applicable). To represent the source term, radionuclide partitioning and decay in PFLOTRAN, the "Waste Form" (https://documentation.pflotran.org/theory_guide/pm_waste_form.html) and "UFD Decay" (https://documentation.pflotran.org/theory_guide/pm_ufd_decay.html) process models are used.

A.2.3 Creep Closure

Basic Approach

Salt creep (convergence) is represented simplistically by reducing material porosity in a pre-defined manner based on results obtained externally from the code LOPOS as provided by the team from the Gesellschaft für Anlagen- und Reaktorsicherheit (GRS gGmbH). Porosity changes feed directly into advective flow and transport (via intrinsic permeability) and diffusive transport (via the effective diffusion coefficient).

Porosity changes are implemented in PFLOTRAN by means of kinetic reactions of "dummy" minerals, whereby the mineral precipitation rates are calibrated so as to obtain the desired rates of porosity reduction as a function of time. Importantly, this approach ensures mass conservation during porosity reduction. Therefore, for example, water pressurization due to salt convergence is represented.

Calibration of the model is briefly described in the next subsection.

Model Calibration

As discussed, porosity reduction in the PFLOTRAN model is roughly approximated based on the results of the LOPOS model. The LOPOS model allows salt porosity evolution to be calculated at discrete locations over time. As part of the task effort, GRS provided average porosity time series for selected salt components of the disposal system (Figure A.3) – refer to Task Specification for further details.

The PFLOTRAN porosity reduction model does not aim to reproduce the results of LOPOS in any specific detail – rather, it reflects general trends and value ranges. For simplicity, only two porosity reduction evolutions are considered in the PFLOTRAN model: (i) one specifically for the salt seal ("PFLOTRAN salt seal") and (ii) one for all other salt components (e.g. disposal drifts and connecting tunnels – "PFLOTRAN salt else"), as shown in Figure A.3.
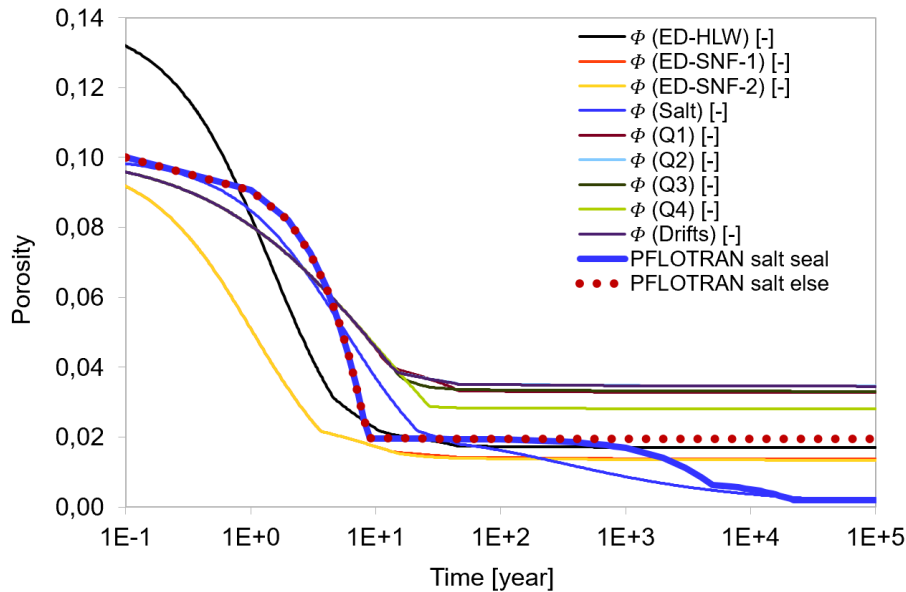

Figure A.3: Time evolution of average porosity in salt at selected locations as calculated by the LOPOS model (labelled with "ɸ" – refer to the task specification document for explanations) and simulated in the PFLOTRAN model for the salt seal ("PFLOTRAN salt seal") and for all other salt materials ("PFLOTRAN salt else").

Porosity changes are dynamically coupled to intrinsic permeability. The PFLOTRAN implementation of permeability update due to porosity changes (https://www.pflotran.org/documentation/theory_guide/mode_reactive_transport.html#changes-in-material-properties) differs from that stipulated in Task Specification (see Equation 4-20). Therefore, the PFLOTRAN implementation was parameterized so as to match the results of the Task Specification formula. Figure A.4 presents a comparison of salt seal intrinsic permeability calculated according to Task Specification ("Eq Task Spec") and the calibrated PFLOTRAN implementation ("Eq PFLOTRAN") – both calculated externally (in a spreadsheet) using as input the PFLOTRAN average porosity evolution of the salt seal shown in Figure A.3. In addition, average intrinsic permeability of the salt seal as calculated by the PFLOTRAN base case model is presented ("PFLOTRAN out"). The results show excellent agreement.
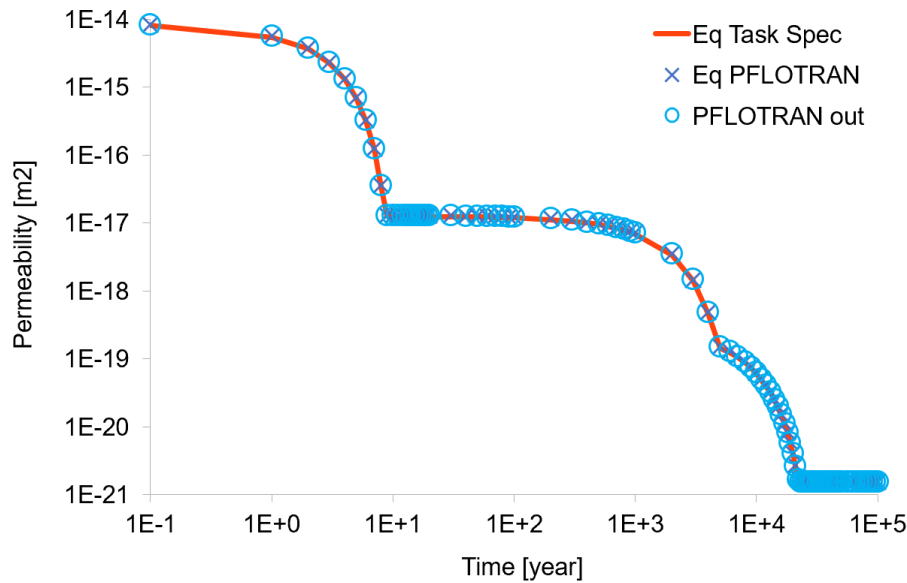
Figure A.4: Salt seal permeability over time calculated as a function of porosity according to: Task Specification ("Eq Task Spec"), the equation used in PFLOTRAN ("Eq PFLOTRAN") and the base case model ("PFLOTRAN out"). Refer to text for explanations.

A.2.4 Simplifications/divergence from the task specification in detail

During model development, some simplifications were necessary to avoid numerical issues (such as slow convergence) and speed up the overall efficiency of the numerical solution given available computational resources (e.g. max. 10 processor threads used in parallel). These simplifications can be categorized as follows:

a) Processes: Stage 1+2 (flow, radionuclide mobilization and transport, and salt consolidation – refer to Task Specification) are considered. Additional processes (heat flow, non-isothermal conditions, gas generation) will be implemented in future iteration of the project.
   o Variably-saturated liquid flow is represented using the Richards model (refer to Section A.2.2 for further details)

b) Geometric: all simplifications made relative to Task Specification are discussed in Section A.2.1.

c) Flow and transport model parameterization:
   o Homogenous shaft material model is used (bulk shaft material properties as per Tables 4-7 and 4-8 of Task Specification)

d) Flow and transport initial and boundary conditions:

- Initial radionuclide inventories are averaged across the entire volume of deposition drifts

  e) Representation of salt creep: salt convergence is represented in a simplified manner as discussed in Section A.2.3.

A.3 Reference Base Case Results

A.3.1 Flow Modelling Results

The overall hydraulic evolution of the repository system is illustrated in Figure A.5 (relative liquid saturation of the repository system at selected times) and Figure A.6 (average relative liquid saturation of the whole repository system and of selected components as a function of time). In addition, fluid fluxes at selected locations (refer to Task Specification for details) are presented (Figure A.7, Figure A.8, and Figure A.9).

The following main features of the repository system's hydraulic evolution can be distinguished:

- Rapid liquid saturation (approaching unity) of salt during the initial ca. 10 years due to salt convergence (Figure A.5 and Figure A.6)
- Salt convergence drives gradients in saturation (Figure A.5and Figure A.6) and liquid pressure (not shown) between the converging salt and cement seals
- As a result, liquid flows from the salt (e.g. salt seal, access and disposal tunnels) towards the cement seals Figure A.7 and Figure A.8), causing portions of the former to de-saturate (Figure A.5 and Figure A.6)
- Shaft failure at 1 000 years drives rapid liquid ingress (Figure A.9), causing the shaft and infrastructure area to saturate, while liquid saturation of salt elements beyond the seal (near waste) is impeded by the seal (Figure A.5 and Figure A.6)
- After ca. 10 000 years, relative liquid saturation of the whole system slowly approaches unity, but remains incomplete at 100 000 years (Figure A.6)

In summary:

- The seal constitutes a barrier that hydraulically decouples the "inner" (deposition drifts and tunnels) and "outer" (access shaft and infrastructure area) parts of the repository system

- Liquid saturation of the inner parts of the repository system is driven primarily by salt convergence
- Liquid saturation of the outer parts of the repository system is driven by water inflow from the surface (especially following shaft failure)
- Water re-distribution transients are observed within and near the seal (especially at material interfaces)
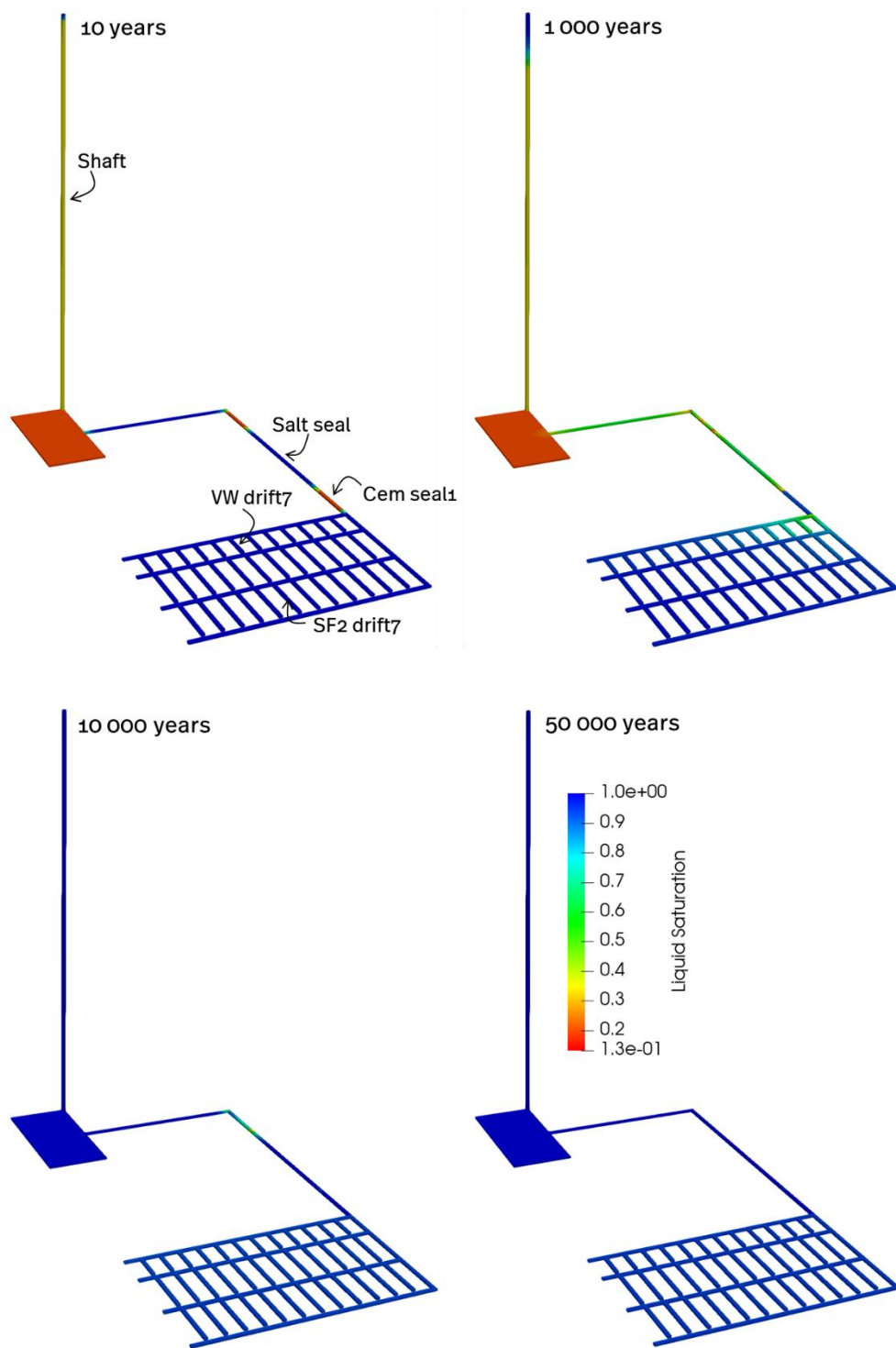
Figure A.5: Relative liquid saturation of the repository system at selected times (10, 1 000, 10 000 and 50 000 years). Initial saturation is 0.35 in the shaft and 0.20 elsewhere.
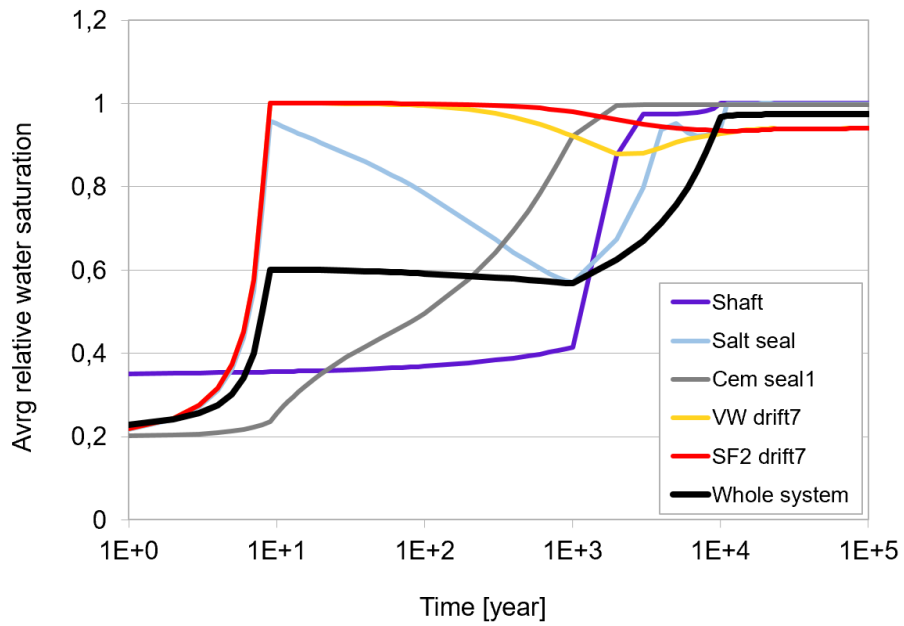
Figure A.6: Average relative liquid saturation of the whole repository system ("Whole system") and of selected components as a function of time. Refer to Figure (top, left) for explanation on labels.
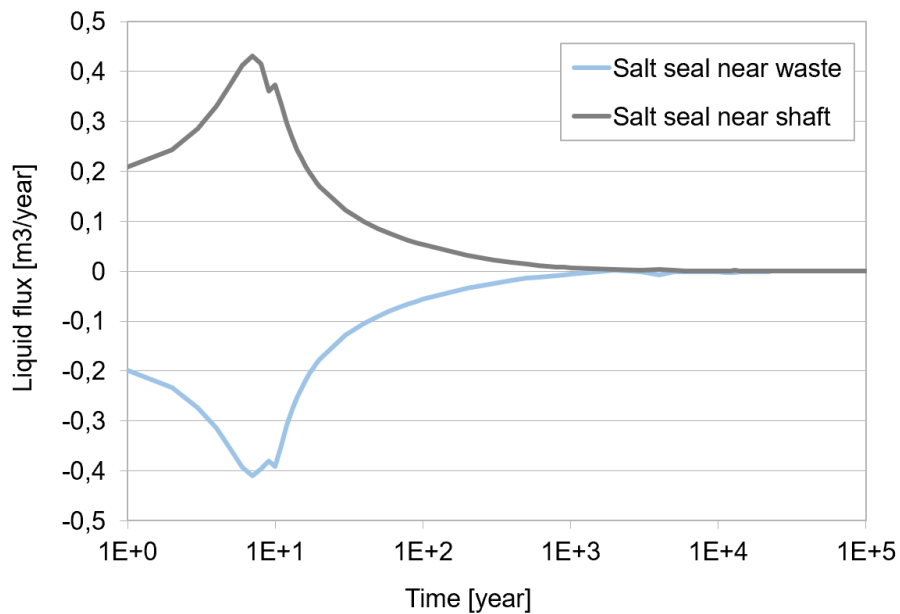
Figure A.7: Liquid fluxes [m3/year] at the salt seal interfaces with the cement seals near the waste ("Salt seal near waste") and near the shaft ("Salt seal near shaft") – refer to Task Specification for details. Positive values indicate flow from waste towards shaft.
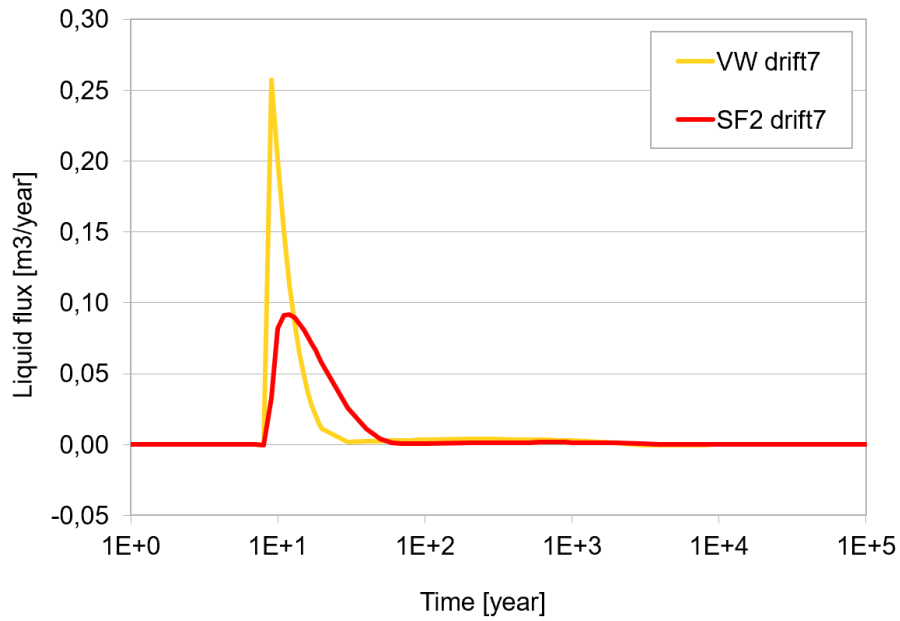
Figure A.8: Liquid fluxes [m3/year] from the vitrified waste drift 7 ("VW drift7") and from the spent fuel 2 drift 7 ("SF2 drift7") across their intersection with the access drifts – refer to Task Specification for details. Positive values indicate flow from waste towards shaft.
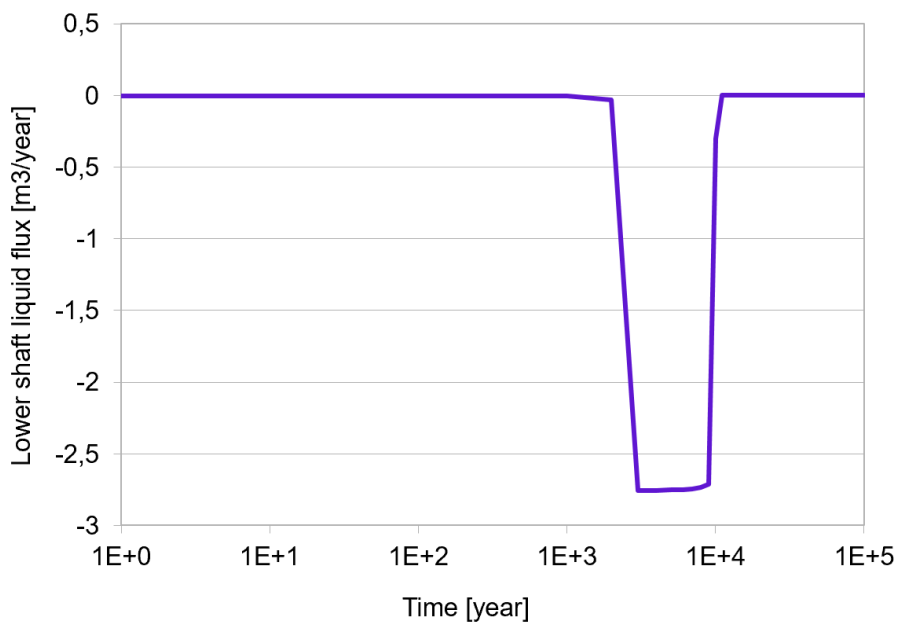
Figure A.9: Liquid flux [m3/year] across a plane in the shaft 25 m above the ceiling of the infrastructure area – refer to Task Specification for details. Positive values indicate flow from waste towards shaft.

A.3.2 Tracer/Radionuclide Release and Transport Results

Tracer and radionuclide releases start at time zero and at 500 years for the vitrified waste (VW) and spent nuclear fuel (SF), respectively. All SF canisters are assumed to fail simultaneously at 500 years in agreement with Task Specification.

As liquid saturation of the repository proceeds quickly (Figure A.6), only minor advective fluid flow occurs (Figure A.7 and Figure A.8), and the transport of tracers and radionuclides in the long term is dominated by diffusion (in the liquid phase).

In agreement with Task Specifications, Tracer-1 and Tracer-3 are modelled after (i.e. are characterized by identical source terms, but ignore radioactive decay) the instant release fraction (IRF) of I-129 (spent fuel) and Tc-99 (vitrified waste), respectively.

Commencing at time zero, Tracer-3 is released from VW by congruent dissolution at an approximately constant rate. The mass of Tracer-3 in the VW drifts increases steadily (Figure A.10) indicating that its supply by waste dissolution is greater than the (almost constant) rate of its diffusion out of the drift (Figure A.11).

In contrast to Tracer-3, Tracer-1 is released instantly from SF into the liquid at 500 years (Figure A.10) – approximating a "pulse source". The tracer is discharged into the adjacent sections of the disposal tunnels at a rate that decreases sharply over time (Figure A.11), as the initial concentration gradients between the disposal drifts and their surroundings decline (Figure A.12).
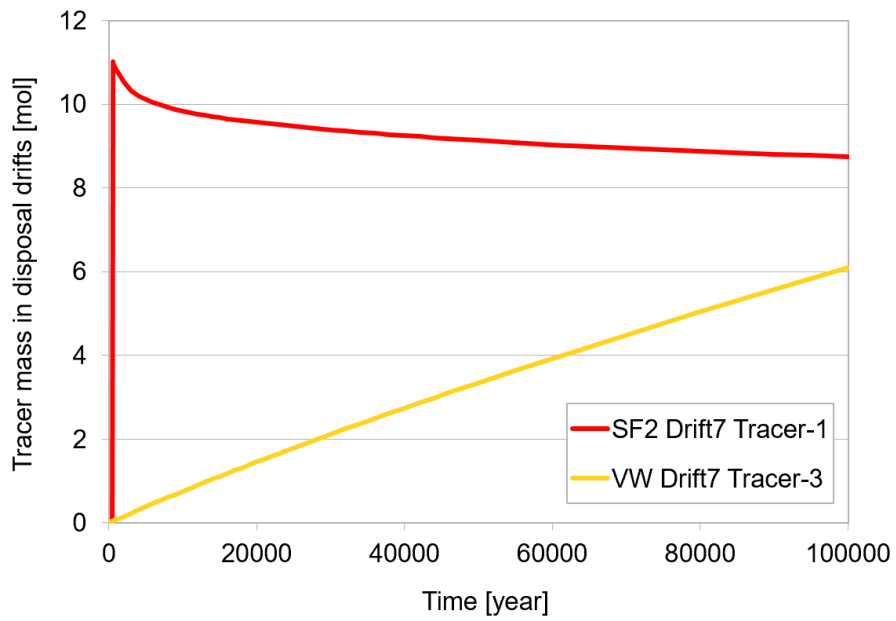
Figure A.10: Total mass [mol] of Tracer-1 and Tracer-3 in the SF2 Drift7 and VW Dritf7 disposal drifts, respectively, as a function of time.
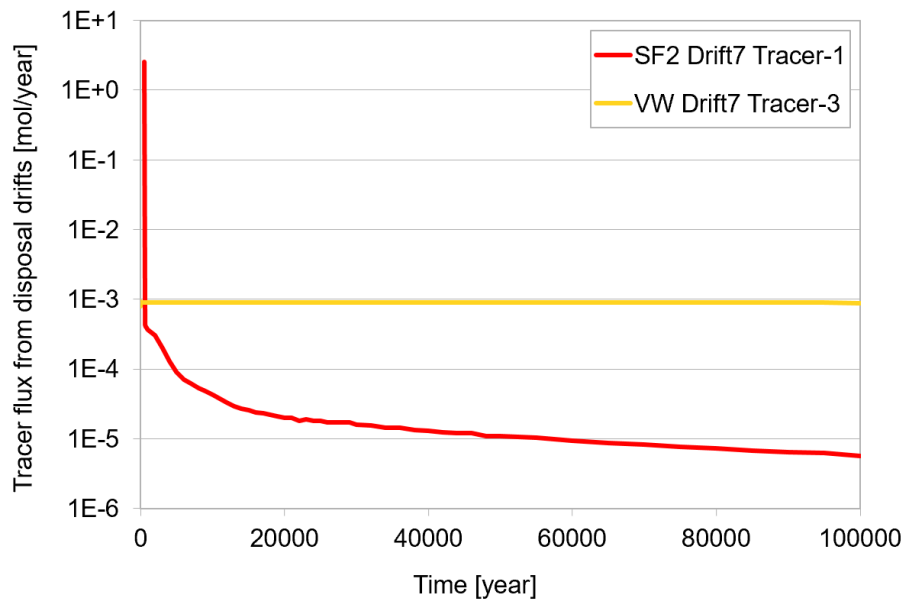
Figure A.11: Mass flux [mol/year] of Tracer-1 and Tracer-3 from the SF2 Drift7 and VW Dritf7 disposal drifts, respectively, as a function of time.
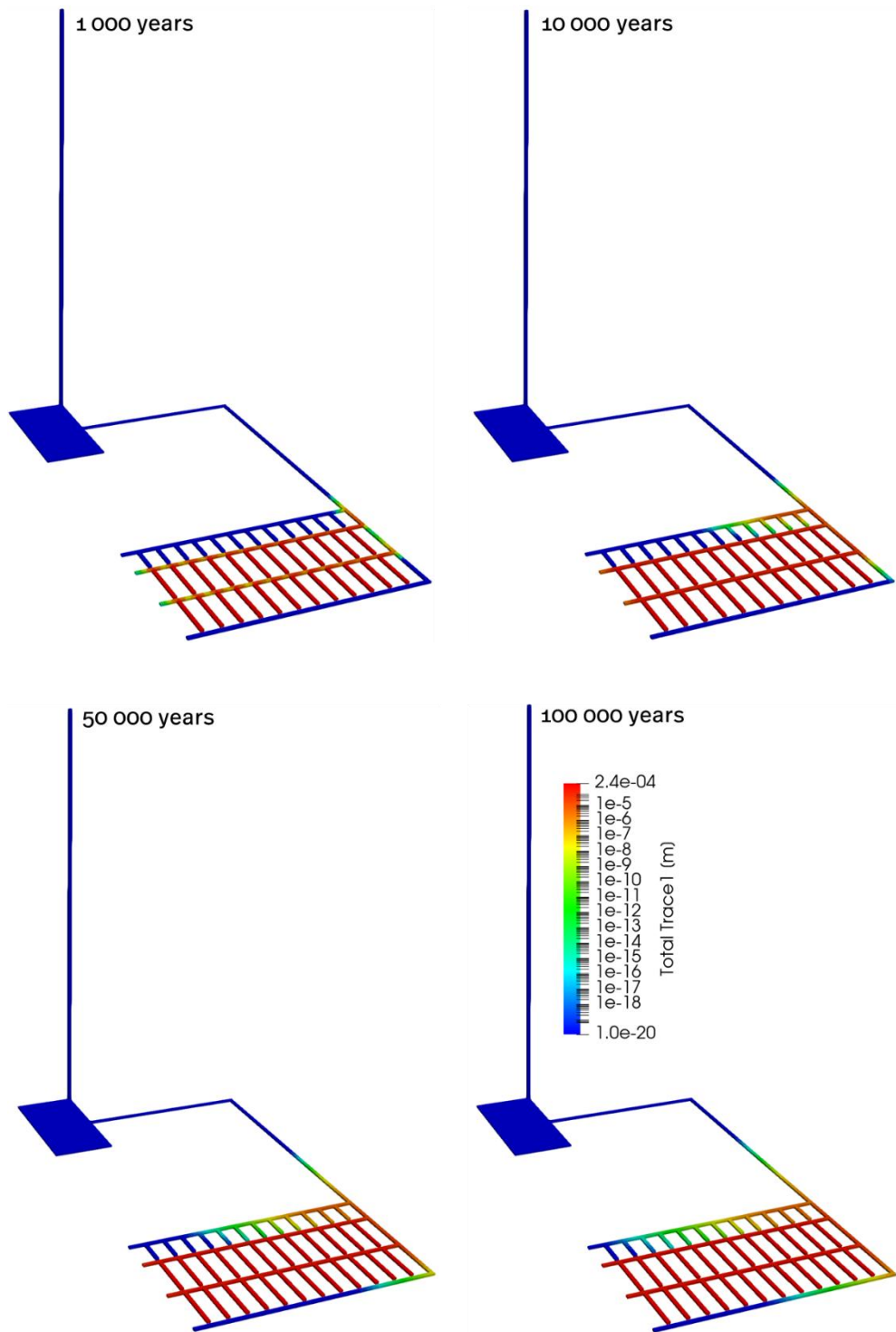
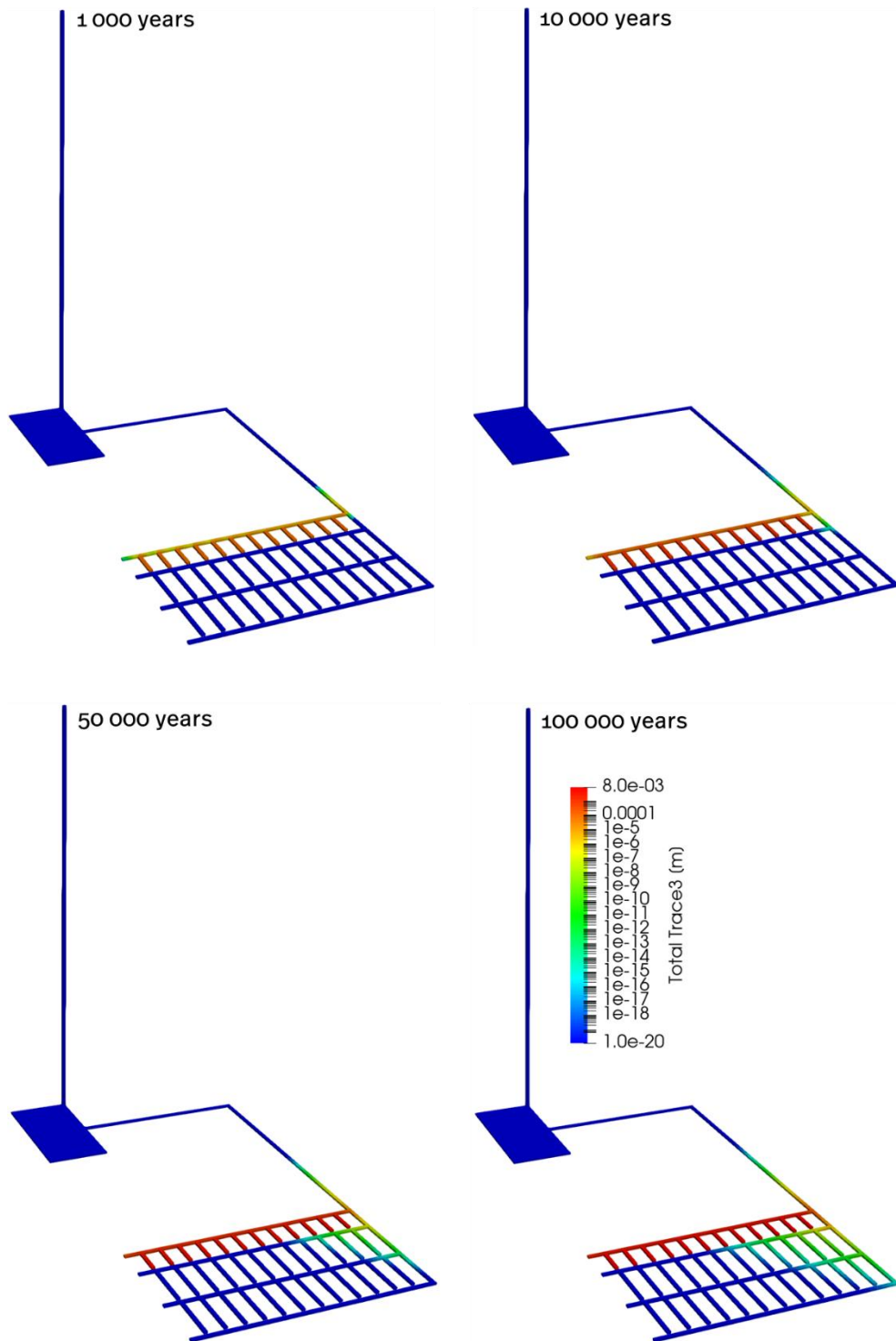**Figure A.12: Concentration [mol/L$_{liquid}$] of Tracer-1 in the repository system at selected times.**

Figure A.13: Concentration [mol/L$_{liquid}$] of Tracer-3 in the repository system at selected times.
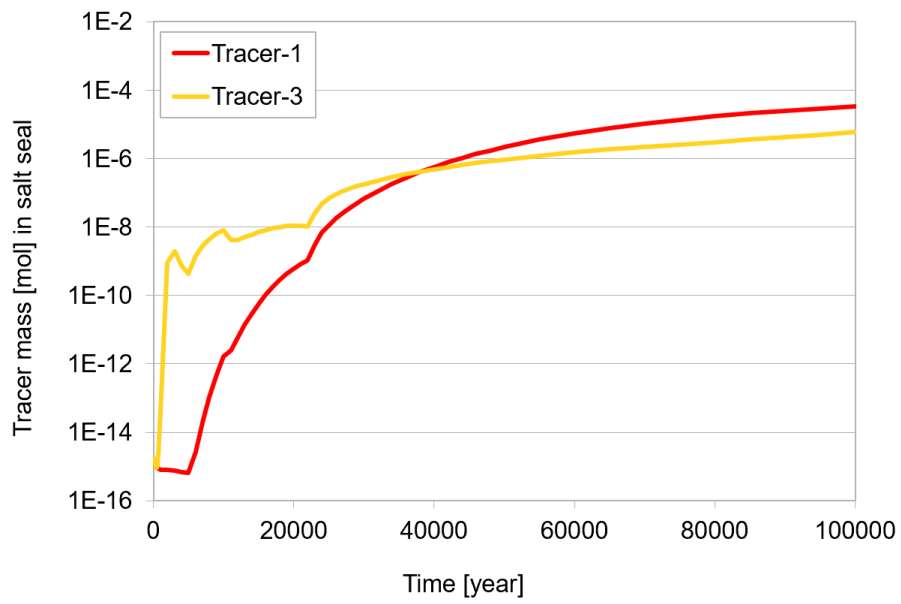
Figure A.14: Tracer mass [mol] in the salt seal as a function of time.
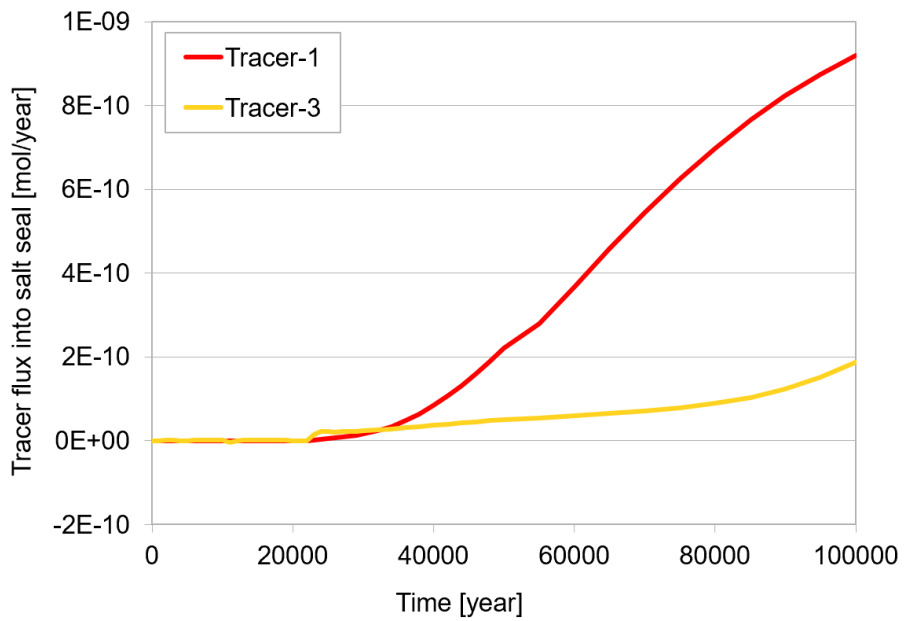
Figure A.15: Tracer flux [mol/year] into the salt seal (from the waste) as a function of time.

No fluxes of Tracer-1 and Tracer-3 from the salt seal towards the access shaft are predicted (not shown).

Radionuclide mass in the salt seal as a function of time are presented in Figure A.16. Worth noting is the behavior of U-238 and Tc-99: the total mass inventory of the former is more than twice that of the latter (refer to Table 4-1 and 4-2 of Task Specification), while both are released congruently at (roughly) the same rate by waste dissolution. Notwithstanding, the mass of Tc-99 reaching the seal is greater than that of U-238 by about a factor of 4. This is due to a limited U solubility (note that radioactive decay for both Tc-99 and U-238 is insignificant over 100 000 years, while no retardation due to sorption is considered for either element).

In the case of Ra, its limited solubility and fast decay lead to Ra-226 mass in the seal decrease below its initial value (corresponding to the initial background concentration of 10^{-20} mol/L_{liquid}) – this indicates that the rate of Ra-226 supply from the waste is lower than the rate of its in-situ decay.

No radionuclide releases from the salt seal towards the access shaft are predicted (not shown).
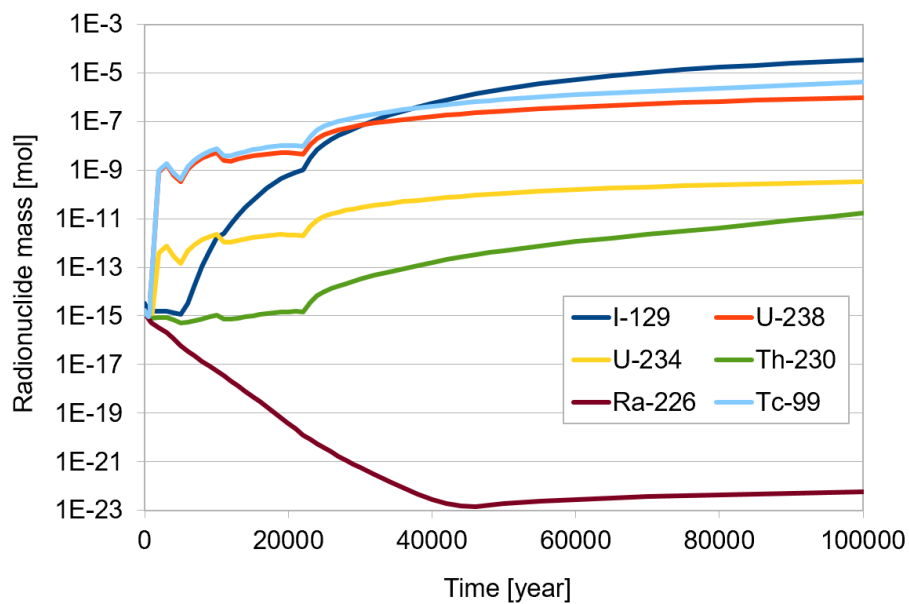
Figure A.16: Radionuclide mass [mol] in the salt seal as a function of time.

A.3.3 Creep closure results

The salt creep model used is discussed in Section A.2.3. A comparison to the GRS model is presented in Figure A.3.

A.4 Discussion of QOI Results

A.4.1 Waste Drift Quantities

Brine Saturation and Flux

Relative liquid saturation of the drifts (as per the agreed QOI) is discussed in Section A.3.1 and shown in Figure A.6. Likewise, liquid flux from the drifts is discussed in Section A.3.1 and presented in Figure A.8.

Porosity

Porosity evolution in the drifts corresponds to that indicated by "PFLOTRAN salt else" in Figure A.3.

Tracer 1/Tracer 3

The evolution of Tracer-1 and Tracer-3 in the drifts is discussed in Section A.3.2 and presented in Figure A.10 and Figure A.11.

A.4.2 Seal Quantities

Brine Saturation and Flux

Relative liquid saturation and fluxes in the salt seal (as per the agreed QOI) are discussed in Section A.3.1 and presented in Figure A.6 and Figure A.7.

Tracer 1/Tracer 3

The evolution of Tracer-1 and Tracer-3 in the salt seal (as per the agreed QOI) is discussed in Section A.3.2 and presented in Figure A.14 and Figure A.15.

A.5 References

Hammond, G.E., Lichtner, P.C., Lu, C., Mills, R.T., 2012. PFLOTRAN: reactive flow and transport code for use on laptops to leadership-class supercomputers. In: Zhang, Fan, Yeh, G.T., Parker, Jack C. (Eds.), Groundwater Reactive Transport Models. Bentham Science Publishers, Sharjah, UAE, pp. 141–159, 2012.

Hammond, G.E., Lichtner, P.C., Mills, R.T., 2014. Evaluating the performance of parallel subsurface simulators: an illustrative example with PFLOTRAN. Water Resour. Res. 50, 208–228.

Hammond, G.E., Lichtner, P.C., Lu, C., Mills, R.T., 2019. PFLOTRAN: reactive flow & transport code for use on laptops to leadership-class supercomputers. In: Groundwater Reactive Transport Models, pp. 141–159. United States.

Appendix B: COVRA

B.1 Introduction

B.1.1 Brief introduction to team

Radioactive substances and ionizing radiation are widely used in medicine, industry, agriculture, research, education, and electricity production. These activities generate radioactive waste. In the Netherlands, The Central Organization for Radioactive Waste (COVRA) is the only company in the Netherlands that is qualified to collect, process, and store all the Dutch radioactive waste. COVRA is responsible for the disposal of the radioactive waste.

The current policy in the Netherlands is that radioactive waste is collected, treated, and stored for at least 100 years above ground until approximately 2130. After this period of storage, this waste must be disposed (Ministry of infrastructure and the Environment, 2016). A definitive decision on this disposal method will be taken around 2100. While a definitive decision on the disposal method has not been taken yet, the Netherland already started research on geological disposal in the early 80's. Research initially focused only on the Zechstein rock salt the focus gradually shifted to poorly indurated clay: both are considered potential host rocks for disposal in the Netherlands. However, the most recent research programme (COPERA) will again focus on both host rocks (Verhoef et al., 2021).

B.1.2 Why team is participating

At the end of 2023 and the start of 2024, a non-site-specific safety case needs is expected to be published in the Netherlands. An important part of the safety case is the safety assessment. The safety assessment is to demonstrate the safety of the repository through time but also to optimize the design, identify knowledge gaps and steer the development. While there are differences between both repositories (e.g., layout, waste), this generic safety assessment can be used as a starting point for the Dutch safety assessment.

B.2 Reference case construction

B.2.1 Software (versions), method of calculations

For the reference case calculation, COMSOL Multiphysics is used. COMSOL is a commercially available software finite element method software. It is a general-purpose simulation software that can be used for a wide variety simulation in the field of engineering, manufacturing and in the field of scientific research including safety assessments. COMSOL can run both single physics models but also models in which different types of physics that are loosely or fully coupled. While COMSOL is general purpose, it can be expanded with additional modules that contain a collection of similar processes.

B.2.2 Flow and transport model construction

For the model, a triangular grid was used that was automatically created by COMSOL. To ensure the model results are independent, convergence test were performed. While both the surrounding formations and the salt dome were specified in the task specification, we here only model the engineered barrier system (shaft, backfill and seals). This is the only pathway to the biosphere since the salt dome itself is essentially impermeable: permeability is ultra-low and diffusion through the salt dome is limited and possibly non-existing. Excluding the salt dome and the biosphere helps to decreases the compactional time without effecting the results. For the same reasons, a two-dimensional symmetric model was used to represent the repository. This will not affect the model results as the flow and consequently transport of radionuclides towards will dominantly be in the horizontal plane. Following the same line of reasoning although transport will be in the vertical rather than horizontal direction, the shaft is modelled as a 1D model.

One simplification made compared to the task specification was to split the model into two separate independent models: the shaft and the repository. First the saturation of the shaft is modeled. The resulting evolution of the head pressure at the bottom of the shaft is subsequently used as an input for the repository. The latter is then run as an separate model. Furthermore, both models will not reach full saturation. This is achieved by setting the maximum head pressure used as input for the repository model to -20 meter: at 0 meters, the model would be considered to be fully saturated. These two simplifications are made to reduce the computational time needed. This because, there

is a sharp increase in pressure (pressure jump) when the model reaches full saturation which increases the computational time needed significantly.

Another simplifications made are the waste packages. In the model, the waste packages (Pollux and stainless canister surrounding the vitrified waste) are not explicitly modelled. They are modeled as a open space. Furthermore, the vitrified HLW is assumed to be placed inside the disposal gallery. There is thus no salt plug between the vitrified waste and the salt backfill in the disposal gallery and hence radionuclide directly enter the backfill.
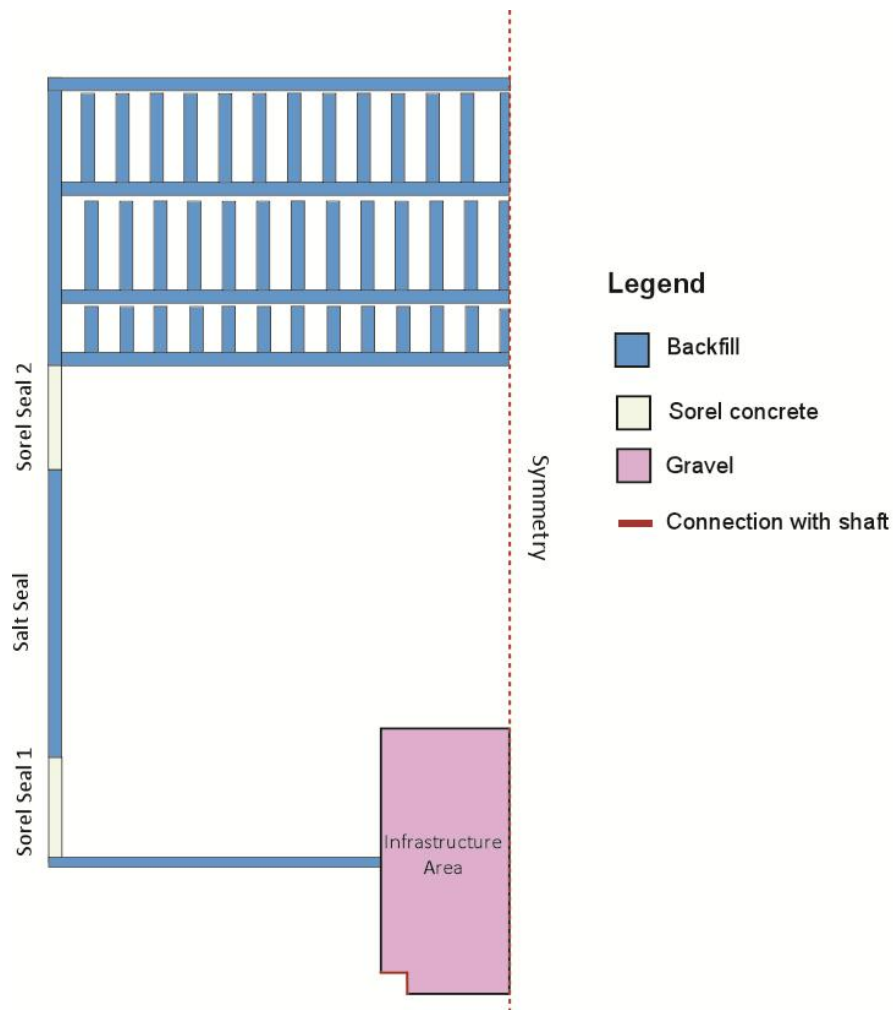
Figure B.1 Model layout of the 2D model with the different materials used throughout the repository.

Initial and boundary conditions (if different from base case)

Initial conditions are and boundaries are implemented as close as possible to the specified in the base case. For the repository, an initial head pressure of -463 meter was selected which corresponds with an initial saturation of about 20% as specified in the task. The infrastructure area has a slightly higher head pressure of -330 meter. This head pressure corresponds roughly with the specified initial saturation of around 20% although it is actually a bit higher (21%). Together, they give an average saturation of 20.7%.

For the shaft, a similar constant head pressure of -330 meter is assumed. This will, however, results in an average saturation of 31%. This is somewhat lower than the task specified saturation of 35%. Along the edges of the tunnels and the disposal gallery, no flow boundary conditions are assumed. Where the shaft connects with the infrastructure area, a head pressure boundary condition is thus used.

Implementation of tracer/radionuclide source terms, solubility limits, partitioning

Release of the tracers and radionuclides was modeled in two ways. For the gradual dissolution of SNF and VW, a simple function was used that reproduced the specified behavior of both waste. In case of radionuclides, additional calculations were preformed to account for the decay of radionuclides and hence the changing source term. For the instant release traces and radionuclides, it is assumed that they are homogenous distributed within a disposal gallery from the start of the model. They will, however, only start to be transported (advection/diffusion) after 500 years: failure of the Pollux-10 waste container.

For radionuclides, solubility limits were implemented. However, it was not possible to make a distinction between different isotopes (e.g., 238U and 234U). Therefore , the maximum solubility of these elements was increased with the number of isotopes. For example, as we have two uranium isotopes in the model, the maximum solubility of uranium is increased by a factor of two. Furthermore, the solubility limits are implemented as a processes with a specific rate that aims to stay at our below the solubility limit. Since it is a rate, the concentration of a specific radionuclide within the brine might occasionally under or overshoot the solubility limits: it takes time to reach the maximum solubility. Furthermore, deposition due to the solubility limits of an element does already occur before the solubility limits are reached.

B.2.3 Creep Closure

Assumptions

In the model, we have adopted a different creep model to ensure that the model can be run. While different, the compaction model aims to reproduce the specified compaction model as closely as possible.

Method of calculation

For the creep closure, a different compaction model was thus implemented. To calculate the compaction rate, the equation shown here below is used:

$$\frac{\partial (K_0 \cdot (H_p(t) + h_{add})/-850[m])}{\partial t}$$

In this equation, K_0 is the constant compaction rate which is set to 0.005[1/a], $H_p(t)$ is the head pressure in the repository at any given point, h_{add} (5 m) is a positive constant which is added to the H_p(t) and together they are subsequently divided by -850 meter. The latter determines together with K_0 how fast compaction is. Since both the $H_p(t)$ and $H_{p,initial}$ are negative, h_{add} is added to ensure that that the porosity of the backfill does not start to increase. Another difference with the task specified compaction is that the equation used here is a continues equation. The compaction rate within a single SNF drift is thus not constant: it varies within drift. To ensure that the model is stable, the porosity cannot become lower then 0.0058 although this value is never reached as the compaction will stop before full saturation is reached.

B.2.4 Simplifications/divergence from the task specification in detail

As described in previous sections, the simplifications are:

- Two separate model one for the shaft and one for the repository. First the shaft model is ran and the resulting head pressure evolution at the bottom of the shaft is used as a boundary condition of the repository.
- Waste packages are not explicitly modeled and the vitrified waste is assumed to be located within the disposal gallery.

- The host rock and the overburden are not modeled. Based on the result, this is also not needed
- To ensure mass conservation, the residual saturation was set to zero. Furthermore, the relative permeability function was set equal to equal the saturation rather then using Corey, Van Genuchten or Mualem - Van Genuchten. This is done to ensure that flow does occur through the model. Using the relative permeability function of Corey, Van Genuchten or Mualem - Van Genuchten would have resulted in a very low saturation in the backfill near the sorel seals which in turn would have resulted in a very low relative permeability.

B.3 Reference Base Case Results

The reference case takes about 14 hours to run for hydrological part of the model while another 6 hours is needed for the transport of diluted species (tracers).

B.3.1 Flow Modelling Results
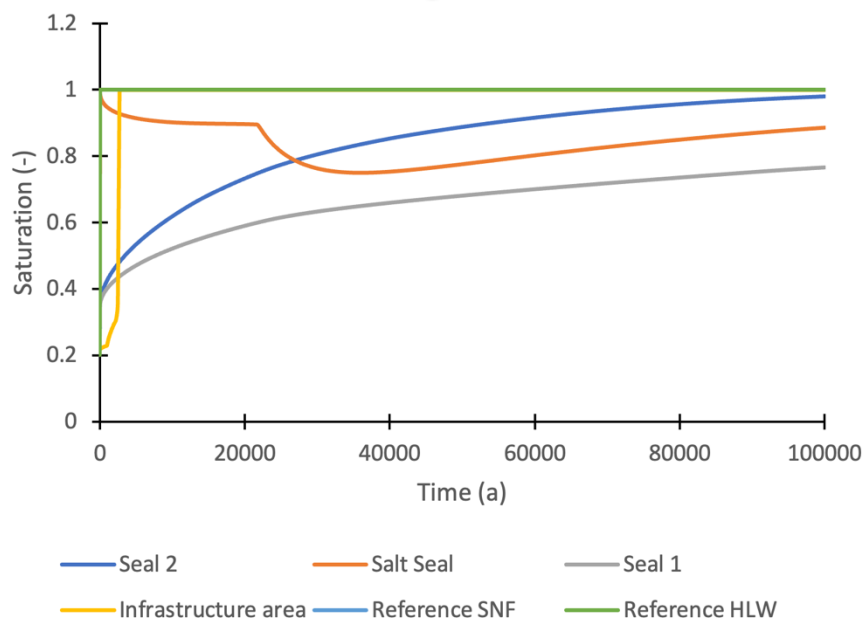
Figure B.2 Saturation through time of the different components of the repository through time.
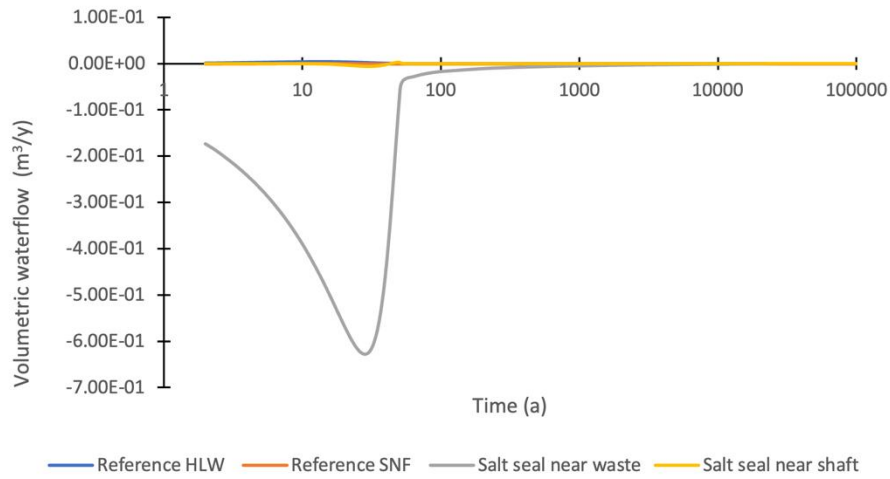
Figure B.3 Volumetric waterflow through specific interfaces within the repository. Positive is towards the waste while negative is flow away from the waste. Compared to the other flows, the flow from the seal 2 into the salt seal is the highest while the other flows are an order of 2 lower. Note that the time scale is logarithmic.
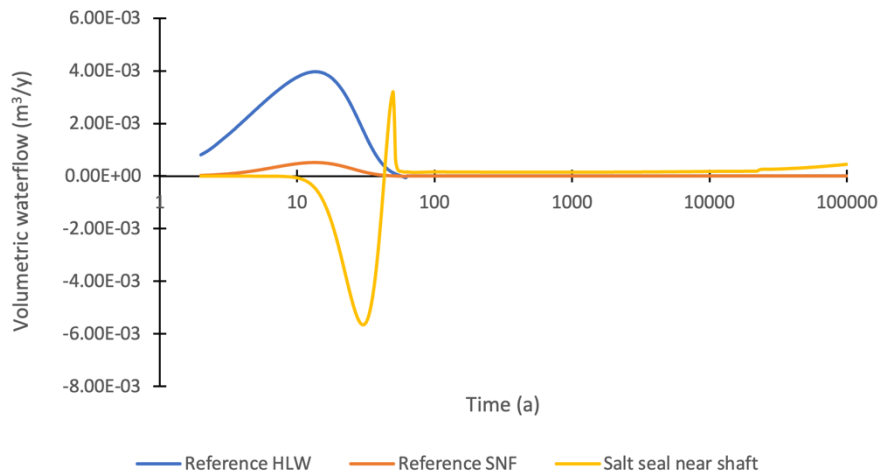
Figure B.4 Zoom in Volumetric waterflow through specific interfaces within the repository. Positive is towards the waste while negative is flow away from the waste. Note that the time scale is logarithmic.

B.3.2 Tracer/Radionuclide Release and Transport Results
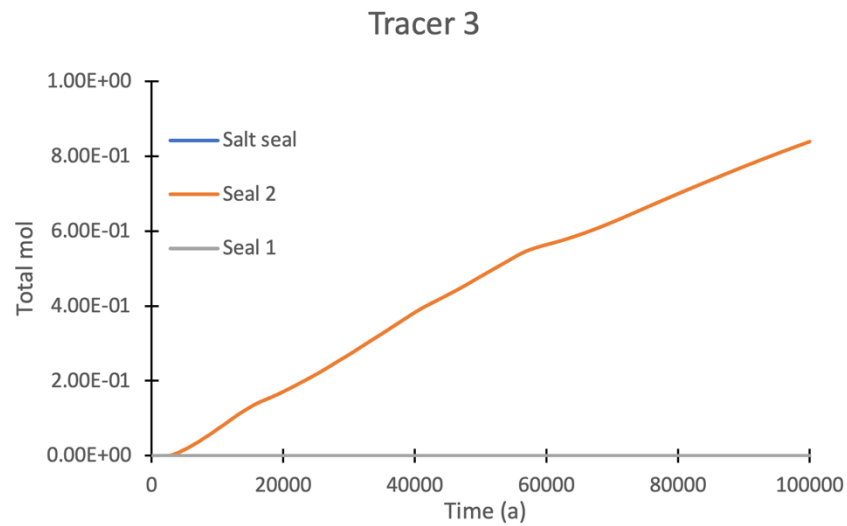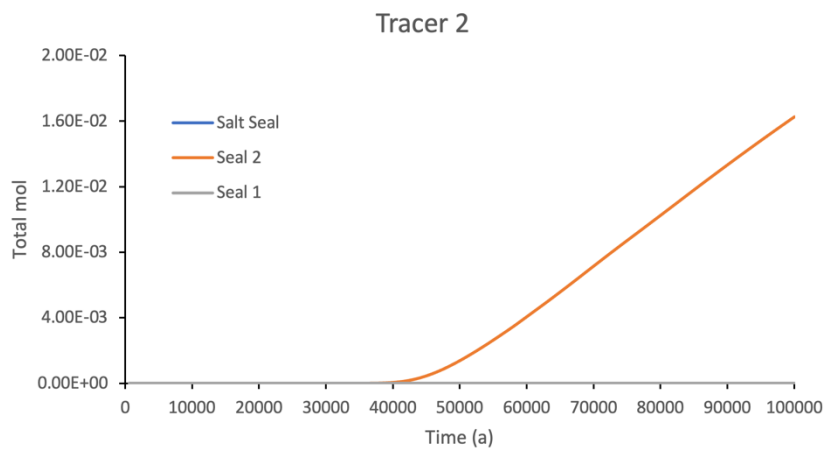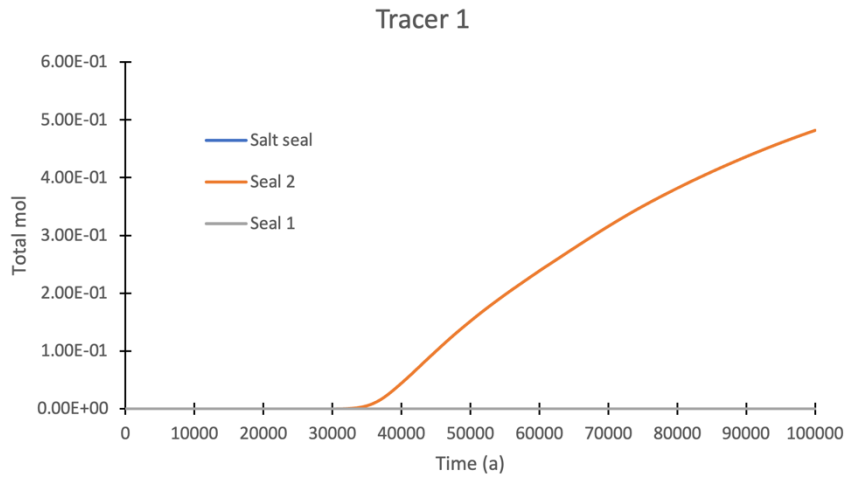
Figure B.2 The total amount of mol of each tracer in either the salt seal, seal 1 and seal 2. For all tracers, the amount in seal 1 and the salt seal is limited. This suggest that the tracers do not reach either of them.

B.3.3 Creep closure results

As shown in Figure B.6, the porosity in this model decreases more slowly and the remaining (residual) porosity is also higher compared to the specified compaction (compare with GRS curve). This slow compaction is a result of the compaction model implemented and specifically from the division by -850 [m] which makes the compaction going even slower. Interestingly, away from the sorel seal the backfill has an higher porosity; compaction is slower here. This higher porosity is a result of compaction near the concrete seals. Close to the seals, brine flows into the seal more easily as the porosity and therefore the permeability is initially still relatively high. Flowing into the seal, the saturation decreases and the backfill can compact further resulting in a lower porosity and therefore permeability close to the seal and so on. Because of the very low permeability of the backfill close to the seal, brine further away becomes essentially trapped essentially forming a brine front impeding further compaction. This brine front does move backward with time as permeability is still high enough to allow some brine flow.
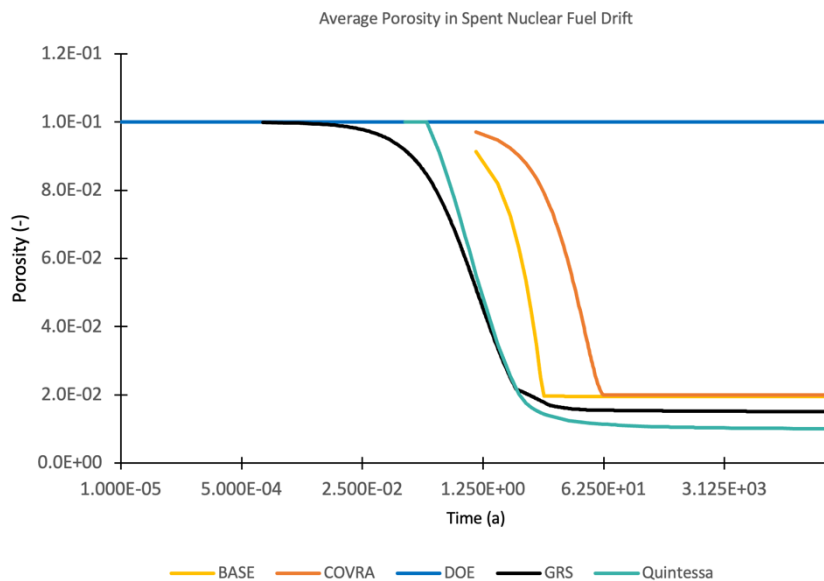
Figure B.6 Porosity change through time for the different models. Note that the COVRA's model is the slowest model to compact.
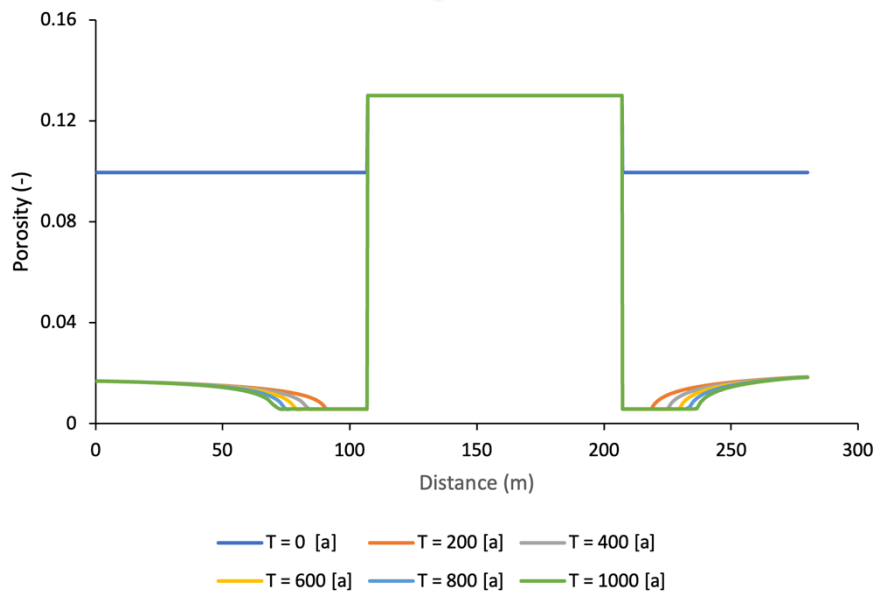
Figure B.7 Porosity change through one of the sorel seals and the area next to it that are backfilled with run of the mine salt. The porosity inside the sorel seal, does not change while it does inside the areas next to it in a backstepping manner. First, the area near the sorel seal compacts resulting in a lower porosity and consequently permeability essentially resulting in a low permeability zone. This makes it more difficult for the brine behind this zone to flow towards the sorel seal resulting in a higher porosity.
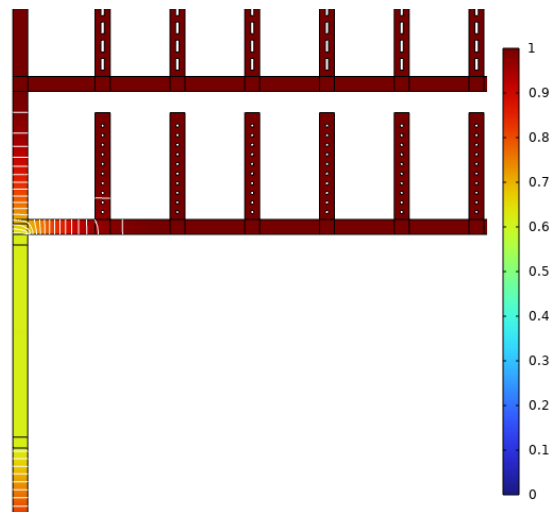
Figure B.8 Saturation of the model. Close to seal 2, the saturation in the run of the mill salt used as backfill is lower compared to the other areas. This is because brine can gradually flow into the concrete seal desaturating the backfill.

B.4 Discussion of QOI Results

As shown in previous sections, there are two processes that saturate the repository in time: the compaction of the backfill and the fluid entering the repository through the shaft. The first processes results in the initial saturation of the repository especially in areas that are backfilled with run of the mill salt. Here, saturation increases quickly and the maximum saturation is reached after 625 years with a porosity of around 0.018; higher then the minimum porosity of 0.0058. Afterwards, the saturation will slowly decrease again as brine start to saturate the concrete seals and the whole system strives to an equilibrium. This only occurs in areas close to the seal (Figure B.7 and B.8). As discussed in the previous section this is caused by the fact that the brine near the sorel seal can flow into the seal resulting in a low permeability zone near the sorel seal. Form Figure B.2 it is also clear that saturation of seal two is slower. This because the brine can also flow to the infrastructure area with relative ease. There is thus essentially less brine available to saturate the seal resulting in a lower saturation rate of this seal.

At around 1000 years, brine from the shaft enters the repository filling the infrastructure area which suddenly increases at around 2000 years. Around this time, the infrastructure area becomes essentially fully saturated. While brine enters the repository via the shaft, there is no notable increase in the rate of saturation of the seals. This is likely related to the low permeability zone of the backfill near the seals making it difficult for the brine entering via the shaft to reach the concrete seal. However, as the porosity is not zero and there is thus still a permeability ($5 \cdot 10^{-20}$ m^2), brine continues to flow slowly but steadily into the seal. It should be noted that the porosity does not decrease further near the sorel seals: it has reached the minimum porosity possible in the model. Because of this, the area near the sorel seal becomes partially saturated.

As shown in Figure B.5, all three tracers reach sorel seal 2. However, while tracer 2 does reach this seal, it's total mol in sorel seal 2 through time is a magnitude lower compared to the other 2 tracers. This because it is only release after 500 years and the quantities in which it is released is limited through time. Furthermore, tracer 1 is homogenous distributed in the SNF drift and essentially starts an bit closure to the seal compared to the tracer 2 which is simulated as a boundary flux.

B.5 References

Ministry of infrastructure and the Environment, 2016. The national programme for the management of radioactive waste and spent fuel, p. 61.

Verhoef, E., Neeft, E., Bartol, J., Vuorio, M., Scholten, C., Buitenhuis, A., Veen, G.v.d., Chapman, N., McCombie, C., 2021. COVRA's Long-term research programme for geological disposal of radioactive waste., p. 89.

Appendix C: DOE

C.1 Introduction

C.1.1 Brief introduction to team

The US DOE team is represented by Richard Jayne and Tara LaForce of Sandia National Laboratories (SNL).

C.1.2 Why team is participating

Sandia National Laboratories is leading Task F of DECOVALEX-2023 on behalf of the Spent Fuel and Waste Science and Technology (SFWST) Campaign of the US Department of Energy Office of Nuclear Energy (DOE-NE) office of Spent Fuel and Waste Disposition (SFWD). The goal of SFWST is to develop US technological readiness and expertise on generic performance assessment modelling in three host rocks: salt, crystalline, and argillite. International leadership and learning from international best-practice have been identified an important step in developing expertise, which is furthered by participation in DECOVALEX-2023.

The primary objectives of Task F are to build confidence in the models, methods, and software used for performance assessment (PA) of deep geologic repositories, and/or to bring to the fore additional research and development needed to improve PA methodologies. As part of our contribution to the Task F2-salt project we are also building a simulation model and utilizing the task to develop an early career scientist at SNL to provide training to the next generation of scientists. Both of these DECOVALEX goals align closely with the goals of SFWST.

C.2 Reference case construction

C.2.1 Software (versions), method of calculations

The simulator used for this study is PFLOTRAN (Hammond et al., 2014), an open source, state-of-the-art massively parallel subsurface flow and reactive transport code. PFLOTRAN solves a system of generally nonlinear partial differential equations

describing multiphase, multicomponent and multiscale reactive flow and transport in porous materials. The code is designed to run on massively parallel computing architectures as well as workstations and laptops.

C.2.2 Flow and transport model construction

Model Domain and Flow Mode

Richards' mode is chosen to simulate mass transport within the repository which applies to single phase, variably saturated, isothermal systems.

The workflow used here to create the cartesian mesh utilizes PFLOTRAN's internal structured meshing method. Inputs for the cartesian mesh include the total dimensions of the model domain with the number of grid cells in the X, Y, and Z directions. The current model domain is 490 m × 932 m × 940 m consisting of 4,309,900 grid cells. The dimensions of each grid cell are 7 m × 3.5 m × 4 m – these dimensions were chosen to match the height and width of the drifts and shaft proposed for the Task F2 repository. The final mesh (Figure C.1) utilizes ½ symmetry to reduce computational demand associated with the given repository scenario. The model domain contains 24 SNF disposal drifts, 12 HLW drifts, a drift seal contains two 100 m cement abutments with 300 m run-of-mine (ROM) salt in-between, an infrastructure area, a simplified shaft seal (homogenous material properties), and an overburden layer where an aquifer is located. The centremost drift is omitted due to challenges with meshing and simulating half a drift along the line of symmetry.
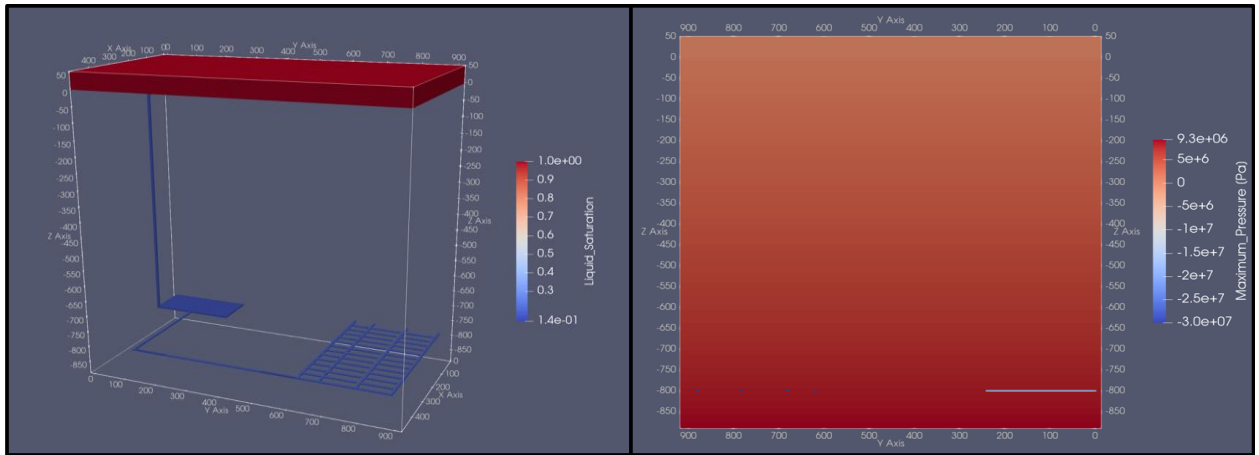
Figure C.1. Left: The repository, shaft, and overlying aquifer showing initial fluid saturation. Right: A Y-Z plane view of the model domain illustrates fluid pressure is hydrostatic within the intact salt and negative within the repository to create atmospheric gas phase pressure.

Initial and boundary conditions (if different from base case)

The initial pressure and saturation profiles are shown in Figure C.1. Initial conditions for fluid pressure within the intact salt are hydrostatic from the surface at 50 m above mean sea level (amsl) at 101325 Pa to 9.6 MPa at 890 m amsl (940 m below land surface). The initial fluid pressure conditions within the repository are -30 MPa, due to the use of Richards' flow; to set an initial saturation near 20% within the repository, negative fluid pressure is required to compute a liquid saturation less than 100%.

C.2.3 Creep Closure

The only creep closure accounted for in the Team DOE simulations is permeability decreasing with time. Porosity change is not accounted for.

C.2.4 Simplifications/divergence from the task specification in detail

With the geomechanical limitations of the current version of PFLOTRAN, simplifications are made to implement some of the geomechanical effects of drift convergence. Porosity does not change with time; this simplification is important for the conservation of mass with a finite-volume code. Instead, here we make a stepped permeability change with time. At 1000 years when the shaft fails the drift convergence is considered complete, resulting in any crushed salt within the repository assuming the properties of intact salt, in this case permeability (1.0×10^{-17} -> 1.0×10^{-21} m^2). This assumption speeds

up the drift convergence process with respect to permeability as described in the Task Specification. However, increasing the rate that permeability decreases is done here to offset the lack of porosity closure. In reality, when porosity decreases, saturation increases and eventually pore fluid pressure increases. As pore fluid pressure increases it causes the pressure gradient from the shaft to the drifts to decrease, resulting in slower brine flow within the repository. In order to compensate for the lack of porosity closing slowing brine flow, we have chosen here to decrease permeability rapidly. For comparison in future simulations a stepped permeability change with time may be used to match drift convergence more accurately.

Steps were taken to reduce the complexity of the meshing and simulations; additional assumptions are made to help with numerical convergence:

- The domal salt and overburden geologic formations are accounted for explicitly in the model and all other geological units are omitted.
- Drifts are meshed, but individual waste packages are not. Each disposal drift is treated as one waste package containing the sum of all radionuclides from each waste package within an individual drift.
- The shaft seal is simplified into one homogeneous material.

C.3 Reference Base Case Results

C.3.1 Flow Modelling Results

Figure C.2 illustrates how the repository is predicted to re-saturate slowly over time. At 500 years (Figure C.2A) the shaft is slowly becoming saturated starting near the surface and liquid is migrating down towards the repository. The drifts leading away from the infrastructure area towards the waste drifts have also increased in saturation slightly. This is due to a small amount inflow from the intact salt. Once the shaft seal fails at 1000 years the bulk permeability of the shaft seal increases by two orders of magnitude and it can be seen in Figure C.2B at 2500 years the shaft is fully saturated, the infrastructure area is becoming saturated, as well as the drifts near the infrastructure area. Figure C.2C and D illustrate how the remaining drifts become saturated at 5000 and 10000 years, respectively. The entire repository is 100% saturated by 15000 years.

Figure C.3 helps illustrate the evolution of liquid saturation over time in six regions of interest within the repository. The infrastructure area begins saturating rapidly after 1000 years when the shaft seal fails, then the drift seal closest to the shaft, the ROM salt

in the drift seal, the drift seal nearest to the waste, the HLW drift, and finally the vitrified waste drifts all become fully saturated.
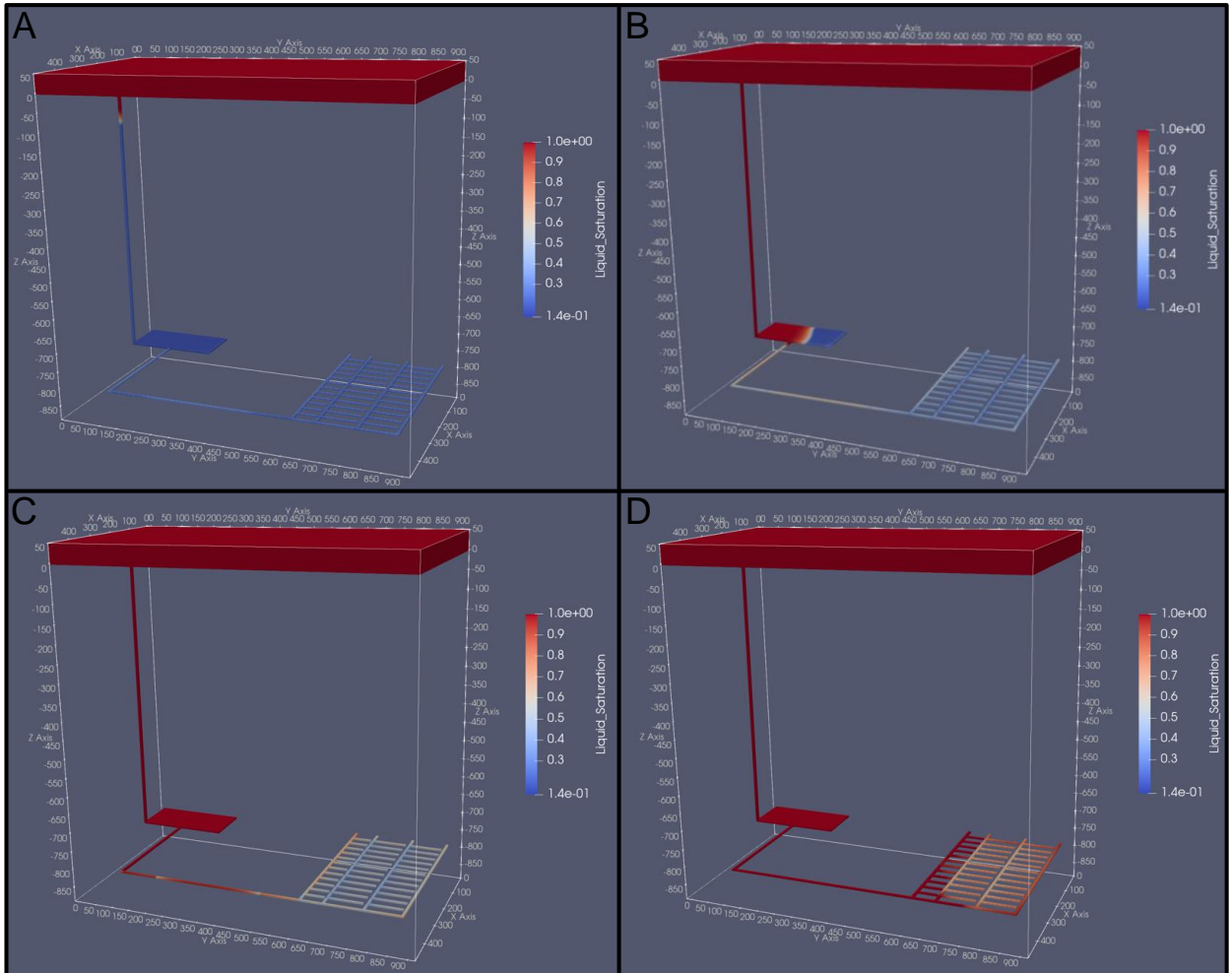

Figure C.2. Liquid saturation in the repository at A) 500 years, B) 2500 years, C) 5000 years, and D)10000 years.
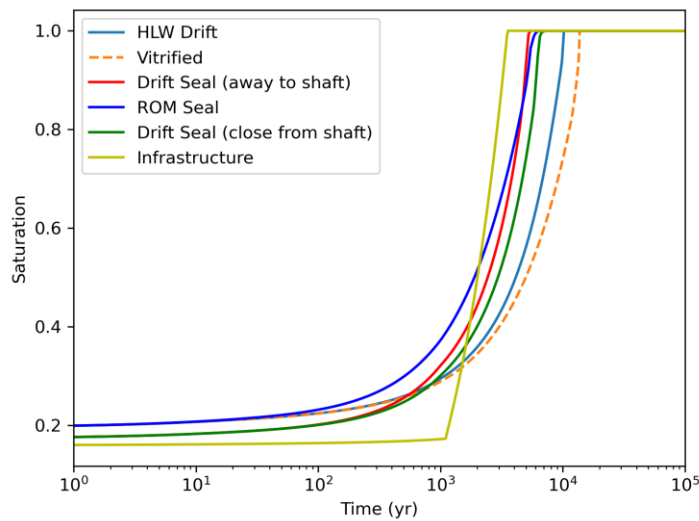
Figure C.3. Liquid saturation over time at regions of interest within the repository.

C.3.2 Tracer/Radionuclide Release and Transport Results

Tracer and radionuclide transport within the repository is kept to the disposal drifts, the first cement drift seal, and the ROM salt within the drift seal (Figure C.4 – C.5). There is no appreciable amount of tracer or radionuclide transport past the drift seal into the infrastructure area or the shaft. Radionuclide and tracer mass within the first grid cell of the 100 m cement abutment of the drift seal closest to the waste is shown in Figure C.4, where Tracer 3 (1.2×10^{-5} moles) and ^{99}Tc (3.8×10^{-6} moles) are most abundant. These results are intuitive given that Tracer 3 and ^{99}Tc have the shortest distance to travel from the vitrified waste drift to the seal.

Figure C.5 shows the tracer and radionuclide masses in the first grid cell of the run-of-mine salt between the two cement abutments within the drift seal. As shown in Figure C.5, Tracer 3 and ^{99}Tc are the most abundant radionuclides, but their total masses have decreased by 2-3 orders of magnitude. This highlights the effectiveness of the drift seal at decreasing the rate of radionuclide transport for the given scenario and material properties.

Finally, moving onto the drift seal closest to the shaft (Figure C.6) and the shaft seal 25 m above the infrastructure area (Figure C.7) we see no radionuclides transported past the drift seal. The values shown in Figure C.6 and Figure C.7 are insignificant with the most abundant radionuclide at ~1×10^{-20} moles, which is the order of magnitude of the background concentration in the simulation. Additionally, multiple tracer and radionuclide data plot directly on top of each other resulting in both Figure C.6 and

Figure C.7 appearing to only have three different curves, highlighting how small the changes in radionuclide and tracer mass over the 100,000-year simulation.
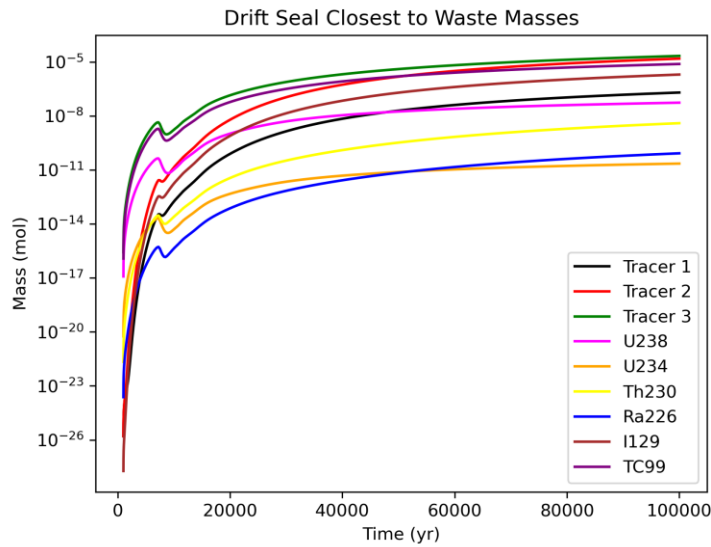

Figure C.4. Radionuclide and tracer masses within the concrete abutment of the drift seal closest to the waste disposal drifts.
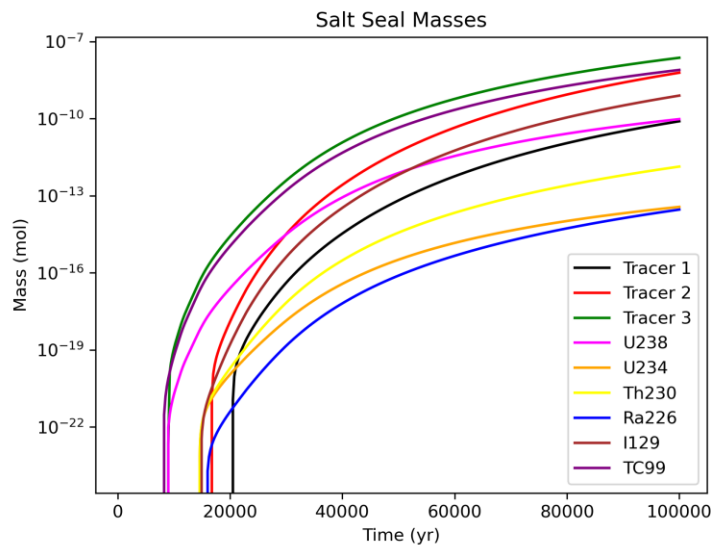

Figure C.5. Radionuclide and tracer masses within the Run-of-Mine (ROM) salt between the two concrete abutments within the drift seals.
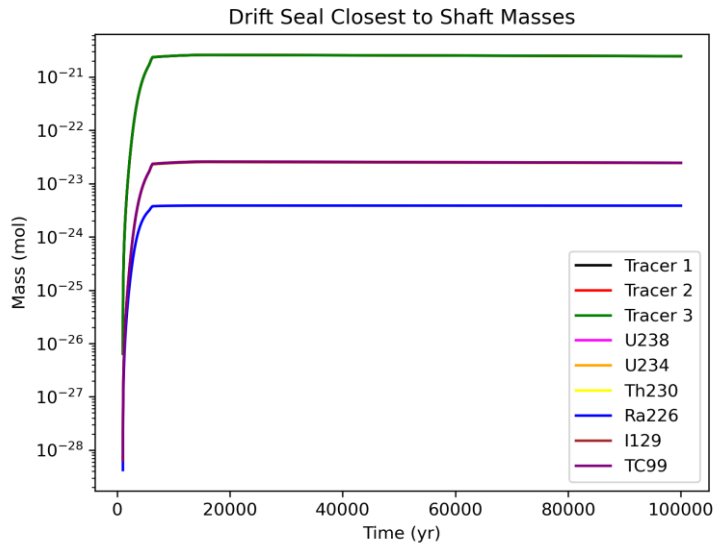
Figure C.6. Radionuclide and tracer masses within the concrete abutment within the drift seal closest to the shaft. Note that some masses are not seen because the data plot on top of one another.
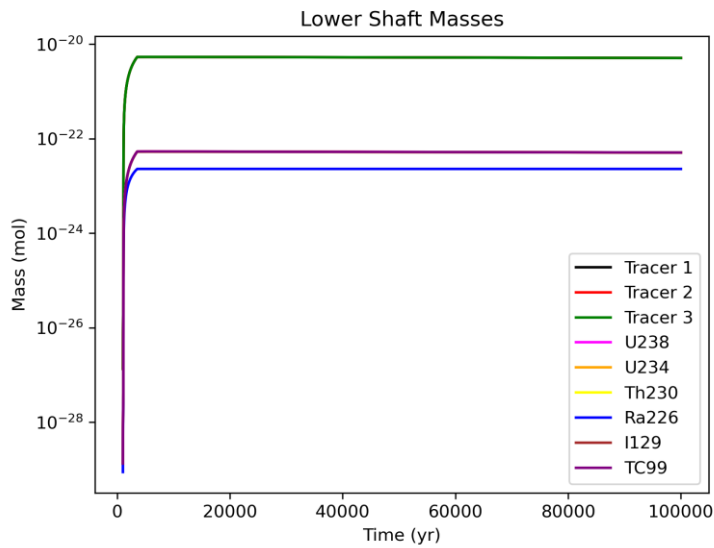
Figure C.7. Radionuclide and tracer masses within the shaft 25 meters above the infrastructure area. Note that some masses are not seen because the data plot on top of one another.

C.3.3 Creep closure results

There is no creep closure modelled here, instead a stepped permeability change is implemented as described above in Section C.2.3.

C.4 Discussion of QOI Results

C.4.1 Waste Drift Quantities

Brine Saturation and Flux

Brine flow into the disposal drifts occurs via two mechanisms, inflow from the intact salt and from the surface as a result of the failed shaft seal. The processes take place at different times and different scales. Figure C.8 shows brine flow into or out of the interface between emplacement drift and the drift it connects to. There is a clear difference between the vitrified and SNF drifts. The vitrified drift has a small amount of brine flowing into the drift from the connecting drift between ~300-1000 years. This inflow is based on the geometry of the repository, the connecting drift for the vitrified emplacements drifts has no excavations between itself and the infrastructure area so all available brine from the intact salt flows into this drift. As the connecting drift begins to saturate in early time a small amount of this brine flows into the vitrified emplacement drift. After the shaft seal failure at 1000 years a large increase of flow into both the SNF and vitrified drifts is observed. The increased brine inflow occurs in the vitrified emplacement drift before the SNF drift, this is also caused by the geometry of the repository because the SNF drift is further from the shaft. The same result is illustrated by Figure C.9, where the average liquid saturation is shown for both emplacement drifts. The inflow from the intact salt is the same for both drifts and then after 1000 years the saturation curves begin to separate, where the vitrified waste drift becomes fully saturated at 10,200 years and the SNF drift at 13,700 years.
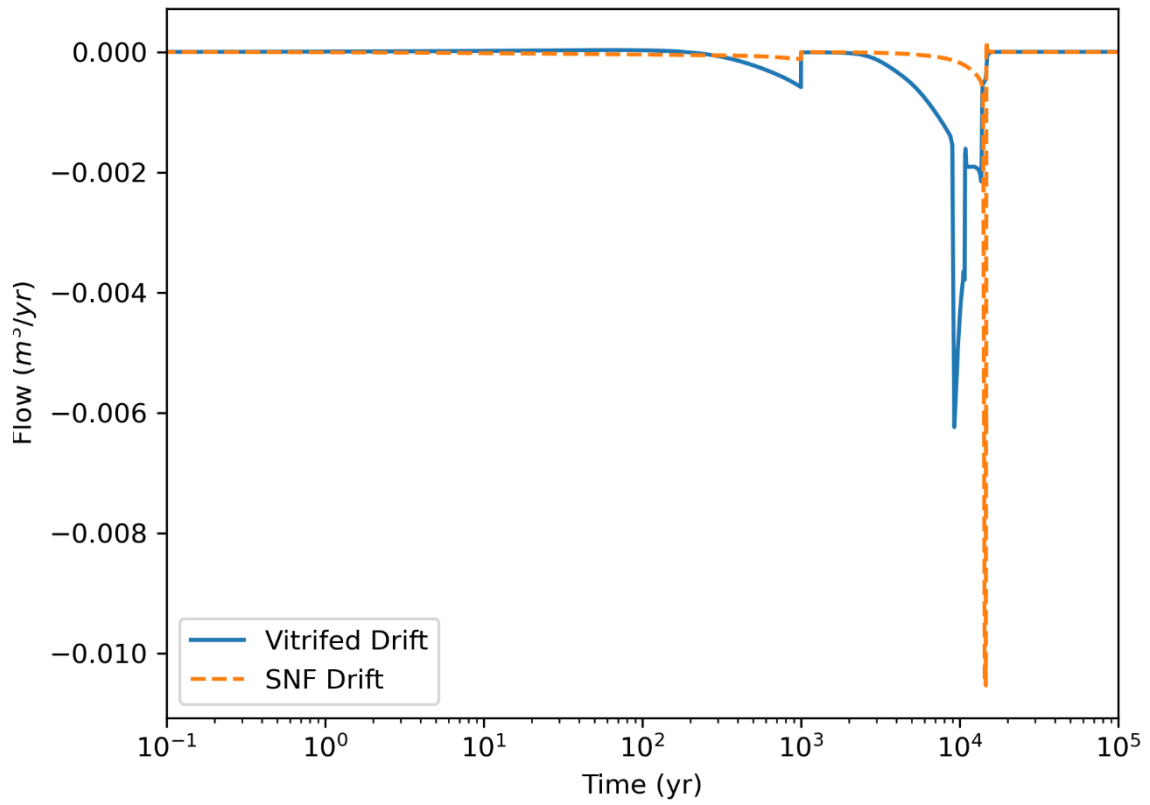
Figure C.8. Brine flow into (positive) or out of (negative) the waste disposal drifts.
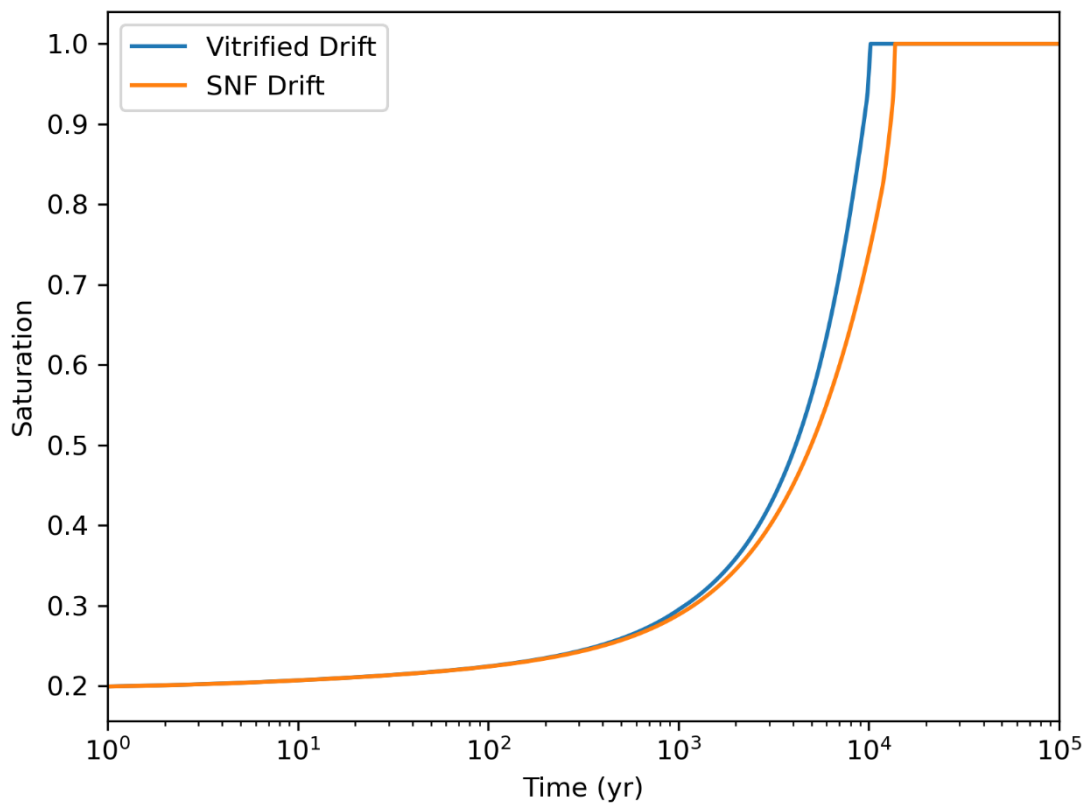
Figure C.9. Liquid saturation within the waste disposal drifts.

Porosity

Porosity does not change with time within the simulations presented by Team DOE.

Tracer 1/Tracer 3

Tracer transport out of the SNF and HLW emplacement drifts follows a similar trend to brine flow where there are two time-dependent phases of transport. First, Tracer 3 transport out of the emplacement drift begins around 100 years where the drifts are ~25% saturated with brine. Second, Tracer 3 transport begins before Tracer 1 because Tracer 3 begins releasing at t = 0 and Tracer 1 doesn't begin until the canisters fail at 500 years. Tracer 3 flow increases steadily until ~9000 years where a sharp decrease occurs before continuing to increase. This is caused by an increase in brine inflow into the drift as shown in Figure C.8 and once the drift is mostly saturated and brine flow into the drift decreases, the outward transport of tracer 3 increases. Tracer 1 flow out of the emplacement drift begins at 500 years and increases quickly until 1000 years where it

begins to steadily decrease. After the drift becomes fully saturated a spike of Tracer 1 out of the drift is observed and then flow steadily falls to around 0 after 80000 years. Tracer 3 transport increases with time because its concentration in the repository increases as the glass waste form dissolves, while Tracer 1 transport decreases after waste package failure when all of it is released into the repository at once.
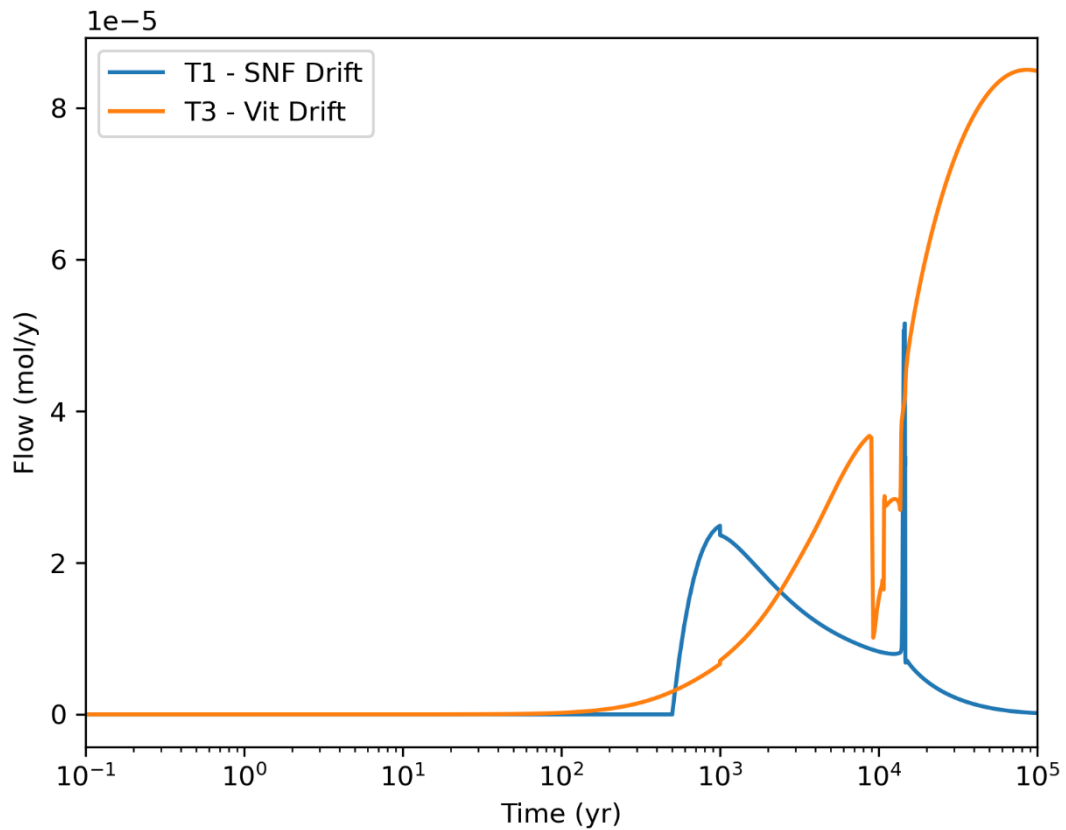

Figure C.10. Flow of Tracer 1 and Tracer 3 out of the SNF and Vitrified waste drifts, respectively.

C.4.2 Seal Quantities

Brine Saturation and Flux

Brine flow into and out of the drift seals also occurs in two distinct phases. Prior to the shaft failure at 1000 years flow slowly increases and occurs in opposite directions (Figure C.11). The drift seal closest to the shaft has brine traveling away from the shaft, while the drift seal closest to the waste has brine flowing towards the shaft. This is caused by an increase in pressure within the salt backfill in the drifts outside of the two seals.

Figure C.12 illustrates how the pressure within the backfill is higher than the pressure in the drift seals at 500 years; this increase in pressure drives the brine into the drift seals from the backfill. When the shaft seal fails at 1,000 years the drift seal closest to the shaft has increased brine flow around 2000 years, and brine flow into this seal stops when it becomes fully saturated around 6000 years. The drift seal furthest from the shaft has a significant increase in brine flow around 6000 years, this delay is caused by the low permeability of the seals and ROM salt between the seals. The average saturation of each seal and the ROM is shown in Figure C.13. The increase in saturation within each part of the seal begins at different times, which is expected based on the distance from the shaft. The ROM begins with a higher initial saturation due to the relative permeability models implemented, but the order of becoming fully saturated is drift seal closest to the shaft, the ROM, and finally the drift seal furthest from the shaft. This illustrates that the timing associated with resaturation of these seals is dominated by the shaft failure at 1000 years.
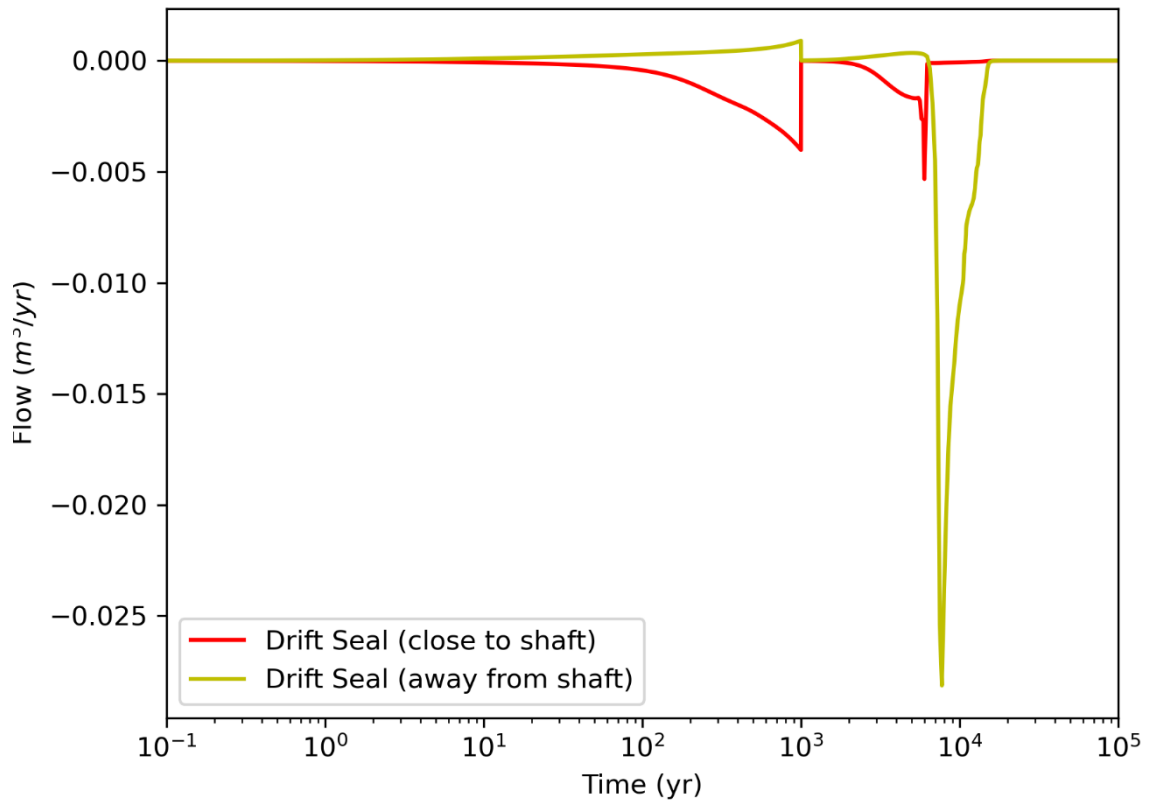
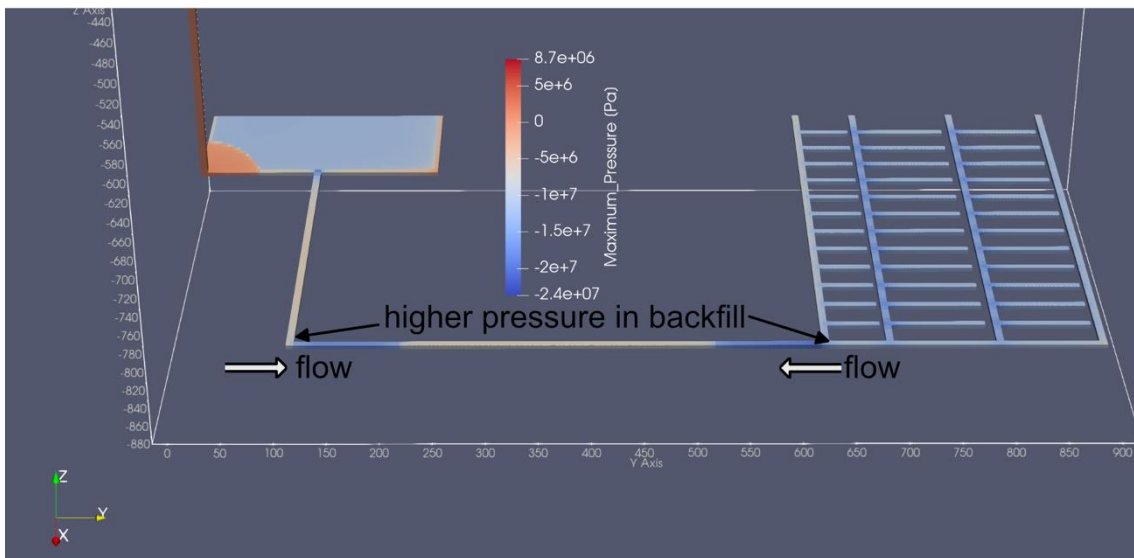**Figure C.11. Brine flow into or out of drift seals.**

Figure C.12. Liquid pressure within the repository at 500 years. The higher pressure within the backfill causes flow into each drift seal.
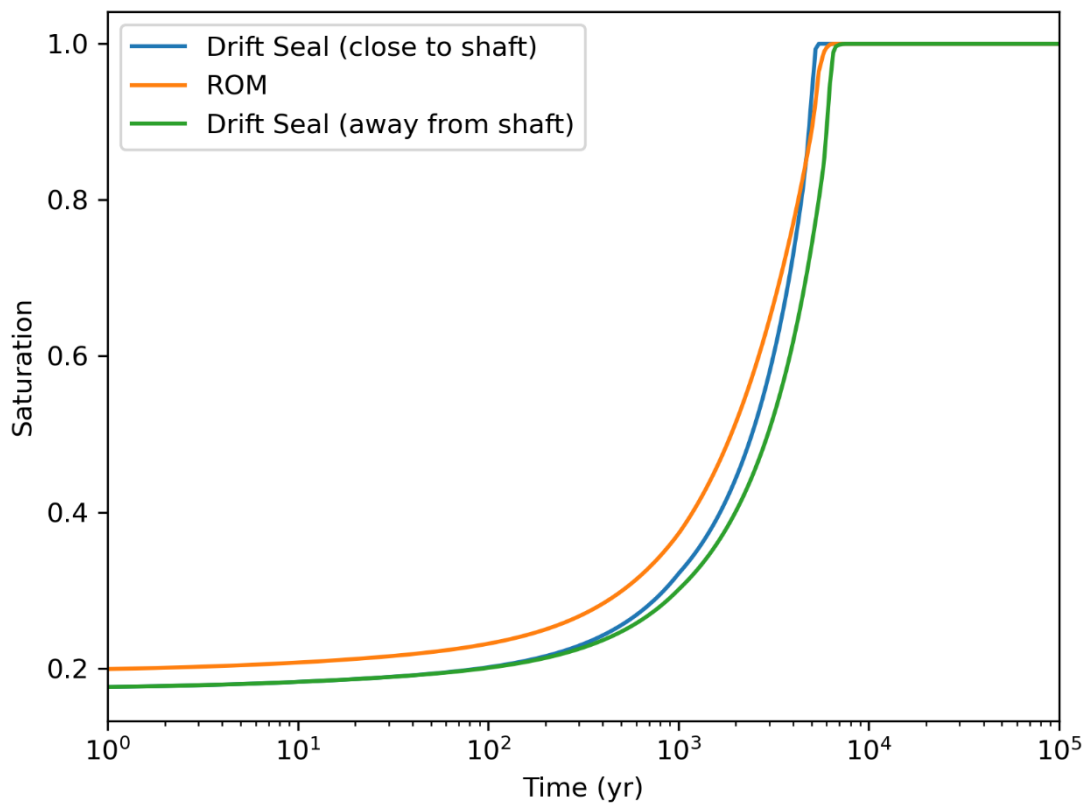
Figure C.13. Average saturation of each drift seal and the run-of-mine (ROM) salt.

Tracer 1/Tracer 3

Tracer 1 and 3 transport are observed in the drift seal furthest from the shaft (Figure C.14). Tracer 3 transport into the drift seal begins slowly before the seals and drifts are fully saturated, and after ~10000 years the diffusive transport of tracer 3 steadily increases to 1.2×10^{-5} mol/y at 100000 years. Transport of Tracer 1 is minimal into the drift seal furthest from the shaft where a maximum flow of 1.4×10^{-7} mol/y is reached at 100000 years. There is no Tracer 1 or 3 transported through the ROM salt into the drift seal closest to the shaft.
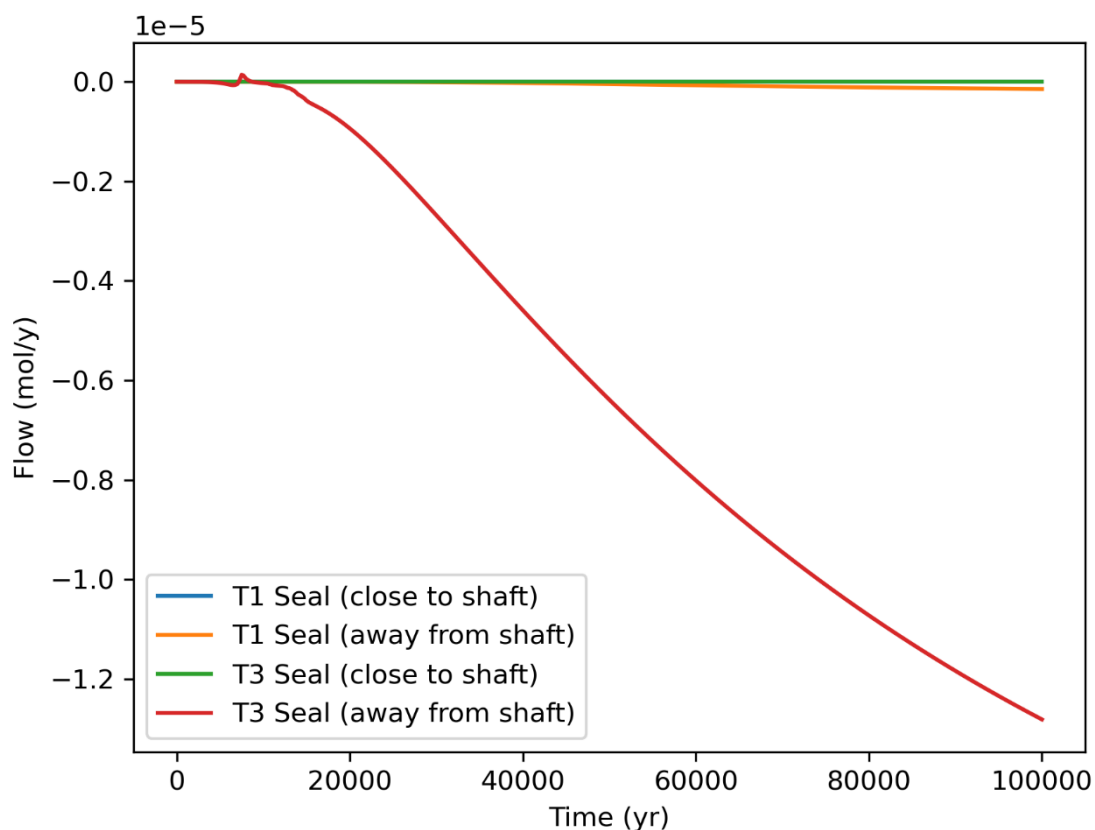
Figure C.14. Flow of Tracer 1 and Tracer 3 within the drift seals. Flow is shown as negative here because the transport of these tracers is towards the shaft.

C.5 Investigation of Variant Cases

C.5.1 100-year vs. 1000-year vs. 10,000-year Shaft Failure

Here three shaft failure times are investigated: 100-, 1000-, and 10000-years. The main differences between these variants are evident in Figure C.15 and Figure C.16. Figure C.15 shows liquid saturation within the repository at 1250 years. The shaft and half the infrastructure area are fully saturated in the 100-year failure scenario, the shaft and a small portion of the infrastructure area are fully saturated in the 1000-year failure scenario, and only a small portion of the shaft is saturated in the 10,000-year failure scenario. Figure C.16 shows liquid saturation within the repository at 10,000 years. There is no difference in liquid saturation at 10,000 years throughout the repository in

the 100- and 1000-year failure scenarios. In the 10,000-year failure scenario the shaft seal is still fully competent and as a result the infrastructure area is still near initial liquid saturation, but the drifts have all become mostly saturated due to inflow from the intact salt. While the liquid saturation within the repository is affected by changing the time at which the shaft seal fails, the transport of tracers and radionuclides within the repository remains largely unaffected. Figure C.14 shows the flow of Tracer 1 and 3 into the drift seal closest to the waste for the base case and these results do not differ from those presented in Figure C.17 for the variants. The investigation of these variants illustrates that the early time behaviour of the repository may be slightly affected, but over the course of 100,000 years the end results are very similar. This suggests that the drift seal and the reconsolidation of the backfilled salt largely control the transport of radionuclides within the repository given the scenarios investigated here.
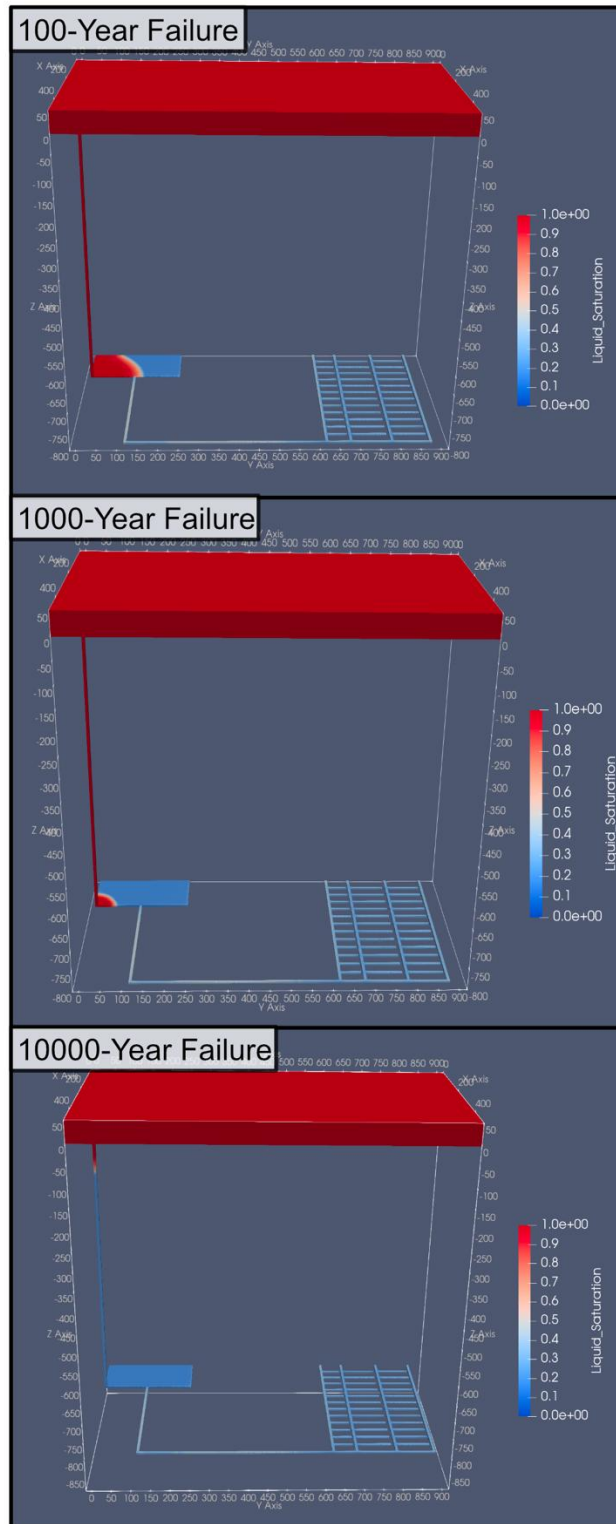
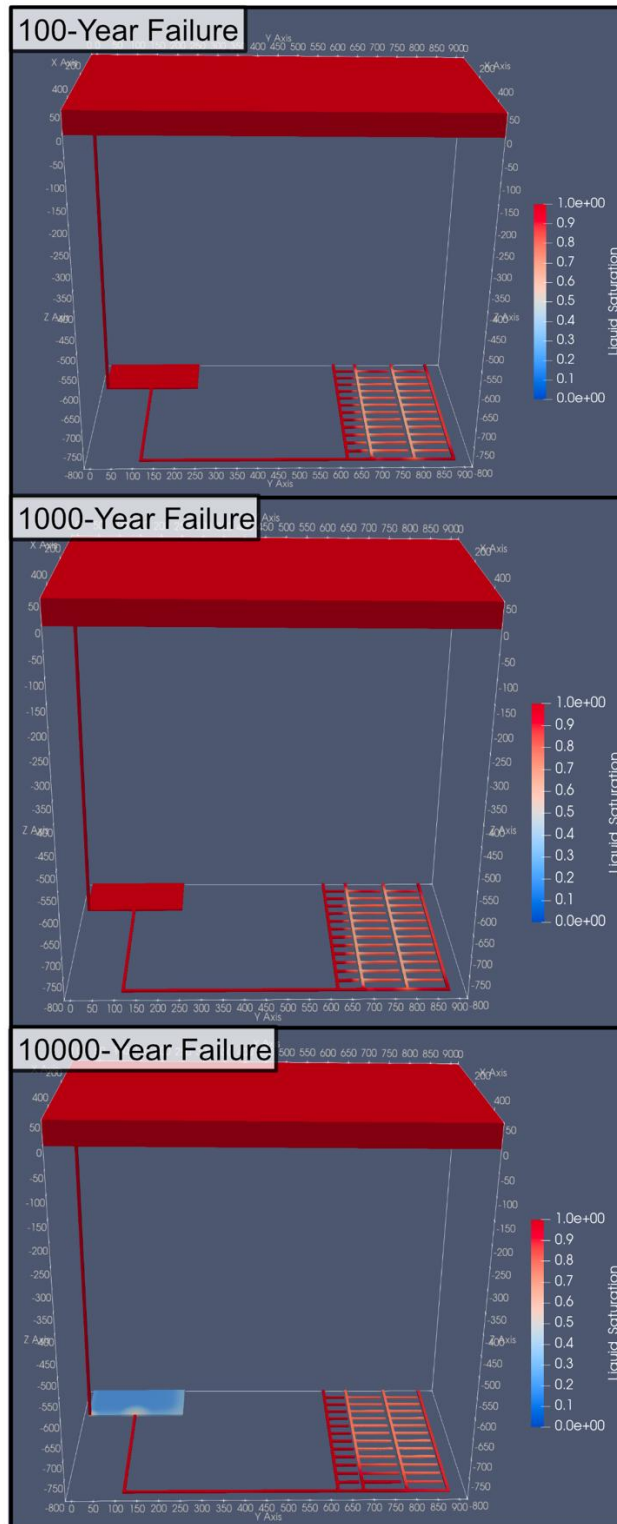**Figure C.15. Liquid saturation after 1250 years for each variant.**

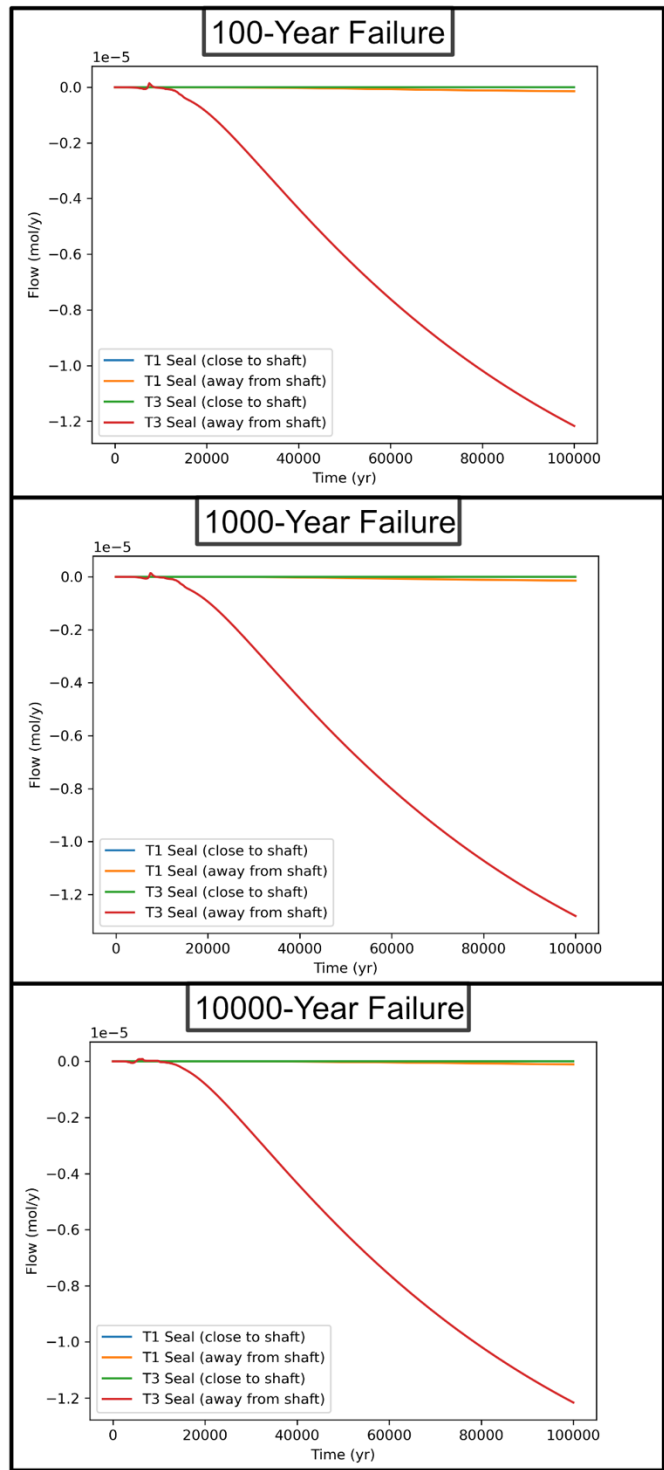**Figure C.16. Liquid saturation after 10,000 years for each variant case.**

Figure C.17. Tracer 1 and 3 flow within the drift seals.

C.6 References

G.E. HAMMOND, LICHTNER, P.C., & MILLS, R.T., "Evaluating the performance of parallel subsurface simulators: An illustrative example with PFLOTRAN" Water Resources Research, 50 (2014)

Appendix D: GRS

D.1 Introduction

D.1.1 Brief introduction to team

GRS gGmbH is a non-profit technical-scientific research and expert organization. Since 1977, GRS has been Germany's central expert organization for nuclear safety issues. GRS research focuses on reactor safety, decommissioning and dismantling, interim storage, disposal, physical protection, and radiation protection as well as environment and energy in general. GRS carried out long-term safety analyzes for generic and real radioactive waste repositories in various national and international projects. Research activities are carried out to continuously expand knowledge regarding several questions related to safe disposal of radioactive waste.

D.1.2 Why team is participating

GRS gGmbH is participating in Task F to examine the need for further development of their performance assessment code, enhance the features of the applied code and learn about different approaches and methods in performance assessment.

D.2 Reference case construction

D.2.1 Software (versions), method of calculations

GRS is using a sequentially coupled model framework called RepoTREND. RepoTREND is a modularly structured code, that contains modules for simulating processes in the nearfield, the farfield and the biosphere (Reiche et al., 2016). The integrated nearfield code LOPOS is a compartment model, which is used to simulate single-phase Darcy flow and radionuclide transport in a repository in salt (Hirsekorn et al., 1999).

D.2.2 Flow and transport model construction

How the space is represented and gridded

In LOPOS, a compartment structure can be defined to represent a network of chambers, drifts, shafts and boreholes. The shaft and the other components of the repository are modelled as LOPOS segments. Fluid flow and contaminant transport between them is modelled as a fully coupled process. The layout of the repository as represented in LOPOS near-field model is shown in Fig. D.1. Only half of the repository is represented, due to the model symmetry. The three sets of emplacement drifts are lumped together in three compartments, as simulations with each waste emplacement drift modelled separately showed no significant difference in the simulation results. The shaft is divided into two compartments, one that describes the lower 25 m of the shaft and one main shaft segment, which is above and reaches to the surface. This division was made in order to evaluate the quantities of interest regarding the shaft.

Initial and boundary conditions (if different from base case)

The salt reference case was set up according to the requirements of the task specification (LaForce, et al., 2023). The deviations from the task specification are summarized in the following. LOPOS is simulating single-phase Darcy flow, therefore relative permeability and capillary pressure functions cannot be taken into account. Also, tortuosity and compressibility of the engineered barrier system are not considered in the setup of LOPOS. Further, the natural barrier system is not modelled, because there is no significant radionuclide release from the shaft.

Implementation of tracer/radionuclide source terms, solubility limits, partitioning

The near-field code LOPOS calculates single-phase flow, driven by a pressure gradient and based on Darcy's law. According to Storck et al. (1996) the transport equation implemented in LOPOS is:

$$\frac{\partial}{\partial t}(\phi A R_k c_k) = \frac{\partial}{\partial x}\left(\phi A (D_m + \alpha u)\frac{\partial c_k}{\partial x}\right) - \frac{\partial}{\partial x}(\phi A u c_k) + \sigma_k A$$

$$- \lambda_k \phi A \left(R_k c_k - \sum_{k'} R_{k'} c_{k'} \right)$$

with

t time,

Φ porosity,

c radionuclide concentration,

A cross section of a compartment,

V volume of the compartment,

R   Retardation factor,

u   velocity,

D_m molecular diffusion coefficient,

α   longitudinal dispersion length

λ   decay constant,

σ   volume-related source term,

k   nuclide index,

k′   index for mother nuclide.

The tensor of hydrodynamic dispersion, which includes molecular diffusion D_m and longitudinal dispersion, is defined as follows:

$$(D_h)_{ij} = \Phi \cdot D_m \cdot \delta_{ij} + \alpha_L \cdot |u_j| \cdot \delta_{ij}$$

with

D_m molecular diffusion,

α_L longitudinal dispersion,

$|u_j|$ darcy velocity (Hirsekorn et al., 1999).

Since the LOPOS approach is one-dimensional transverse dispersion is neglected (Hirsekorn et al., 1999).

Solubility limits and mobilization of radionuclides are considered as described in the following.

As LOPOS is simulating single-phase flow, only radionuclides dissolved in liquid are taken into account in the transport calculation. If solubility limits are exceeded, the excess will precipitate and no longer take place in radionuclide transport. It is assumed that all isotopes of an element behave chemically identically, so that the precipitated nuclides have the same isotope ratio as the dissolved ones. The part $a_{L,i}$ of the dissolved nuclides available for transport is then:

$$a_{L,i} = \frac{V_L L_{e(i)}}{I_{e(i)}}$$

Here V_L is the liquid volume, $L_{e(i)}$ is the solubility limit of the element e to the nuclide i and $I_{e(i)}$ is the amount of substance of all isotopes of element e(i) (Hirsekorn et al., 1999).

The LOPOS approach to simulate mobilization for vitrified waste is based on the results of experiments for C31-3EC borosilicate glass (PSE, 1985). This approach describes an incongruent glass dissolution, which can consider temperature dependence. Glass dissolution is proportional to the surface of the glass assumed. The following applies for the surface-related reaction rate $j(\tau)$

$$j(\tau) = j_r \exp\left(-\frac{Q_G}{R}\left(\frac{1}{T(\tau + t_L)} - \frac{1}{T_r}\right)\right)$$

with

j_r surface related reaction rate for reference temperature,

Q_G activation energy,

R general gas constant,

T current temperature,

T_r reference temperature.

The mobilization of radionuclides from the glass matrix begins when liquid gets to the glass. If $n_B(\tau)$ is the proportion of containers that have failed at time τ and $m_G(0)$ is the initial glass mass of a container, this results in the mobilization rate for a waste container

$$\dot{\mu}_{eff}(\tau) = \frac{n_B(\tau) O_{\text{eff}} j(\tau)}{m_G(0)}$$

Here O_{eff} is the effective surface area of the glass matrix of a container on which the brine is corrosive.

Further for the calculation of radionuclide release from the Pollux container the assembly is divided into three areas: Metal, gas and fuel pellet. The total inventory is distributed to the three areas by defining relative element-specific proportions. The element-specific mobilization rates are described for all three areas (1<x<3) in the following form:

$$\dot{\mu}_{\text{eff},x,i}(\tau) = n_B(\tau) a_{x,e(i)} r_{M,x}$$

where $r_{M,x}$ are the mobilization rates in area x, n_B is the percentage of failed containers and $a_{x,e(i)}$ is the relative inventory percentage of element e in area x. the rates are all assumed to be constant (Hirsekorn et al., 1999).

D.2.3 Creep Closure

Creep closure is modelled in LOPOS as it is described in the task specification section 4.3.4.1 with the parameters given in Table 4-6 of the task specification (LaForce, et al., 2023).

Method of Calculation

The salt creep model in LOPOS is based on the equations presented in Hirsekorn et al. (1999) and Noseck et al. (2005). Change in salt volume (V) can be calculated as a function of time using:

$$\frac{d}{dt} V(t) = -K(t) \cdot V(t)$$

$$K(t) = L \cdot K_{ref} \cdot f_R \cdot f_P \cdot f_F \cdot f_T \cdot f_Z$$

with:

V(t)   volume [m³] of a compartment at time t,

K(t)   convergence rate [1/s] at time t,

L   factor for local properties of the surrounding salt,

K_{ref} reference convergence rate [1/s],

f_R dimensionless moisture creep enhancement function,

f_P dimensionless fluid pressure function,

f_F dimensionless backfill support function,

f_T dimensionless temperature function,

f_Z dimensionless explicit time dependency function.

The reader is referred to LaForce, et al., 2023 for an extended description of the governing equations for the compaction model approach of LOPOS.

D.2.4 Simplifications/divergence from the task specification in detail

Deviations from the task specification for the salt reference case (LaForce, et al., 2023) are discussed in the following. Fluid flow should be simulated utilizing a single-phase variably saturated (Richards Equation type) model. This cannot be realized in LOPOS, since LOPOS is calculating single-phase flow applying Darcy´s law.

Only half of the specified repository geometry is defined as LOPOS compartments, due to the line of symmetry through the repository and salt dome, to reduce computational effort. Each of the three sets of 25 emplacement drifts is realized as one compartment. The waste packages are not explicitly modelled as defined, but implicitly considered in the vertical borehole and emplacement drifts. Since LOPOS simulates single-phase radionuclide transport, the transport equation is only solved for compartments that have reached full liquid saturation. In 100,000 years, all compartments expect Seal-1 reach full saturation. Since diffusion can also occur in partly saturated compartments, liquid saturation of the Seal-1 compartment is manually set to 1 after 50 years for the simulation of radionuclide transport. This time was chosen because at this time radionuclides reach the neighbouring Salt compartment.

D.3 Reference Base Case Results

This section shows results of the reference case calculated with LOPOS.

D.3.1 Flow Modelling Results

Since LOPOS simulates single-phase Darcy flow, liquid saturation is defined as the ratio between liquid volume and pore volume. The mined repository initially has a liquid saturation of 20 %, while the shaft has a liquid saturation of 35 %. The evolution of the liquid saturation of selected locations in the repository is depicted in Fig. D.2. Full liquid saturation is quickly reached after a few years in case of the emplacement drifts (ED) and the salt seal. This is not due to brine inflow as the shaft is still intact at that time, but because of compaction, which reduces the pore volume (Fig. D.3). Full saturation is reached when the reduced pore volume equals the initial brine volume of 20 % for the mined repository (35 % for the shaft). Brine level increase of Seal-1 is minor at the beginning. When the Salt compartment is fully saturated the liquid flow is hindered due to the decreased pore volume, which causes a smaller transport cross section and reduced hydraulic conductivity. Therefore, brine is accumulated on the right side of the Salt compartment, which leads to brine level increase in Seal-1. Brine inflow to Seal-1 is low, due to the advanced state of compaction of the surrounding salt drifts, so that Seal-1 is not fully saturated within 100,000 years. In LOPOS, the transport equation is only solved for compartments that have reached full saturation. Therefore, for the simulation of the radionuclide transport, the liquid saturation of the Seal-1 compartment is manually set to 1 after 50 years. This time was chosen because at this time radionuclides reach the neighbouring Salt compartment. This modelling decision is also discussed in section D.2.4.

The homogeneous shaft compartment is fully saturated after 18,000 years. Thus, a continuous transport path would be present after that point in time.

Liquid pressure build-up during inflow is due to brine level increase. After a compartment is fully saturated, full hydrostatic pressure is reached instantaneously. Afterwards liquid pressure of the salt compartments (Fig. D.4) is tending towards lithostatic pressure because of the ongoing compaction that reduces the voids.
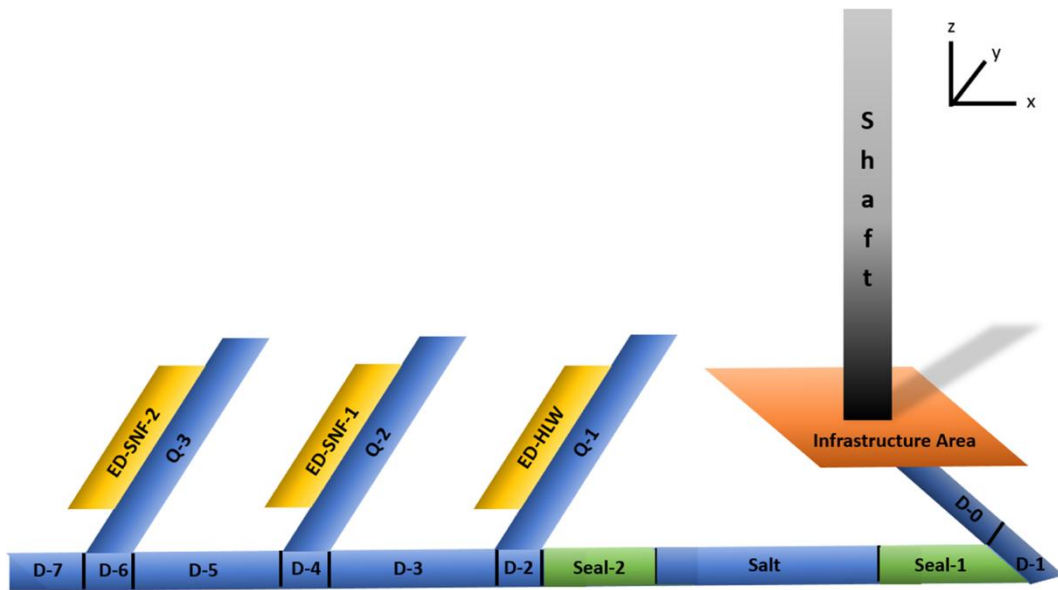
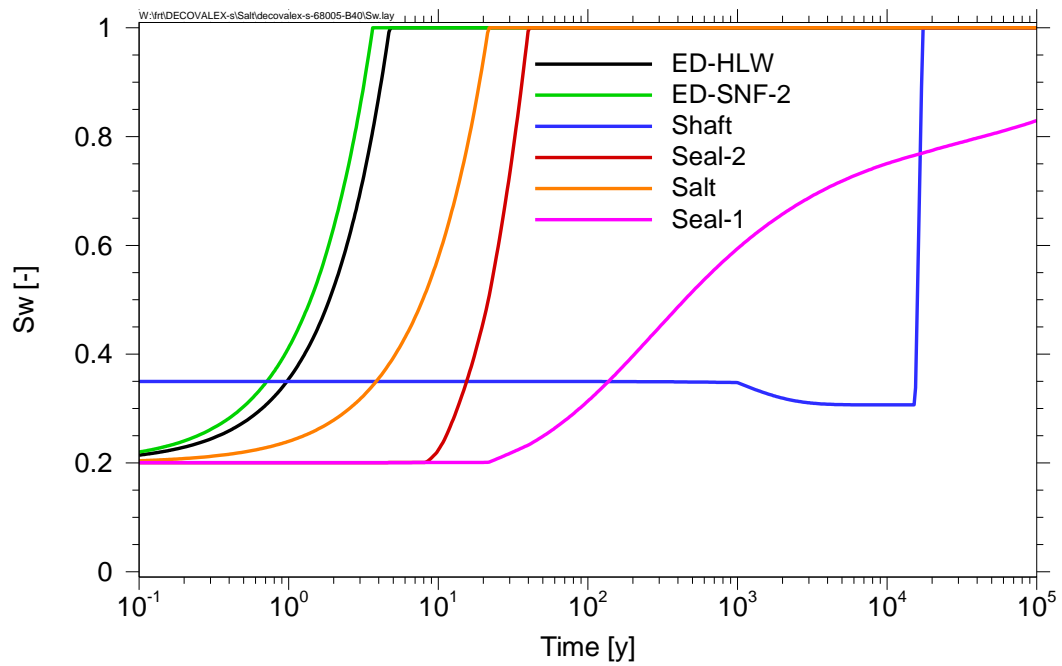**Fig. D.1: Reference case LOPOS layout for the performance assessment case**

Fig. D.2: Liquid saturation of selected compartments
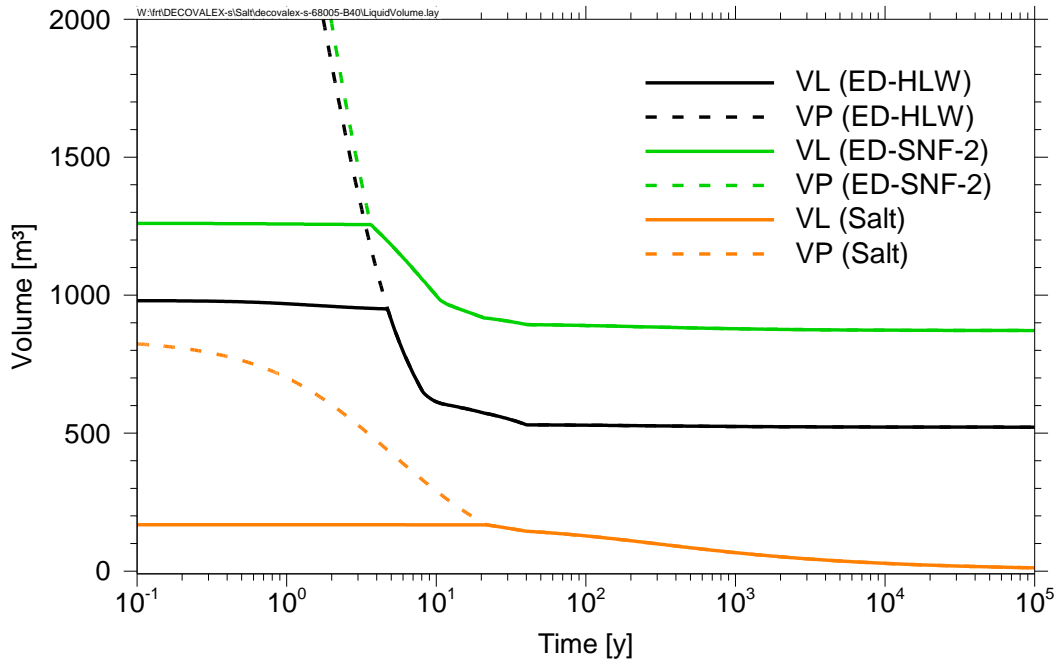
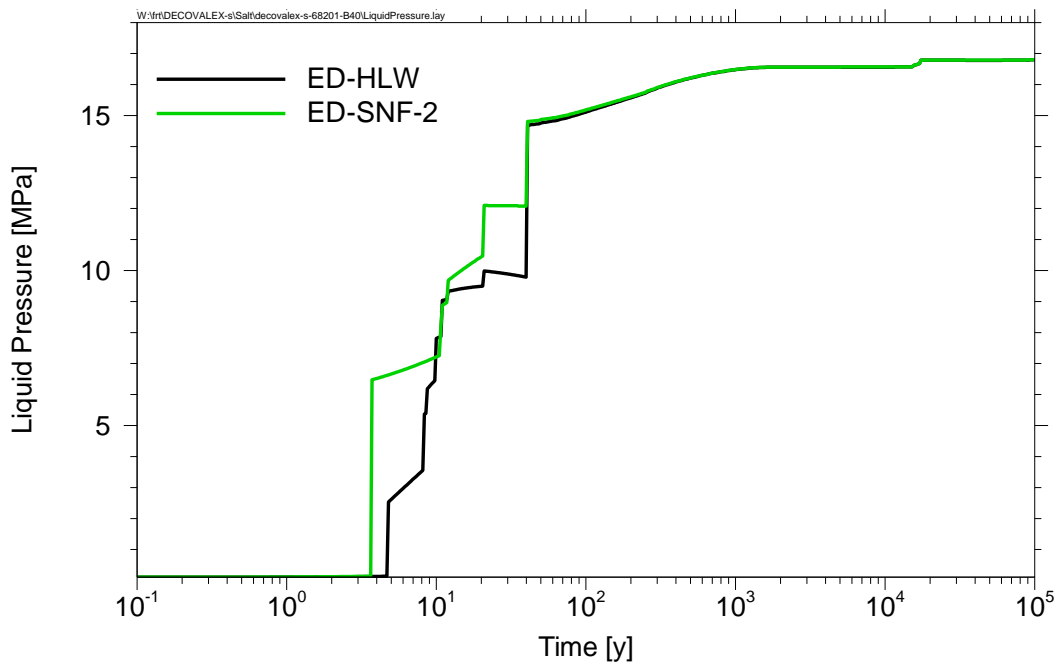**Fig. D.3: Liquid (VL) and pore (VP) volume of compacting compartments**

Fig. D.4: Liquid pressure of ED-HLW and ED-SNF-2 compartment. Temporal pressure decrease is due to LOPOS specifics

D.3.2 Tracer/Radionuclide Release and Transport Results

The discussion in section D.4 focusses on Tracer 1 and Tracer 3, therefore the results of radionuclide release and radionuclide transport are discussed in the following. Fig. D.5 shows the release of radionuclides from the emplacement drift for HLW (left) and SNF (right). Since glass dissolution starts at the beginning, the release from the ED-HLW segment starts initially. After 500 years, the SNF canisters fail, releasing radionuclides from the ED-SNF-2 compartment from that time on. When ED-HLW and surrounding compartments reach full saturation the radionuclide release from ED-HLW and ED-SNF-2 is affected from LOPOS numeric used to simulate salt compaction. The release rates of U-234 and U-238 increase in the beginning but decrease after 500 years, as they reach their solubility limit and are squeezed out of both emplacement drifts due to compaction. I-129 also shows a sharp increase after SNF-canister failure, but this is related to the instant release fraction of this nuclide. The effectiveness of the sealing system depends on how well it contains the radionuclides. To answer that question, Fig. D.6 shows the release of radionuclides from Seal-1 compartment and Fig. D.7 depicts the total amount of each radionuclide that has left the seal system. U-238 and Tc-99 occur with the largest masses followed by I-129. Yet these amounts are still very low.
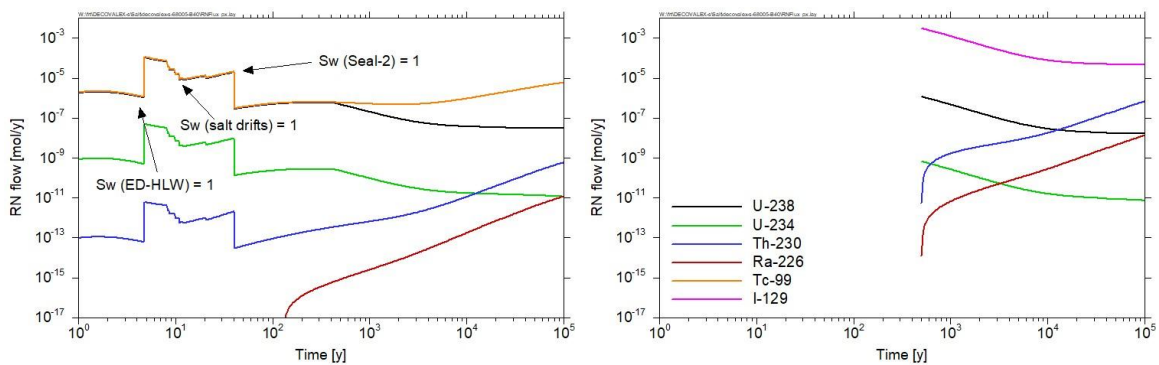

Fig. D.5: Radionuclide release from ED-HLW compartment (left) and ED-SNF-2 compartment (right). The legend applies for both.
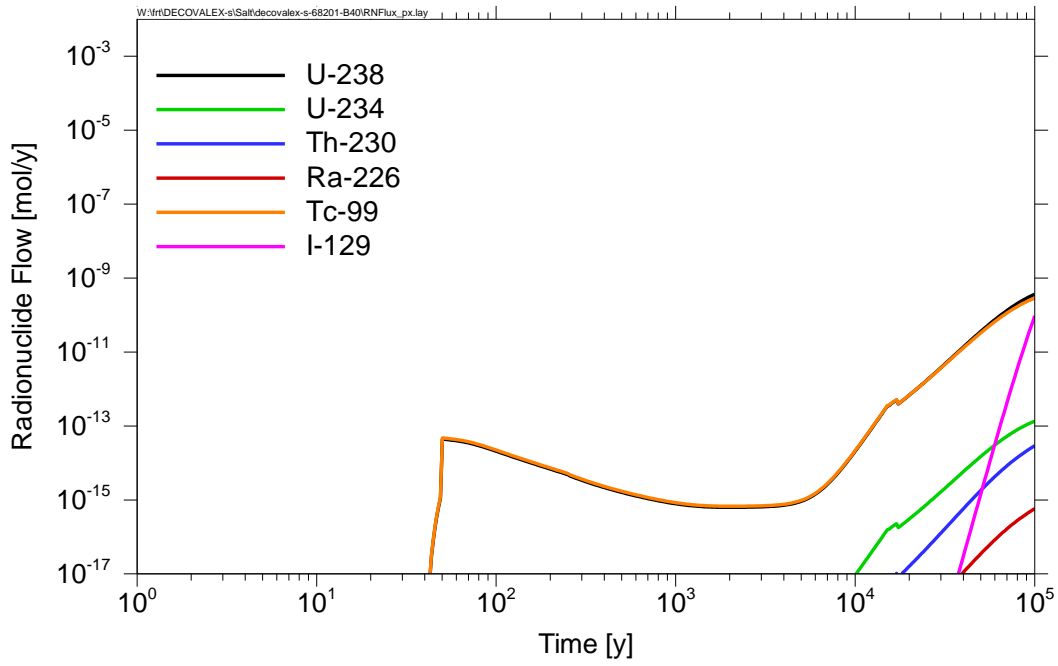
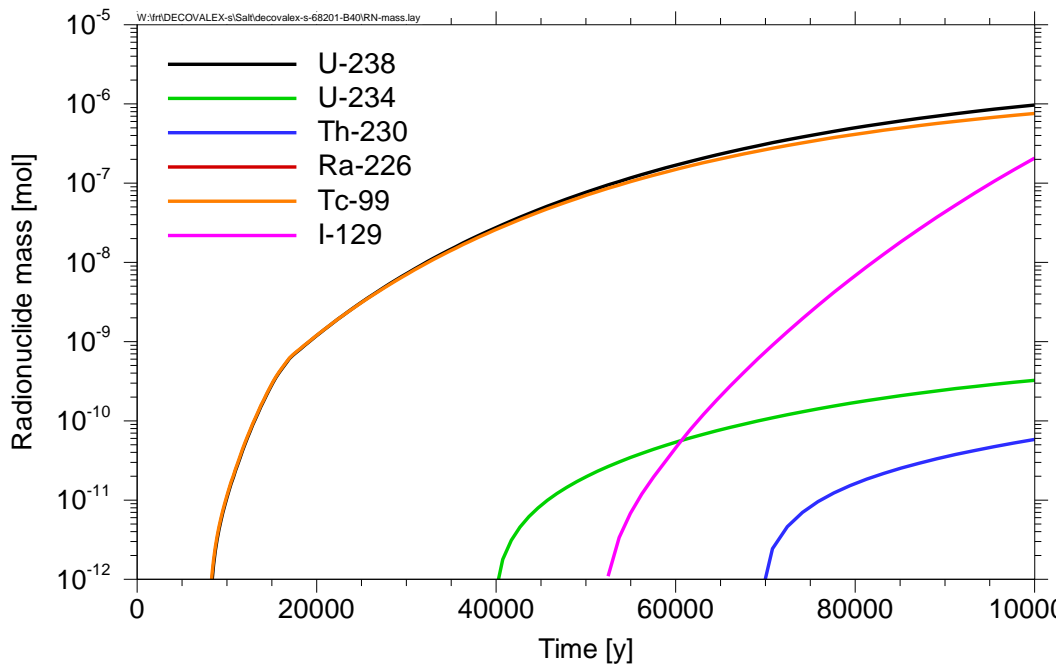**Fig. D.6: Radionuclide flow out of Seal-1 compartment.**

Fig. D.7: Radionuclide mass´ present in the compartments on the right side of Seal-1.

D.3.3 Creep closure results

Fig. D.8 depicts the compaction rates and the related porosity evolution for selected compartments. The main porosity decrease takes place within ten years in case of ED-HLW and ED-SNF-2. The compaction process is quite fast because the initial saturation of 20 % leads to higher compaction rates (wet creep). After 10 years the pore volume has been reduced so far that the initially present liquid volume fills the complete remaining pore space. After that, porosity can only be further reduced by squeezing out liquid. This happens predominantly in the Salt compartment, since it is surrounded by the abutment drifts and squeezing is relatively easy because the surrounding compartments are not compacting and Seal-1 does not reach full saturation during the entire 100,000 years. The drops in the compaction rate are due to the LOPOS numeric approach how to couple compaction and flow processes.
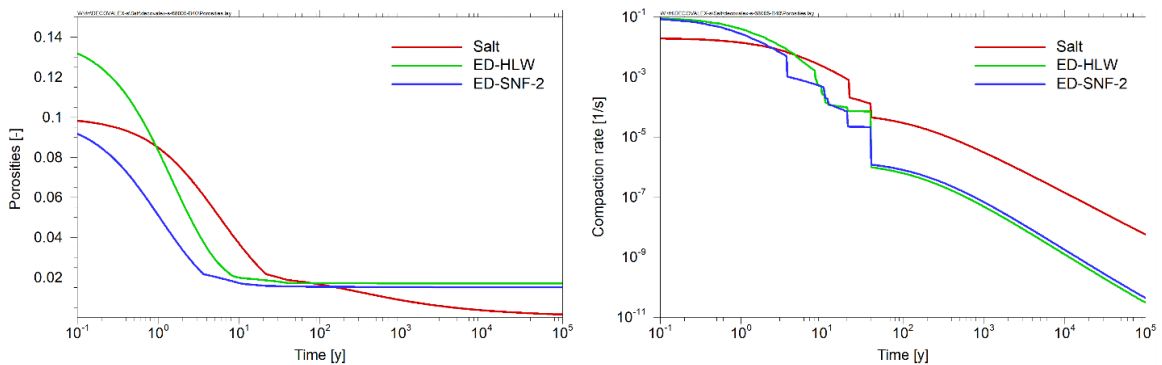

Fig. D.8: Porosity and compaction rate evolution of the compartments Salt, ED-HLW and ED-SNF-2.

D.4 Discussion of QOI Results

The results which are discussed in this section are presented in Section 5 and compared with the results of the other teams.

D.4.1 Waste Drift Quantities

Brine Saturation and Flux

The liquid level of the compartments ED-HLW and ED-SNF-2 rises constantly until full saturation is reached. ED-HLW is fully saturated after five years and ED-SNF-2 after four years. The deviation is due to the higher porosity of ED-HLW. These compartments reach

their full saturation state due to the reduced pore volume and not due to brine inflow. Compaction causes brine outflow of these compartments. In the short and early period prior to full saturation ED-HLW brine flow increases. After full saturation is reached squeezing begins, resulting in a sharp flow peak. As the surrounding compartments are compacting too, the flow resistance becomes larger. Hence brine flow is decreasing with time. Brine outflow of ED-SNF-2 is similar, but occurring earlier, because full saturation is reached earlier. Also, the squeezing peak is less high, which is caused by the lower hydraulic conductivity of that compartment, which is a result of the smaller porosity.

Porosity

The main porosity decrease of the compartments ED-HLW and ED-SNF-2 takes place within the first ten years. Afterwards the pore volume is equal to the initially present liquid volume. After 10 years, porosity is reduced much slower, because of the present liquid.

Tracer 1/Tracer 3

As glass dissolution starts at the beginning, the release from the ED-HLW segment starts initially. The calculated release rate is affected by the numerical method implemented in LOPOS to simulate salt compaction. When the compartments ED-HLW and the surrounding salt drifts are fully saturated because of compaction, the flow of Tracer 3 increases. Full saturation of Seal-2 compartment reduces the flow of Tracer-3 since that limits the advective flow. After 500 years, the SNF canisters fail, releasing Tracer-1 from the ED-SNF-2 compartment at that time. Tracer 1 shows a sharp increase after canister failure, which is caused by the instant release fraction. In the following time a congruent release takes place.

D.4.2 Seal Quantities

Brine Saturation and Flux

It takes 40 years for Seal-2 (closer to the waste) to fully saturate. Seal-1, on the other hand, is not fully saturated during the observation time. After 100,000 years Seal-1 reaches 80 % brine saturation. The seals behave differently because of the compacting salt compartment between the two. The salt seal limits the brine that is squeezed from the repository towards the shaft. Seal-2 can fill up with this brine, but the flow through the salt seal is minor. Seal-1 saturates due to the brine coming from the shaft, but due

to the large infrastructure area this amount is limited too. Consequently, the adjustments discussed in section D.2.4 were necessary for the simulation of the reference case.

Tracer 1/Tracer 3

The flow of Tracer 1 and Tracer 3 into the seal nearest the waste and out of the seal nearest the shaft increase with time. At early times Tracer 3 flow of is affected by compaction and the reduction of the pore volume of the neighboring compartment. After 100,000 years the radionuclide flow is the highest in the order of 10-5/10-6 mol/y.

The largest flow out of the seal nearest the shaft is at the end of the observation time with a small order of magnitude (<10-10 mol/y). Tracer flow is significantly decreased from Seal-2 to Seal-1 due to the efficiency of the salt seal compartment. The deviation between Tracer 1 and I-129 and Tracer 3 and Tc-99 is marginally (compare Fig. D.6).

D.5 Investigation of Variant Cases

Several variants of the reference case were investigated. One variant examines the heterogeneous shaft instead of the homogeneous one. In another variant, each emplacement drift is simulated individually instead of being combined into one large compartment. Furthermore, the influence of an initially dry or residually saturated salt on compaction is investigated.

When comparing the heterogeneous shaft with the homogeneous shaft, minor differences are observed. LOPOS calculates that in the homogeneous case, the shaft becomes completely saturated after 17,400 years, whereas the heterogeneous shaft takes 28,500 years to reach full saturation. This difference is considered negligible over a 100,000-year assessment period. Additionally, what becomes very apparent in the heterogeneuos design is the effectiveness of the sealings. They exhibit low hydraulic conductivity, which is reflected in the fact that the liquid volume in the compartments initially flows into the underlying segments, and less liquid intrudes from above, causing the compartments to desaturate initially (Fig. D.9). The Drainage Layer, Gravel 1, and Abutement 1 desaturate first because Sealing 1 holds the liquid back, causing the liquid to accumulate in the segments Abutement 2 and Crushed Salt. In these two segments, the liquid accumulates due to the low-permeability layer Sealing 2, which is also

responsible for the desaturation of Abutement 3, Gravel 2, Sealing 3, and Abutement 4. In the reference case, the emplacement drifts are united to one large compartment. In order to examine whether this assumption is valid, a simulation was carried out in which each emplacement drift was modelled individually. The liquid saturation of the emplacement drift chosen as location of interest is compared to the liquid saturation of the united emplacement drift compartment in Fig. D.10. The curves are almost identical, the differences in the liquid saturation can only be seen in the third decimal place.

Due to the initial saturation, porosity evolution of Salt and ED-SNF-2 compartment (Fig. D.11) differ mainly in how low the porosity decreases and when this state is reached. The fast porosity decrease that initially occurs is slowed down by the amount of brine initially present. Especially for the Salt compartment, the porosity curves are similar because this is not surrounded by compacting salt (but abutments), which makes squeezing easier for the Salt than the ED-SNF-2 compartment.
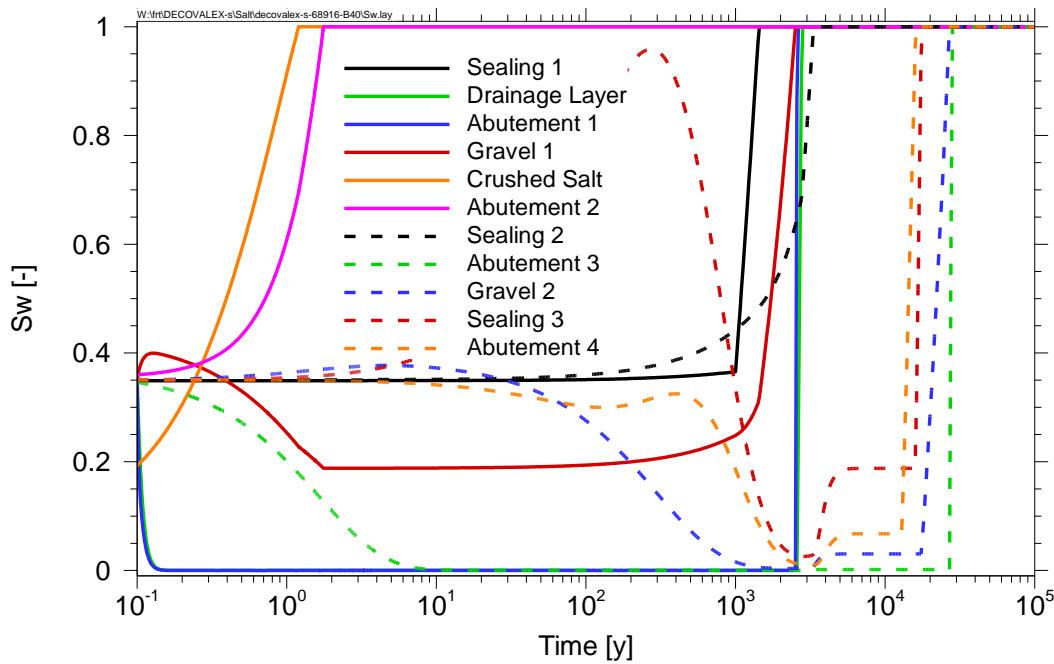
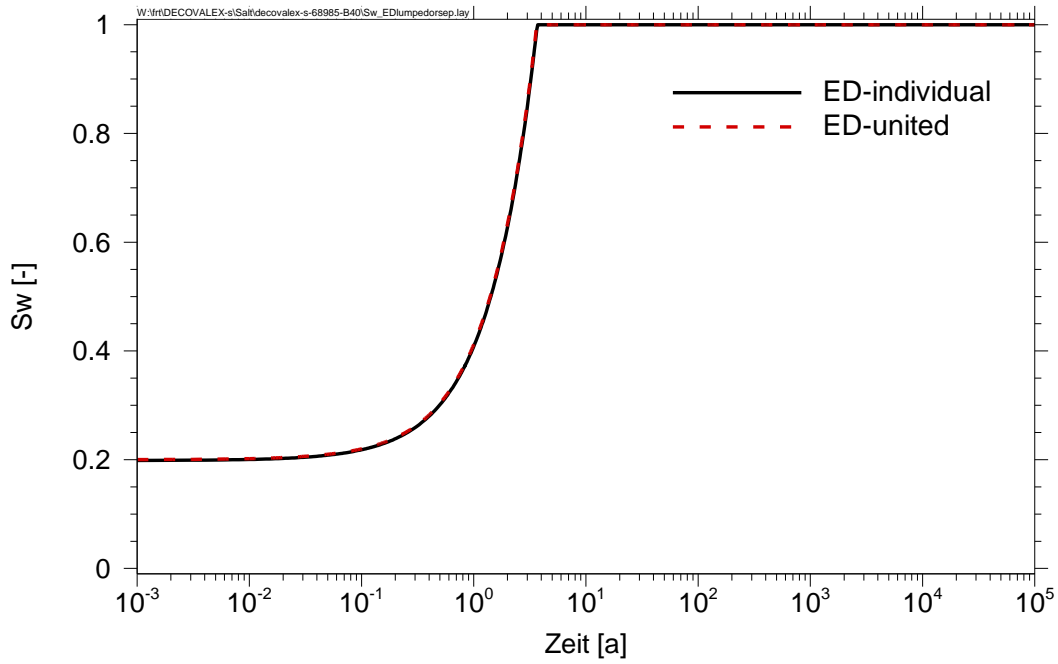**Fig. D.9: Liquid saturation (Sw) of the heterogenous shaft compartments.**

Fig. D.10: Comparison of the liquid saturation (Sw) for the ED-SNF-2, when modelled individually or united to one large compartment.
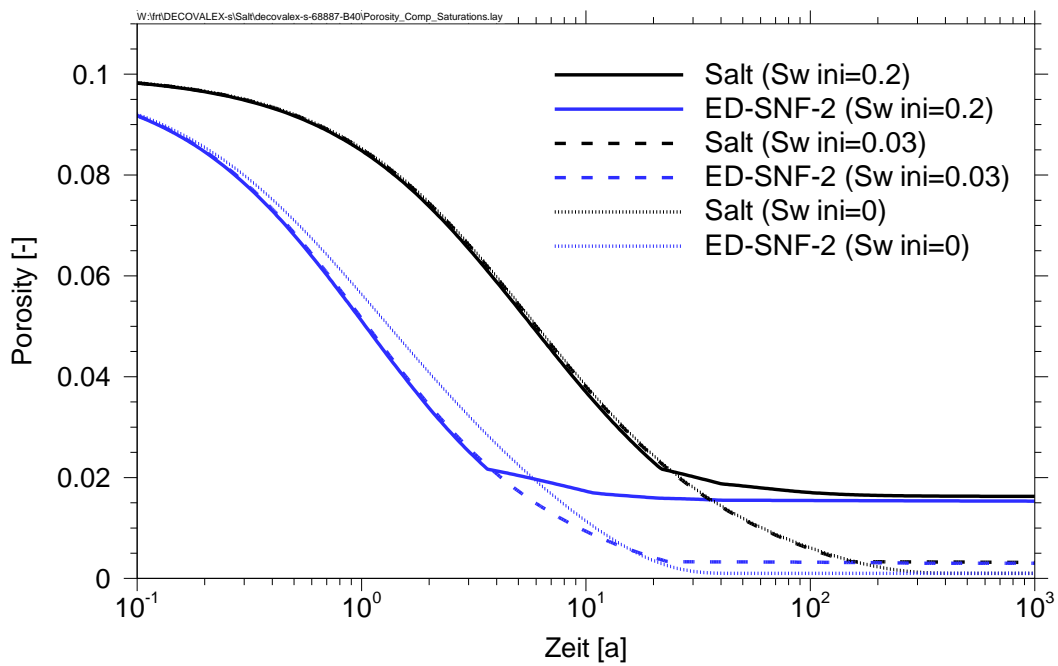

Fig. D.11: Porosity evolution of the compartments Salt and ED-SNF-2 for different initial saturation (Sw ini) assumptions

D.6 References

LaForce, et al., 2023. DECOVALEX-2023 Task F Specification Revision 10. SAND2023-04005R, Sandia National Laboratories, Albuquerque, NM.

Storck, R., Buhmann, D., Hirsekorn, R.-P., Kühle, T., Lührmann, L. (1996): Das Programmpaket EMOS zur Analyse der Langzeitsicherheit eines Endlagers für radioaktive Abfälle. Version 5. GRS-122, GSF-Forschungszentrum für Umwelt und Gesundheit GmbH, ISBN 3-923875-75-4, Braunschweig.

Hirsekorn, R.-P., Boese, B., Buhmann, D. (1999): LOPOS: Programm zur Berechnung der Schadstofffreisetzung aus netzwerkartigen Grubengebäuden. GRS-157, Gesellschaft für Anlagen- und Reaktorsicherheit (GRS) mbH, ISBN 3-931995-19-4, Braunschweig.

Noseck, Ulrich, Wernt Brewitz, Dirk-Alexander Becker, Dieter Buhmann, Christine Fahrenholz, Eckhard

Fein, Peter Hirsekorn, Sven Keesmann, Klaus-Peter Kröhn, Ingo Müller-Lyda, André Rübel,

Anke Schneider, Richard Storck. (2005). Wissenschaftliche Grundlagen zum Nachweis der Langzeitsicherheit von Endlagern. GRS, Germany, GRS-204.

Projekt Sicherheitsstudien Entsorgung (PSE), Abschlußbericht, Fachband 10. Berlin, Januar 1985.

Reiche, T. (2016): RepoTREND – Das Programmpaket zur integrierten Langzeitsicherheitsanalyse von Endlagersystemen. GRS-413, Gesellschaft für Anlagen- und Reaktorsicherheit (GRS) gGmbH, ISBN 978-3-944161-95-2, BMWi-FKZ 02E10367, Braunschweig.

Appendix E: Quintessa

E.1 Introduction

E.1.1 Brief introduction to team

Quintessa's vision is to provide leading-edge scientific, mathematical and strategic consultancy, scientific software development and research to public and private science-based organisations to facilitate a low carbon energy future.

Quintessa was founded in 1999 with the aim of providing an enjoyable and fulfilling working environment in which talented scientists and mathematicians can use their problem solving skills to help clients address key issues. Quintessa operates at the interface between academia and industry, facilitating the application of leading-edge knowledge in a timely and cost-effective manner. Quintessa has been heavily involved in radioactive waste management since its inception and has been active in DECOVALEX since 2007.

Quintessa's contribution to Task F is self-funded with a team comprising of Alex Bond, Steven Benbow, Josh Nicholas and Jodie Stone.

E.1.2 Why team is participating

Quintessa has a general interest in building models that are comprehensive enough to include all relevant processes *at an appropriate level*, but simple enough that they can be readily understood and run repeatedly. The ability to strike this balance between complexity and simplicity is critical to producing models that can be used to generate insights into the potential performance of a complex coupled system while being sufficiently transparent that the results can be presented with confidence.

This task provides an excellent opportunity to understand how to construct numerically robust models that are transparent, representative and practicable for detailed sensitivity/conceptual uncertainty analysis.

E.2 Reference case construction

E.2.1 Software (versions), method of calculations

For the reference case calculations the primary tool was the Quintessa multi-physics code QPAC (https://www.quintessa.org/software/QPAC), currently at version 4.2. The code is implemented using a 'model as input' approach meaning that process modelling equations can be added and modified directly by the user at runtime without changing the code. Several pre-built 'modules' (collections of processes, with associated documentation and testing) are available for QPAC. For the purposes of these calculations, the following modules were used:

- Multiphase flow (water + arbitrary number of phases, including water vapour and dissolution; Darcian flow in porous media)
- Richards' equation (partially saturated Darcian flow)
- Tracer Transport (advection, diffusion, dispersion of tracer contaminant in fluids in porous media; includes retardation, solubility limitation etc.)

As discussed below, bespoke physical relationships were implemented to represent release of contaminants from the waste and creep closure of the access drifts and brine inflow from the host rock (as a variant case only).

QPAC is primarily a finite volume code, with the additional flexibility of being able to specify variables on the interfaces between finite volumes ('compartments'), as well as on the volume centroid. Depending on the choice of formulation, this can yield a mixed-element formulation. QPAC supports both gridded geometries (either using an internal gridding methodology or importing external meshes) and abstract geometries. These different geometry types can be used together, if needed. All calculations are monolithic (all equations solved simultaneously) using a fully implicit time stepping approach, which allows full coupling of all simulated processes, if desired. The solution method is a customised DAE solver with variable-order adaptive timestep control.

QPAC is not a high performance code, so all calculations are single-threaded; the emphasis of the code philosophy is user flexibility and rapid model development rather than pure computational efficiency.

For the benchmarking work GoldSim v14.1 (https://www.goldsim.com/) and COMSOL v6.0 (https://www.comsol.com/) were also used.

E.2.2 Flow and transport model construction

How the space is represented and gridded

A relatively coarse finite volume mesh was used to represent the system. Only the engineered components of the system (access shaft, tunnels and drifts) were represented explicitly. Simple calculations showed that for the purposes of fate and transport (primarily diffusion) through the salt dome, the only pathway that could credibly cause any impact to surface would be via the engineering; hence the host rock was neglected from the calculations, being only represented via a boundary condition that can be optionally included to impose a brine source from the geosphere. The schematic of the model implementation and the gridded model are shown in Figure E.1 and Figure E.2. The length of compartments along each network leg was kept approximately uniform to aid numerical stability and to keep numerical dispersion broadly consistent through the model. Due to the symmetry of the system, only half the repository was modelled. The model contains only 159 finite volumes (compartments). The model is built using QPAC's capability to grid arbitrary Cartesian or cylindrical regions and join them together to create more complex geometries. With the exception of the infrastructure area and waste panels, each 'subgrid' in the model is represented by a 1D section. In particular, tunnels are represented as 1D sections with no vertical discretisation. This choice is investigated in a variant case.

The model was setup so that both the homogenised and detailed representations of the shaft engineering could be modelled. Consistent with the specification, the homogenised representation was the default.
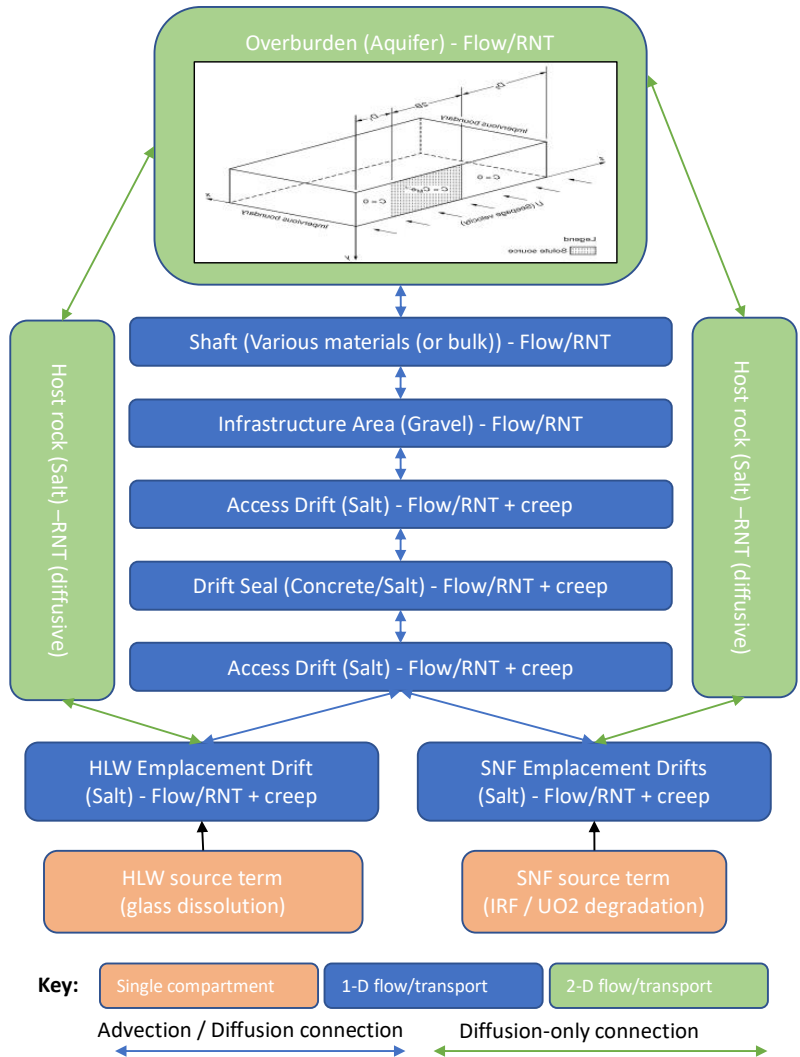
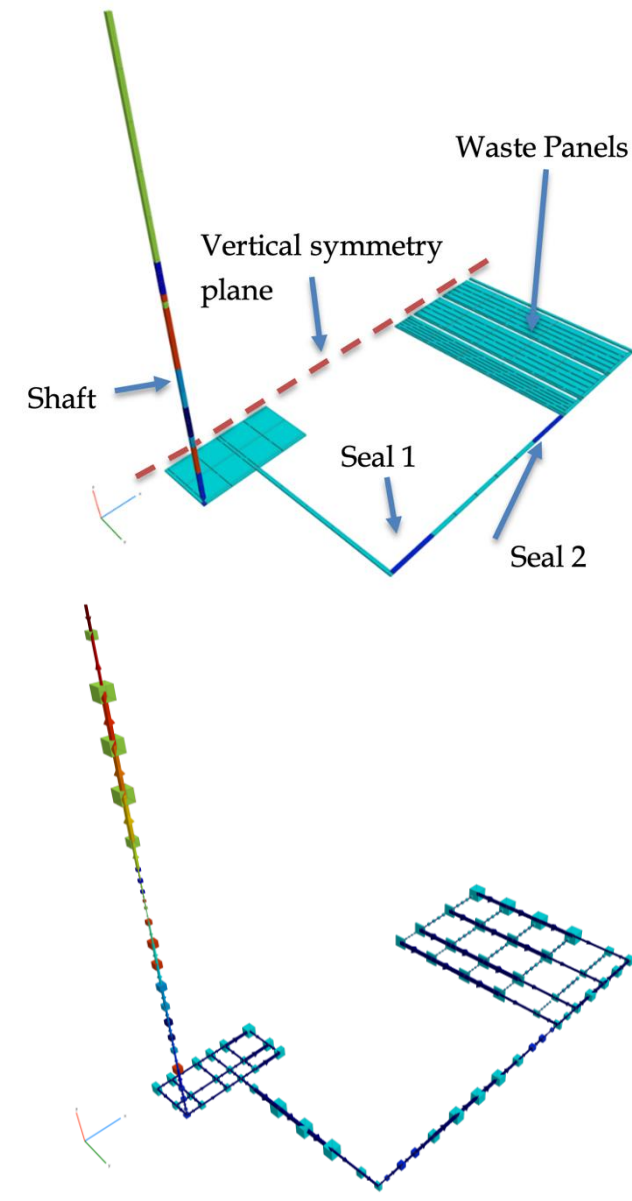**Figure E.1. Conceptualisation of the reference salt repository model**

Figure E.2. Image showing the QPAC model grid (coloured by intrinsic permeability on a log scale) showing the 1D legs making up the model (bottom) and the volumetric representation (top), where compartment volumes represent true cell sizes. The heterogenous shaft infill is shown here.

One simplification of the model was in the waste areas. Rather than model the tunnels explicitly, they were homogenised into larger panels which can contain a non-integer number of disposal tunnels. Waste disposal packages were also not modelled explicitly because the release mechanisms specified do not require an individual treatment due to a lack of spatial variability and no local process coupling (e.g. water saturation, mechanical loading etc). However, the release mechanisms specified were implemented in a homogenised approach using the functions given.

The aquifer was not included in this version of the model because no significant radionuclide concentrations were observed leaving the shaft top.

Initial and boundary conditions (if different from base case)

Initial conditions are and boundaries are implemented as specified in the base case.

Implementation of tracer/radionuclide source terms, solubility limits, partitioning

Release from the wastes is represented via all contaminants having a '*_waste' version with the correct initial mass in each compartment. According to the required release functions the '*_waste' radionuclides and tracers are applied in a source term to corresponding mobile radionuclide. Both the '*_waste' and mobile variants of each radionuclide decay and in-grow as given in the specification.

Solubility of the radionuclides is available in the tracer transport module, and was implemented as specified in the base case.

E.2.3 Creep Closure

Assumptions

The supplied GRS model for creep closure, as given in the specification was adopted directly in the QPAC model and was coupled directly to the solve.

Method of calculation

An additional variable for each volume (only used where salt convergence is active) was added to the model allowing the convergence strain to be calculated, hence giving the converged porosity. The only change to the model was that the 'p-p_{atm}' pressure term in equation 4.6 (LaForce et al., 2023) was limited to a minimum of 0 MPa and a maximum of p_{hydro} to prevent problematic numerical effects, especially the impact of very high suctions which the GRS model was not designed to accommodate. This modification effectively prevents the largely chemical, rather than mechanical, fluid pressures from accelerating convergence and is consistent with the general philosophy of the convergence model.

The GRS model was fully coupled with the rest of the case. This means that fluid pressure influences the creep closure, which impacts porosity, which in turn impacts the fluid pressures (through fluid saturation and fluid compression).

E.2.4 Simplifications/divergence from the task specification in detail

As noted previously, the only simplifications are in the geometrical treatment of the system by:

- Homogenising the waste tunnels into fewer waste 'panels' each containing multiple tunnels.
- No explicit treatment of individual waste packages and representing degradation of barriers and release through the specified release functions.
- No explicit treatment of the host rock, but the capability to allow for brine inflow using a simplified representation of flow was included instead.
- No aquifer representation (unneeded given the lack of release)

In addition to improve run time, the van-Genuchten retention curves were linearised from 90% water saturation to 100% water saturation. This prevents the infinite gradient at 100% water saturation which is numerically challenging. Testing showed that this simplification reduced run-time by a factor of 2 or 3, depending on the case, but made no significant difference to the results.

It is noted that run times were sufficiently fast that the homogenisation of tunnels perhaps wasn't necessary, and explicit representation would have been practicable for this model.

An additional minor difference was that creep convergence only starts after 0.2 y. The capability to allow for delayed convergence was a defensive measure to initially stabilise the model and also represent the operational part of the repository lifetime; however such a capability was not needed in the final version of the specification. The impact on the porosity evolution of having convergence starting immediately is discussed in section E.4.

E.3 Reference Base Case Results

The reference case model runs in approximately 10 minutes on a typical workstation using a single thread.
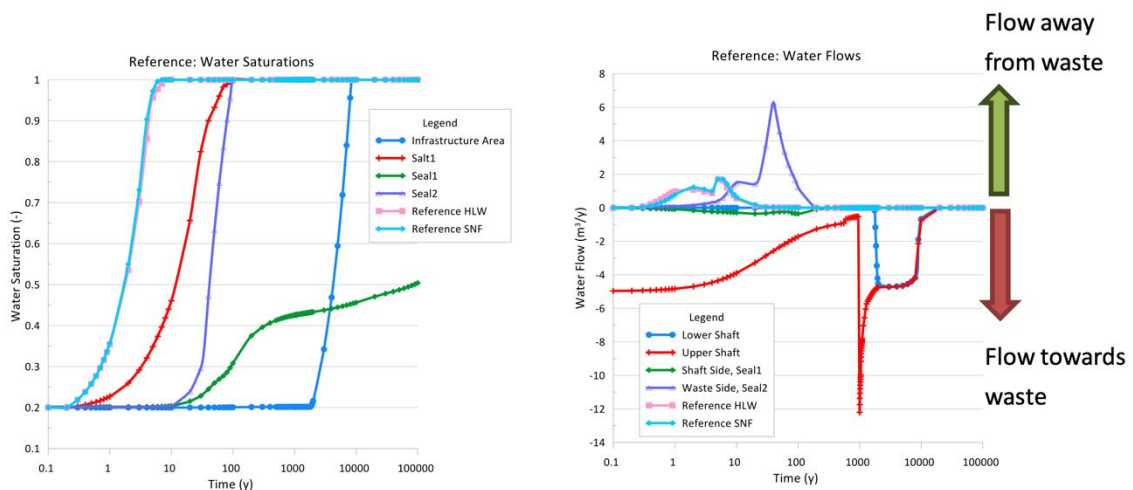
E.3.1 Flow Modelling Results

Figure E.3. Quintessa results, volumetric water flows (right) and saturations (left) in the specified repository regions.
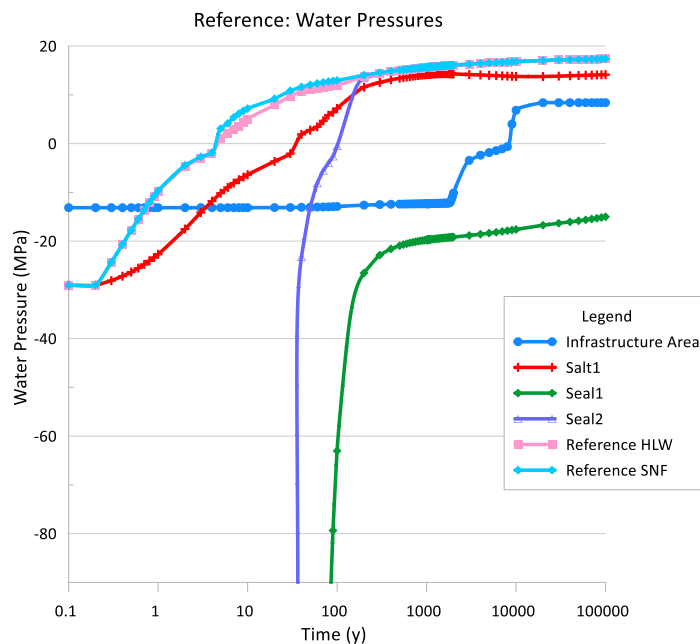

Figure E.4. Quintessa results, water pressures in the specified repository regions.

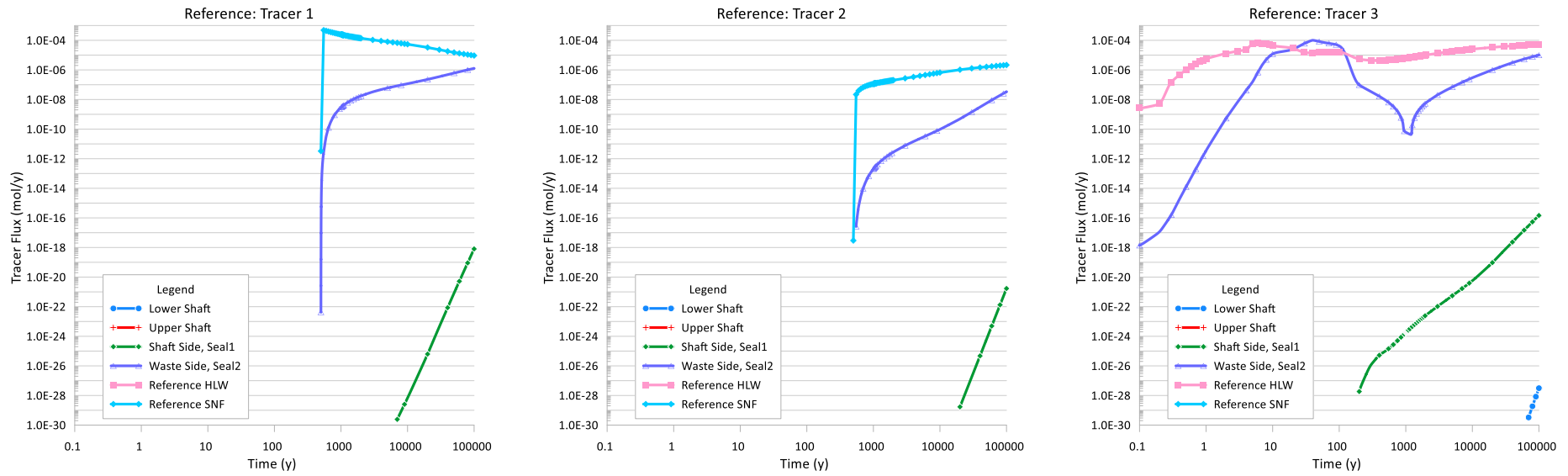## E.3.2 Tracer/Radionuclide Release and Transport Results

Results are shown in Figure E.5 and Figure E.6.

Figure E.5. Quintessa results, tracer 1 to 3 discharges in the specified repository regions.
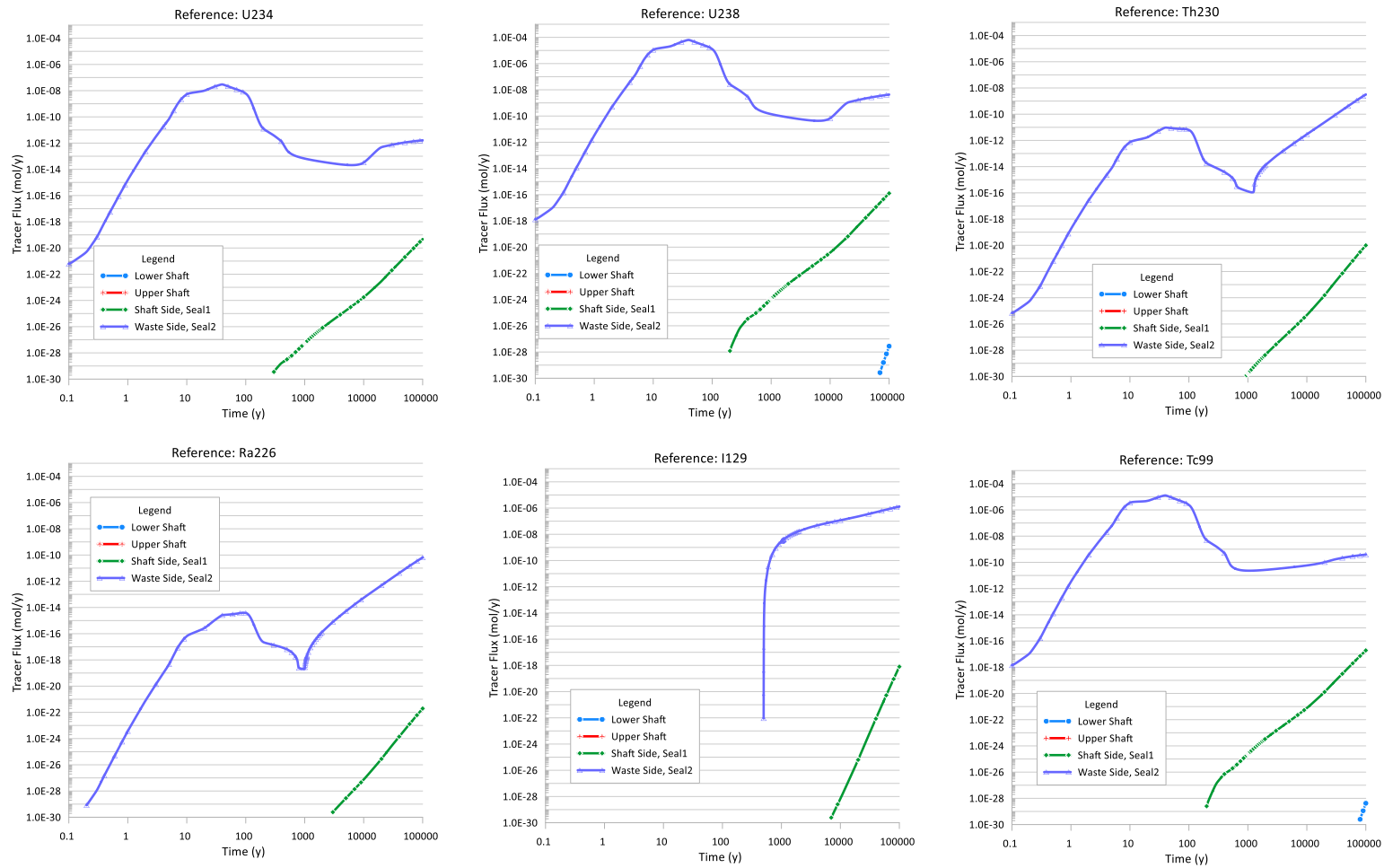
Figure E.6. Quintessa results, radionuclide discharges. Note that the discharges from the SNF and HLW drifts are not included because the results add to the complexity of the plots without adding a great deal of insight above the tracer results.

E.3.3 Creep closure results

The model implemented in QPAC is the GRS model documented by LaForce et al (2023), so deviations in results from the GRS model (see Figure E.7) only come about due to:

- Differences in evolution of fluid pressure in the repository
- An inconsistency in the GRS initial porosity definition for the HLW disposal drifts. The GRS results assume 0.14 initial porosity, whereas the QPAC model reflects the specification with an initial porosity of approximately 0.1
- A slight difference with when convergence starts in the model. For the Quintessa results a small delay is introduced before convergence starts (0.2 y), which is not present in the GRS results.

This initial delay in the convergence was included as a defensive measure to help stabilise the initial rapid transients in the solution at very early times (as well as a capability to allow delay in convergence to be modelled, e.g. representing an operational phase) and is a trivial difference between the models. The current reference case parameterisation shows as an exaggerated difference in the early time porosity behaviour, when plotted with a logarithmic time axis. To confirm this assertion, a variant was run to show this delay could easily be removed if required and that the QPAC and GRS evolutions would be consistent for the SNF and Salt 1 zones– see Figure E.8. All other quantities of interest were essentially unchanged.
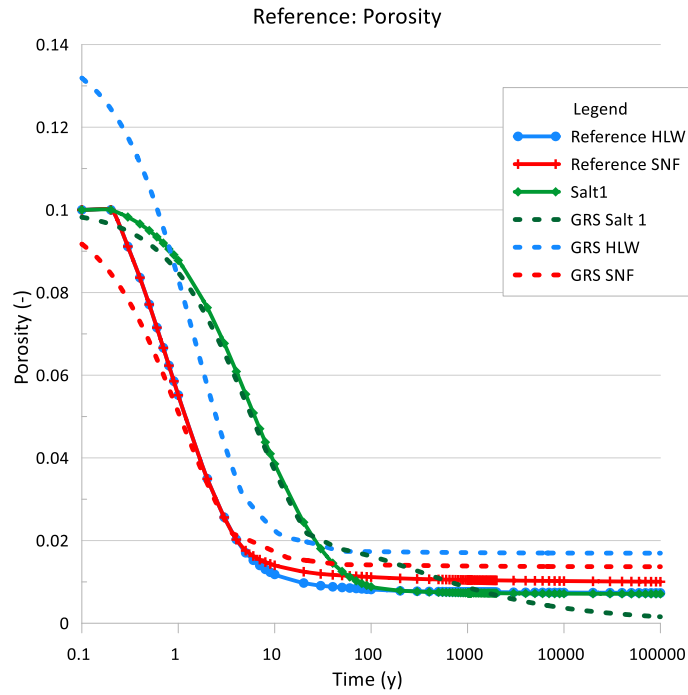
Figure E.7. Quintessa reference case and supplied GRS porosities with time. The inconsistency in the HLW result primarily arises because GRS results assume 0.14 initial porosity, whereas the QPAC model uses an initial porosity of ~0.1, consistent with the specification.
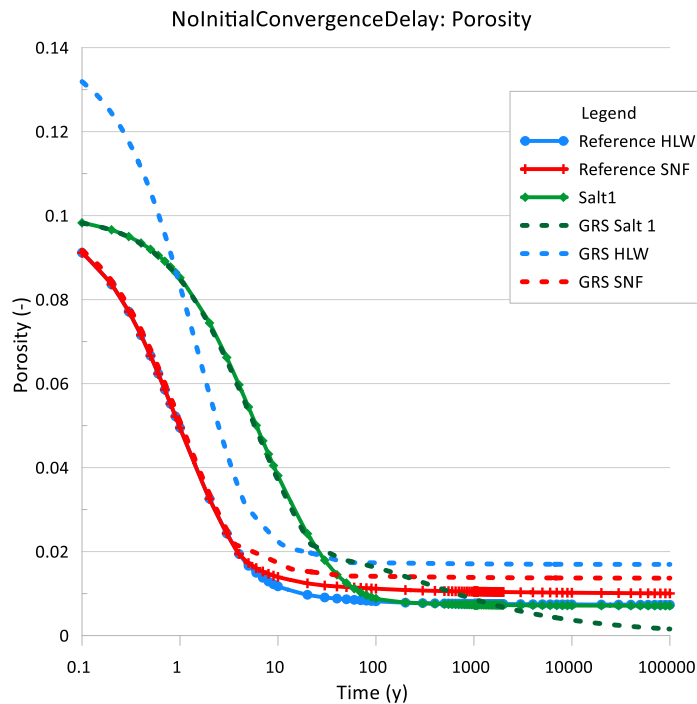

Figure E.8. Quintessa reference case variant (no initial delay on convergence) and supplied GRS porosities with time. The inconsistency in the HLW result primarily arises because GRS results assume 0.14 initial porosity, whereas the QPAC model uses an initial porosity of ~0.1, consistent with the specification.

E.4 Discussion of QOI Results

E.4.1 Brine Saturation and Flux

The results in the previous sections show there are two competing components of repository resaturation. The creep closure of the drifts is the dominant mechanism for the salt-filled portions of the facility, since it displaces in situ porewater and locally reduces porosity, both of which lead to changes in saturation, while for the shaft, infrastructure area and concrete seals it is the flow of water that controls resaturation. In terms of the seals, the seal closest to the waste (Seal 2) resaturates relatively quickly as water is 'squeezed' out of the waste areas into the seal. In contrast Seal 1 remains partially saturated due to the hydraulic connection with the shaft being very limited through creep closure between the infrastructure area and the seal. The low permeability of this zone prevents the resaturation of the concrete seal (Figure E.9). The infrastructure area and shaft (which don't converge in the base case) also provide a sink for any water 'squeezed' out of the gallery between the infrastructure area and the seals. The progressive slow resaturation is caused by equilibration of suction between the concrete seals and adjacent converged salt, but the process is slow. Note that because the reference model uses Richards' equation, the gas is assumed to be infinitely mobile, so no account of gas trapping is taken into account.

Resaturation of the infrastructure area and shaft is entirely dominated by inflow from the surface, and it is clear that this is, in turn, largely controlled by the imposed shaft 'failure' at 1000 years. These behaviours are echoed in the water pressures and illustrate the hydrostatic control in the infrastructure area and lithostatic control at and behind the seal (Figure E.4).
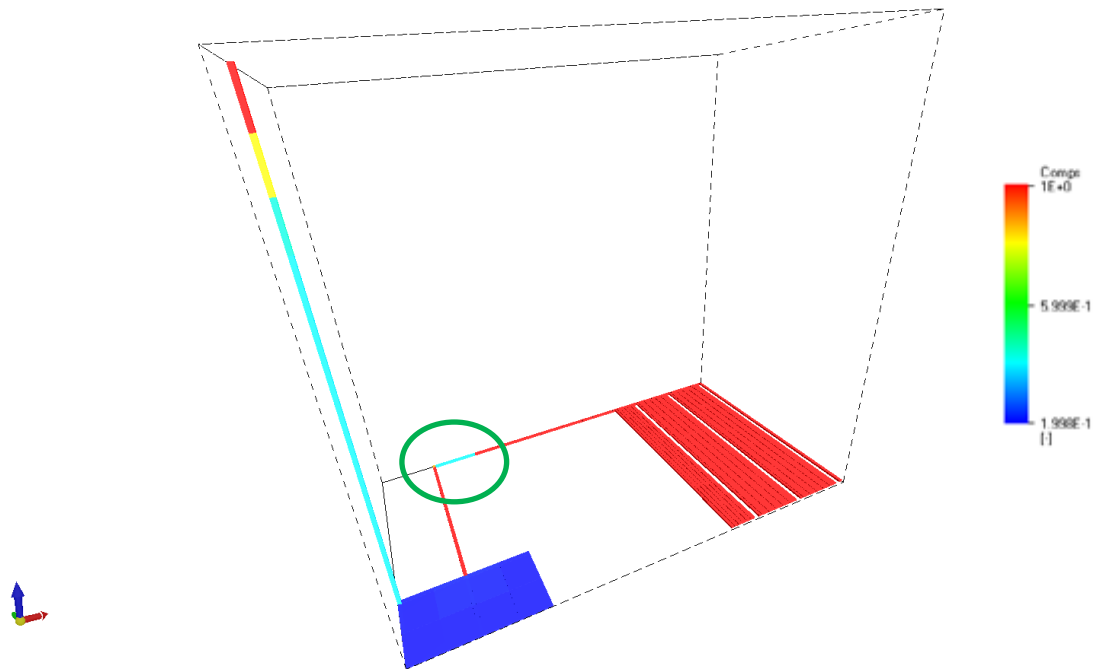
Figure E.9. Water saturation at 1000 years for the reference case, Seal 1 is highlighted (green ellipse)

E.4.2 Porosity

As shown in Figure E.7 creep closure is largely complete after 10 years in the waste drifts, and after approximately 100 years in the salt seal with convergence essentially halted after 1000 years. This illustrates the timescale for the initial advective transport of water due to convergence of the porosity with the water being 'squeezed' out of the waste areas.

E.4.3 Tracer 1/Tracer 3

The results for tracer 3 (which is available for release immediately) shows an initially advectively dominated evolution until just after 1000 years when creep closure is essentially complete, and then a dominantly diffusive phase, once the perturbations from the shaft failure have resolved in the water fluxes (Figure E.3). Tracer 1, in contrast, tend to be diffusively dominated at all times because of the delay in release means that the advective portion fluid flow and tracer transport is largely avoided.

Both sets of results show that the fluxes out of the seal closest to the shaft (seal 1) is extremely small, and much smaller than the other seal. Discharges to the base of the shaft are effectively negligible. However, the results suggest that the very long term trend is for increasing fluxes (albeit extremely small levels), which is thought to reflect the diffusion breakthrough from the waste galleries. Hence this increase is not expected to continue indefinitely, but breakthrough into the shaft is expected eventually.

E.5 Investigation of Variant Cases

The main variants that were required by all teams are discussed in the main text and are not elaborated on here further. However, a range of additional variants were considered. These variants are:

•   Heterogeneous Shaft Infill

•   Geosphere Brine Inflow (with and without total volume restriction)

•   Multi-phase flow (MPF)

•   MPF + Brine Inflow (with and without total volume restriction)

•   MPF + dissolution of air

•   Vertical discretisation in the repository

•   Full initial water saturation

•   and various other variants not discussed here (e.g. convergence delays etc) but were used to ensure the model was behaving sensibly

Those cases warranting a full discussion are summarised in the sub-sections below and overall conclusions from the variants are given. In all the cases shown below, the reference case results are shown using dashed lines.

E.5.1 Heterogeneous Shaft Infill

Comparing the quantities of interest when using a heterogeneous or homogeneous shaft representation we see very little difference in the results. The only significant difference is in the earlier resaturation of the infrastructure area with the heterogeneous shaft infill (Figure E.10). This illustrates that resaturation beyond the seals is mainly controlled by convergence not flow down the shaft.
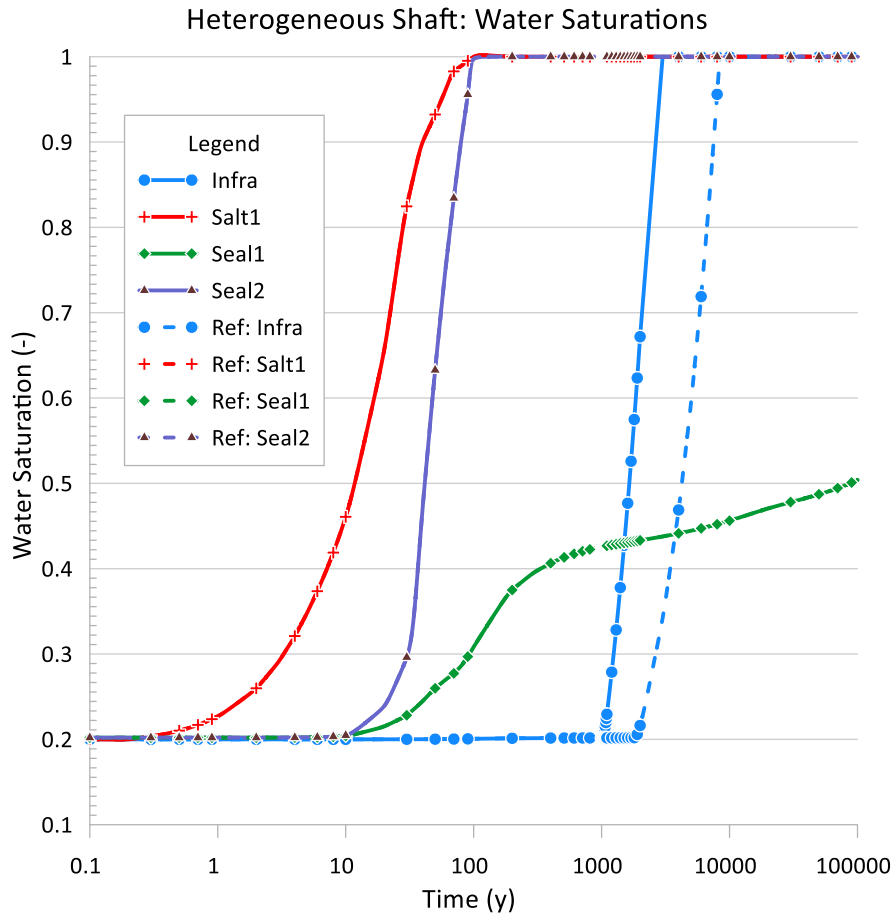
Figure E.10. Quintessa comparison of the reference case water saturation results and the heterogeneous shaft infill variant.

E.5.2 Geosphere Brine Inflow

On the basis of the Task E Brine Availability Task (BATS) work in DECOVALEX-2023, an illustrative brine inflow rate of 1 g/day/m tunnel length was applied to all tunnels at the repository level. The inflow rate was scaled (I_s) in proportion to the difference in fluid pressure in the local tunnel p_f from atmospheric pressure (p_{atm}- full inflow) to zero inflow when the fluid pressure in the tunnel is the same as the specified far-field fluid pressure (p_{ff}) (lithostatic pressure), i.e.:

$$I_s = (p_f - p_{ff})/(p_{atm} - p_{ff})$$

p_f was truncated in the above relationship to be at or above atmospheric pressure, i.e. fluid suction in the tunnels does not enhance inflow. Water pressure exceeding the far-field pressure will cause brine to be expelled from the tunnels, although this is not

expected to happen in the model significantly at present. However, inclusion of gas generation or thermal effects in any future model may change this behaviour. Example results are shown in Figure E.11.

The results show that Seal 1 now resaturates, as it is no-longer starved of a source of brine, and there are slightly increased discharges past seal 2 but reduced discharges past seal 1. Overall, the differences are relatively small however.

This variant essentially assumes an infinite amount of brine is available for resaturation from the geosphere, which is clearly unrealistic. More likely the supply of any host-rock derived brine will be limited to some extent. An option was added to the model to restrict inflow using the following water availability scaling

$$WAs = \begin{cases} \exp\left(-\dfrac{r_i - r_T}{r_I - r_T}\right), & I_S > 0 \\ 1, & I_s \leq 0 \end{cases}$$

where r_i is the current effective radius of influence (m), r_T is the effective tunnel radius (m) and r_I is the additional source radius length (set at 10 m). r_i is calculated using the volume of water that has inflowed into that tunnel section assuming a reference fully saturated hostrock porosity of 0.1% and r_T is the equivalent circular radius of the current tunnel cross-sectional area. The selection of the additional source radius is arbitrary, but could be informed by appropriate more detailed calculations. However, the method helps to illustrate what the behaviour of the system might be as it becomes more difficult to bring brine into the tunnel system. Results are given in Figure E.12 to compare with Figure E.11. The restriction of inflow does very little to the tracer 3 fluxes, but does prevent full resaturation of seal 1 and allows a slight desaturation of Salt 1 as the concrete and salt seals start to equilibrate, bringing forward slightly a process that happens later than the 100,000 year assessment time frame for the reference model. So in this configuration, the brine inflow restriction has a minimal effect.
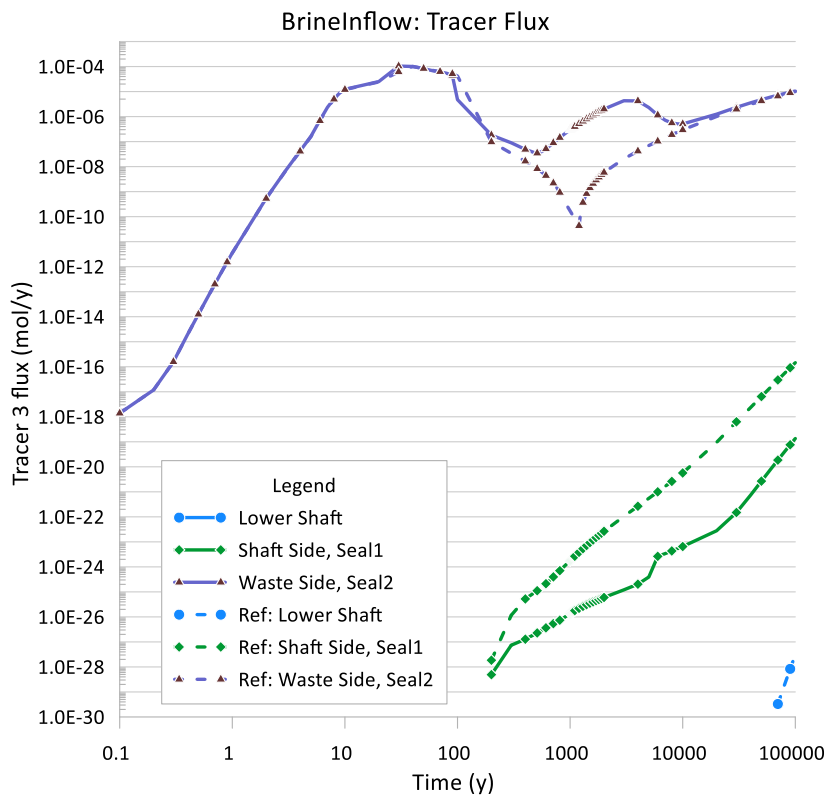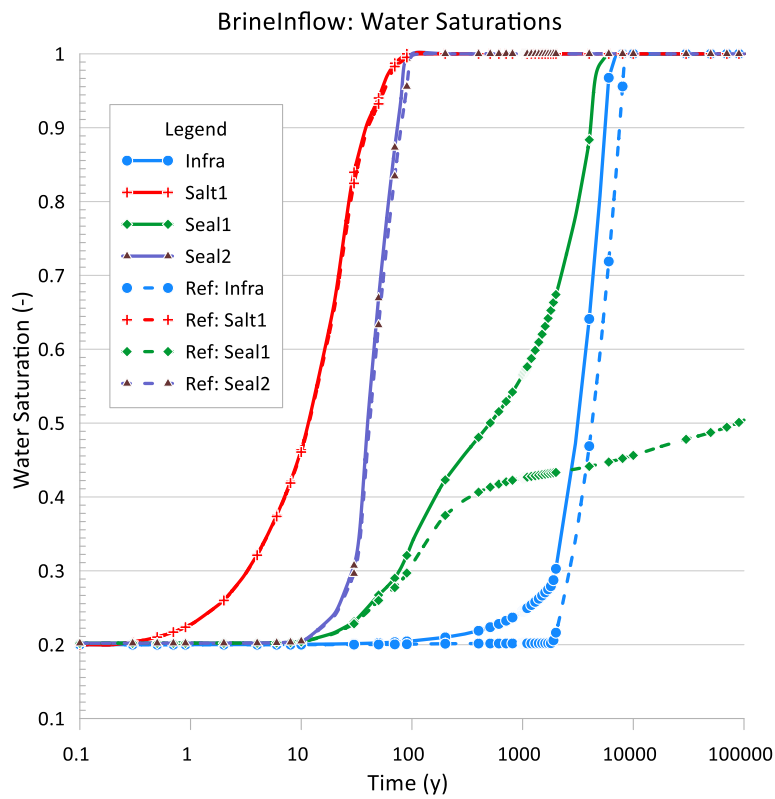
Figure E.11. Comparison of quantities of interest with additional brine inflow from the host rock and the reference case (dashed lines) for water saturations (top) and tracer 3 flux (bottom).
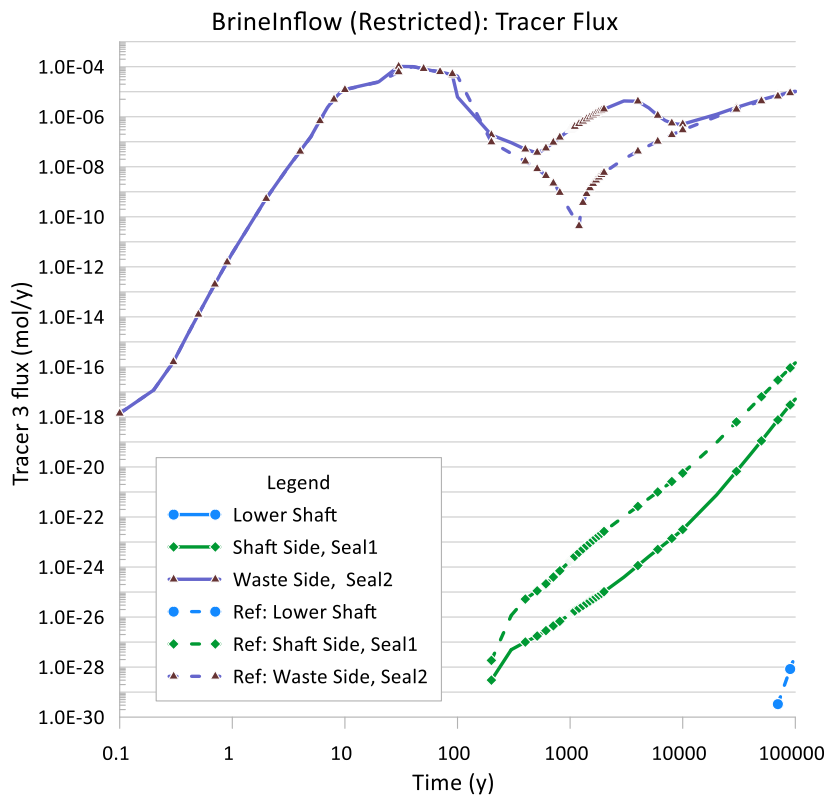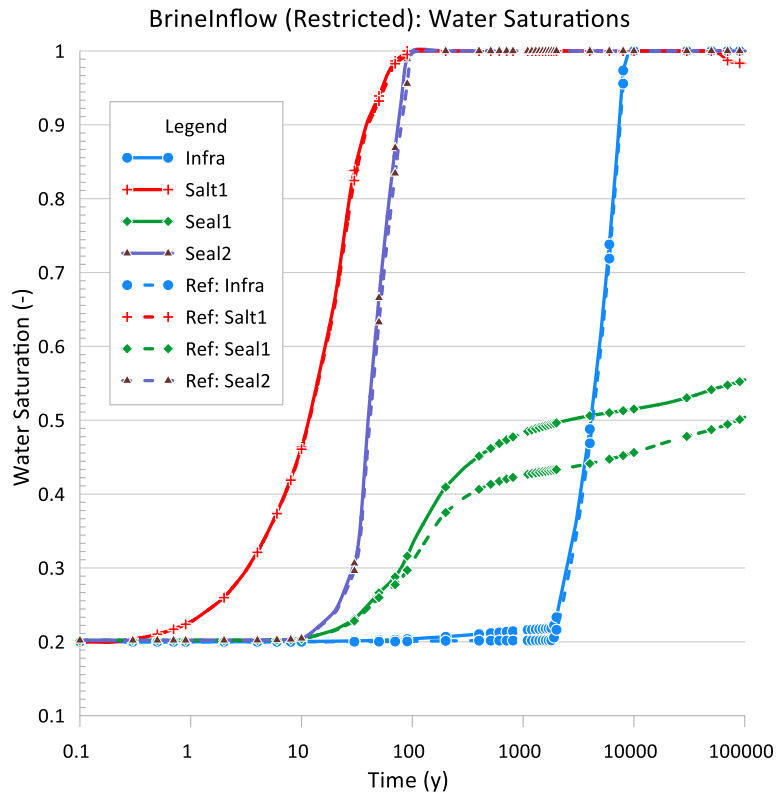
Figure E.12. Comparison of quantities of interest with additional (but restricted) brine inflow from the host rock and the reference case (dashed lines) for water saturations (top) and tracer 3 flux (bottom).

E.5.3 Multiphase Flow Variants

In this variant the Richards' equation formulation is replaced with a full multi-phase flow implementation (Bond et al, 2013; Bond 2014) with air as a distinct phase. Fluid pressure for the creep and brine inflow (note that brine inflow is not enabled by default) is calculated using a simple saturation weighted average. The case is otherwise identical to the reference case. Results are shown in Figure E.13 and show the changes are small. There are differences in the how air gets trapped inside the repository late in life with no part of the sealing system fully saturated, as opposed to the Richards' gas where gas is effectively considered to be infinitely mobile, but otherwise the results are largely unchanged from the reference case.

Additional variants were run with:

- Brine inflow (Figure E.14 – see section E.5.2)
- Restricted brine inflow (Figure E.15 - see section E.5.2)
- Dissolution of air

Including dissolution of air made only small changes to the results, largely in water saturations as the hydrostatic water pressure breaks through from the shaft, so the results aren't presented here.

Adding in unrestricted inflow of brine allows seal 1 to fully resaturate, and this displaces the air into the salt 1 sealing zone; reflecting the differing water retention curves and permeabilities between the two porous media. The additional resaturation of seal 1 causes an advective flow back into the salt 1 zone, which causes the tracer 3 discharge out of the sealing zone to be lower than the reference case.

Restricting the inflow of brine does very little to the results other than preventing the complete resaturation of seal 1, however we still see desaturation of salt 1 later in time, but slightly higher fluxes of tracer 3 out of the sealing zone compared with the unrestricted inflow case.

Clearly the presence of brine inflow has some impact on the brine disposition in the repository, but it doesn't completely change the evolution of the system.
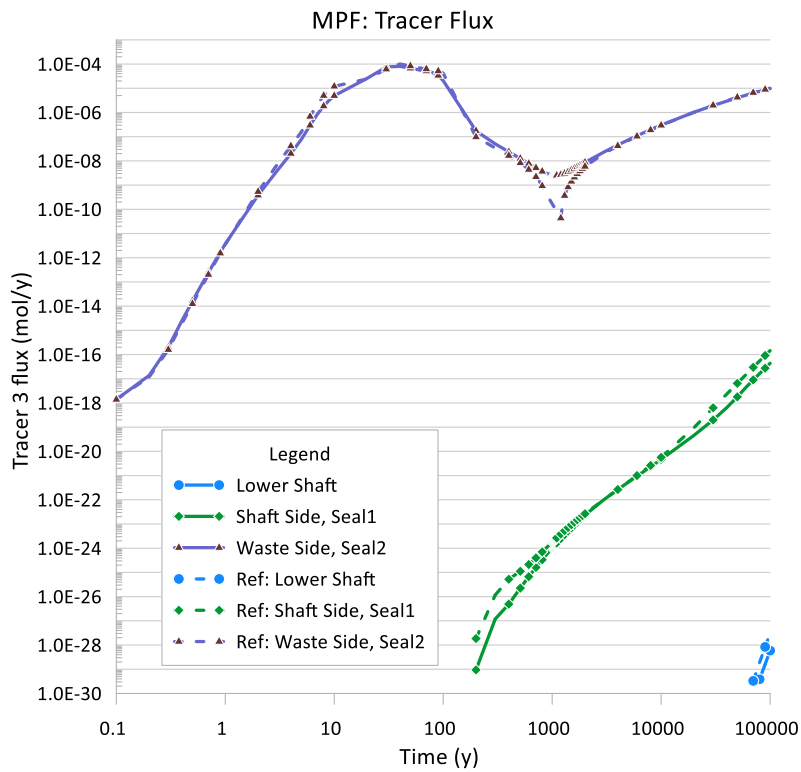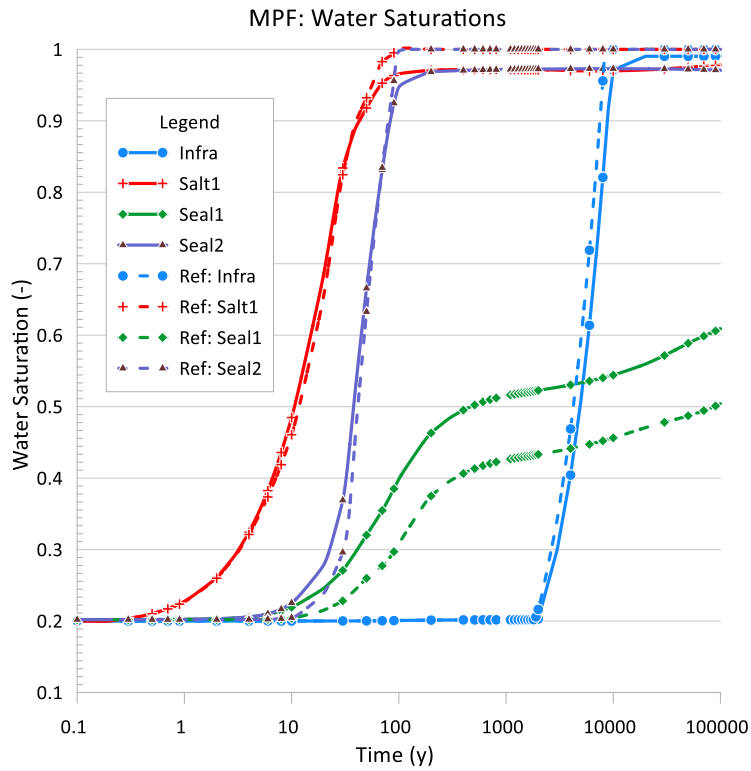
Figure E.13. Comparison of quantities of interest with the multiphase flow formulation and the reference case using Richards' equation (dashed lines) for water saturations (top) and tracer 3 flux (bottom).
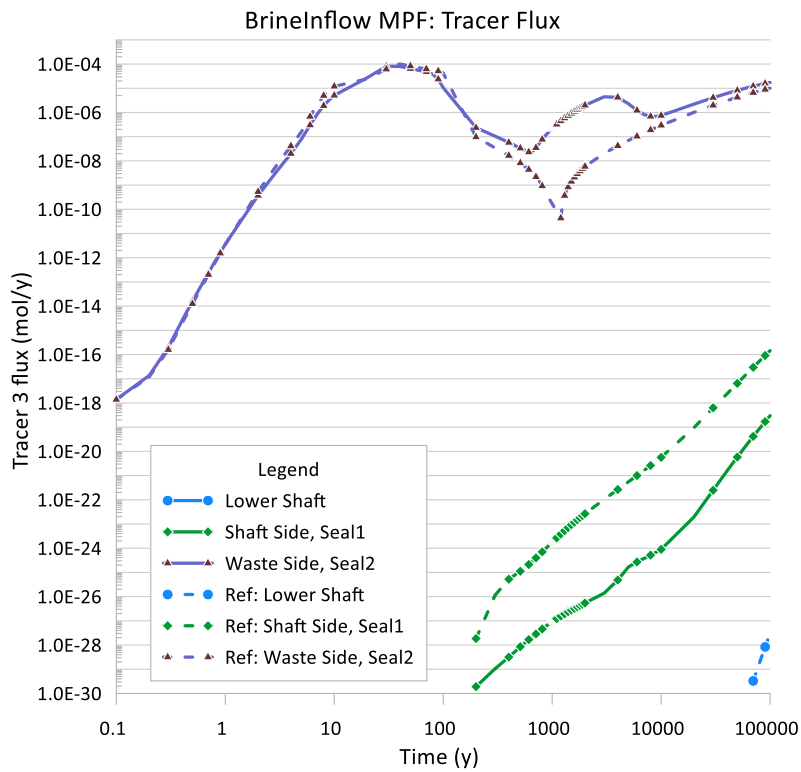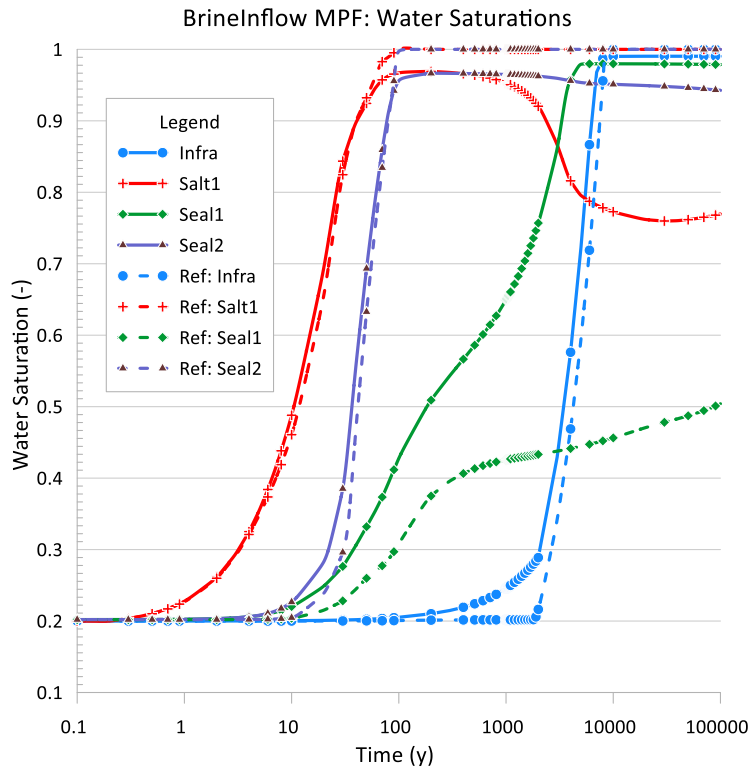
Figure E.14. Comparison of quantities of interest with the multiphase flow formulation with unrestricted brine inflow and the reference case using Richards' equation (dashed lines) for water saturations (top) and tracer 3 flux (bottom).
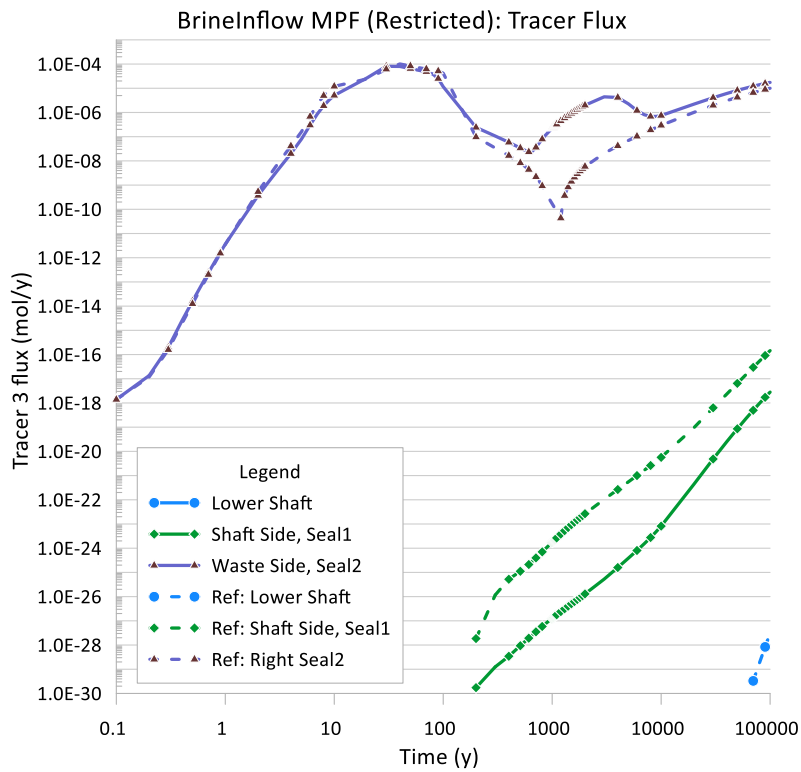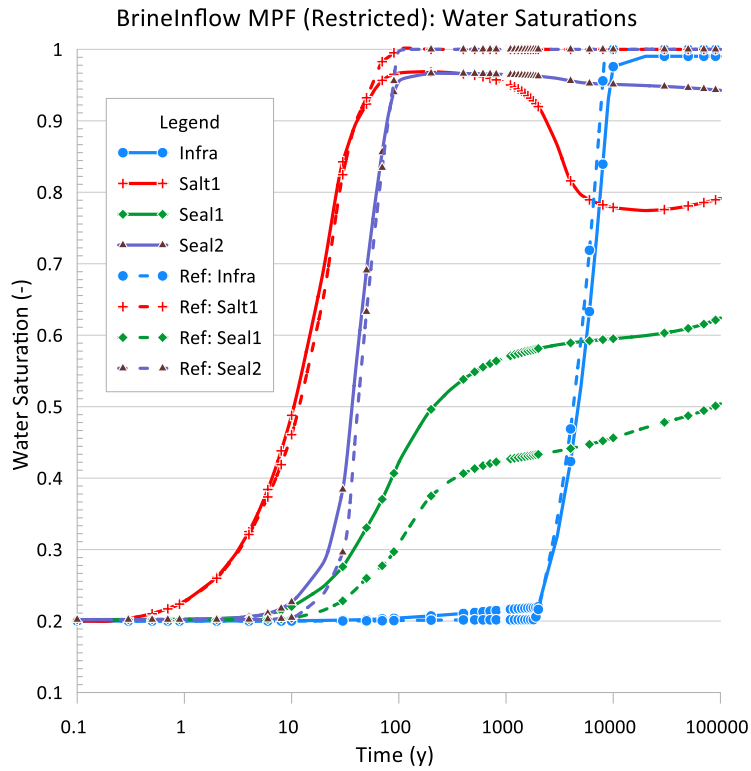
Figure E.15. Comparison of quantities of interest with the multiphase flow formulation with restricted brine inflow and the reference case using Richards' equation (dashed lines) for water saturations (top) and tracer 3 flux (bottom).

E.5.4 Vertical Discretisation in the Repository

The reference model has no vertical discretisation in the tunnel. This was thought to be acceptable because the high suction retention curves means that the water content vertically in a given part of the facility won't change significantly unless very close to full water saturation. Calculations showed that including the vertical discretisation made very little difference to the results and that a single vertical compartment discretisation was appropriate.

E.5.5 Repository Initially Water Saturated

A large part of the evolution of the system is driven by the initial water saturation, the interaction with the creep closure and the inflow down the shaft. In this variant the initial water saturation is set to 1 throughout the repository, with an initial water pressure of 1 atmosphere. Results are shown in Figure E.16. As expected the water saturations remain at 1 throughout the simulation. Tracer 3 fluxes are substantially altered. Discharges into the seal system are generally more constant, just reflecting the convergence of the tunnels and more limited advective migration of the brine in the system as it equilibrates, tending to reflect more of a diffusive discharge profile. Discharges out of the seal system and across the base of the shaft are up to 10 orders of magnitude higher than the reference case (while still being many orders of magnitude lower than the discharge into the sealing structure).

We can see the impact on the creep convergence in Figure E.17 – convergence is greatly reduced by the initial presence of water and the consequently higher water pressures earlier in the calculation. This relative lack of convergence explains the lack of advective tracer movement in the calculation and illustrates the importance of unsaturated advective flow of water in the reference case results.
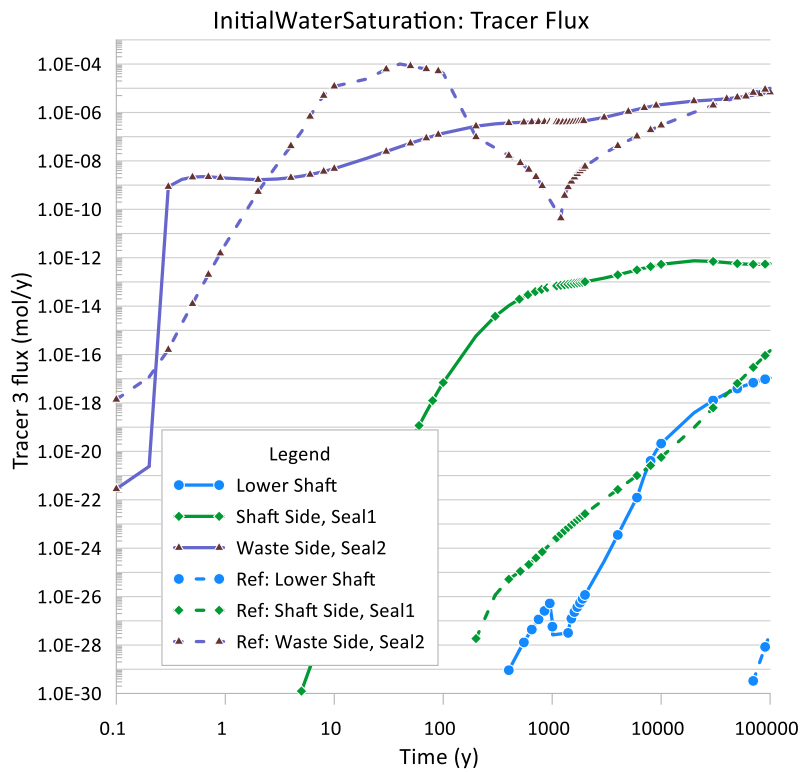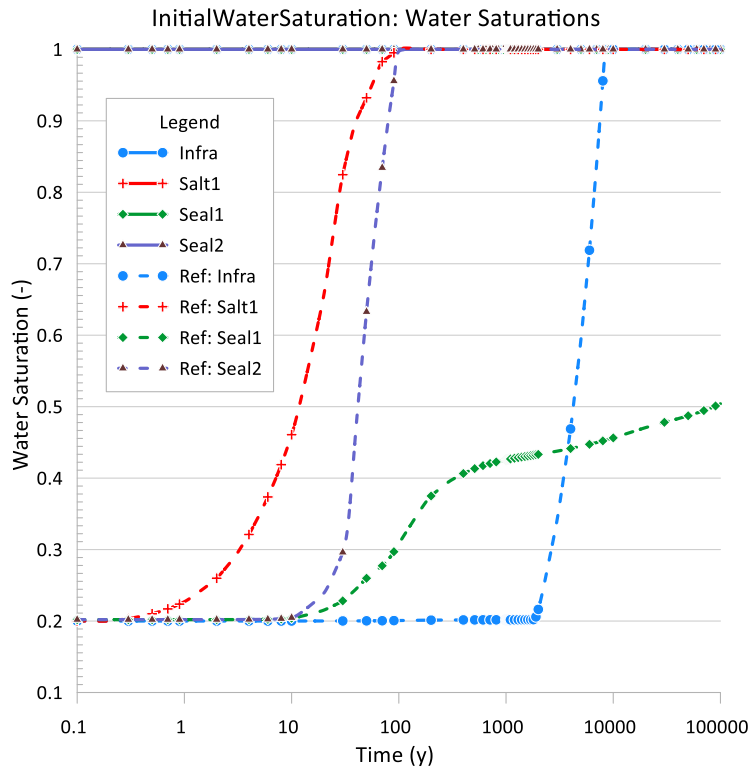
Figure E.16. Comparison of quantities of interest with the initial water saturation of 1 and the reference case (dashed lines) for water saturations (top) and tracer 3 flux (bottom).
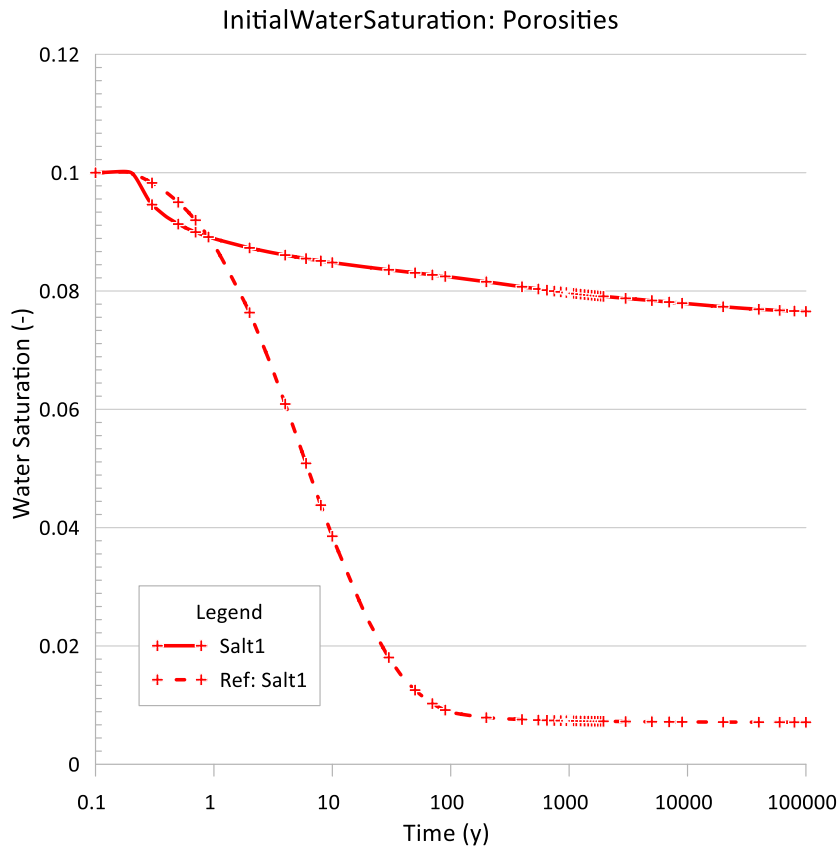
Figure E.17. Comparison of Salt 1 porosities for the reference case (dashed line) and when an initial water saturation of 1 is assumed.

E.5.6 Summary Comments

While the additional variants run here all illustrate that process modelling uncertainties can lead to non-trivial changes in the evolution of the system, none of the changes, with the exception of the full initial water saturation, predicted significant increases in contaminant breakthrough to the bottom of the shaft. Full initial water saturation is highly unlikely to occur in the real system however, so this case was largely investigated out of curiosity as opposed to representing genuine supposed uncertainty.

This suggests that the primary predictions of the reference model - limited contaminant breakthrough to the base of the shaft – are not negatively impacted by the key uncertainties in the system.

The variants do illustrate the important role of tunnel creep convergence in creating advective flow paths in the system, essentially "squeezing" the initial water around the facility. However, this effect might be an artefact of the high initial water content

specified. For a an initially "dry" repository, the behaviour may be quite different, especially as regards contaminants that may be released early in the repository life.

One factor not investigated in the current modelling is the effect of the temperature perturbation transient introduced by the waste forms on brine availability to the tunnel. This coupling is currently being investigated in D-2023 Task E at the level of a single waste package. The combined effect of all heat sources on brine availability could be investigated in the current model to some extent via alternative geosphere flow assumptions, but the effect of thermal stresses at the repository scale on brine inflows is perhaps an open question.

E.6 References

Bond A, Millard A, Nakama S, Zhang C, Garitte B. (2013) Approaches for representing hydromechanical coupling between large engineered voids and argillaceous porous media at ventilation experiment, Mont Terri. Journal of Rock Mechanics and Geotechnical Engineering 2013; 5 (2).

Bond A (2014). The QPAC Multi Phase Flow Module User Guide. QRS-QPAC-HYD-6 Version 2.0 July 20 1 4

Maul P. (2013). QPAC: Quintessa's General-Purpose Modelling Software. QRS-QPAC-11, June 2013. https://www.quintessa.org/qpac-overview-report.pdf

LaForce T, Jayne R, Leone R, Mariner P and Stein E (2023). DECOVALEX-2023 Task F Specification Revision 10. Sandia National Laboratories. SAND2023-04005R